Dissertation zur Erlangung des Doktorgrades
der Fakultät für Chemie und Pharmazie
der Ludwig-Maximilians-Universität München

Chiral Induction in Stereodynamic Catalysts by Non-Covalent Interactions

Ligand Design, Supramolecular Self-Recognition, Deracemization and Enantioselective Self-Inhibition

Jan Felix Scholtes
aus
Karlsruhe, Deutschland

2019

Erklärung

Diese Dissertation wurde im Sinne von § 7 der Promotionsordnung vom 28. November 2011 von Herrn **Prof. Dr. Oliver Trapp** betreut.

Eidesstattliche Versicherung

Diese Dissertation wurde eigenständig und ohne unerlaubte Hilfe erarbeitet.

München, _____21.05.2019_____

.....
(Jan Felix Scholtes)

Dissertation eingereicht am _____15.03.2019_____
1. Gutachterin / 1. Gutachter: ……Prof. Dr. Oliver Trapp.....
2. Gutachterin / 2. Gutachter: ……Prof. Dr. Paul Knochel.....
Mündliche Prüfung am _____02.05.2019_____

Für meine Eltern und meine Schwester.

Publications

J. F. Scholtes, O. Trapp, **Inducing Enantioselectivity in a Dynamic Catalyst by Supramolecular Interlocking**, *Angew. Chem. Int. Ed.*, **2019**, *58*, 6306-6310; A*ngew. Chem.* **2019**, *131*, 6372-6376.

J. F. Scholtes, O. Trapp, **Enantioselectivity through Self-Assembly and Cooperative Self-Recognition – A Novel Core Motif for *Tropos* Ligands**, *Chem. - Eur. J.*, submitted manuscript.

J. F. Scholtes, O. Trapp, **Supramolecular Biphenyl Ligands for Enantioselective Ti-catalyzed Alkylation of Aromatic Aldehydes**, *Organometallics*, submitted manuscript.

J. F. Scholtes, O. Trapp, **Reversal of Selectivity by Enantioselective Self-Inhibition in a Tailor-made, Stereodynamic Catalyst,** *J. Org. Chem.*, submitted manuscript.

Poster presentations

J. F. Scholtes, O. Trapp, 9th CaRLa Winter School 2016, Heidelberg, (Germany).
Enantioselectivity Through Non-Covalent Interactions.

J. F. Scholtes, O. Trapp, 28th International Symposium on Chiral Discrimination (Chirality 2016), Heidelberg, (Germany).
Enantioselectivity Through Non-Covalent Interactions (Poster Prize).

J. F. Scholtes, O. Trapp, 10th CaRLa Winter School 2017, Heidelberg, (Germany).
Induction Enantioselectivity by Self-Recognition.

Table of Content

Abbreviations

α	separation factor
Ac	acetyl
Ala	alanine
BHT	2,6-di-*tert*-butyl-4-methylphenol
BINAP	2,2'-bis(diphenylphosphino)-1,1'-binaphthyl
BIPHEP	2,2'-(diphenylphosphanyl)-1,1'-biphenyl
BIPOL	2,2'-biphenol
Bn	benzyl
Boc	*tert*-butoxycarbonyl
Bu	butyl
calcd.	calculated
Chiraphos	bis(diphenylphosphino)butane
COD	1,5-cyclobutadiene
COMU	(1-cyano-2-ethoxy-2-oxoethylidenaminooxy)dimethylamino-morpholino-carbenium-hexafluorophosphat
CSP	chiral stationary phase
DABCO	1,4-diazabicyclo[2.2.2]octane
DAD	diode array detector
DART	direct analysis in real time
DAST	*N*,*N*-diethylaminosuflur trifluoride
DCM	dichloromethane
de	diastereomeric excess
DHPLC	dynamic high performance liquid chromatography
DIAB	(2*S*)-(−)-3-*exo*-(dimethylamino)isoborneol
DIOP	2,3-*O*-isopropylidene-2,3-dihydroxy-1,4-bis(diphenylphosphino)butane
DiPAMP	bis[(2-methoxyphenyl)phenylphosphino]ethane
DIPEA	diisopropylethylamine
DMAP	N,N-dimethylaminopyridine
DMF	dimethylformamide
DMSO	dimethylsulfoxide
DPEN	diphenylethylenediamie
DPPE	diphenylphosphinoethane
DPPF	diphenylphosphinoferrocene
dr	diastereomeric ratio
EA	elemental analysis
EDCI.HCl	1-ethyl-3-(3-dimethylaminopropyl)carbodiimide hydrochloride

ee	enantiomeric excess
eq.	equivalents
er	enantiomeric ratio
Et	ethyl
FDHM	full duration at half maximum
FTIR	Fourier-transform infrared spectroscopy
GC	gas chromatography
HOBt	1-hydroxybenzotriazole
HPLC	high performance liquid chromatography
HR-EI	high resolution – electron impact ionisation
HR-ESI	high resolution – electron spray ionisation
HMBC	heteronuclear multiple-bond correlation spectroscopy
Hz	hertz
i.d.	inner diameter
IPA	isopropyl alcohol
^{i}Pr	isopropyl
k	retention factor
LDA	lithiumdiisopropylamide
L-DOPA	L-3,4-dihydroxyphenylalanine
M	molar
MAA	methyl 2-acetamidoacrylate
MALDI	matrix assisted laser-desorption/ -ionization
Me	methyl
min	minute(s)
MOF	metal organic framework
MOM	methoxymethyl
MS	mass spectrometry
NMR	nuclear magnetic resonance
NOE	nuclear Overhauser effect
NOESY	nuclear Overhauser enhancement spectroscopy
Phe	phenylalanine
pm	picometer
ppb	parts per billion
ppm	parts per million
R_F	retardation factor
s	seconds
t	retention time
TEA	triethylamine
THF	tetrahydrofuran
TS	through space

v	volume
Val	valine
$\Delta G^{\ddagger}$	Gibbs free energy
$\Delta S^{\ddagger}$	entropy
$\Delta H^{\ddagger}$	enthalpy

Kurzfassung

Enantioselektive Interaktionen zwischen Molekülen spielen in vielen biologischen Vorgängen eine entscheidende Rolle. Sind diese Wechselwirkungen von nicht-kovalenter Natur, bilden sie häufig die Grundlage für Vorgänge der molekularen Erkennung, des Chiralitätstransfers oder der Selbstorganisation. Es wird vermutet, dass solche Mechanismen an der Entstehung der Homochiralität in der Natur beteiligt waren.[1-4] Das Verständnis darüber, wie solche nicht-kovalenten Interaktionen ausgenutzt werden können, um die stereochemische Kontrolle über asymmetrische Reaktionen zu erlangen, verspricht weitreichende Möglichkeiten für das zukünftige Design neuer Katalysatoren in der Chemie.

Die vorliegende Dissertation beschreibt die Synthese und Untersuchung stereodynamischer Liganden und Komplexe sowie ihre Anwendung in asymmetrischen Reaktionen. Im Zentrum stand die Beeinflussung der Chiralität axial chiraler Liganden durch nicht-kovalente Wechselwirkungen zwischen am Ligandenrückgrat befestigten Bindungsstellen (Selektoren) und anderen Molekülen. Die Dissertation ist in vier Themengebiete untergliedert.

Das erste Themengebiet in Kapitel 2 beinhaltet die Untersuchung chiraler, L-Aminosäure-basierter Interaktionsstellen mit sekundären Amiden, deren Natur von Interaktionsstellen der Hochleistungs-Gaschromatographiesäule CHIRASIL VAL abgeleitet wurde (Abbildung 1a). Verschiedene 5,5‘-selektormodifizierte, 2,2‘-biphenyl-basierte Liganden wurden synthetisiert und es konnte gezeigt werden, dass eine derartige Substitution im Rückgrat eine spontane, mitunter quantitative Anreicherung eines Ligandrotamers bewirkt. In detaillierten strukturellen Untersuchungen konnte nachgewiesen werden, dass ein intermolekulares Netzwerk aus Wasserstoffbrückenbindungen zwischen Selektoreinheiten zur diastereoselektiven Ausbildung von Ligand-Dimerstrukturen führt, welche im Folgenden die Anreicherung nach sich zieht. Die verschiedenen Ligandtypen konnten abschließend erfolgreich in enantioselektiven Hydrierungs- und Alkylierungsreaktionen eingesetzt werden.

Im darauffolgenden Kapitel 3 wird die Thematik auf achirale Bindungsstellen ausgeweitet (Abbildung 1b). Nach dem Vorbild „schaltbarer“ Katalysatoren sollte die gezielte Deracemisierung von racemischen Liganden mittels chiraler Additive durchgeführt werden. Hierbei wurden unter anderem, aufbauend auf Erkenntnissen aus dem vorangegangenen Kapitel, racemische Bisphosphinite mit Glycin- sowie racemischen Phenylalanin-basierten Selektoren modifiziert. Durch Wechselwirkung mit chiralen Additiven konnte das Rotamerverhältnis der Liganden entsprechender Rhodiumkomplexe selektiv beeinflusst werden und somit Katalysatoren für enantioselektive Hydrierungsreaktionen erzeugt werden.

Kapitel 4 behandelt die Entwicklung eines autoinduktiven Katalysatorsystems (Abbildung 1c). In Anlehnung an eine von Trapp *et al*. beschriebene enantioselektive Reaktion mit autoinduktiven, selbstamplifizierenden Eigenschaften wurde ein komplementäres System entwickelt, bei dem der Selektivität einer Reaktion ein selbstinhibierender Ablauf zugrunde liegt. In einem zweistufigen Prozess wurde zunächst ein neuartiges Phenylalanin-basiertes Amidoester-Selektormotiv auf sein Potential der Stereoinduktion hin untersucht. Durch stereoselektive Interaktion mit einer Reihe chiraler L-Aminosäurederivate, die gleichzeitig potentielle Hydrierprodukte darstellten, gelang es, eine signifikante Rotameranreicherung bei einem der untersuchten Bisphosphinitliganden und seinem Rhodiumkomplex herbeizuführen. Dies führte gleichzeitig zu einer signifikanten Selektivitätssteigerung in nachfolgenden Hydrierreaktionen, wobei verstärkt das (*R*)-Produktenantiomer gebildet wurde. Basierend auf diesen Ergebnissen wurden im

zweiten Schritt ein hochdynamischer, selektormodifizierter Phosphoramiditligand und verschiedene Olefine synthetisiert, wobei letztere sich von einem der chiralitätsinduzierenden Aminosäurederivate ableiten. In folgenden Hydrierreaktionen konnte gezeigt werden, dass ein ursprünglich bevorzugt gebildetes Produktenantiomer durch Interaktion mit dem Katalysator seine eigene Entstehung im weiteren Verlauf der Reaktion inhibiert und so eine Selektivitätsumkehr herbeiführt.

Der letzte Teil der Arbeit in Kapitel 5 beschreibt das Konzept und initiale Studien eines neuartigen, aliphatischen Ligandengrundkörpers für selektormodifizierte *tropos* Liganden, der auf *meso*-Weinsäure basiert (Abbildung 1d). Die Erprobung von Synthesen für einen Bisphosphin- und einen Bisphosphinitliganden und Untersuchungen zur Konformerverteilung werden beschrieben.

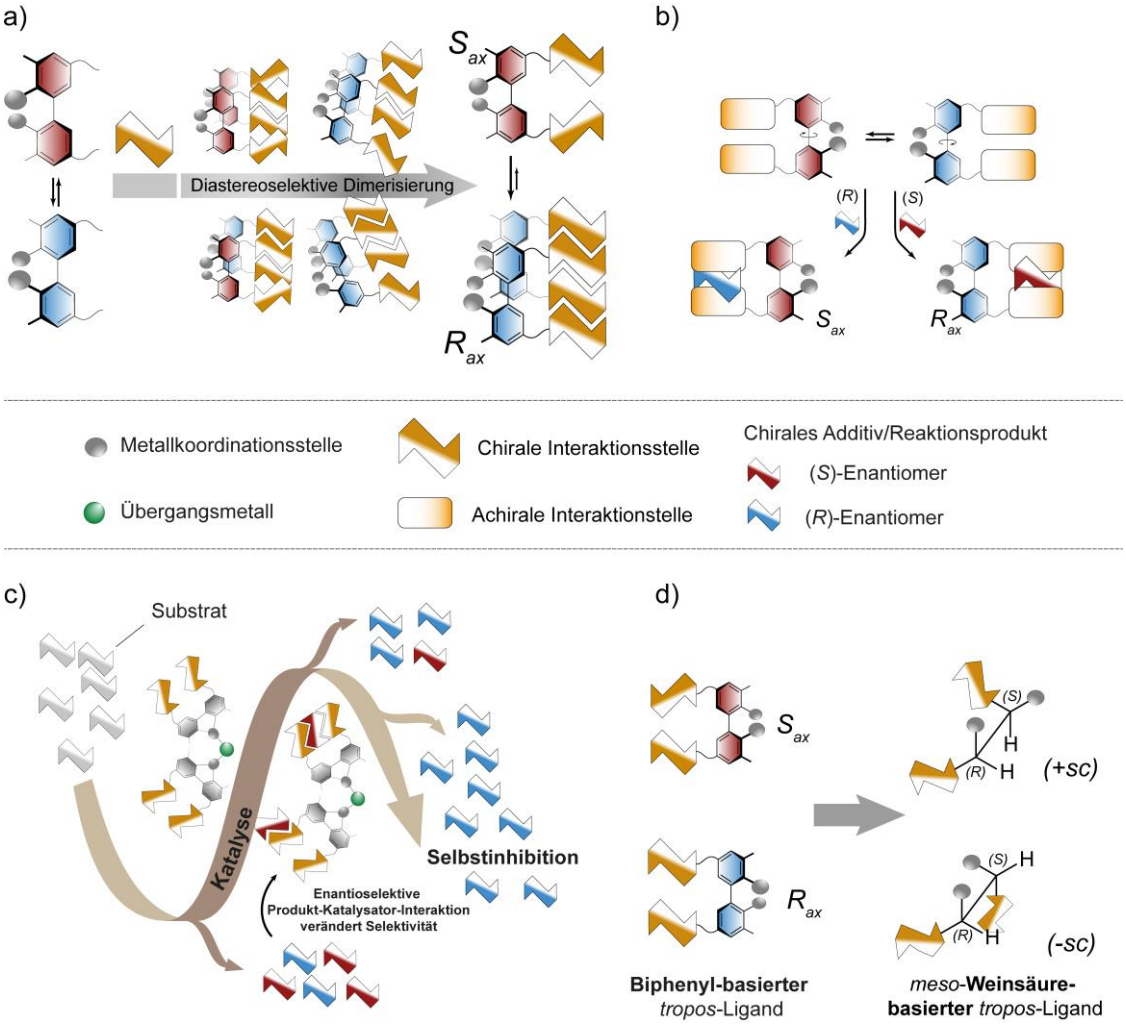

Abbildung 1: Übersicht der in der vorliegenden Dissertation beschriebenen Forschungsprojekte. Im Zentrum steht das Bestreben mittels nicht-kovalenter Wechselwirkungen Einfluss auf die Stereochemie der untersuchten, stereodynamischen Liganden und Katalysatoren zu nehmen, um so Enantioselektivität in asymmetrischen Reaktionen zu erzeugen.

Abstract

Enantioselective interactions between molecules play a crucial role in a wide range of biological transformations. Where these interactions are of non-covalent nature, they can form the basis for molecular recognition, chirality transfer and self-organization, processes believed to be deeply involved in the origin of natural homochirality.[1-4] Understanding how non-covalent interactions can be utilized to exert stereochemical control over chemical reactions promises far-reaching opportunities for the prospective design of novel chiral catalysts in chemistry. The strive to harness this potential has sparked great efforts to find pathways that allow for enantiocontrol on a molecular level.

In this dissertation, the synthesis and study of stereodynamic ligands and respective complexes as well as their application in asymmetric reactions is described. The focus is on investigating possibilities to influence the axial chirality of *tropos* ligands through non-covalent interactions between binding sites (selectors), covalently attached to the ligand backbone, and other chiral and achiral molecules, thus inducing enantioselectivity in subsequent asymmetric reactions. The dissertation is divided into four topics.

The first topic in chapter 2 covers investigations on chiral L-amino acid-based interaction sites with secondary amides, derived from selector sites of the gas chromatography CSP CHIRASIL VAL. Different 2,2'-biphenyl-based ligands with interaction sites in 5,5'-position were devised and it was found that such a substitution entails spontaneous enrichment of one ligand rotamer (Figure 1a). Detailed structural investigations revealed an intermolecular network of hydrogen bonds between selector units to cause diastereoselective formation of ligand dimers. Lastly, the ligands could successfully be employed in transition metal-mediated asymmetric hydrogenation and alkylation reactions yielding products in very high enantioselectivities.

In chapter 3, investigations are extended to achiral binding sites for non-covalent interaction. Inspired by the model of "switchable" catalysts, hydrogen-bond driven deracemization of racemic catalysts was examined (Figure 1b). Based on the findings in the previous chapter, bisphosphinite ligands with glycine- and racemic phenylalanine-based diamide selectors were devised. By interaction with chiral additives, the rotational distribution of the ligands in corresponding rhodium complexes could be selectively influenced and catalysts for enantioselective hydrogenation reactions could be obtained.

Chapter 4 deals with the development of an autoinductive catalyst system. Based on a "by design" self-amplifying reaction previously described by Trapp *et al*., a complementary system was developed in which the selectivity of a reaction is based on enantioselective self-inhibiting properties (Figure 1c). In a two-stage process, a novel, phenylalanine-based amidoester selector motif was first investigated for its potential of non-covalent stereoinduction. Using a series of chiral amino acid derivatives, all of them representing potential hydrogenation products, it was possible to induce significant rotameric enrichment in one investigated ligand and its respective rhodium complex. A concomitant increase in selectivity for the *R* product enantiomer in subsequent hydrogenation reactions was detected. In the second stage of the project, a highly dynamic, selector-modified phosphoramidite ligand and different olefins were synthesized, the latter being structurally based on one of the amino acid derivatives that had earlier exhibited strong stereoinducing capabilities. In subsequent hydrogenation reactions, it could be shown that over the course of the reaction, an originally preferential product enantiomer inhibited its own production

by changing the catalyst's selectivity through non-covalent interaction, thus inducing a reversal of the catalyst's enantioselectivity.

The last part of the dissertation in chapter 5 describes initial studies concerning a novel ligand motif for selector-modified *tropos* ligands that is based on an aliphatic ligand backbone derived from *meso*-tartaric acid (Figure 1d). The synthetic outline and initial syntheses for a bisphosphine and a bisphosphinite ligand as well as preliminary studies on ligand conformers and interaction behaviour are described.

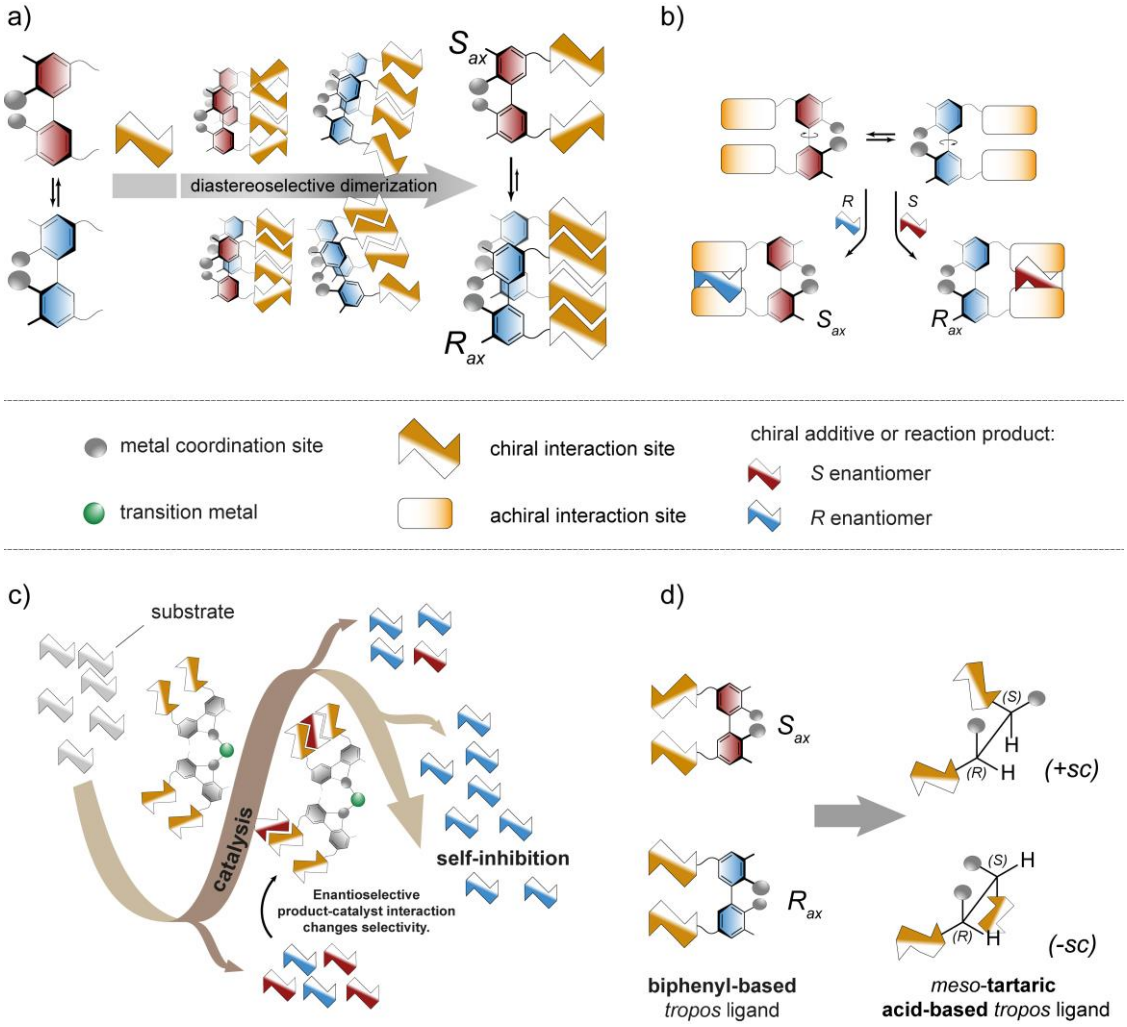

Figure 1: Overview of the research projects described in this dissertation. The investigations focused on influencing the stereochemistry of stereodynamic ligands and catalysts by means of non-covalent interaction in order to generate enantioselectivity in asymmetric reactions.

1 Introduction

Nature provides us with countless patterns illustrating the importance of a stereochemical information for the successful functioning of biochemical processes. One example is provided by the fact that in some processes only the correct stereoisomer produces the desired effect, while other isomers have reduced to no effect. One example is the herbicide metolachlor for which four different stereoisomers exist, only two of which are biologically active (see Figure 1-1, *left*).[5]

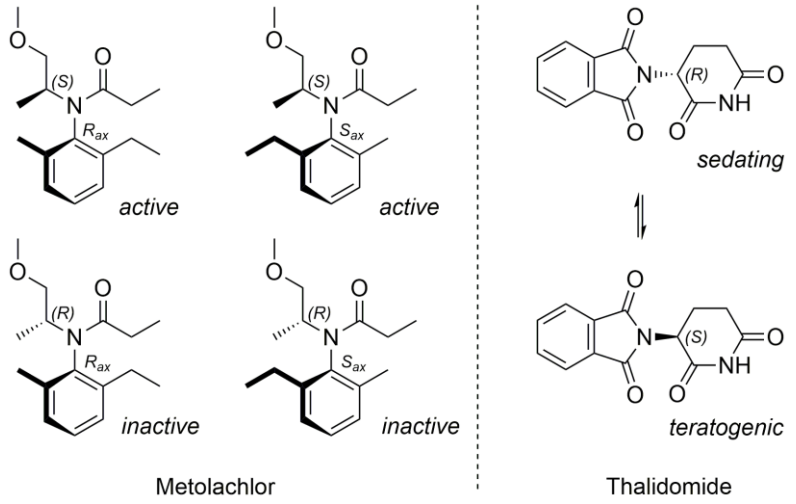

Figure 1-1: Four diastereomers of the herbicide Metolachlor and both enantiomers of Thalidomide.

Another example can be found in cases where two enantiomers have opposite biological effects. One of the most prominent examples is thalidomide, a immunomodulatory drug which became infamous during the Contergan scandal.[6] While (*R*)-thalidomide successfully countered nausea and alleviated morning sickness for expecting mothers, tragically, the corresponding *S* enantiomer was found to have a teratogenic effect on the unborn child (see Figure 1-1, *right*). It was also observed that both enantiomers can interconvert[7,8] under physiological conditions[9], strongly limiting the medical applicability of the compound. These examples illustrate that the optical purity of chiral compounds is of vital importance for the pharmaceutical, cosmetic and agrochemical industries, among others.[10-12]

In general, this is achieved by employing enantiomerically pure catalysts, whose preparation requires enantioselective syntheses or the cumbersome separation of a racemate themselves. The best-known examples are the synthesis of L-menthol, developed by BASF, in which neral is reduced to *D*-citronellal using a Chiraphos-Rh catalyst,[13] the JosiPhos-Ir-catalyzed imine reduction during the preparation of the aforementioned metolachlor[14] and the enantioselective hydrogenation using DIPAMP- or BINAP-Rh complexes for the synthesis of the Parkinson's drug L-DOPA ((*S*)-3,4-dihydroxyphenylalanine) that was originally established by Knowles.[14,15] The fact that the development of optically pure catalysts is so time-consuming and expensive is the underlying reason for present trends to investigate alternative approaches to generate optically enriched compounds. Naturally, interest arises to understand and imitate underlying mechanisms nature has developed for this purpose.

The stereochemical specialisation of biological processes in nature is generally summarised under the term *homochirality*. At the very center of this concept are amino acids and sugars, with

few exceptions naturally only found in their L-form and in their D-form, respectively, and making up the essential building blocks for the most important molecules of life. The question of the origin of homochirality is a heavily discussed topic among experts.[16-19] As early as 1953, Frank published a theoretical model dealing with the spontaneous emergence of asymmetric reactions.[20] Todays consensus assumes a two-stage procces. In the first stage, a local deviation from racemic equilibrium is assumed. While Frank's model uses statistical, locally limited fluctuation as the original trigger, it has been shown that irradiation of racemic amino acids with circularly polarized light leads to enantioselective degradation.[1] Furthermore, it was found that spontaneous deracemization can occur during the crystallization of racemic compounds.[21,22] In the second stage, stereochemical fluctuations must be amplified, leading to an enantiomerically pure final state. In this context, non-linear effects play a decisive role, because they allow for an enlargement of initially small enantiomeric excesses. [23] It has already been achieved to transfer this concept to reactions catalysed by biologically relevant compounds such as amino acids.[24,25] A special case is auto induction or self-amplification, where a chiral reaction product influences the enantioselectivity of its own production. If the product serves as the catalyst itself, this is also referred to as autocatalysis.[26]

2 Cooperative chiral induction in stereodynamic catalysts

2.1 State of knowledge

Asymmetric reactions using chiral, organometallic catalysts is one of the most versatile and widely applied methods for the preparation of enantioenriched compounds.[27] The most common approach is to employ optically pure ligands for which a number of privileged structures have emerged following the diligent research in the past decades.[28] Among the most popular examples are bidentate ligands like BINAP,[29] where the chiral information is stored in a rigid, atropisomeric axis and widespread research has been conducted to understand how this information can efficiently be transferred onto a given substrate.[30-32] Since the enantiopure synthesis of these ligands can be quite challenging to begin with, numerous strategies have emerged that allow employment of racemic ligands in asymmetric reactions.

Yamamoto *et al.* were the first to employ a strategy now referred to as *chiral poisoning*, when they treated racemic BINOL-Al complexes with chiral ketones to reduce catalytic activity of one catalyst enantiomer in hetero-diels-alder reactions (see Figure 2-1).[33]

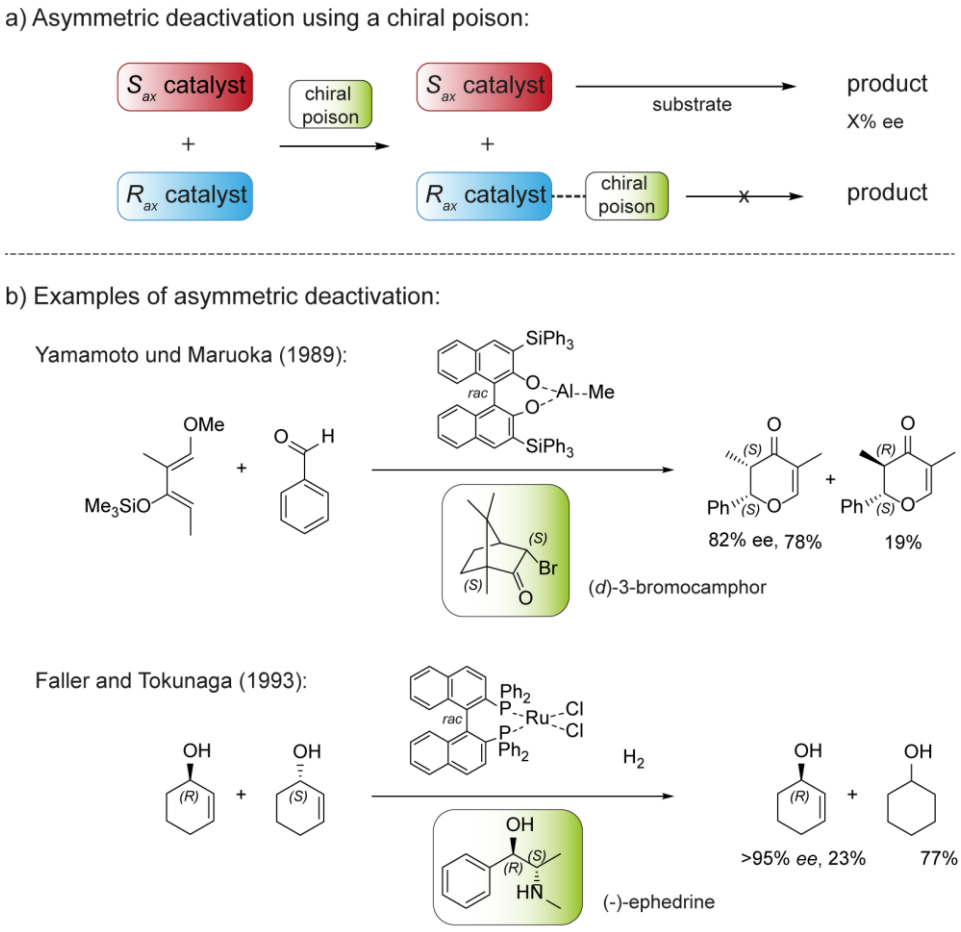

Figure 2-1: a) Schematic illustration of enantioselective reactions with racemic catalysts where a chiral agent (*chiral poison*) selectively decreases the reactivity of one catalyst isomer. b) Reaction schemes for the enantioselective deactivation of a *rac*-BINOL-Al catalyst using (*d*)-3-bromocamphors as chiral poison for enantioselective hetero-diels-alder reactions by Yamamoto and Maruoka[33] and for the kinetic resolution of allylic alcohols using a *rac*-BINAP-$RuCl_2$ catalyst and (-)-ephedrine as deactivator, published by Faller and Tokunaga.[34]

This effect was also studied by Faller and Parr, among other, who could employ racemic Chiraphos-Rh complexes in the presence of (*S*)-methophos for the enantioselective hydrogenation of olefins[35] and by Faller and Tokunaga, who achieved the asymmetric kinetic resolution of allylic alcohols with a racemic BINAP-Ru catalyst in presence of (-)-ephedrine.[34] In the complementary approach of "chiral activation", Mikami and Noyori used (*S*,*S*)-diphenylethylendiamine (DPEN) as co-ligand for *rac*-TolBINAP-Ru complexes to selectively enhance the reactivity of one catalyst enantiomer, allowing for the highly enantioselective reduction of various ketones (see Figure 2-2).[36]

This concept, too, was widely adopted and further developed.[37] It bears the intrinsic advantage, that – unlike in the case of chiral poisoning – the activated catalyst species can have a higher selectivity and reaction rate than a comparable enantiopure catalyst. A general drawback in both concepts results from the fact that either one relies on only half of the catalyst stock to conduct the reaction.

Stereolabile, biphenyl-based *tropos* ligands offer a substantially different approach. The term "*tropos*" generally refers to chiral ligands where the two chiral ligand states have a low barrier of interconversion and isomerize readily.[38] The overwhelming majority of these ligands is based on 2,2'-biphenol (BIPOL) and a relevant selection of ligand types is shown in Figure 2-3.

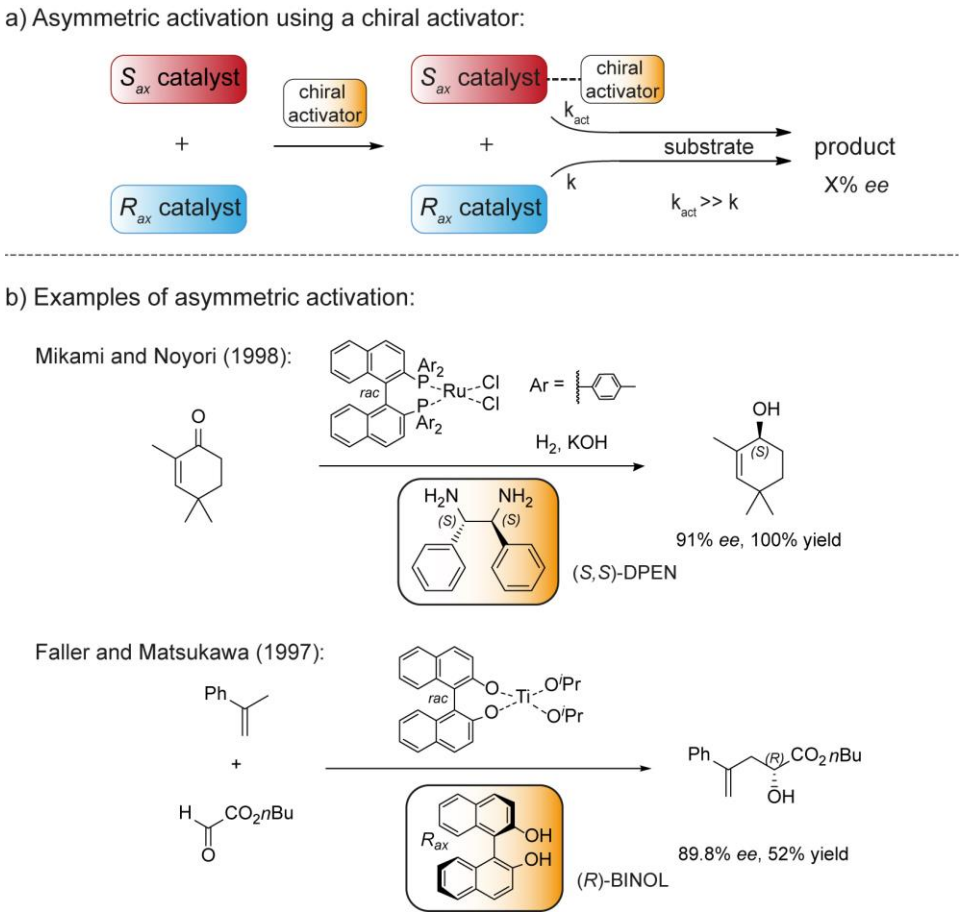

Figure 2-2: a) Schematic illustration of enantioselective reactions using a chiral activator, which selectively enhances the catalytic performance of one catalyst isomer to generate enantiomeric excess in an asymmetric transformation. b) Reaction schemes for the enantioselective activation of a *rac*-TolBINAP-Rh catalyst using (*S*,*S*)-DPEN during enantioselective hydrogenations of prochiral ketones by Mikami and Noyori[36] and for an enantioselective carbonyl-ene reaction using a *rac*-BINOL-Ti(O^iPr)$_2$ catalyst and (*R*)-BINOL as activator, published by Mikami and Matsukawa.[39]

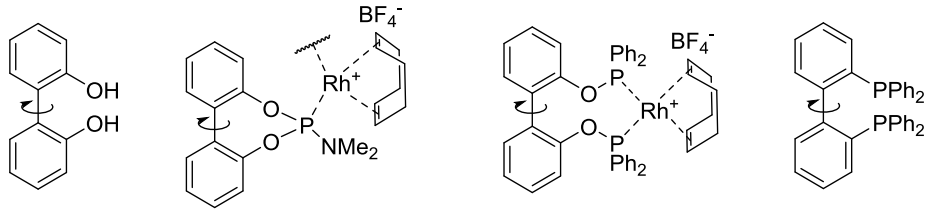

BIPOL	phosphoramidite (Rh complex)	bisphosphinite (Rh complex)	BIPHEP
$\Delta G^{\ddagger}_{298}$ =	37.8 kJ mol^{-1}	78.8 kJ mol^{-1}	86.8 kJ mol^{-1}

Figure 2-3: Relevant selection of biphenyl-based *tropos* ligands or their respective Rh complex. Rotational barrier increases from left to right and references for the values for the rhodium-phosphoramidite complex,[40] the rhodium-bisphosphinite complex[41] and the BIPHEP ligand[42,43] can be found in the respective reference(s). In general, complexated ligands have an increased barrier of rotation in comparison to the uncoordinated ones.

To generate enantioselectivity, a stereochemical bias on the dynamic chiral axis is needed to trigger the enrichment of one ligand rotamer. This can be accomplished by interaction of the racemic catalyst with a chiral molecule. The energetic difference between the resulting diastereomeric complexes leads to concomitant adaptation of the rotamer distribution. This was impressively pioneered by the groups of Gagné, Mikami and Noyori, who used enantiopure diamines and amino alcohols as co-ligands to generate diastereomerically enriched 2,2'-bis(diphenylphosphinyl)biphenyl (BIPHEP) transition metal complexes for the use in asymmetric transformations (see Figure 2-4).[44-47] Similarly, Brown and Faller employed chiral diene ligands, while Klankermayer, Leitner and Franciò used proline-based ionic liquids that coordinate to a metal center across from the *tropos* ligand to achieve similar degrees of stereoinduction.[48-51] Because of the dynamic nature of the ligand, this approach demands suitable conditions to preserve the chiral enrichment, if the stereoinducing co-ligand is displaced during the catalytic reaction cycle. To circumvent this issue, RajanBabu und Parquette *et al.* designed a system where stereodirecting, chiral oxazoline substituents were covalently attached in the 3,3'-position of a biphenol-based 2,2'-bisphospinite to allow for spontaneous rotameric enrichment of the ligand based on central-to-axial chirality transfer.[52] Similarly, Trapp *et al.* modified a BIPHEP-core with chiral esters in the 3,3'-position to obtain diastereoenriched catalysts for the enantioselective hydrogenation of olefins, whose selectivities could be changed by temperature treatment.[53,54]

In a more recent development, supramolecular chemistry has emerged as a new pillar in asymmetric synthesis. However, as with original *atropos* catalysts, many systems reported rely on employment of established ligand motives such as BINOL, which bear a static chiral information and need to be provided in high enantiomeric purity. Enhanced enantioselectivity is subsequently achieved through rigidification of the complex geometry based on non-covalent interaction between ligands or ligand parts.[55,56] The share of published examples, where the chiral information in the ligand or catalyst is defined by intermolecular interaction itself (e. g. a chiral axis or a helical structure) is much smaller. Inspired by the well-defined geometry of DNA base pairs, Breit *et al.* devised chiral, nucleobase-derived ligands with complementary binding motives to form supramolecular, out-of-plane ligand dimers that were used in enantioselective hydrogenation reactions.[57,58] Both groups of Breit and Kirin employed peptidyl-substituted phosphines that formed PhanePhos-like complexes with helical chirality (see Figure 2-7, page 8).[59-61] Reek and co-workers developed a "cofactor"-controlled catalyst, where a chiral guest binds to the pocket of an achiral ligand to determine its helical conformation.[62]

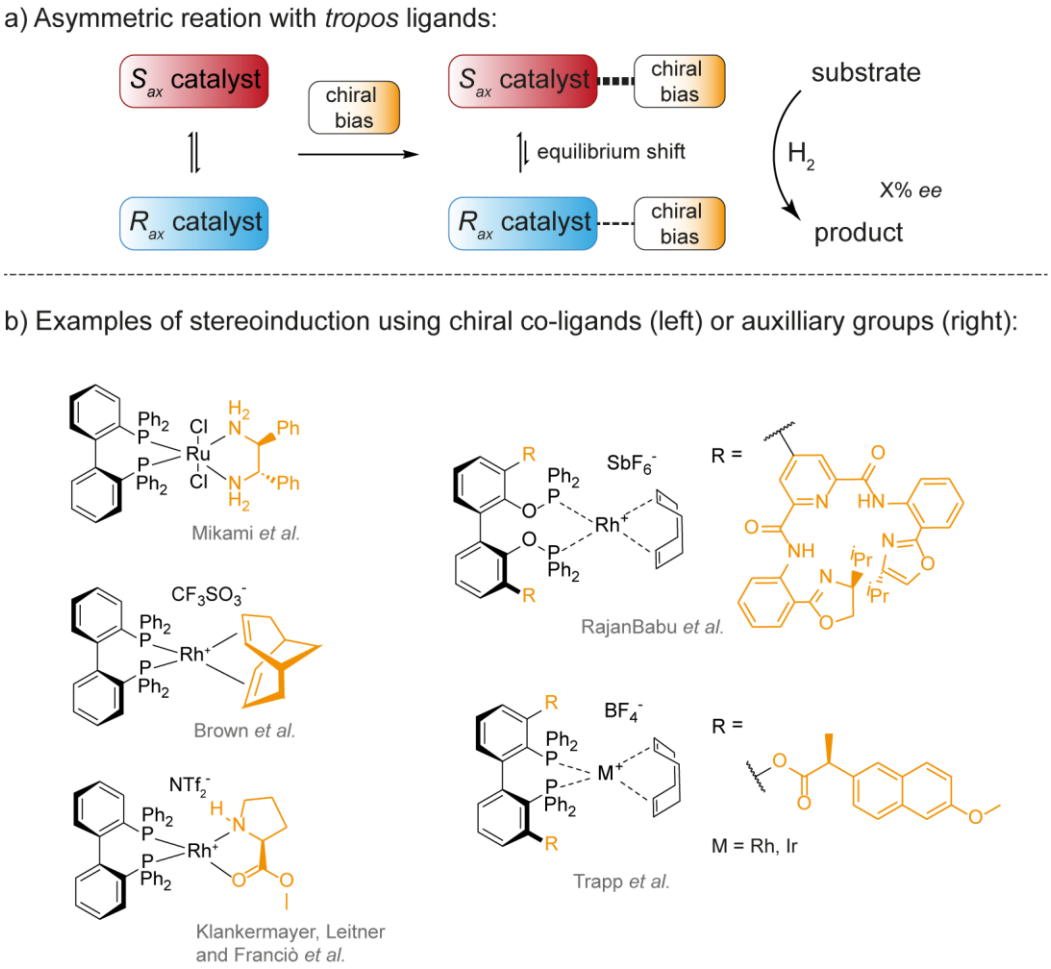

Figure 2-4: a) Schematic illustration of an enantioselective reaction using tropos ligands. The previously racemic catalyst experiences a stereochemical bias rendering the two rotamers unequal in energy. The low rotational barrier allows for an equilibrium shift generating a diastereomerically enriched catalyst. b) The rotameric enrichment of the ligand can be achieved using a chiral co-ligand coordinating across the metal center (*left*)[45,49-51] or by covalently attaching a chiral auxiliary group to the ligand core achieving central-to-axial chirality transfer (*right*).[52-54]

The interplay of chiral and achiral components in supramolecular systems became of particular interest with the development of the "sergeant-soldier principle", also known as the "majority rule effect", where a chiral moiety, the "sergeant", aligns an achiral neighbour, the "soldier", who conveys this bias further down the line.[63] Most prevalent approaches are implementations in larger self-assembling systems[63-67] or helical polymers.[68-70] Suginome *et al*. published several examples where such helices were employed in a number of different stereoselective transformations .[71-74]

Trapp and co-workers combined the concept of previously discussed *tropos* biphenyl-based ligands with that of non-covalent interactions on a molecular level. They modified ligands with interaction sites (selectors) and succeed to change the rotamer distribution of the ligand, solely relying on non-covalent interactions between the ligand's selector moieties and its chiral environment. This requires formation of well-defined, transient diastereomeric associates between the two ligand rotamers and surrounding, chiral molecules. Selector-modified BIPHEPs were successfully employed in *on-column* deracemization experiments using chiral HPLC columns to achieve an equilibrium shift in the previously racemic ligand that could later be used in enantioselective double aldol reactions.[75] In other examples, strong additive-selector interaction was achieved by modifying stereodynamic ligands with HPLC column selector-derived interaction

groups, such as 3,5-dichlorobenzoyl amide from Chiralpak® IC and IE[41,76] or (*S*)-*N*-pivaloylproline,[40] originally employed on a high-performance stationary phase reported by Pirkle and Murray.[77,78] In both cases, a shift of the equilibrium ration of the catalyst species was observed in the presence of amino acid-derived additives and enantiomerically enriched products were obtained in asymmetric hydrogenation experiments (see Figure 2-5).

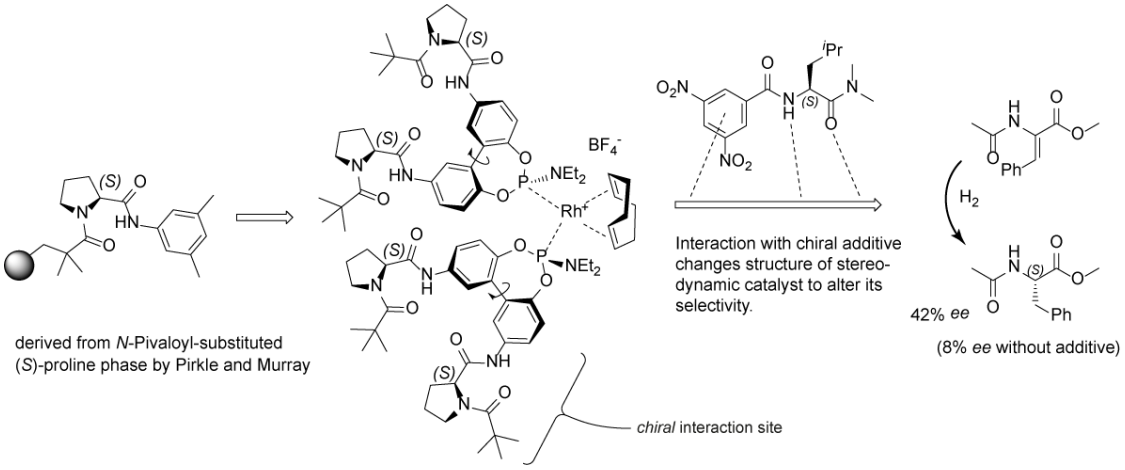

Figure 2-5: Example of a stereodynamic phosphoramidite ligand developed by Trapp *et al.* with interaction sites derived from HPLC column selectors, originally developed by Pirkle and Murray.[77,78] The catalyst shows structural change in presence of specifically designed additives, which alters its selectivity and was featured in self-amplifying reactions which will be discussed in a later chapter (see chapter 4, page 49).[40]

The design of such stereodynamic systems requires careful consideration of the ligands rotational barrier and of the strength of molecular interaction between the ligand's selector and the chirality-inducing agent. If the selector moiety contains a chiral information, the stereoselectivity of the interaction has to be taken into account as well (see also chapter 7.9, page 176). This is relevant if the selector is simultaneously serving as stereoinducing unit or if autoinductive reactions – which will be covered in a later chapter – are considered. It appears self-evident to derive interaction sites from state-of-the-art chromatography selectors, such as the HPLC column selector-based examples mentioned above.

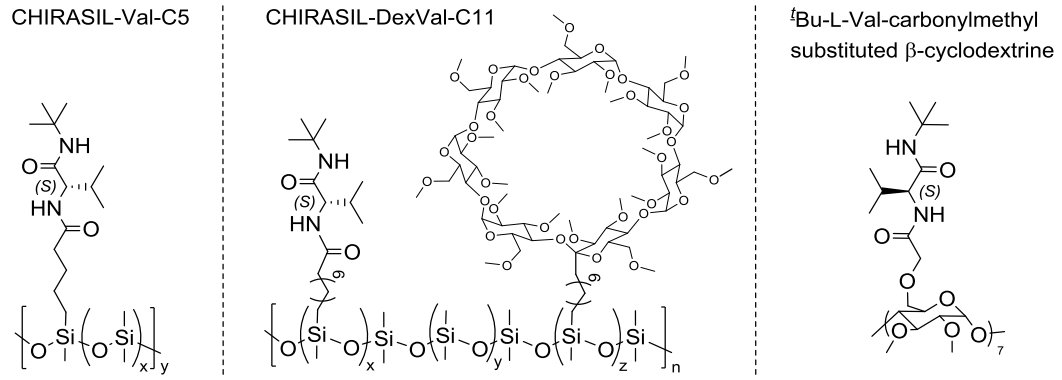

Figure 2-6: Different examples of CSP's that incorporate the motive of (*S*)-valine with two secondary amide functionalities and that allow for the simultaneous separation and enantiodiscrimination of a wide range of amino acid derivatives and amino alcohols.[79-81]

Most promising, yet unexamined as selectors for *tropos* biphenyl-based ligands, are amino acid-derived diamides such as the one found in the chiral high-performance CSP CHIRASIL-Val for

GC (see Figure 2-6).[82,83] This selector is highly appreciated for its versatility and its excellent chiral separation capabilities which are based on strong and well defined hydrogen bonding.[81,84-87] The number of hydrogen bond acceptor and donor sites allow for a multitude of possible interaction modes which appears promising for broad applicability and particularly selective interaction with other amino acid-derived additives. Chiral amino acid-derived diamide interaction sites have previously been used in combination with other stereodynamic frameworks. Apart from earlier mentioned peptidyl-modified phosphine ligands by the groups of Breit and Kirin (see Figure 2-7a),[59-61] Herradón *et al.* published findings of crystallization-induced dynamic resolution of axial isomers of 2,2'-peptidyl-modified biphenyls, a process based on the stereoselective formation of a network of intra- and intermolecular hydrogen bonds (see Figure 2-7b).[88,89] Similarly, it was found that chiral 1,1'-disubstituted ferrocenyl dipeptides, who exist in interconverting rotamers based on the twist around the Cp-Fe-Cp axis, undergo spontaneous transformation into one single species due to a β-turn-like interaction between the opposite peptidyl chains (see Figure 2-7c).[90-92]

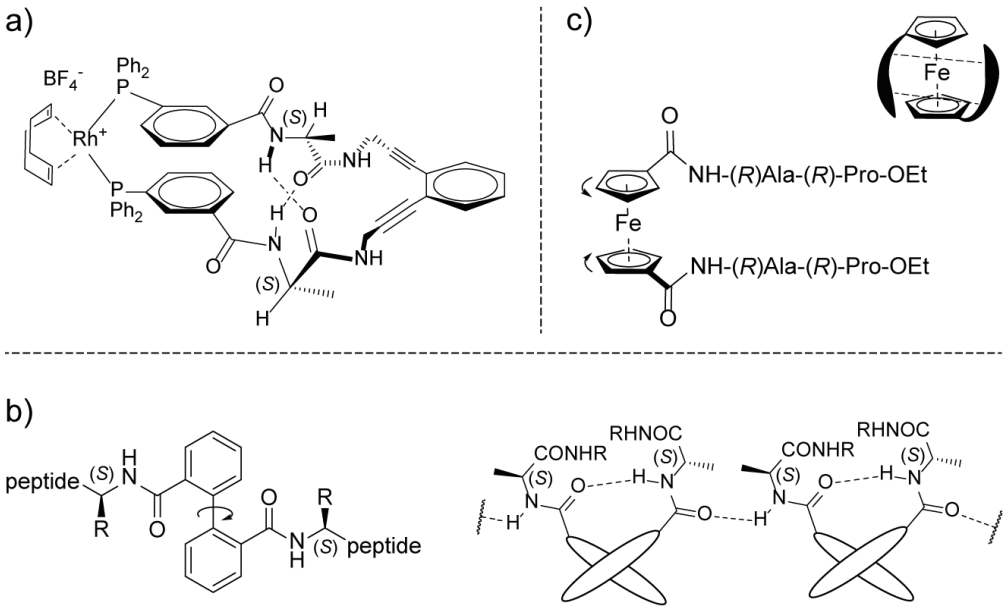

Figure 2-7: Illustration of previously published stereodynamic systems with amino acid-derived interaction sites. a) *m*-peptidyl-substituted bisphosphine ligand as "PhanePhos" analogue published by Kirin et al.[60] b) Diastereoselective crystallization of 2,2'-peptidyl-substituted biphenyls based on stereoselective formation of intra- and intermolecular hydrogen bonds published by Herradón *et al.*[88,89] c) Bis(peptidyl)-substituted ferrocene molecules exhibit diastereoselective β-turn-like interaction between the amide chains forcing the two cyclopentadienyl rings into a preferential conformation.[90-92]

2.2 Objective

The objective was the preparation and investigation of stereodynamic 2,2'-biphenol-based ligands bearing amino acid-derived selector moieties, which are based on selector sites from the high-performance GC column CHIRASIL-Val. Selectors were placed in 5,5'-position of the ligand core in order to enable efficient chirality transfer onto the ligand while maintaining rotational flexibility. Attachment of the selectors in 6,6'-position would render the ligand *atropos*. Sterically demanding substituents in 3,3' position are expected to strongly increase the rotational barrier (buttressing effect)[93] and potentially affect coordination of the ligand to the metal center. Little information is available in literature on substitution effects at the 4,4'-position, however, a rather minor influence on the axial stereochemistry of the ligand was assumed.[94]
A very short linking group between selector and ligand backbone would enhance rigidity and, consequently, improve chirality transfer onto the ligand axis. Methoxy groups in the 3,3'-position were included as stereodirecting groups to enhance the ligand's performance in enantioselective catalytic reactions through increased steric hindrance around the catalyst metal center.[95]

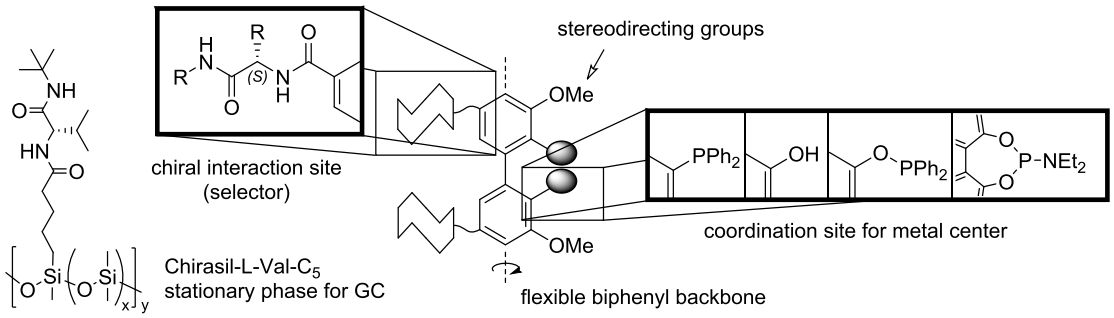

Figure 2-8: Schematic illustration of targeted *tropos* biphenyl-based ligands of different types bearing amino acid-derived selector sites in 5,5'-position and stereodirecting groups in 3,3'-position. Chiral interaction sites are derived from those found in the stationary GC phase Chirasil-Val.

Accordingly, a synthetic scheme was to be devised to synthesize a set of ligand bearing (*S*)-amino acid-derived, secondary diamide moieties, with different isomerization barriers, namely a biphenol, a bisphosphine, a bisphosphinite and a phosphoramidite ligand. Following successful syntheses, ligands were to be studied for their stereodynamic behaviour. The investigated selector sites were believed to be particularly capable of engaging in strong and stereoselective interaction with surrounding hydrogen bond donors and acceptors, which was thought to allow for increased stereocontrol over the chiral axis of the biphenyl backbone. Finally, ligands were to be tested for their performance in asymmetric aldol reactions (biphenol ligand) and in enantioselective hydrogenation reactions (the phosphorus-based ligands).

2.3 Investigation of a selector-modified bisphosphine ligand

2.3.1 Synthesis

Initial synthetic attempts to synthesize the ligand were based on modification of a corresponding 2,2'-biphenol with appropriate triflate leaving groups and subsequent transition metal-mediated C-P cross coupling. This approach failed, however, supposedly due to increased steric demand around the triflate groups. In a more successful approach, shown in Figure 2-9, 3-bromo-5-hydroxybenzoic acid **1** was reacted in a Fischer esterification and subsequently treated with chlorodiphenylphosphine oxide to give phosphinate **2**. Reaction with LDA induced an anionic phosphorous Fries rearrangement,[96,97] that gave the desired product **3** where the diphenylphosphine oxide moiety had migrated to the position adjacent to the bromine substituent. Subsequent methylation of the newly formed hydroxy group gave diphenylphosphine oxide **4**. The biphenyl backbone was constructed by a pyridine-free Ullmann coupling[98] to yield bis(diphenylphosphine oxide) **5**, which was reduced in phenylsilane yielding the free bisphosphine **6**. To attach the selector moieties, the methyl esters in 5,5'-position where saponificated and ^{t}BuNH-(*S*)Val-NH selector groups were attached employing standard peptide coupling reagents EDCI·HCl/HOBt under inert conditions yielding the desired bisphosphine **7** as a white powder. With the Phospho-Fries rearrangement as an exception, good yields were obtained for all transformations, especially at the end of the sequence, where compound value increases.

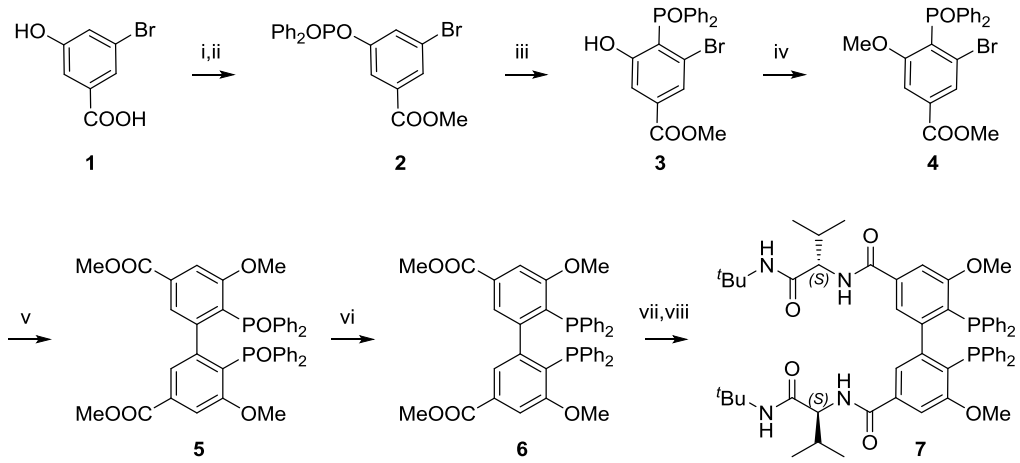

Figure 2-9: Synthesis of bisphosphine ligand **7**, i) MeOH, H_2SO_4, 84%, ii) $POPh_2Cl$, 4-dimethylaminopyridine, NEt_3, 83%, iii) lithium diisopropylamine, 29%, iv) MeI, 98%, v) Cu, 91%, vi) $PhSiH_3$, 95%, vii) KOH, 99%, viii) ^{t}BuNH-(*S*)Val-NH_3Cl, EDCI·HCl, HOBt, DIPEA, 63%.

2.3.2 Structural investigations

Bisphosphine ligand **7** was obtained as a mixture of two species with a ratio of 16:84, as detected by ^{31}P NMR analysis. While the minor species showed no unexpected characteristics with regard to its NMR data, the major compound exhibited a two-fold set of signals of identical intensity in ^{1}H, ^{13}C{^{1}H} and ^{31}P{^{1}H} NMR spectra. For the phosphorus atoms, the two signals additionally split due to mutual coupling which indicates that both observed signal sets belong to the same C_1 symmetric molecular scaffold. The two species of bisphosphine **7** could be separated by precipitation and were individually characterized. Both compounds gave identical HR-ESI$^+$-MS spectra with a signal at m/z = 979.4666. Heating a pure sample of either species in $CDCl_3$

to 60 °C for 14 hours resulted in complete re-equilibration to the same previously observed diastereomeric ratio of both species, indicating their conformational relationship, *i.e.* interconversion of the two diastereomeric forms by rotation (see Figure 2-10).

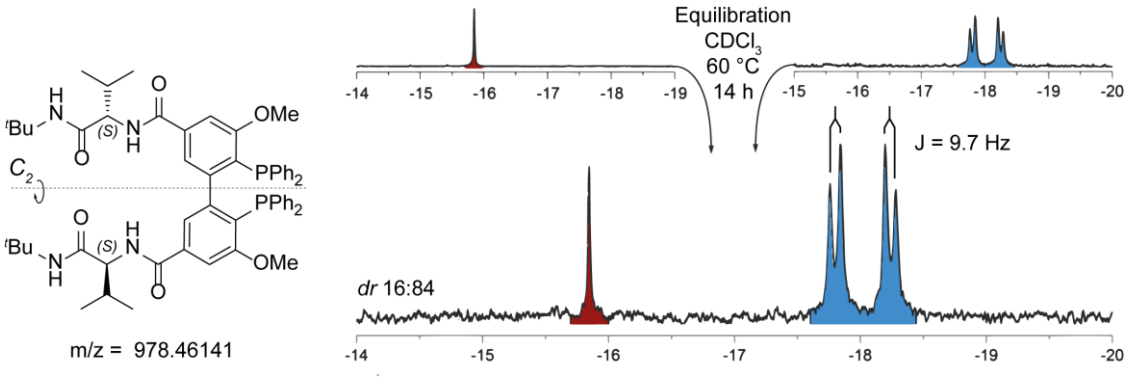

Figure 2-10: ^{31}P NMR spectra of isolated samples of both ligand species of **7** (top). Heating the samples for several hours yields identical distribution of both species, which indicates their conformational relationship.

^{31}P NMR spectra taken in steps of 20 °C between -40 and 80 °C revealed significant line broadening for the major species with increasing temperature until the signal had completely vanished at 80 °C. The minor species, however, underwent no such change (for spectral data see chapter 7.2.13, page 107). This indicates that the major rotamer experiences a dynamic change of its chemical environment with rising temperature, *e.g.* by dissociation of hydrogen bonds.

A single crystal suitable for X-ray analysis was obtained from a purified sample of the major species. The obtained structure shows a C_2 symmetric dimer comprising two R_{ax} rotamers of **7** that are connected through multiple hydrogen bonds (see Figure 2-11). The supramolecular complex can be divided into two parts. In the *inner sphere* part, two selectors align in a Herrick conformation,[92] imitating a [β²]-turn, by forming a C5:C5 associate.[1] In the *outer sphere* part, two remaining selector moieties engage in a chelating, "tweezer"-like assembly by forming two additional hydrogen bonds each (C7:C5) with the backside of the *inner sphere* selector of the respective other ligand molecule.

The *inner sphere* aromatic rings of the biphenyl units arrange spatially offset in parallel plane. The free electron pairs of the two diphenylphosphine groups in each molecule point towards the aromatic backbone on the respective other side of the same molecule. Assuming that these supramolecular features are retained in solution, this data identifies the minor species as the rotational isomer (S_{ax})-**7** and the major species as (R_{ax})-**7**. It also provides a plausible explanation for the unexpected asymmetry of the latter, that was illustrated by NMR spectroscopic data.

[1] Within the nomenclature CX:CY of cyclic two-component hydrogen bond networks, X and Y represent the number of atoms (= the length) of each chain that connect over two non-covalent bonds.

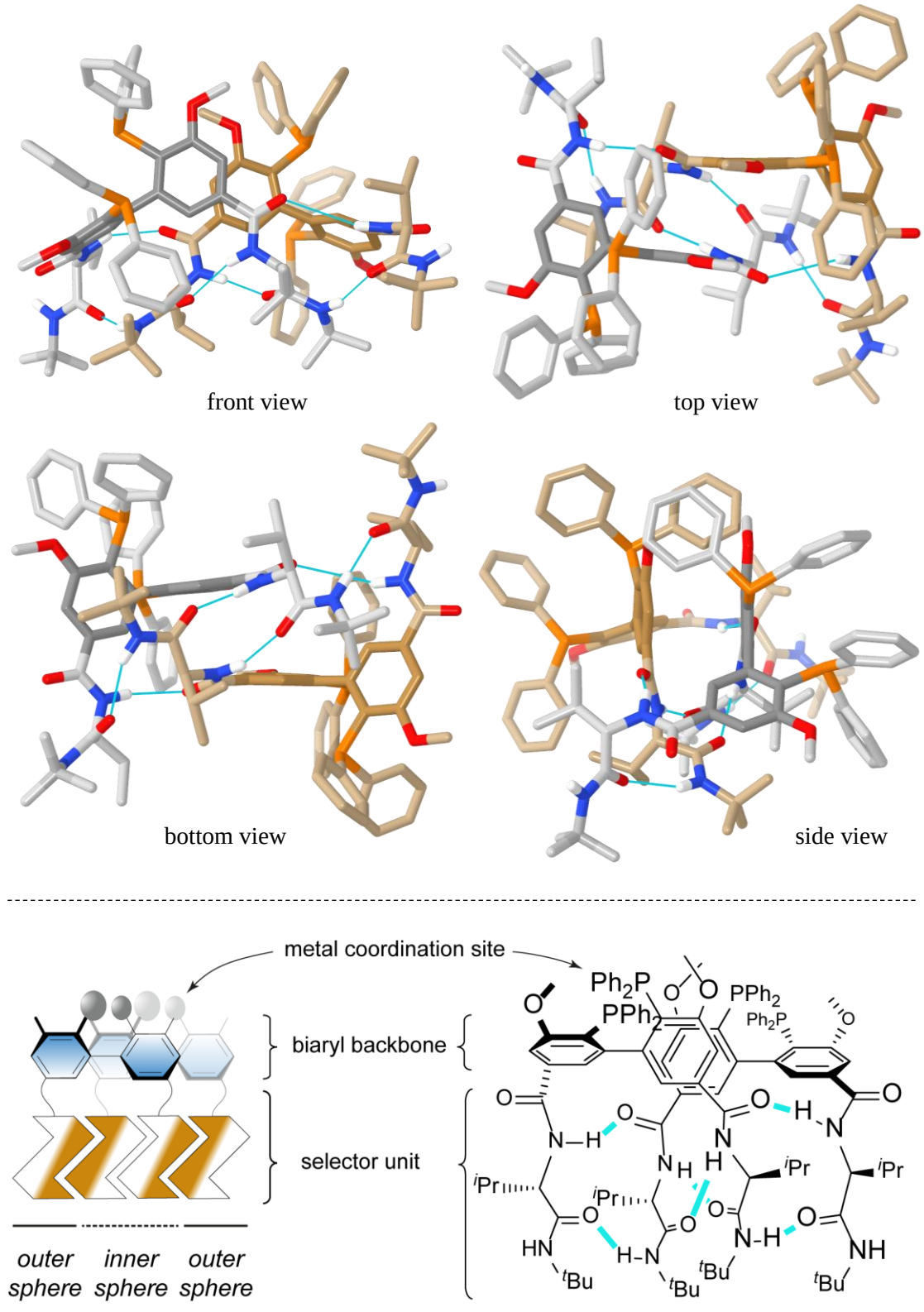

Figure 2-11: Representation of the single crystal X-ray structure of (R_{ax})-**7** from different viewpoints (*top*). Two R_{ax} molecules form a supramolecular C_2-symmetric dimer of C_1-symmetric subunits (indicated in beige and grey, biphenyl core atoms are coloured darker). Nitrogen = blue, oxygen = red, phosphorus = orange. Hydrogen bonds are indicated as blue lines. Non-relevant hydrogen atoms and solvent molecules are omitted for clarity. Images were produced using UCSF Chimera.[99] Also shown are simplified model structures representing the "Front view" arrangement (*bottom left*) and a detailed depiction of the selector interaction pattern (*bottom right*).

The supramolecular structure renders both halves of each molecular subunit diastereotopic, thus doubling the number of detectable NMR signals. Moreover, the spatial orientation of the free electron pairs on the phosphorus atoms provides a pathway for their coupling through π* orbital interaction (*through space* coupling) through the adjacent backbone phenyl ring (^{TS}J(P,P) = 9.7 Hz), which is a known phenomenon for bidentate ligands with diastereotopic phosphorus atoms.[100,101]

^{1}H NMR signal shifts of amide protons of (R_{ax})-**7** were found to be 9.05, 8.34, 6.96 and 5.75 ppm. This this suggests that three out of four protons of each molecular subunit are strongly engaged in non-covalent interactions, the forth, unbonded one being one of the two terminal ^{t}BuN*H* protons, which is in agreement with bonding pattern found by single crystal X-ray analysis (see Figure 2-11 for comparison). It is unlikely that the minor rotamer (S_{ax})-**7** does not engage in some sort of non-covalent interaction, however, these bonds seem to be much less stable. ^{1}H NMR shifts of amide protons for this rotamer showed a comparably high field shift (6.38 and 5.84 ppm), indicating much weaker bonding. At the same time, a higher molecular symmetry contradicts the formation of aggregates of the kind found for (R_{ax})-**7** even at temperatures as low as -40 °C, as visible from the obtained NMR data. Also, since the formation of a hydrogen bond is accompanied by energetic stabilization, the strong enrichment of the R_{ax} rotamer suggests that significant differences exist in the saturation level of hydrogen bond donor and acceptor sites between both rotamers. Moreover, heterodimeric species comprising both ligand isomers were not observed.

From this can be concluded, that the key feature of the investigated ligand motif, which causes rotameric enrichment, is the diastereoselective and cooperative self-recognition process during selector interaction of two ligand molecules. The stereoinformation imbedded in the selector sites dictates the axial orientation of the biphenyl units during formation of the hydrogen bond network allowing only one rotamer to form dimers. In itself, this phenomenon can also be seen as a form of stereoselective *narcissistic self-sorting*,[102] which is a concept that has been found to govern non-covalent interaction in a variety of chiral systems.[3,103-108]

To investigate the effect of hydrogen bonding on the rotational barrier, respective energies for bisphosphines **6** and **7** were compared. Ligand precursor **6** was previously investigated for its isomerization barrier of its enantiomers using dynamic HPLC[109] and was found to have a barrier of interconversion of $\Delta G_{298}^{\ddagger}$ = 97.8 kJ/mol. NMR-spectroscopically assisted kinetic measurements of compound **7**'s epimerization at 60 °C were conducted assuming an opposing reaction of first order. Rate constants of $k(R_{ax}\text{-}S_{ax})$ = 1.3692 x 10^{-5} s^{-1} and $k(S_{ax}\text{-}R_{ax})$ = 6.9798 x 10^{-5} s^{-1} were found, which correspond to free enthalpies of $\Delta G_{333K}^{\ddagger}(R_{ax}\text{-}S_{ax})$ = 112.9 kJ/mol and $\Delta G_{333K}^{\ddagger}(S_{ax}\text{-}R_{ax})$ = 108.4 kJ/mol, respectively (correlation factor R^2 = 0.978, see chapter 7.2.9, page 98 for experimental details). The increased energetic barriers of isomerization can be explained by additional sterical pressure of the larger diamide substituents compared to the smaller methyl esters. It is also plausible to assume that strong hydrogen bond stabilization of the ground state of (R_{ax})-**7**, that needs to be overcome for an epimerization, is responsible for the observed difference in transition state energies.

2.3.3 Interaction studies

Since stereoselective formation of hydrogen bonds was found to be the cause of the ligand's self-enriching behaviour, interfering with its bonding pattern was expected to have a profound effect. Consequently, the effects of chiral and achiral hydrogen bond donors and acceptors on ligand **7** was investigated by adding them in excess to a solution of the equilibrated ligand (*dr*

14:86 S_{ax}:R_{ax}) in $CDCl_3$. The re-equilibration of the resulting mixtures at 60 °C was monitored by ^{31}P NMR spectroscopy.

Given the excellent enantioselectivity of the GC stationary phase CHIRASIL Val in separating amino acid derivatives, compounds **8-10** from the same class, all with different steric and electronic properties, were employed as chiral additives. Because of the matching interaction pattern[83] of the valine-based selector, these where believed to be effective competitors for the ligand's self-interaction. As achiral additives, dicyclohexyl urea (**11**) and DMSO-d6 (as solvent instead of $CDCl_3$) were used, both expected to unselectively interfere with hydrogen bonds of (R_{ax})-**7** and diminish beneficiary stabilization effects. Intriguingly, mixing the bisphosphine ligand with amino acid-based additives (*S*)-**8**, (*S*)-**9** and (*S*)-**10**, all of which have the same chirality as the ligand's selector unit, immediately gave rise to a new singlet species, (R_{ax}^{C2})-**7** at the expense of the two doublets of (R_{ax}^{C1})-**7** (see Figure 2-12 and Table 2-1).

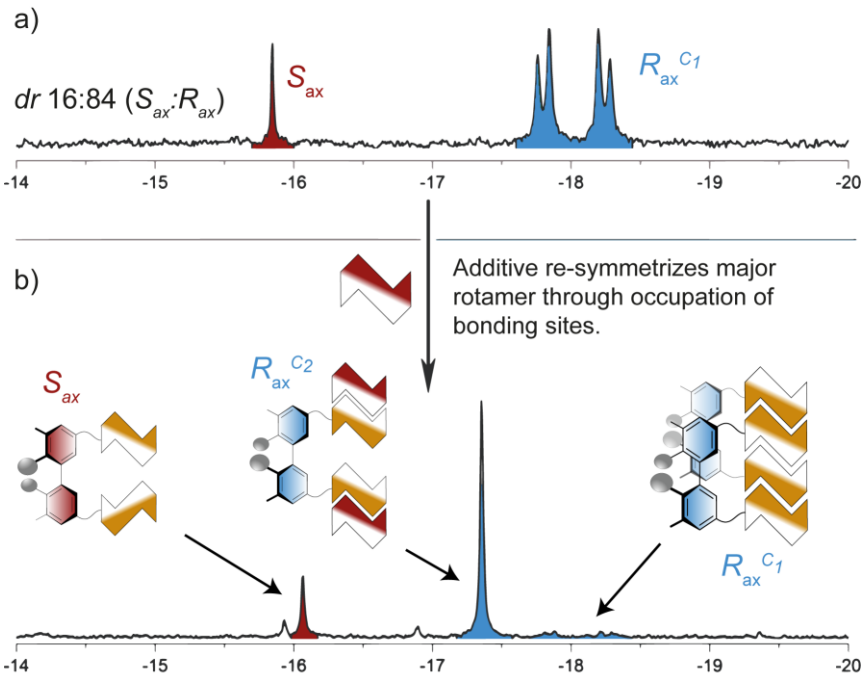

Figure 2-12: Exemplary ^{31}P NMR spectra of interaction studies between equilibrated ligand **7** (a) and (*S*)-amino acid derived additives **8**-**10** that shows formation of a new singlet species (b), which was assigned to a "re-symmetrized" monomer (R_{ax}^{C2})-**7** that forms at the expense of dimeric (R_{ax}^{C1})-**7** when the additives inhibit dimerization and occupy binding sites instead. Re-equilibration of these mixtures changes the ligand distribution (see Table 2-1). The exact stoichiometry of (R_{ax}^{C2})-**7** and the shown structure serves as an example.

Interactions between ligand and additive break the supramolecular dimer (R_{ax}^{C1})-**7** and binding sites are instead occupied by excessive additive molecules, thus yielding a labile, "re-symmetrized" additive-ligand hydrogen bond adduct (R_{ax}^{C2})-**7** of unknown structure and stoichiometry. The process was found to be reversible. Placing a sample of ligand and poorly soluble diamide (*S*)-**9** in the fridge led to crystallization of the additive. As a result, (R_{ax}^{C2})-**7** vanished and (R_{ax}^{C1})-**7** reformed. The extent of re-symmetrisation was found to be depending on the type of substituents on the diamide additive (see Table 2-1, entries 2, 4 and 5). Apart from hydrogen bond donor and acceptor sites, bulky aromatic moieties for π-interactions or additional steric repulsion were found vital to maximize the effect, indicating a three-point interaction pattern.[110] After re-equilibration, a further increase of the diastereomeric excess (*de*) of **7** was observed for all samples mentioned above. The strongest enrichment was found to occur in presence of phenylalanine derivative (*S*)-**8** (*dr* 7:93 S_{ax}:R_{ax}, Δ*de* = +18%). When "mismatched" diamide (*R*)-**8** was used, almost no re-symmetrisation was observed (Table 2-1, entry 3). This demonstrates the stereoselective nature of the interactions and is in line with the enantiodiscriminatory capacity of the ^{t}BuNH-(*S*)Val-NH moiety as a selector site in CSPs. Equilibration of this sample led to a slight decrease of the *de* of (R_{ax})-**7** (*dr* 24:76 S_{ax}:R_{ax}, Δ*de* = -16%). As expected, both achiral additives DMSO-d6 and **11** were also found to reduce the excess of the ligand's major rotamer (Table 2-1, entries 6 and 7). While a high excess of DMSO-d6 lead to significant line broadening and uninterpretable NMR spectra, DCU, like compound (*R*)-**8**, only shifted the ligand's equilibrium distribution without changing the unsymmetrical appearance of (R_{ax})-**7**. Beyond these differences, observations confirm the assumption that the rotameric enrichment of the bisphosphine is based

Table 2-1: Distribution of ligand species of bisphosphine 7 after equilibration in presence in different chiral and achiral compounds.

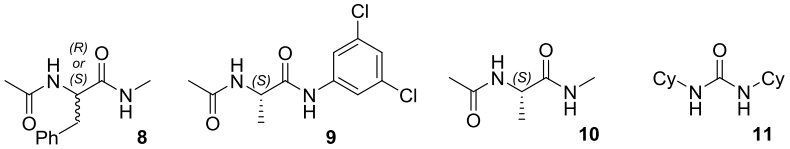

Entry[a]	Solvent/Additive (eq.)	Ligand Species of **7** [%]			
		S_{ax}	R_{ax}^{C2}	R_{ax}^{C1}	*de*[d]
1	$CDCl_3$/no additive	16	0	84	68
2	$CDCl_3$/(*S*)-**8** (10 eq.)	7	82	11	86
3	$CDCl_3$/(*R*)- **8** (10 eq.)	24	5	71	52
4	$CDCl_3$/(*S*)-**9** (5 eq.)[b]	9	59	32	82
5	$CDCl_3$/(*S*)-**10** (10 eq.)	11	38	51	78
6	DMSO-d6	35	nd[c]	65	30
7	$CDCl_3$/**11** (10 eq.)[b]	33	0	67	34

a) Detailed experimental protocol can be found in the experimental section. b) Solute did not fully dissolve. c) Not determined. Measured in $CDCl_3$ after equilibration to circumvent heavy line broadening. d) $de = (R_{ax}^{C1}+R_{ax}^{C2})-S_{ax}$

on non-covalent interactions of highly enantioselective nature, which is governed by the central chirality of the selector moieties.

2.3.4 Enantioselective hydrogenation experiments

Ligand **7** was subsequently employed in Rh-catalyzed hydrogenation experiments. Ligand precursor **6** was tested in the same context to assess the stereoselectivity provided by the ligand core during the asymmetric hydrogenation of methyl 2-acetamidoacrylate (**12**). Ligand (S_{ax})-**6** has been enantiomerically purified by preparative HPLC and isolated with 91 % *ee* S_{ax}. *In situ* reaction with $[Rh(COD)_2]BF_4$ gave a catalyst that converted substrate **12** with 90 % *ee* in favour of the (*S*)-enantiomer, verifying that the ligand's rotamer distribution closely correlates with the selectivity of the asymmetric transformation, as previously found for the 3,3'-methoxy substituted BINAP ligand.[95] Hereafter, equilibrated ligand **7** (*dr* 16:84 S_{ax}:R_{ax}, 68% *de* R_{ax}) was employed under identical conditions generating (*R*)-**13** with 65% *ee* (see Figure 2-13).

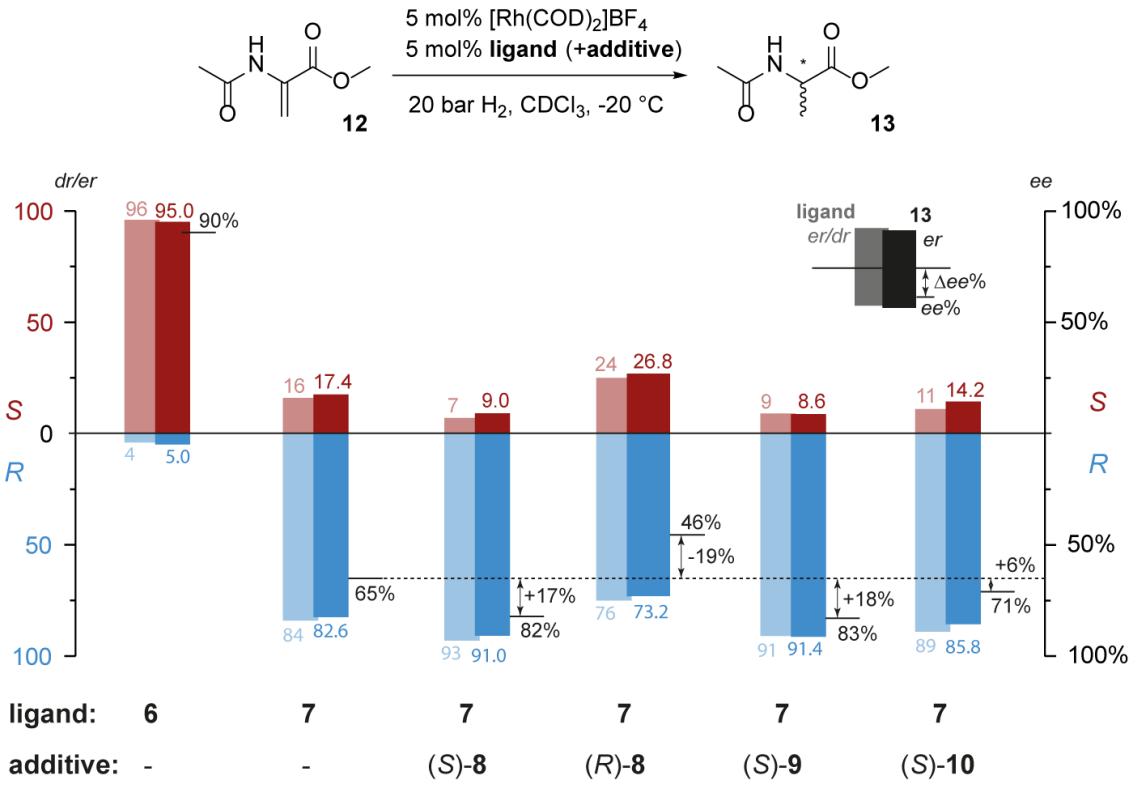

Figure 2-13: Asymmetric hydrogenation of methyl 2-acetamidoacrylate **12** using bisphosphine ligands **5** and **7**. The diagram shows the diastereomeric/enantiomeric ratio (*er*/*dr*) of ligand rotamers and the corresponding enantiomeric ratio of **13** (colored bars), as well as the enantiomeric excess (*ee*%) of the latter (black lines) and its change when the ligand was aligned by an additive (Δ*ee*%). Additives were added to the ligand in a 10-fold excess and the mixture was equilibrated at 60 °C prior to complexation. In case of (*S*)-**9**, only a 5-fold excess was used and not all solids dissolved. All reactions showed full conversion. Detailed experimental procedure can be found in the experimental section in chapter 7.2.17 on page 121.

Assuming the same degree of stereoinduction as ligand **6**, given identical substituents on the ligand core in 3,3'-position,[95] these findings corroborate the assignment of ligand rotamers that was originally based on the crystal structure. Hydrogenation experiments of complexated ligands previously pre-conditioned in presence of a chiral diamide gave product enantiomer distributions of **13** that correlated with the change of the ligand rotamer equilibria mentioned above. While equilibration with (*R*)-**8** led to a selectivity drop to 46% *ee R* (Δ*ee* = -19%), all other

additives allowed for a conversion of **12** with higher selectivity. Best results were achieved with AcNH-(*S*)Ala-NH(3,5-dichlorophenyl) (*S*)-**9**, which increased the catalysts selectivity to 83% *ee R* (Δ*ee* = +18%).

2.4 Investigation of selector-modified bisphosphinite ligands

2.4.1 Syntheses

For the synthesis of stereodynamically flexible bisphosphinite ligands, a precursor derived from 2,2'-biphenol (BIPOL) was found to be the most convenient approach (see Figure 2-14). Due to the ease of synthesis, it a was also decided to investigate changes in the selector structure. Apart from the previously employed selector (^{t}BuNH-(*S*)Val-NH, **a**), a modified version with terminal 1-adamantyl group, which was supposed to act as a more sterically demanding terminal substituent, was devised (1-AdNH-(*S*)Val-NH, **b**). Moreover, a phenylalanine-based selector was synthesized (^{t}BuNH-(*S*)Phe-NH, **c**), to incorporate an aromatic moiety into the selector structure and potentially benefit from an additional π-interaction after those where found beneficial during interaction studies between bisphosphinite **7** and differently substituted additives. Lastly, a glycine-derived bisphosphinite was synthesized (^{t}BuNH-Gly-NH, **d**) to allow for investigation of achiral selector sites, as well (see chapter 3 for details).

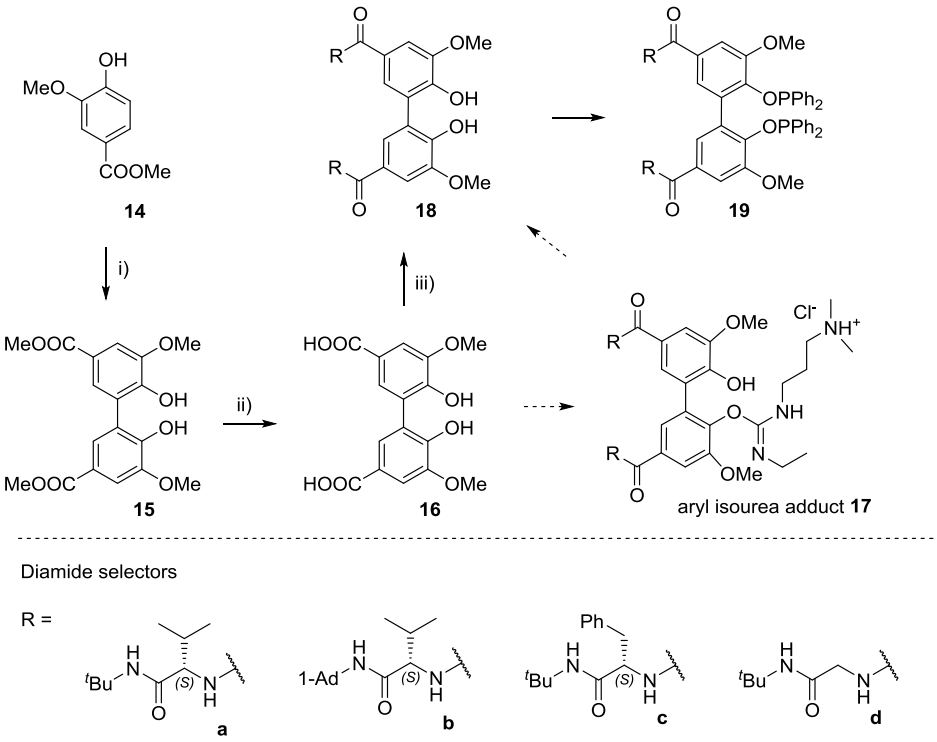

Figure 2-14: Synthesis of phosphinite ligands **19a-d**, i) $PhI(OAc)_2$, 51%, ii) KOH, 97%, iii) amide selector hydrochloride, EDCI·HCl, HOBt, DIPEA, then excess $Me_2NCH_2CH_2NH_2$, 89% **a**; 51% **b**, 91% **c**, 80% **d**, iv) PPh_2Cl, 1,4-diazabicyclo[2.2.2]octane, 49% **a**, 53% **b**, 83% **c**, 53% **d**.

In a straightforward synthesis, methyl vanillate **14** was initially oxidatively dimerized using (diacetoxyiodo)benzene to build the biphenyl backbone (**15**).[111] Subsequent saponification gave dicarboxylic acid **16**. Notably, introduction of the selectors by amide coupling could be conducted without protection of the phenolic hydroxyl groups. After initial EDCI·HCl/HOBt-mediated amide coupling between compound **16** and 2.5 equivalents of the corresponding selector

amine hydrochloride, excess carbodiimide reacted with the free hydroxy groups on the phenol to form adduct **17**. It was found that this addition could be reversed by treating **17** with an excess of *N*,*N*'-dimethylethylenediamine to aminolyse the isourea. Aqueous workup gave selector-modified biphenols **18a-d** without further purification in high purity. Final treatment of the BI-POLs with chlorodiphenylphosphine in presence of DABCO[112] yielded the desired bisphosphinite ligands **19a-d** as white solids.

2.4.2 Structural investigations

As structural similarities to bisphosphine **7** suggest, dimerization was also observed for bisphosphinite ligands **19a-d**. Formation of the supramolecular hydrogen bond complexes could be verified by NMR spectroscopy, where two sets of signals could be detected in ^{1}H, ^{13}C{^{1}H} and ^{31}P{^{1}H} NMR spectra. In contrast to the bisphosphine, no coupling was observed between the two phosphorus atoms. However, strong cross peaks in two-dimensional ^{1}H-^{13}C HMBC spectra were found that link both signal sets to the same molecular scaffold (for spectral data see chapter 7.2.11, page 102). Intriguingly, bisphosphinites **19a-c** were found to exist as one diastereomerically pure species and no minor rotamer was be detected for any of them. This indicates that the energy gap between the two rotamers is increased due to enhanced hydrogen bond-driven stabilization of the enriched species, which, in analogy to previous example of bisphosphine **7**, was assigned to the R_{ax} isomer. For ligand **19d**, the achiral nature of the selector sites consequently leads to formation of racemic S_{ax} and R_{ax} dimers. When ligands where complexated to a rhodium center, significant line broadening was observed, but the dimerization and the associated enrichment process were found not to be affected.

Suitable crystals for X ray analysis were obtained of glycine-based ligand **19d**. The resulting crystallographic data showed close resemblance the one obtained for (R_{ax})-**7**. The same supramolecular arrangement was found, where two ligands of the same axial chirality form a C_2-symmetric dimer that is stabilized by six hydrogen bonds and that renders the molecular halves of each subunit chemically and magnetically inequivalent, hence resulting in the additional set of NMR signals. (see Figure 2-15).

^{1}H NMR signals of amide protons were found to be strongly shifted to low fields. Signals for compound **19a** were observed at 9.43, 9.12, 8.11 and 7.56 ppm, while ligands **19b-d** showed shifts between 9.46 and 7.44 ppm, between 9.75 and 7.59 ppm and between 10.22 and 7.67 ppm, respectively. The stronger lowfield shift compared to bisphosphine (R_{ax})-**7** is in line with the observation of complete diastereoenrichment, since a stronger shift represents stronger hydrogen bonding which, in turn, increases ground state stabilization of the dimer and is the driving force for the rotameric enrichment.

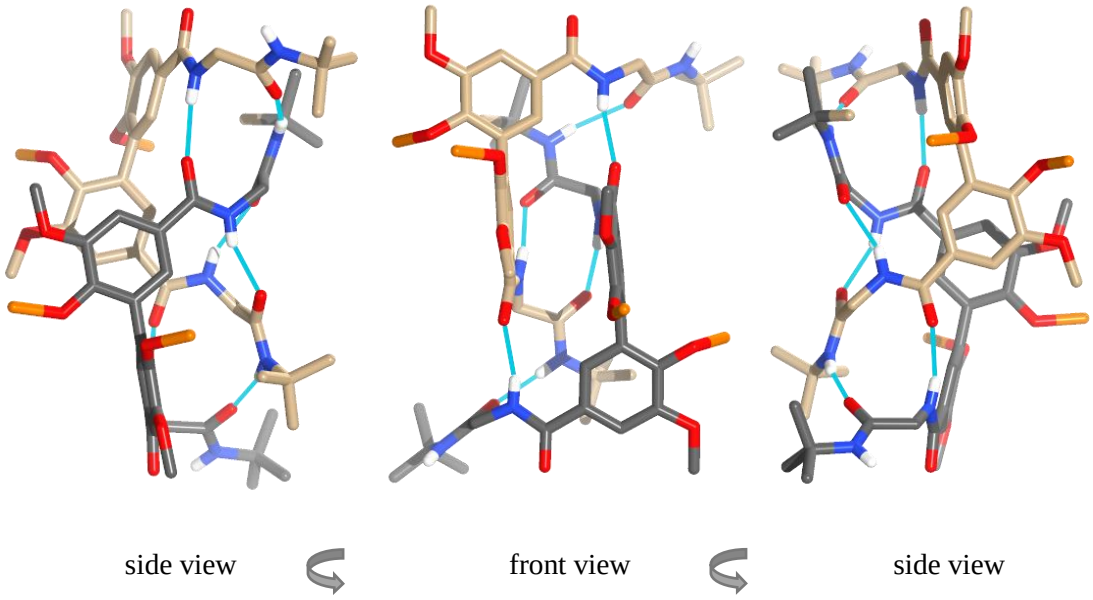

Figure 2-15: Representation of the single crystal X-ray structure of **19d**, which closely resemble that of bisphosphine **7** shows on page 12. Two R_{ax} molecules form a supramolecular C_2-symmetric dimer of C_1-symmetric subunits (carbon atoms of different subunits are indicated in beige and grey). Hydrogen bonds are indicated with light blue lines. To improve clarity, $OPPh_2$ moieties are abstracted as orange placeholder atoms and non-relevant hydrogen atoms as well as solvent molecules are omitted. Nitrogen = blue, oxygen = red. Images were produced using UCSF Chimera.[99]

Temperature-dependant NMR spectra of **19a** were collected in steps of 20 °C between -40 and 100 °C. Shifts of the amide protons with rising temperature can be used to qualitatively asses the strength of hydrogen bonds. Protons shifting with 0 to -4 ppb K^{-1} are either strongly bonded or not bonded at all, hence insignificantly changing their chemical surrounding with increased temperature, while chemical shifts >4 ppb K^{-1} indicate weakly bonded hydrogen atoms.[113,114] The three amide protons, believed to be participating in the hydrogen bond network according to the established binding model, exhibit shifts of -0.84, -2.76 and -3.58 ppb K^{-1}, whereas the forth, "unbonded" one shifts with -6.25 ppb K^{-1} (see chapter 7.2.13, page 107, page for spectral data). Since absence of hydrogen bonds for the first three protons can be ruled out on the basis of previous experiments, the obtained values indicate a much stronger hydrogen bonding strength for those protons in comparison to the last one, which is in good agreement with the assumed arrangement of the ligand subunits.

When respective ^{31}P NMR spectra were compared, significant line broadening was observed at higher temperatures. At 40 °C, a new singlet species appeared and vanished again when another spectrum was collected at room temperature afterwards (see chapter 7.2.13, page 108 for spectral data). As with bisphosphine ligand **7**, this indicates that the ligand loses a stabilizing force at elevated temperatures and regains structural flexibility due to breaking of weak non-covalent, intermolecular bonds. Formation of the new singlet species after very moderate heating additionally signifies that the dimeric complex retains enough dynamic at ambient temperatures to disengage and undergo chemical exchange with other complexes. This indicates that the state of rotameric enrichment is self-reinforced by dynamic exchange among the complex subunits, which is a form of stereocontrol that resembles that found in *sergeant-soldier*-type self-organizing, supramolecular systems. Nonetheless, attempts to interfere with the dimeric hydrogen

bond network by adding diamide **8** failed, and no re-symmetrisation was observed, which supports the assumption that a comparably stronger binding force is the cause of the quantitative rotational enrichment.

In order to corroborate the supramolecular nature of the hydrogen bonding, a crossover experiment was conducted by mixing ligands **19a** and **19b**, which only differ with respect to their terminal amide substituents. While each individual ligand gave two singlet signals in their respective ^{31}P NMR spectrum, a 1:1 mixture of both ligands immediately gave rise to new species represented by four additional singlet signals of identical intensity (see Figure 2-16). In accordance with previous observations, the additional four signals were attributed to a heterodimeric ligand complex comprising both ligand types, where all four phosphorus atoms become diastereotopic. The ratio of the dimers was found to be 1:2:1 (**19a**^{2}:**19a·19b**:**19b**^{2}) A 2:1 mixture of the same ligands resulted in formation of the same species in a 4:4:1 ratio (**19a**^{2}:**19a·19b**:**19b**^{2}), signifying a statistical distribution of ligand species with no preferential interaction with respect to the two different selector types. Kinetic considerations as well as spectral data for the latter experiment can be found in chapter 7.2.12.1, page 105.

Comparing the ligand mixtures to the respective pure ligand samples revealed a very similar behaviour. NMR signals of heterodimeric species showed similar signal patterns and, most notably, all amide protons exhibited similarly strong downfield shifts. Also, when conduction ^{31}P NMR measurements at elevated temperatures, similar line broadening and formation of a new singlet signal representing monomeric ligand molecules was observed, both of which was reversed when the same sample was re-measured at room temperature again afterwards.

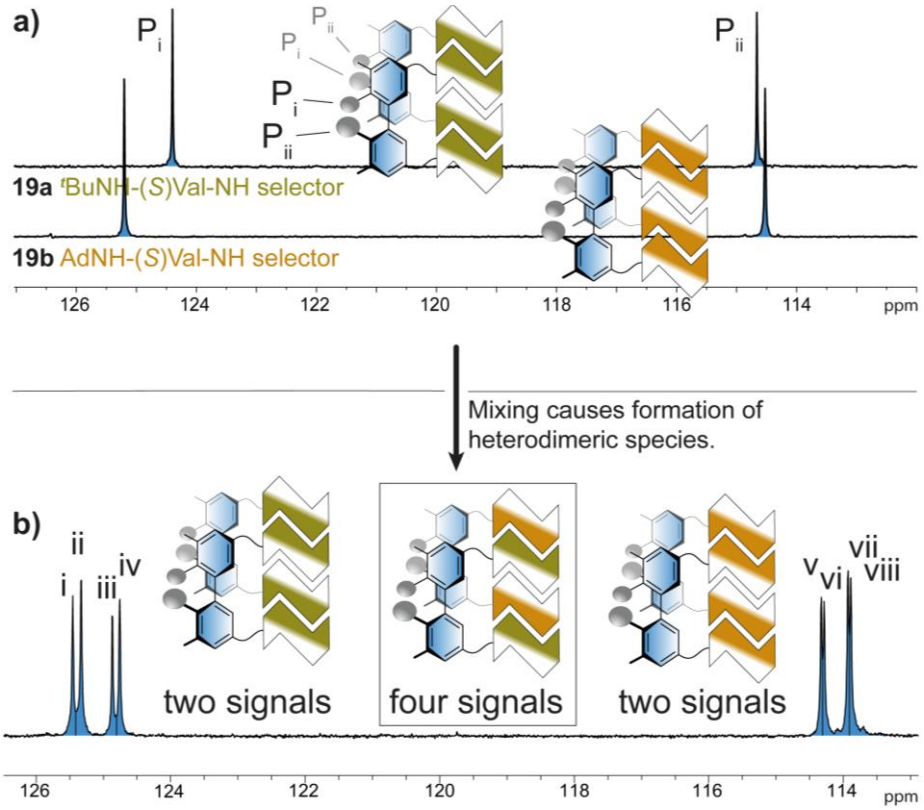

Figure 2-16: ^{31}P NMR spectra of (a) individual ligands **19a** and **19b** and of (b) an equimolar mixture of two ligands where a total of eight signals could be observed and the four new signals were assigned to a supramolecular heterodimer comprising both ligand types. Results for the experiment with a 2:1 mixture as well as kinetic considerations can be found in chapter 7.2.12.1, page 105.

Most crucially, as with the individual ligands, newly formed heterodimers where not affected by the presence of chiral diamides and no inhibition of the intermolecular interactions were observed, when diamide (*S*)-**8** was added to compete over hydrogen bonding sites.
The swift formation of the mixed ligand dimer supports the assumption mentioned above that chemical exchange still occurs at room temperature and individual molecules change interaction partners rapidly despite strong hydrogen bonding. Furthermore, the findings provide definite proof for the formation of supramolecular structures in solution. Assuming that the investigated enrichment phenomenon and the C_1-symmetric appearance could also be caused by intramolecular selector interactions or other conformational changes (e.g. amide *cis-trans* isomerism),[115,116] formation of a mixed ligands species clearly disproves these possibilities.
To analyse the spatial atomic arrangement in a supramolecular structure, NOE-based two-dimensional spectroscopy is usually a convenient approach. NOESY experiments on hydrogen bonded structures with intrinsic symmetry are problematic, however, if the subunits retain sufficient dynamic for chemical exchange on the NMR timescale. It results in the difficulty to distinguish proximity-based cross peaks from chemical exchange or dynamic TOCSY transfer.[117,118] Conveniently enough, this was not the case for bisphosphinite **19a** and NOESY spectra could be collected without signs of chemical exchange. Since crystallographic data on **19a** was unavailable, a model structure was generated in order to allow a qualitative comparison of NOE cross peaks with atomic distances within the ligand dimer. The structure **model-19a** was based on the crystallographic data obtained for glycine derivative **19d** and the stability of the dimer was verified by geometry optimization using DFT calculations on the B3LYP/(aug)-cc-pVDZ level (see chapter 7.2.14, page 109 for details). The most prominent atomic proximities extracted from the NOESY spectrum are illustrated in Figure 2-17 (see SI for spectral data). Cross peaks were found between protons H4 and H6'.[2] Comparing atomic distances in **model-19a** suggests that intramolecular coupling of corresponding atoms within the same molecule is not possible (d(H4,H6', intra) = 5.818 Å). Intermolecular coupling, however, seems likely (d(H4,H6', inter) = 2.703 Å). Coupling was also observed for protons H9 and H8' and for H9 and H10', which both accounts for the interaction between *inner* and *outer sphere* selector and where atomic distances of d(H9,H8', inter) = 2.543 Å and d(H9,H10', inter) = 2.334 Å were found in the model structure. Respective atomic distances for the other halve of the dimer were found to be similar with a maximum deviation of 0.05 Å.

[2] In the following notation, HX refers to an *inner sphere* proton and HX' to an *outer sphere* proton.

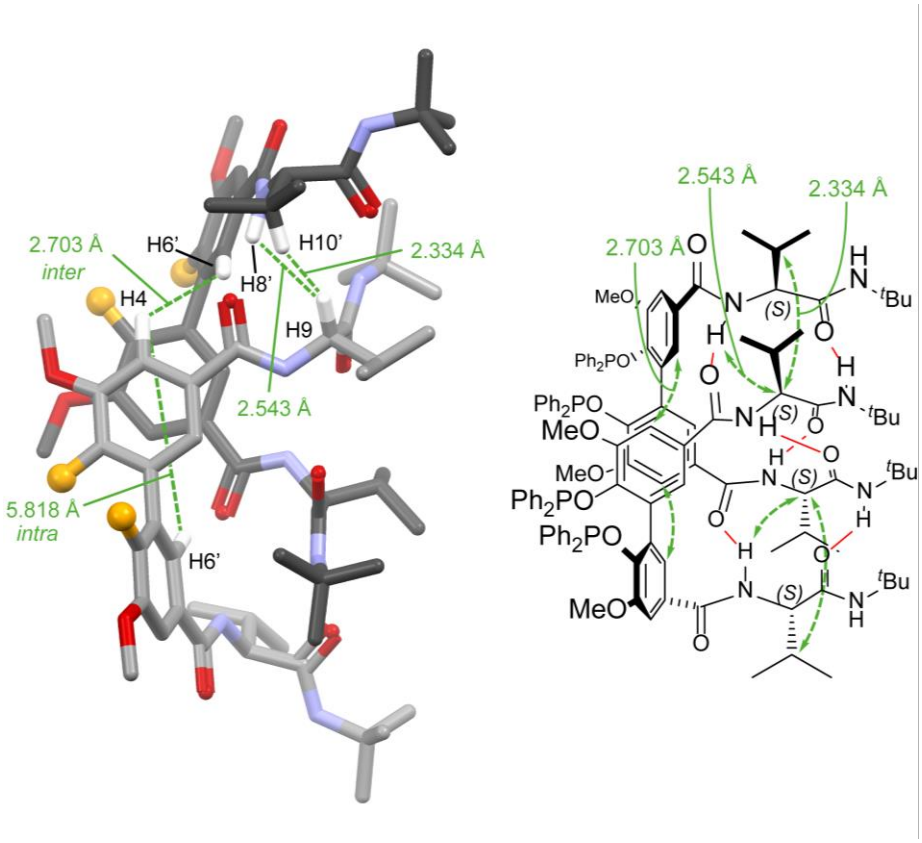

Figure 2-17: Calculated structure (R_{ax}/R_{ax})-**model-19a** after geometry optimization on the theoretical level B3LYP/(aug)-cc-pVDZ (left). Initial guess of **model-19a** was based on the crystal structure of **19d** (see chapter 7.2.14, page 109 for details). To improve clarity, only annotated hydrogen atoms are shown and $OPPh_2$ moieties are abstracted as orange placeholder atoms. Image was produced using UCSF Chimera.[99] The two molecular subunits of the dimer are coloured in light and dark grey. Nitrogen = blue, oxygen = red, $OPPh_2$ moiety = orange. A simplified representation of the structure is also given (right). Atomic distances are depicted in green dashed lines. Respective atomic distances for the lower side of the dimer were found to be similar with a maximum deviation of 0.05 Å.

2.4.3 Enantioselective hydrogenation experiments

Diastereomerically pure ligands **19a-c** were employed in Rh-catalyzed hydrogenation experiments of prochiral olefins **12** and **20**-**22**.[3] Catalysts were formed by treating a solution of the ligand with $[Rh(COD)_2]BF_4$. All three ligands exhibited high to very high enantioselectivities. Phenylalanine derived ligand **19c** performed slightly better than valine-based bisphosphinites. It allowed conversion of methyl 2-acetamidoacrylate **12** with an enantiomeric ratio of 4.0:96.0 (*S*:*R*), methyl *N*-acetylcinnamate **20** with a ratio of 5.5:94.5 (*S*:*R*) and dimethyl-2-methyl succinate **21** with 94.9:5.1 (*S*:*R*). For enamide **22**, a selectivity of 6.3:93.7 (*S*:*R*) was obtained. An overview over all hydrogenation experiments can be found in Figure 2-18. Conveniently enough, obtained selectivities were comparable to those found for enantiopure *atropos* ligands of similar built.[119] In a second set of experiments, substrate loadings and hydrogen pressure was varied yielding identical outcomes. These experiments were designed to prove that the catalyst's selectivity is independent of the turnover number (TON). Consequently, these findings exclude selective catalyst activation or structural change of the catalyst over time as a source of selectivity. Catalyses were also conducted in THF and MeOH to evaluate solvent effects. While THF, a weakly coordinating solvent, gave a similar product distribution for the hydrogenation

[3] For experiments concerning glycine-based ligand **19d**, see chapter 3.4.1, page 44.

of substrate **12** using ligand **19c** (4.8:95.2, *S*:*R*) compared to $CDCl_3$, employment of methanol as reaction solvent led to a significant drop in selectivity (19.2:80.8, *S*:*R*), which can be attributed to the solvent inhibiting ligand-ligand interaction that drive the rotameric enrichment.

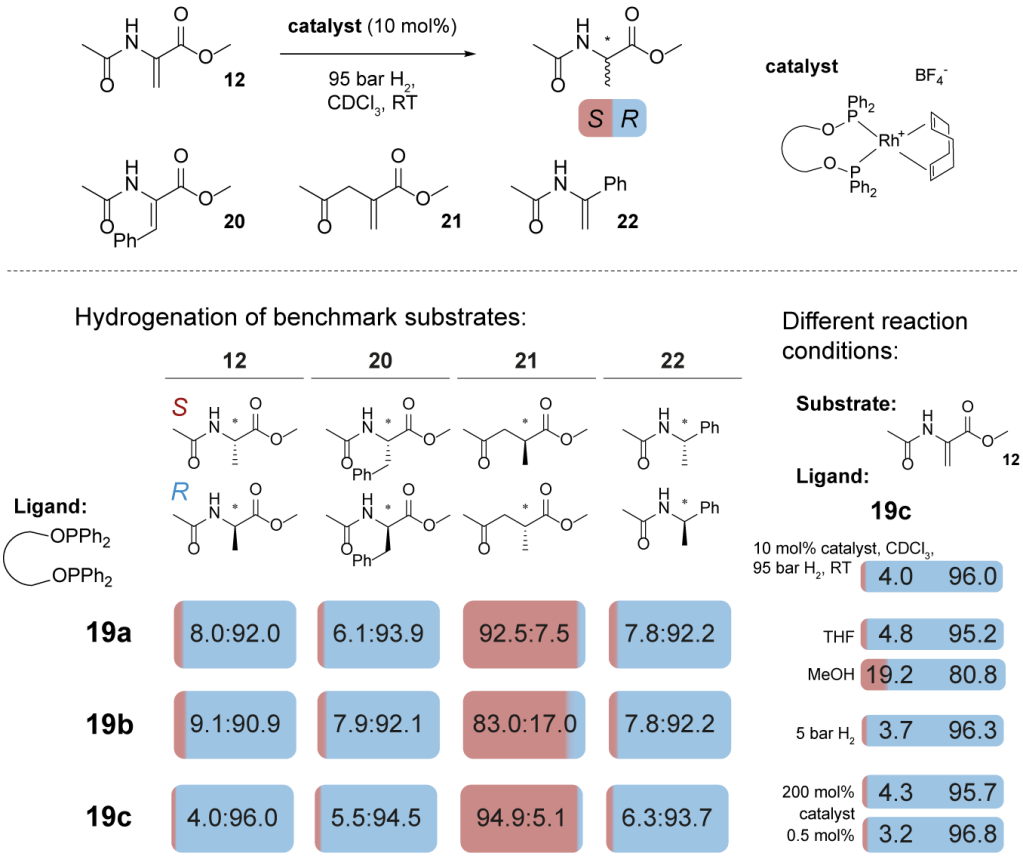

Figure 2-18: Overview over asymmetric hydrogenation experiments of prochiral olefins **12** and **20**-**22** using diastereomerically pure ligands **19a-c** (left) and control experiments under differing reaction conditions to evaluate the origin of the catalyst's selectivity (right). All reactions showed full conversion. Enantiomeric ratios were determined by chiral GC or HPLC. Detailed experimental procedures can be found in chapter 7.2.17 on page 121.

2.4.4 Selector comparison

Comparison of the ligands **19a-c** with respect to their selector types shows no significant difference (for further investigations concerning ligand **19d**, see chapter 3.4.1). Full rotameric enrichment and very similar behaviour during structural investigations was observed in all three cases. Additional sterical pressure provided by the adamantyl moiety had no adverse effect on dimerization as evident from the crossover experiment, where distribution of species was found to be purely statistical. Strongest low-field shifts of amide protons were observed for phenylalanine derivative **19c**, which is an indicator for increased binding strength. Accordingly, this ligand was found to exhibit the highest selectivities during asymmetric hydrogenation reactions, which might either be caused by higher supramolecular stability or by a change in the ligands dihedral angle[120,121] due to the difference in the selector's substitution pattern.

2.5 Investigation of selector-modified phosphoramidite ligands

2.5.1 Synthesis

Stereodynamic phosphoramidite ligands could be conveniently synthesized from the same BINOL precursors as the respective bisphosphinite ligands (see Figure 2-19). Valine-based ligand **23a** was prepared by refluxing a suspension of biphenol **18a** in toluene in the presence of tris(diethylamino)phosphine to give the desired phosphoramidite in good yields. Phenylalanine derivative **23b** was synthesized by treating the corresponding diol with diethylphosphoramidous dichloride in presence of triethylamine.

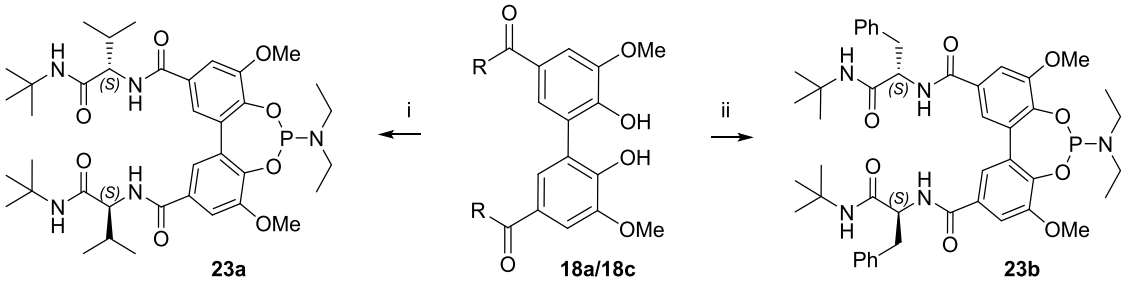

Figure 2-19: Synthesis of phosphoramidite ligands **23a,b**. Diols **18a** and **18c** were prepared as shown in Figure 2-14, page 17. i) $P(NEt_2)_3$, 56%, ii) NEt_2PCl_2, NEt_3, 74%.

2.5.2 Structural investigations

Based on structural similarites to previously discussed bisphosphine and bisphosphinite ligands, the synthesized phoshoramidites were expected to undergo the same dimerization process that entails cooperative chiral induction to yield diastereomerically pure ligands. Since this ligand type has a very low isomerization barrier, it is exceedingly difficult to distinguish between the two ligand rotamer states by means of NMR spectroscopy. Both ligands, however, were found to exhibit C_1-symmety leading to a doubling of NMR signals in ^{1}H and ^{13}C NMR spectra and amide protons exhibited low field ^{1}H NMR shifts between 10.64 and 7.63 ppm (**23a**) and between 10.72 and 7.32 ppm (**23b**), which proves very strongly engagement in hydrogen bonding. These findings have previously been identified as indicators for the supramolecular arrangement for these types of diamido-modified ligand structures (see chapter 2.3.2 and 2.4.2). Intriguingly, the reduction of symmetry for ligands **23a** and **b** was found to have another consequence. Since the two sides of each ligand subunit within the hydrogen bonded complex are chemically non-equivalent, the phosphorus atom becomes chiral. As a result, diastereomeric adducts with different chirality at the phosphorus atom form. In the resulting ^{31}P NMR spectrum, the two C_2-symetric homomers (S,S,R_{ax},P^*_R)/(S,S,R_{ax},P^*_R) and (S,S,R_{ax},P^*_S)/(S,S,R_{ax},P^*_S) produce one singlet signal each while the C_1-symmetric heteromer (S,S,R_{ax},P^*_R)/(S,S,R_{ax},P^*_S) gives two more singlet signals (see Figure 2-20). Consequently, another fourfold increase in signals is observed in ^{1}H and ^{13}C NMR spectra.

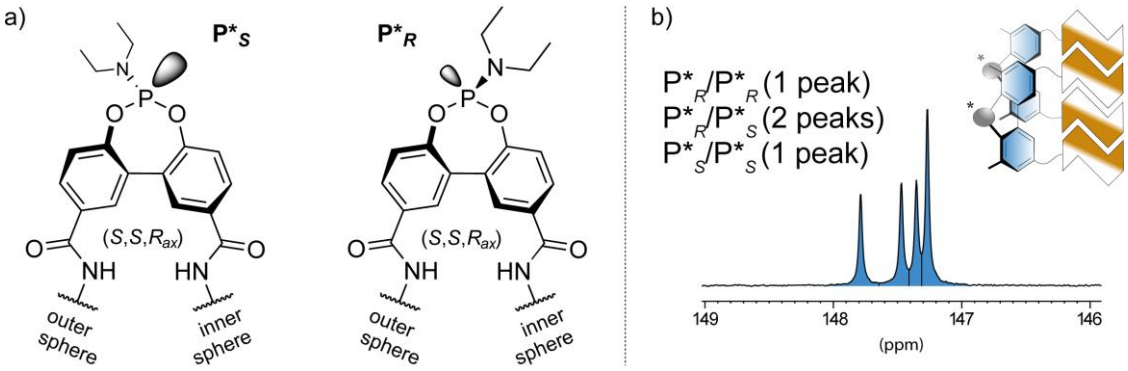

Figure 2-20: a) Reduction of symmetry renders phosphorus atoms in phosphoramidite ligands 23a und 23b chiral. b) Three different diastereomeric adducts form during dimerization that can be distinguished by NMR. For annotation of stereogenic phosphorus atoms, each *inner sphere* ligand half was given priority over the *outer sphere* half.

Finally, assumptions that the observation of additional signals is related to the formation of hydrogen bond dimers comprising both R_{ax} and S_{ax} ligand isomers, instead, can be dismissed. Previously discussed geometrical considerations of the selector interaction patterns make S_{ax}/R_{ax}-adducts unfeasible due to the divergent selector orientation (see crystal structures in Figure 2-11 and Figure 2-15).

2.5.3 Hydrogenation experiments

Phosphoramidite ligands **23a** and **23b** were also employed in rhodium-catalyzed asymmetric hydrogenations of olefins **12** and **20-22**. It is worth stressing that due to the monodentate nature of this ligand type, two molecules were needed to saturate a rhodium center. Since the ligands form supramolecular dimers, it is plausible that structurally dynamic oligomers or polymers with many catalytically active centers were formed during complexation. This is supported by the observation that complexes formed *in situ* using rhodium precursor $[Rh(COD)_2]BF_4$ gave baseline-broadened ^{31}P NMR signals ranging over multiple ppm along with intense line broadening in the corresponding ^{1}H NMR spectra, both of which is common for polymeric, dynamic structures.

Both catalysts, formed *in situ*, were found to be less selective in comparison to their bisphosphinite-based counterparts. Enantiomeric ratios ranged from 56.2:43.8 (*S*:*R)* for the reduction of 1-phenyl-1-acetamidoethylene **22** using ligand **23a** to 73.2:26.8 (*S*:*R*) when the same catalyst was employed with olefin **12**. All other transformations were found to occur with similar selectivities (see Figure 2-21). Most intriguingly, it was found that changing the selector motive from (*S*)-valine to (*S*)-phenylalanine was accompanied by an inversion of selectivity during later catalysis for all tested substrates. While the former ligand exhibited selectivity for the generation of the *S* enantiomer during the reduction of substrates **12**, **20** and **22** and for the *R* enantiomer in case of substrate **21**, the latter proved to predominantly produce the opposite enantiomer in each case. Also, when both ligands were employed during reduction of olefin **22** in a ratio of 1:1, a very low *er* of 51.2:48.8 (*S:R*) was obtained. This clearly indicates that for these catalysts, the selectivity of the transformation is not exclusively based on the axial chirality of the ligands. Arguably, the diastereomeric distribution of the P*-chiral ligands might depend on the nature of the selector and cause this phenomenon. Another possible explanation is that the substitution pattern on the selector units affects the degree and dynamic of the catalyst oligomerization mentioned above. Lastly, it is also known that phosphoramidite complexes exist as a mixture of several different Rh-P rotamers, whose distribution might also affect the catalyst's selectivity

and is possibly being affected by the structure of the ligand backbone. Still, it remains unclear, how such an inversion of selectivity can be evoked by a subtle change of the selector's substitution pattern and without changing its chiral information. Clearly, an answer to this question necessitates further investigation on the exact structure and dynamics of the catalytic system.

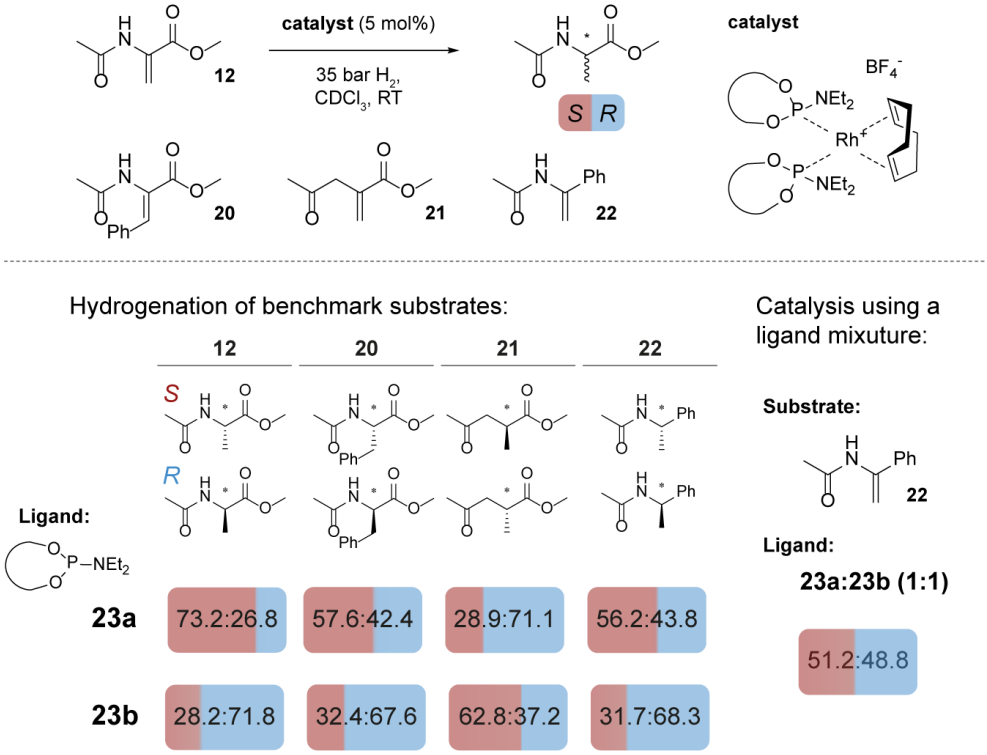

Figure 2-21: Overview over asymmetric hydrogenation experiments of benchmark olefins **12** and **20-22** using phosphoramidite ligands **23a** and **23b**. All reactions showed full conversion. Enantiomeric ratios were determined by chiral GC or HPLC. Detailed experimental procedures can be found in chapter 7.2.17 on page 121.

2.6 Investigation of selector-modified BIPOL ligands

2.6.1 Structural investigations

BIPOL compounds **18a-c** were observed to undergo the same transformation into diastereomerically pure dimers that was identified for bisphosphinite ligands **18a-c** and phosphoramidite ligands **23a-b** derived thereof. Formation of the supramolecular hydrogen bond complexes could be identified by NMR spectroscopy, where two sets of signals could be detected in both ^{1}H and ^{13}C NMR spectra (see exemplary spectrum in Figure 2-22b) and again, strong cross peaks in two-dimensional HMBC spectra were found that link both signal sets to the same molecular scaffold (for spectral data see chapter 7.2.11, page 102). In all three cases, no minor species was observed.

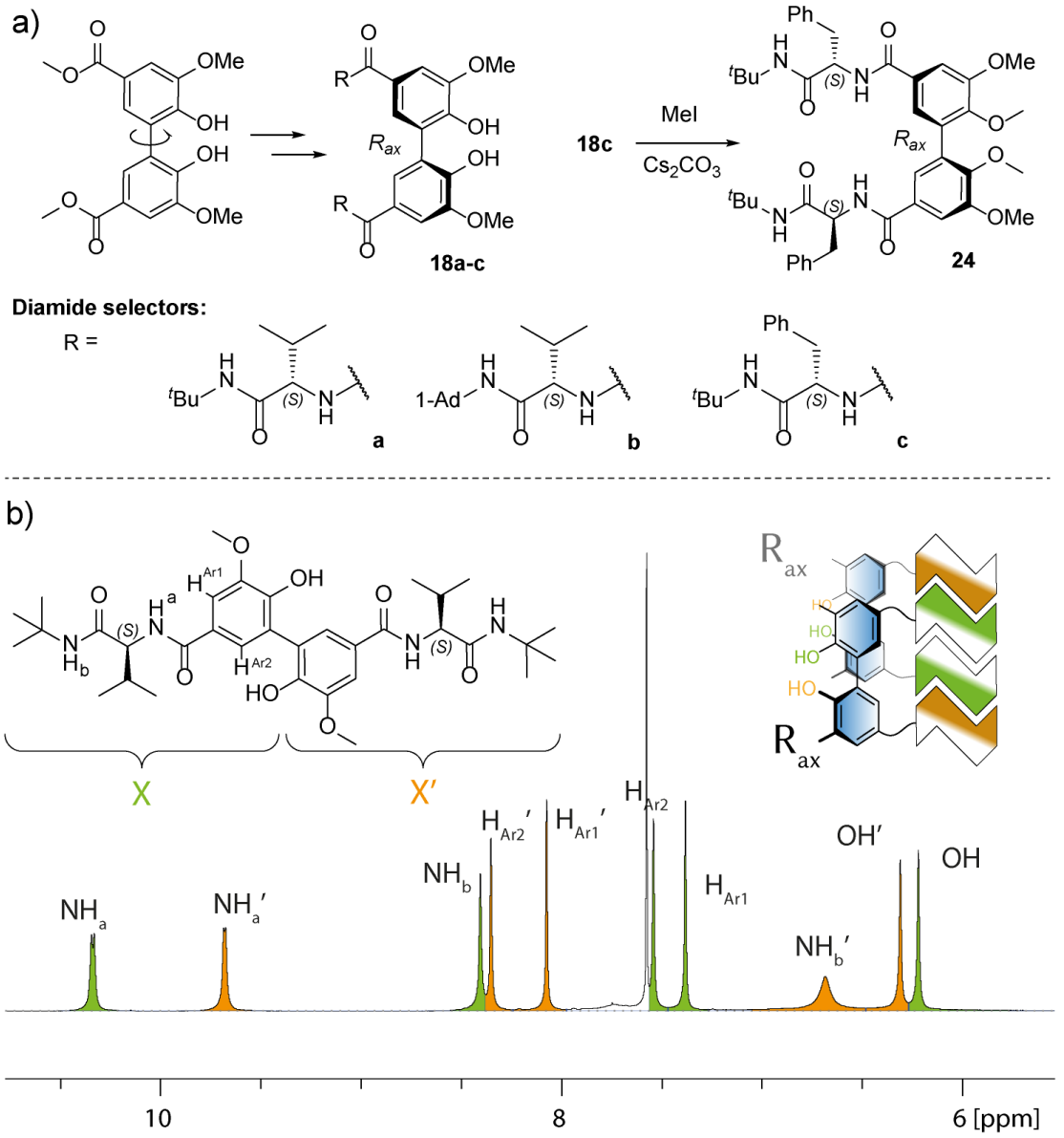

Figure 2-22: a) Overview of investigated BIPOL compounds and synthesis of methylated biphenol **24**. b) Aromatic section of the ^{1}H NMR spectrum of BIPOL **18a** at -20 °C. Two sets of signals of equal intensity were observed representing the *inner sphere* (green) and the *outer sphere* (orange) of the supramolecular dimer.

The dynamic of the *tropos* biphenols was found to depend on the substitution pattern of the selector. While NMR spectra for valine-based BIPOLs **18a** and **18b** needed to be collected at -20°C to avoid excessive line broadening, phenylalanine-derived BIPOL **18c** exhibited sharp, well-defined NMR signals at room temperature.

To verify the dimeric structure of the biphenol compounds, BIPOL **18c** was methylated with iodomethane to afford compound **24** from which single crystals suitable for X-ray analysis could be grown (see Figure 2-22a). The structure shows the same characteristics that were found for that of bisphosphine (R_{ax})-**7** and bisphosphinite **19d** (see Figure 2-23).

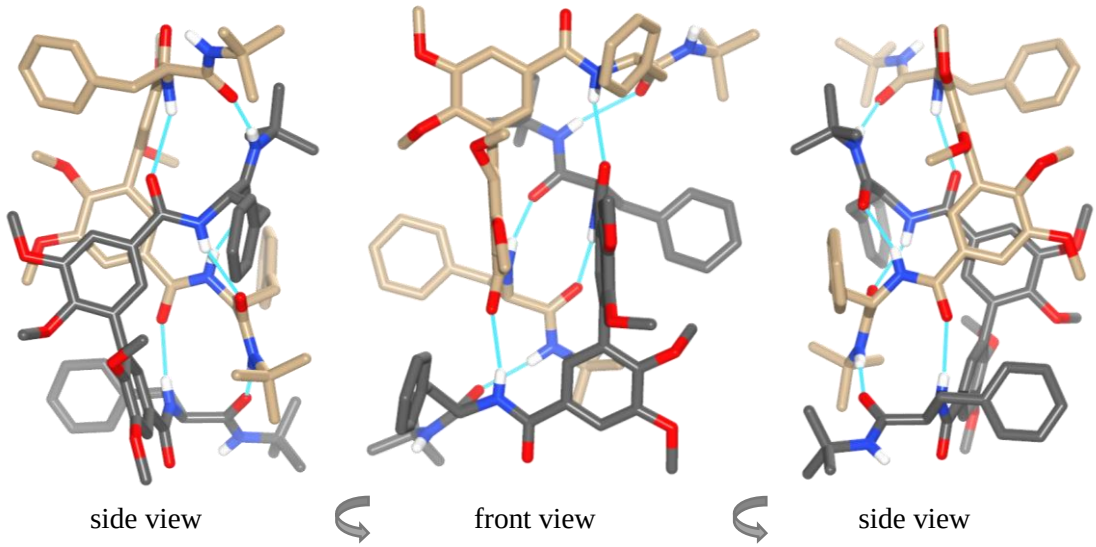

Figure 2-23: Representation of the single crystal X-ray structure of **24**. Two R_{ax} molecules form a supramolecular C_2-symmetric dimer of C_1-symmetric subunits (carbon atoms of different subunits are indicated in beige and grey). Hydrogen bonds are indicated with light blue lines. Non-relevant hydrogen atoms as well as solvent molecules are omitted for clarity. Nitrogen = blue, oxygen = red. Images were produced using UCSF Chimera.[99]

The stability of the diols towards oxygen, moisture and protic solvents subsequently allowed to conduct additional experiments to verify that the structural arrangement found in the solid state is identical to that in solution. In analogy to previous experiments with bisphosphinite ligands **19a** and **19b**, formation of a heterodimeric species was observed, when BIPOLs **18a** and **18b** were mixed in solution (see Figure 7-14, page 106 for spectral data). In a subsequent titration experiment, phenylalanine-based BIPOL **18c** was dissolved in mixtures of $CDCl_3$ and CD_3OD with ratios of 99:1, 90:10, 50:50 and 0:100 (*v*:*v*) and ^1H NMR spectra were collected in order to investigate the impact of solvent molecules capable of hydrogen bonding on the amide protons of the BIPOL dimer (see Figure 2-24).

In accordance with previously suggested bonding patterns, proton H_a, which is part of the C5:C5 interaction in the *inner sphere* of the dimer, and protons H_a' and H_b, that form the *outer sphere* C7:C5 interaction, show very subtle overall shift differences between δ = -0.18 ppm for NH_a and NH_a' and δ = +0.20 ppm for NH_b. The "unbonded" and exposed amide proton NH_b', however, underwent a downfield shift of δ = +1.97 ppm due to increased solvent interaction.

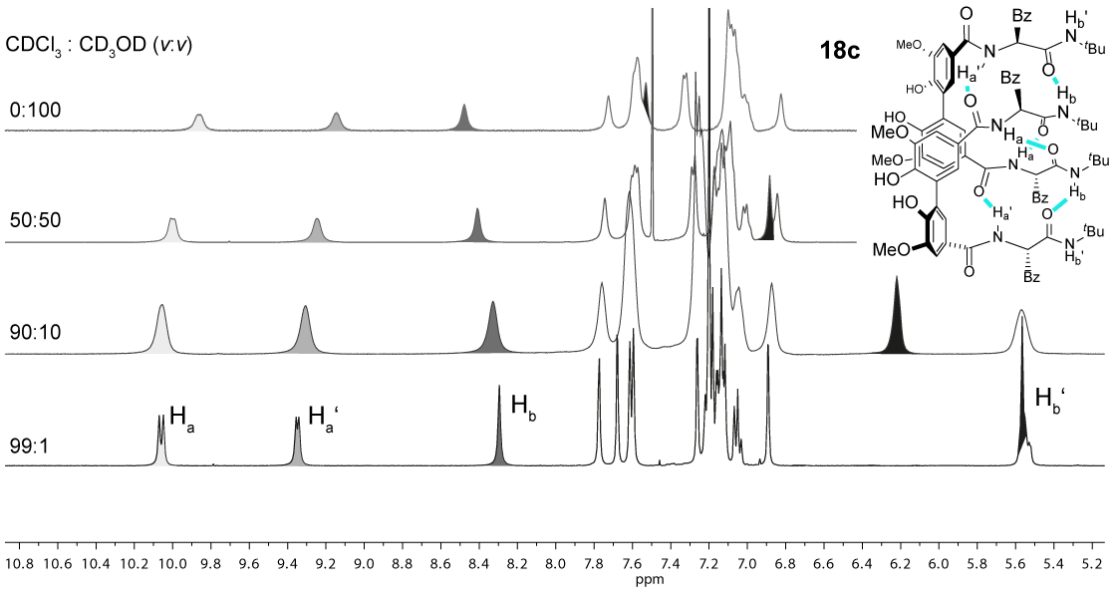

Figure 2-24: ^{1}H NMR spectra showing the titration experiment of BIPOL **18c**. Dissolving the compound in different mixtures of $CDCl_3$ and CD_3OD gave different shifts for amide protons corresponding to their exposure to solvent as predicted by the structural model shown in the top right corner.

In a follow-up experiment, HD exchange rates of the amide protons were investigated. These are reliable indicators for non-covalent interactions of amide groups as these rates are strongly influenced by proton fixation through hydrogen bonding. The speed of exchange also depends on both substitution pattern and electronics of the amide moiety.[122,123] To obtain reference values, model compound (*S*)-**25** was synthesized, which provides exchangeable protons in the same electronic and steric environment compared to the selector moieties of **18c**, but which was considered not to engage in strong self-interaction due to the lack of a comparable chelating effect. Solutions in freshly opened, deuterated methanol were prepared (20 mM **18c**, 40 mM (*S*)-**25**) and spectra were collected periodically to monitor the decrease of the amide proton signals. Due to high excess in methanol, exchange kinetics were calculated based on a pseudo-first order reaction (see chapter 7.2.16, page 119 for details). Half-life times $t_{1/2}$ and corresponding exchange rates k_{ex} are shown in Table 2-2. As expected, amide protons of model compound (*S*)-**25** were found to undergo deuterium exchange significantly faster. Proton H_a^{25} had already fully exchanged before the first measurement could be conducted and the signal for H_b^{25} had vanished after two hours. For BIPOL **18c**, however, exchange took place on a different timescale. Amide protons H_a^{18c} and $H_a{}'^{18c}$ took roughly 20 hours while H_b^{18c} and $H_b{}'^{18c}$ took about nine weeks to undergo complete deuterium exchange. Evidently, hydrogen bonding immobilizes amide protons, which greatly decreases the rate of deuteration. In order to analyse the bonding pattern, retardation factors were calculated to normalize exchange rates of **18c** with those of diamide (*S*)-**25** allowing for a direct comparison of the deceleration for each individual amide proton of the BIPOL ligand (see Table 2-2). Exchange rate constants decreased by a factor of 2554 and 2402 for H_a^{18c} and $H_a{}'^{18c}$, respectively. For the terminal amide protons H_b^{18c} and $H_b{}'^{18c}$, retardation factors of 917 and 731 were found. These values are in good agreement with the proposed binding model: Amide proton H_a^{18c}, located in the *inner sphere* center of the complex, profits from a strong and stabilizing chelating effect of the surrounding hydrogen bonds and shows the

Table 2-2: Half-life times and exchange rates for HD exchange in deuterated methanol.

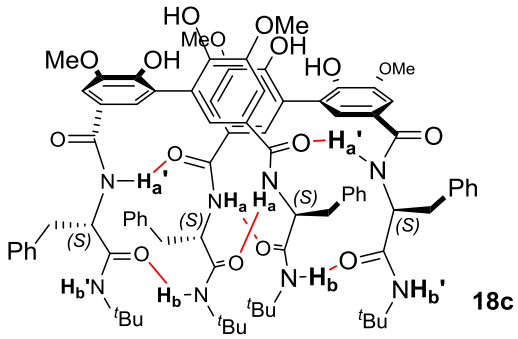

18c

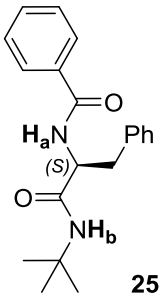

25

Compound[a]	Diol **18c**				Diamide (*S*)-**25**	
	H_a	H_b	H_a'	H_b'	H_a	H_b
$t_{1/2}$ [10^2 min]	1.91	253.3	1.80	201.6	0.0008[b]	0.28
k_{ex} [sec^{-1}]	$6.0 \cdot 10^{-5}$	$4.6 \cdot 10^{-7}$	$6.4 \cdot 10^{-5}$	$5.7 \cdot 10^{-7}$	$1.5 \cdot 10^{-1}$	$4.2 \cdot 10^{-4}$
Retardation Factor[c]	2554	-	2402	-	1	-
	-	917	-	731	-	1

a) Experiments were conducted at room temperature with a 20 mM solution of **18c** and a 40 mM solution of (*S*)-**25** in deuterated methanol. b) Complete exchange was observed already after 30 seconds when the first spectrum was measured. Half-life time was therefore estimated (see chapter 7.2.16, page 119). c) Retardation Factor = $k_{ex}(H_X^{\mathbf{25}}) / k_{ex}(H_X^{\mathbf{18c}})$

strongest exchange slowdown. Proton $H_a'^{\mathbf{18c}}$ benefits to a similar extent but is deuterated slightly faster because of its peripheral position. In comparison, exchange of terminal amide proton $H_b^{\mathbf{18c}}$ is decelerated 2.5 times less since only one hydrogen bond needs to be broken. Finally, proton $H_b'^{\mathbf{18c}}$ experiences the smallest exchange retardation due to the exposed position on the outside of the complex and the measured slowdown can be attributed to chemical exchange of the subunits within the dimer.

2.6.2 Enantioselective alkylation of aromatic aldehydes

2,2'-biphenols have found successful application as ligands in homogeneous catalysis.[124,125] Among the most prominent examples is the Ti-catalyzed alkylation of aromatic aldehydes. Chan *et al.* pioneered the use of *atropos (S)*-BINOL and diethyl zinc to convert a range of substrates with excellent selectivities.[126,127] Using these studies as a starting point, stereodynamic BIPOLs **18a-c** were employed for the same reaction type.

Prior to catalytic experiments, formation of the BIPOL-titanium complex and the interplay with $ZnEt_2$ was investigated. When ligand **18c** was mixed with an equimolar amount of $Ti(O^iPr)_4$ in dichloromethane, yellow solids formed and almost quantitative precipitation of the ligand was confirmed by ^1H NMR spectroscopy (see chapter 7.2.18.1, page 122 for spectroscopic data). When the solids were treated with another six equivalents of the titanium precursor, a clear, yellow solution was produced and formation of a variety of complex species comprising dimerized ligands was spectroscopically observed. These findings suggest that stoichiometric employment of biphenol **18c** and titanium tetraisopropoxide gives hardly soluble complexes of unknown composition. Their dissolution upon addition of more titanium precursor implies coordi-

nation of two or more BIPOL units to the same titanium atom. Combined with the self-aggregating behaviour of the BIPOL compounds, formation of larger clusters or MOF-like oligomers is assumed that fragment when the titanium concentration is increased. Subsequent addition of diethyl zinc resulted in additional line broadening but did not impair the integrity of the dimerized diol complexes.

In a first set of screening reactions with benzaldehyde as a benchmark substrate and diethyl zinc as alkylating agent, all three ligands were employed and the reaction conditions such as temperature, solvent and reagent ratios were varied (see Table 2-3). Differences in the diols' dynamics that were initially identified by comparison of their NMR spectra are reflected in their enantioselectivities as ligands (entries 1-3). More dynamic valine-based compounds **18a** and **18b** alkylated benzaldehyde at 0°C with selectivities of 37.4% *ee R* and 29.4% *ee R*, respectively, and conversions below 62% after 16 hours. In contrast, phenylalanine-based ligand **18c** gave 75.6% *ee R* and a conversion of 92.7% after the same amount of time. Consequently, further screening experiments were limited to this diol. When the reaction was run under identical conditions and stopped after eight hours, the same *ee* and reduced conversion was observed, which indicates

Table 2-3: Reaction screening for the enantioselective alkylation of aromatic aldehydes using BIPOL ligands 18a-c.

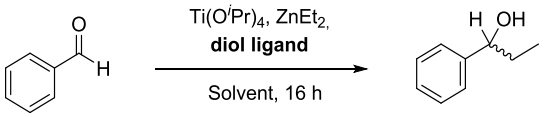

Entry[a]	Solvent	Ligand	Ratio	Temp.	Product analysis [%][e]		
			Ti/Ligand		*Conv.*	*ee*	
1	DCM	**18a**	1.4/0.2	0 °C	61.8	37.4	*R*
2	DCM	**18b**	1.4/0.2	0 °C	41.4	29.4	*R*
3	DCM	**18c**	1.4/0.2	0 °C	92.7	75.6	*R*
4[b]	DCM	**18c**	1.4/0.2	0 °C	76.2	75.4	*R*
5	DCM	**18c**	1.4/0.2	**25 °C**	98.0	66.0	*R*
6	DCM	**18c**	1.4/0.2	**-20 °C**	22.1	57.9	*R*
7[c]	DCM	**18c**	**1.4/0.2**	0 °C	16.0	77.2	*R*
8[d]	DCM	**18c**	**1.4/0.2**	0 °C	98.5	37.8	*R*
9	DCM	**18c**	**1.4/0.4**	0 °C	65.1	79.8	*R*
10	DCM	**18c**	**1.4/0.05**	0 °C	57.7	32.2	*R*
11	**THF**	**18c**	1.4/0.2	0 °C	11.5	12.4	*R*
12	**Toluene**	**18c**	1.4/0.2	0 °C	86.4	27.6	*R*
13	**Et_2O**	**18c**	1.4/0.2	0 °C	78.1	34.5	*R*
14	**MeCN**	**18c**	1.4/0.2	0 °C	36.3	18.5	*R*
15	**EtOAc**	**18c**	1.4/0.2	0 °C	35.0	77.2	*R*

a) Benzaldehyde/Ti(O^{i}Pr)$_4$/ZnEt$_2$ = 1.0/1.4/3.0 (molar ratio) and 125 mM solution with respect to substrate. All reactions were stopped after 16 hours by quenching with NH_4Cl solution. Detailed experimental procedure can be found in chapter 7.2.18.2, page 122. b) Reaction was stopped after eight hours. c) 20.0 mM solution with respect to substrate. d) 375 mM solution with respect to substrate. e) Conversion and *ee* were determined using chiral GC (Chirasil β-Dex). Benzylic alcohol was found to only form in traces and is not considered.

that the catalyst does not change selectivity over time (entry 4). Variation of the reaction temperature to 25 °C or -20 °C slightly in- or significantly decreased the yield but both changes resulted in a drop in enantioselectivity to 66.0% *ee R* or 57.9% *ee R*, respectively (entries 5 and 6). Similar outcomes were observed when the reaction was run at higher concentrations (entry 8), while a 6.5 times more diluted setup gave almost no conversion, but a slight increase in selectivity (entry 7). While the change in conversion along with in- or decreased concentration seems plausible, a lower selectivity at higher ligand concentration seems counterintuitive since the dimerization of a supramolecular ligand should be positively affected by this. These findings suggest that aside from the ligand's diastereopurity, selectivity of the reaction is profoundly influenced by the interplay of the complex network of equilibria that is also affected by the change in concentration. As previously demonstrated, the ratio of titanium tetraisopropoxide and diol ligand also has a strong impact on the course of the catalysis, based on various reversible ligand exchange steps during the reaction cycle.[128] A decreased ligand loading (5 mol% to substrate, 28:1 Ti:ligand) negatively affected both conversion and selectivity, while an increased amount of diol (40 mol% to substrate, 3.5:1 Ti:ligand) gave an equally reduced conversion, but slightly increased the enantiomeric excess to 79.8% *ee R* (entries 9 and 10). Varying solvents led to significantly smaller yields in all instances and only ethyl acetate gave enantioselectivities comparable to those of DCM (35.0% conversion and 77.2% *ee R*, entry 15). In total, conditions found optimal for the investigated catalytic system were found to match those previously identified by Chan *et al*. for the employment of BINOL for the same purpose. Moreover, a high selectivity for the formation of the product was observed and benzylic alcohol, which can be found as side product of this reaction, formed only in traces.

In a second set of experiments, the origin of enantioselectivity during the catalytic cycle was investigated. Apart from diol-titanium complexes of various kinds, zinc complexes of small, bifunctionalized molecules such as amino alcohols or bis(sulphonamides) are also well known to selectively catalyze the reaction.[129-131] For this reason, control experiments were conducted to ensure that selectivity was indeed induced by the axial orientation of diastereoenriched biphenol ligands and not simply by coordination of chiral diamide selector groups to a transition metal center (Table 2-4). A strong, inhibiting effect was found when selector-type diamide (*S*)-**8** was added resulting in a drop of conversion and selectivity (entry 2). When a catalytic solution from racemic 2,2'-biphenol **26** and two equivalents of diamide (*S*)-**8** was prepared, a very low enantiomeric excess of 5% in favour of the *R* enantiomer was obtained indicating involvement of the diamide as ligand (entry 3). Indeed, when the incubation time prior to substrate addition was increased from 10 minutes to two hours, the same catalyst showed an increased enantioselectivity of 11.3% *ee R* along with greatly reduced activity (entry 4). Employment of diamide (*S*)-**8** as sole ligand led to an even higher enantiomeric excess of 38.5% *ee R*, but only in the presence of the titanium precursor (entries 5 and 6). These experiments illustrate, that amino acid-derived diamides can coordinate to a titanium center in the presence of strong bases such as diethyl zinc, forming a less active and less selective catalyst for the alkylation reaction that can compete with the BIPOL-Ti complex. Since acidity of amide protons is affected by hydrogen bond formation, it seems plausible to assume that dimerization reduces the availability of the selector units on the investigated BIPOL ligand **18c** to be deprotonated by a strong base and act as coordination units themselves. To verify this, the "capped" version of the ligand (**24**) was employed as ligand and the resulting catalytic mixture gave a full racemate (entry 7). These experiments allow for the conclusion that enantioselectivities of experiments with diol ligands **18a-c** solely originate from the axial chirality of the self-assembling diol ligand.

Table 2-4: Investigation of the origin of chiral induction during the asymmetric alkylation.

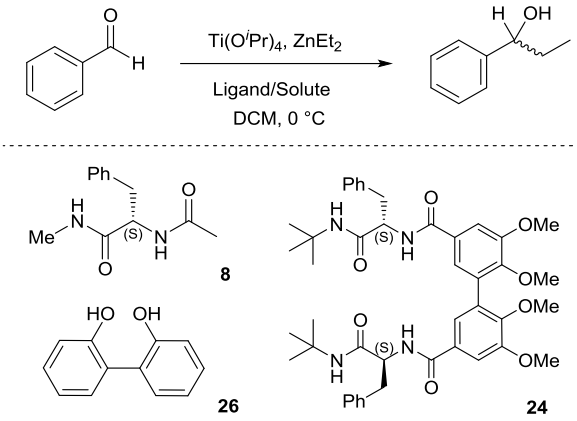

Entry[a)]	Ligand	Solute	Reagents	Product analysis [%][d)]		
	0.2 eq.	0.4 eq.	Ti/Zn	*Conv.*	*ee.*	
1	**18c**	-	1.4/3.0	92.7	75.6	*R*
2	**18c**	(*S*)-**8**	1.4/3.0	52.7	54.0	*R*
3	**26**	(*S*)-**8**	1.4/3.0	82.7	5.0	*R*
4[b)]	**26**	(*S*)-**8**	1.4/3.0	52.4	11.3	*R*
5[c)]	-	(*S*)-**8**	1.4/3.0	33.0	38.5	*R*
6	-	(*S*)-**8**	0.0/3.0	9.1	3.8	*R*
7	**24**	-	1.4/3.0	38.9	0.3	*R*

a) Benzaldehyde/Ti(O^{i}Pr)$_4$/ZnEt$_2$ = 1.0/1.4/3.0 (molar ratio) and 0.125 M solution with respect to substrate. All reactions were stopped after 16 hours. Detailed experimental procedure can be found in chapter 7.2.18.2, page 122. b) Biphenol, diamide and titanium precursor were incubated in presence of ZnEt$_2$ for two hours prior to catalysis. c) 0.375 M solution of diamide with respect to substrate. d) Conversion and *ee* were determined using chiral GC (Chirasil β-Dex).

Finally, a variety of different aromatic aldehydes were tested under standard reaction conditions (see Table 2-5). Most noticeable was the significant variation in conversion. While *m*-nitro-, 2-methoxy- and α-naphthaldehyde (entries 7, 9 and 10) gave good yields (94.7%, 79.5% and 77.0%), 4-substituted aldehydes generally performed worse with yields ranging from 19.3% for 4-methoxybenzaldehyde (entry 5) to 56.7% for 4-fluorobenzaldehyde (entry 4). When comparing the enantiomeric distribution of the products, selectivity was found to scale inversely with sterical pressure around the aldehyde moiety. While most 4-substituted aldehydes were alkylated with enantiomeric excesses that were similar to that of benzaldehyde, substitution of the 1-position caused a significant deterioration of selectivity. As an exception, 4-acetylbenzaldehyde was converted with a selectivity of 49.8% *ee R* (entry 6) similar to the more sterically crowded substrates. Best selectivity was achieved for 4-fluorobenzaldehyde being alkylated with 76.9% *ee R* (entry 4), which slightly exceeded the benchmark value. Altogether, the observed trends reflect those previously found for *atropos* ligand (*S*)-BINOL by Chan *et al*. The lower selectivity can be attributed to the ligand's residual stereodynamic or to a differing dihedral angle compared to BINOL. Furthermore, the spatial arrangement of the ligand dimer brings the transition metal centers of two interlinked titanium complexes closely together, which results in increased sterical pressure when large substrates coordinate during the catalytic cycle. All of these issues could potentially be addressed by optimizing selector and biaryl substituents on the diol in order to

further strengthen the hydrogen bond network and tune sterical hindrance around the catalytically active center.

Table 2-5: Enantioselective alkylation of different aromatic aldehydes.

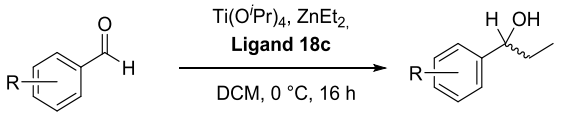

Entry[a)]	Substrate	Conversion and *ee*[b)]	Entry	Substrate	Conversion and *ee*[b)]
1		92.7% 75.6% *R*	**6**	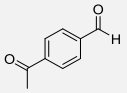	25.3% 49.8% R
2		41.5% 63.3% *R*	**7[c)]**	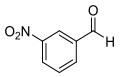	94.7% 49.8% *R*
3	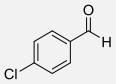	24.9% 62.4% *R*	**8**		67.0% 55.9% *R*
4		56.7% 76.9% *R*	**9**		79.5% 46.5% *R*
5	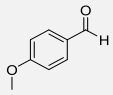	19.3% 69.4% *R*	**10[c)]**	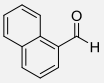	77.0% 53.7% *R*

a) Benzaldehyde/Ti(O^{i}Pr)$_4$/ZnEt$_2$/Ligand = 1.0/1.4/3.0/0.2 (molar ratio) and 0.125 M solution with respect to substrate. All reactions were stopped after 16 hours. Detailed experimental procedure can be found in the 7.2.18.2, page 122. b) Unless stated otherwise, conversion and *ee* were determined using chiral GC (Chirasil β-Dex). c) *ee* was determined by chiral HPLC (Chiralcel OD-H).

2.7 Results

This chapter details the investigation of a novel core motif for *tropos* biphenyl-based ligands. These were equipped with (*S*)-amino acid-based diamido groups (selectors) in the 5,5' position, that are inspired by selector units in the high-performance CSP for GC CHIRASIL VAL. Based on this motif, synthetic routes for bisphosphine **7** and for BIPOLs **18a-c**, bisphosphinites **19a-d** and phosphoramidites **23a-b** were developed.

The investigated substitution pattern was found to trigger a process of spontaneous rotamer enrichment of the R_{ax} isomer. The phenomenon was investigated, *inter alia*, by NMR spectroscopy, X-ray structure analysis and HD exchange experiments. It was found that highly diastereoselective, intermolecular non-covalent interactions of the selector groups lead to formation of well-ordered ligand dimers. The central chirality of the amino acid-based selector units thereby dictates the axial chirality of the ligand's biphenyl backbones within the supramolecular structure. It allows only for R_{ax} rotamers to dimierise causing selective stabilization of one rotamer that drives the ensuing rotameric enrichment. The entire process is controlled by cooperative chiral

induction that results from the self-recognition properties of the selector units. It evokes a stereoconvergent response from the dynamic ligand core that can be described as a form of diastereoselective *narcissistic self-sorting* and the state of rotameric enrichment is self-reinforced by dynamic exchange among the complex subunits, which is a form of stereocontrol that resembles that found in *sergeant-soldier*-type self-organizing, supramolecular systems.

The strength of the supramolecular hydrogen bonds was found to be slightly influenced by the substitution pattern of the selector. A much greater influence was exerted by the ligand-defining substituents in 2,2'-position of the biaryl backbone, which was found to affect the degree of rotameric enrichment. For bisphosphine **7**, a strongly weighted equilibrium between a monomeric S_{ax} rotamer and a dimeric R_{ax} rotamer with a ratio of 16:84 (S_{ax}:R_{ax}) was found. This ratio could be influenced by interfering with the ligands self-interaction by addition of various chiral and achiral hydrogen bond donors and acceptors that would occupy the interaction sites. BIPOL ligands **18a-c**, phosphinite ligands **19a-c** and phosphoramidite ligands **23a-b** were found to undergo complete transformation into one diastereomerically pure R_{ax} species each.

All ligands were subsequently investigated for their potential as ligands in asymmetric reactions. BIPOL ligands were used in titanium-mediated enantioselective alkylation reactions of aromatic aldehydes. The path of chiral induction was examined and a variety of different alcohols could subsequently be generated with selectivities of up to 79.8% *ee R*.

All phosphorus-based ligands were employed in asymmetric, rhodium-catalyzed hydrogenation reactions. Enantioselective reduction of methyl 2-acetamidoacrylate **12** with bisphosphine **7** produced methyl 2-acetamidoalanate **13** with an enantiomeric distribution of 17.4:82.6 (*S*:*R*), which closely corresponds to the previously determined rotamer distribution and indicates high selectivity for each individual ligand rotamer. The enantiomeric excess of the product could subsequently be influenced by employing ligand mixtures whose rotameric distribution had previously been adapted by equilibration in presence of chiral amino acid derivatives. The best selectivity was obtained by using Ac-(*S*)Ala-NH(3,5-dichorophenyl) (**9**) as an additive, which enabled hydrogenation of **12** with a selectivity of 8.6:91.4 (*S*:*R*, Δee = +18%). Diastereomerically pure phosphinite ligands **19a-c** were used for the rhodium-catalyzed hydrogenation of benchmark substrates **12** and **20-22** where all ligands were found to reduce these substrates with high to very high selectivities. Best results were obtained with the phenylalanine-based ligand **19c**, which reduced olefin **12** with a selectivity of 4.0:96.0 (*S*:*R*). Enantiomeric product distributions were additionally shown to be independent of the catalyst's turnover number proving that ligand selectivity is solely governed by the stereodynamic enrichment of the energetically stabilized R_{ax} rotamer, whose enrichment occurs prior to catalysis.

Phosphoramidite ligands **23a** and **23b** were found to perform less selectively and the highest enantiomeric ratio of 73.2:26.8 (*S*:*R*) was achieved with ligand **23a** in the reduction of **12**. Interestingly, a reversal in selectivity was observed when the valine-based selector was replaced by a phenylalanine-based one indicating a more complex path of stereoinduction for this ligand type.

3 Deracemization of selector-modified *tropos* ligands

3.1 State of knowledge

Nature has developed eloquent methods to exert comprehensive control over the path of a catalytic chemical reaction by modulating participating enzymes or other small, catalytically active molecules in manifold ways.[132] Of particular importance in this context is the concept of allostery, which allows to create complex, switchable systems with various ligand states.[133-135] The versatility of such catalysts creates a great incentive to develop artificial, bio-mimetic systems that copy those mechanisms. As result, a variety of catalysts have been developed[136,137] that can undergo structural changes in response to external stimuli such as light,[138,139] pH changes[140,141] or redox-based electron transitions[142-144] to simultaneously change selectivity or reactivity.
One field of particular interest is that of enantioselective reactions, where asymmetric catalysts change their selectivity in response to an external influence.[145] Feringa and colleagues developed a light- and temperature-controlled system, based on the core structure of a molecular motor, where an alkene with catalytically active substituents can be sequentially switched between helical states of different selectivity (see Figure 3-1, *top*).[146-148] Yu *et al*. realized a photoswitchable helicene containing a 4-aminopyridine unit for enantiodivergent Steglich rearrangements.[149]
A heat-controlled system for enantioselective hydrogenation reactions, developed by Trapp and co-workers has already been mentioned in the previous chapter. They modified Rh- and Ir-BIPHEP complexes with chiral esters as auxiliary groups in 3,3'-position. The resulting catalyst underwent heat-driven conversion of the previously major ligand rotamer into the minor one changing the selectivity of the catalyst as a result (see Figure 3-1, *bottom*).[53,54] In other examples, helical polymer structures were equipped with catalytically active centers that gave high enantioselectivities in a number of different transformations. Controlling the helicity of the polymer by solvent change allowed for a reversal of selectivity.[73,150]
In nature, many allosteric systems are controlled by co-factors and system change is evoked by non-covalent interaction. This requires a stereodynamic element within the catalyst structure that responds to interaction with a chiral or achiral molecule. In a system where exchange occurs between two enantiomeric conformers of the catalyst, this interaction produces two diastereomeric, energetically different states of which the more energetically favourable one subsequently accumulates. This concept of *deracemization* as a result of *chirality transfer* was employed in the context of chiral sensing, where chiral analytes interact with a stereodynamic sensor (see Figure 3-2). Canary and Anslyn developed copper complexes that could be used to determine the enantiomeric composition of different coordinating compounds in solution.[151] Wolf and coworkers developed stereodynamic phosphine-palladium complexes for the same purpose.[152]

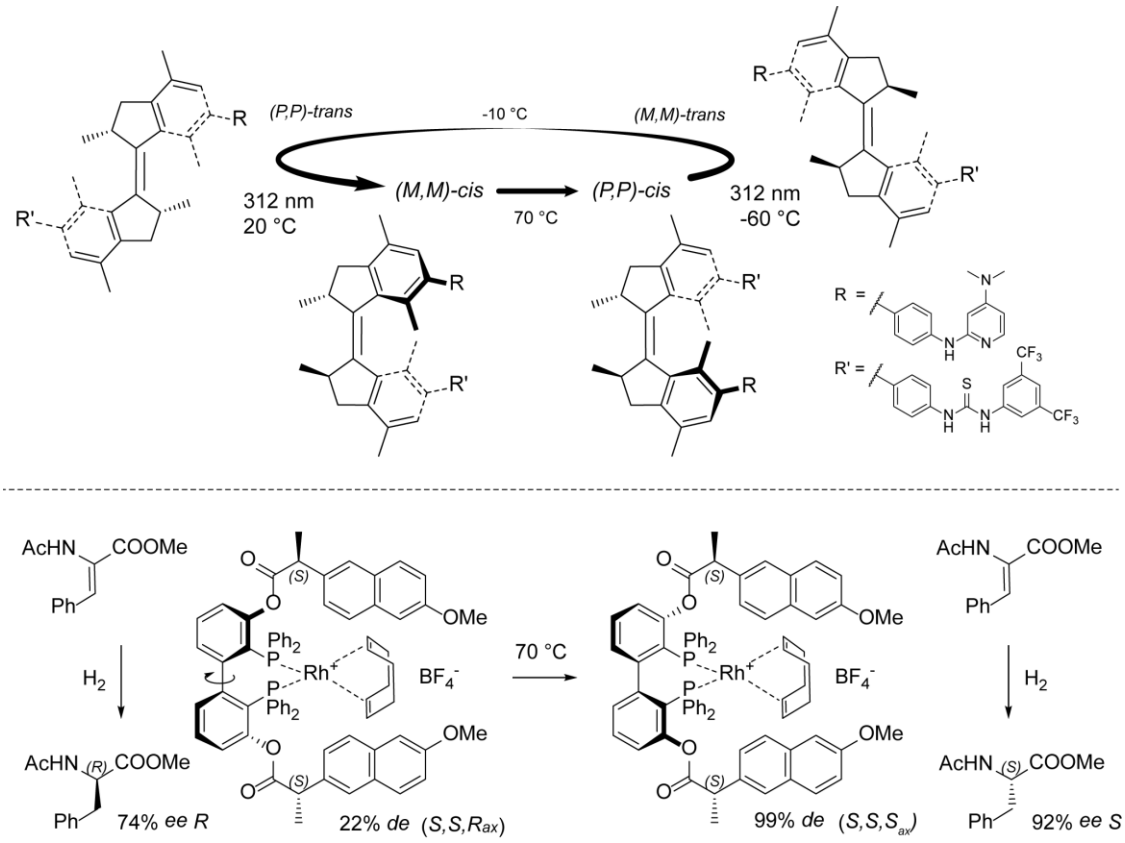

Figure 3-1: *Top*: Light- and heat-driven switch by Feringa *et al.* that serves as organocatalyst in asymmetric 1,4-addition reactions between thiols and α,β-unsaturated ketones.[146] Changing the ligand state alters selectivity of the reaction. *Bottom*: Example for temperature-controlled selectivity during asymmetric hydrogenation reactions by Trapp *et al*. Naproxene-based auxiliary groups on a bisphosphine ligand yield thermodynamically unfavourable rotamer as major species, whose isomerization is kinetically inhibited.[53] Thermal treatment allows for reversal of catalyst selectivity.

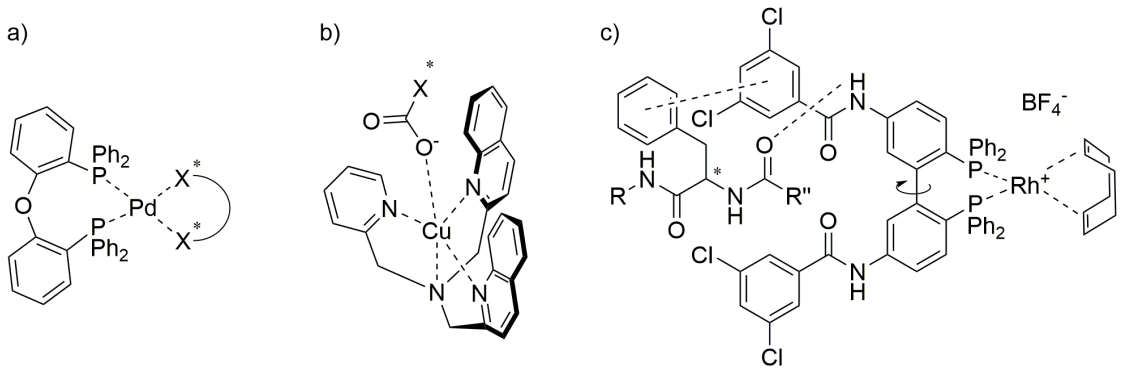

Figure 3-2: Chiral sensors for determination of enantiomeric compositions of small molecules in solution including a) biaryl ether developed by Wolf *et al.* for sensing of bidentate diamines or amino alcohols,[152] b) quinoline-based copper complex coordinating chiral carboxylic acids by Canary and Anslyn[151] and c) *tropos* BIPHEP ligand for sensing of chiral, amino acid-derived diamides by Trapp *et al*.[76] A suggested interaction patterns is shown.

Regarding enantioselective catalysts, some examples of *tropos* catalysts that were enantiomerically enriched by employing chiral co-ligands have already been covered in the previous chapter (see page 6). Furthermore, Suginome *et al*. presented the deracemization of helical polymer structures in presence of chiral additives[153]. Supramolecular structures could be realized in which enantioselective self-aggregation of achiral ligands takes place in the presence of a chiral co-monomer to yield a supramolecular, helical copper catalyst for enantioselective ketone reduction.[154]

In all these systems, a fundamental requirement is strong and diastereoselective non-covalent interaction between the stereoinducing additive and the two enantiotopic catalyst structures in order to generate a large energy gap between the two catalyst states. As already set out in the previous chapter, it serves the purpose to lent structural elements from interaction sites of established HPLC and GC phases. Originally developed by Okamoto *et al*. as selectors in cellulose-based CSPs,[155,156] Trapp and Storch implemented 3,5-dichlorocarbamate-derived moieties into stereodynamic Rh complexes to act as non-covalent interaction sites.[157,158] The respective racemic 5,5'-substituted BIPHEP complex could be used as a chiral sensor to determine the enantiomeric composition of different amino acid derivatives in solution.[76] In addition, a similar racemic phosphinite ligand was devised whose Rh complex **H-32** undergoes rotamer enrichment of the ligand in the presence of a chiral amino acid-derived additive (see Figure 3-3). Employing AcNH-Phe-NHMe (**8**) as additive, a deracemization of the complex to 10% *ee* could be achieved at room temperature, which increased up to 38% *ee* when the mixture was cooled to -38 °C. Due to the achiral nature of the ligand, the S_{ax} rotamer and the R_{ax} rotamer could be enriched by employing either the *S* or the *R* additive. Stereo-enriched catalyst mixtures could subsequently be employed in enantioselective hydrogenation experiments to give up to 12 % *ee* during reduction of methyl 2-acetamido cinnamate.[41]

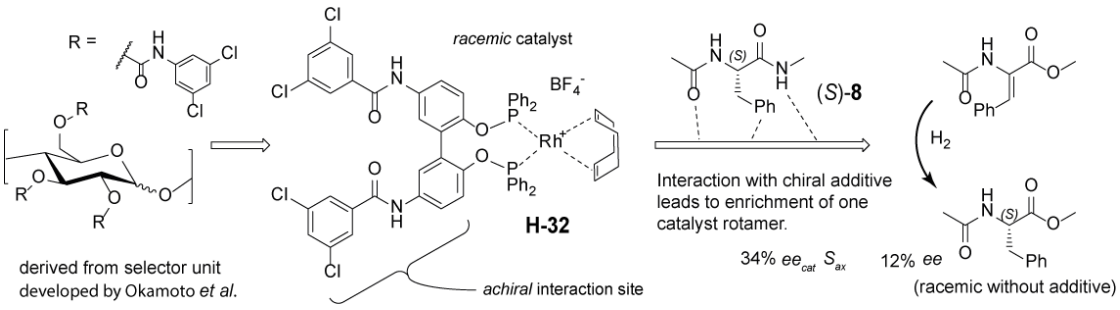

Figure 3-3: Stereodynamic ligand developed by Trapp *et al.* bearing interaction sites derived from high-performance HPLC column selectors. Phosphinite ligand undergoes rotameric enrichment in the presence of amino acid-derived diamides generating optically active hydrogenation products in subsequent asymmetric transformations.[41]

3.2 Objective

The first part of this project was set around the attempt to increase the selectivity of the previously investigated, racemic complex **H-32**. Since non-covalent interactions between the selector site and various additives had already been extensively investigated in the previous study, present efforts focused on modification of the ligand core by introducing stereodirecting groups in the 3,3' position of the ligand. Very little detailed information is available on how substitution of the ligand core of *tropos* biphenyl-based bisphosphinite ligands affects the stereodynamic behaviour. Unquestionably, large substituents increase the barrier of rotation due to the *buttressing*-effect,[93] which could impede de-racemization at lower temperatures. It was thus decided to modify the racemic bisphosphinite developed by Trapp *et al*. with small methyl groups. A synthetic strategy was to be developed and the impact of the 3,3'-substituens on the deracemization process as well as the improvement of selectivity during subsequent catalysis was to be investigated.

By extending the ligand spectrum, the second part of the project was built on knowledge gained on diamido-substituted bisphosphinite ligands, presented in the previous chapter. In this context, it was to be investigated whether achiral, diamide-based selectors such as ^{t}BuNH-Gly-NH or racemic *rac*-^{t}BuNH-Phe-NH are also suitable for generating racemic, switchable ligands whose stereoselectivity can be controlled by chirality transfer from chiral additives.

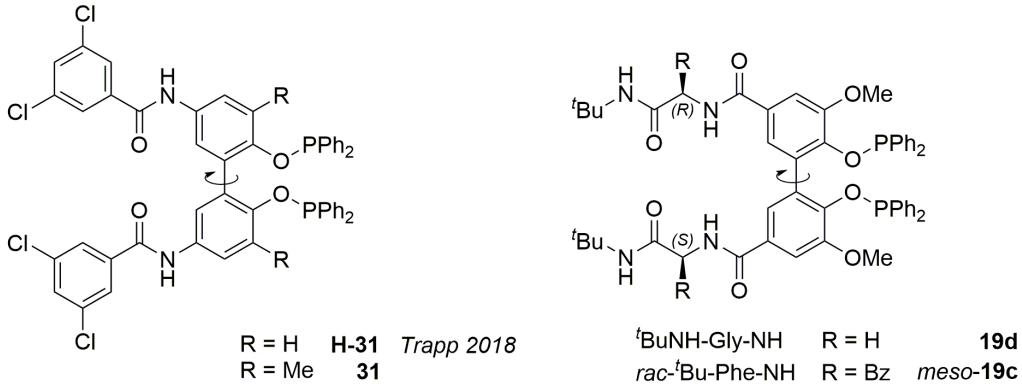

Figure 3-4: Racemic bisphosphinite ligands with achiral or chiral, racemic selector moieties in 5,5'-position to be investigated for their capacity in chirality transfer experiments to give enantiomerically enriched catalysts for asymmetric hydrogenation reactions.

3.3 Investigation of *tropos* ligands with achiral 3,5-dichlorobenzoyl selector sites

3.3.1 Synthesis

In the original approach, synthesis of the ligand was realized by nitration of biphenol in HNO_3/AcOH, protection of the phenol groups with allyl bromide, subsequent reduction of nitro groups using $SnCl_2$ and coupling of resulting amines with 3,5-dichlorobenzoic acid chloride. Final deprotection with a palladium catalyst and treatment of the diol with chlorodiphenylphosphine yielded the desired ligand. Unfortunately, implementation of a reaction step to methylate the biaryl backbone in 3,3'-position into this reaction sequence was unsuccessful due to insolubility of intermediates or compound decomposition under previously employed reaction conditions.

Consequently, an alternative reactions sequence was developed (see Figure 3-5). According to a known procedure by Pfaltz and co-workers, biphenol was methylated in 3,3'-position.[159] Attempts to nitrate compound **28** using nitric acid repeatedly failed due to product decomposition. Employing a slightly modified procedure from Gaude, Le Goaller and Pierre allowed for the synthesis of **29** in a biphasic system under mild conditions.[160] Subsequent reduction of the nitro groups and introduction of the achiral selector moieties was done using the previously established protocol by Trapp *et al.*, which was slightly adapted.[41] Finally, treatment of the resulting biphenol **30** with PPh_2Cl in presence of DABCO yielded the desired bisphosphinite ligand **31** which was complexated to a rhodium precursor to give the final catalyst **32**.
A phosphoramidite-based catalyst was also synthesized. The respective ligand could easily be prepared from diol precursor **30** by refluxing in toluene in presence of $P(NEt_2)_3$ to yield compound **33**. Subsequent complexation gave catalyst **34** (see Figure 3-6).

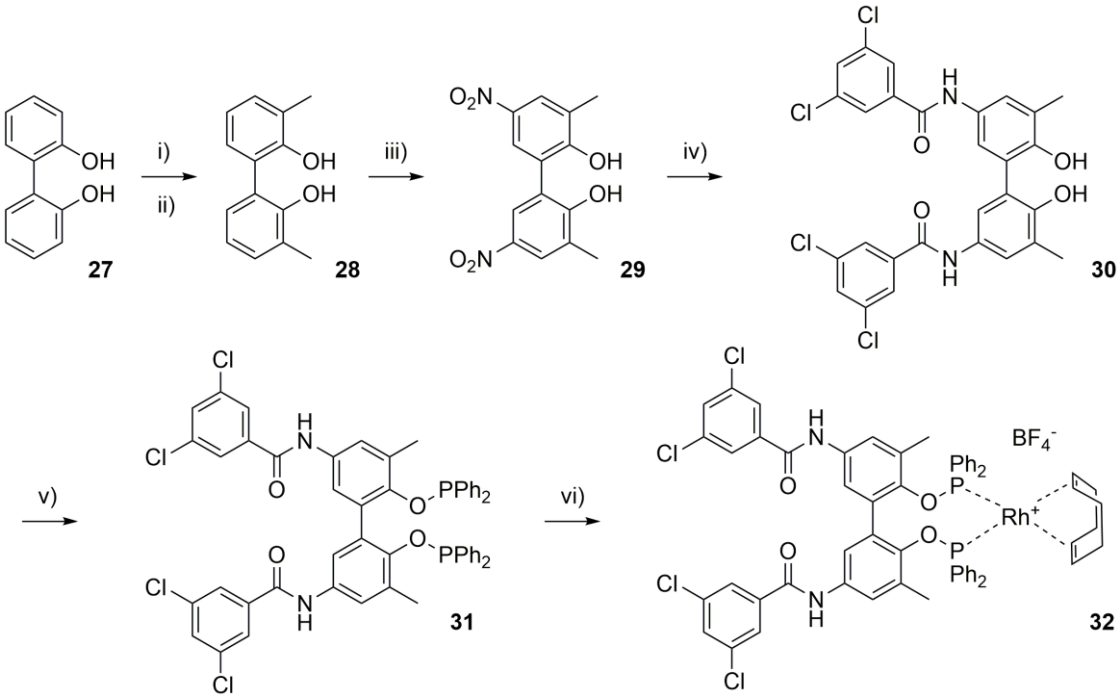

Figure 3-5: Synthesis of bisphosphinite complex **32**, i) CH_3OCH_2Cl, NaH, 61%, ii) BuLi, MeI, then HCl in isopropanol 38%, iii) $NaNO_3$, HCl, 64%, iv) $SnCl_2$, HCl, $Cl_2C_6H_3COCl$, triethylamine, then $H_2NCH_2CH_2NMe_2$, 83%, v) PPh_2Cl, 1,4-diazabicyclo[2.2.2]octane, 73%, vi) $[Rh(COD)_2]BF_4$, 71%.

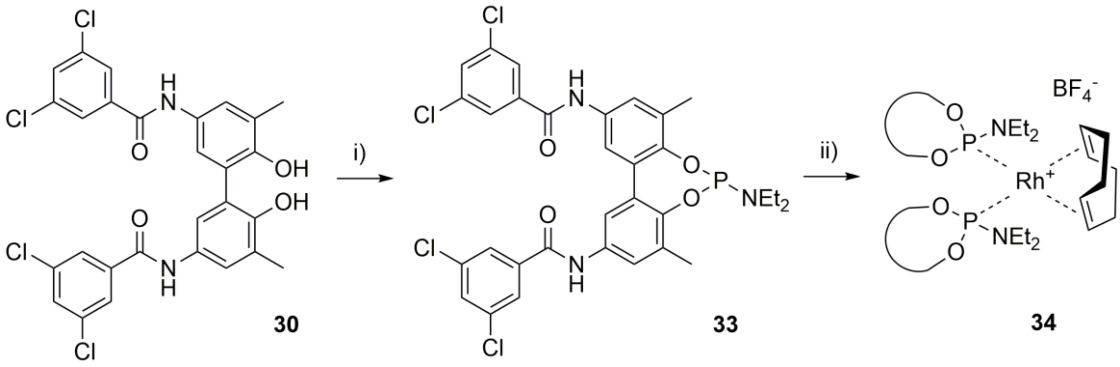

Figure 3-6: Synthesis of phosphoramidite complex **34**: i) $P(NEt_2)_3$, 91 %, ii) $[Rh(COD)_2]BF_4$, *in situ.*

3.3.2 Ligand deracemization and hydrogenation experiments

To compare complex **32** to previously investigated catalyst **H-32**, the same chirality transfer experiment was conducted. Catalyst **32** and diamide (*S*)-**8** were dissolved in dry and degassed chloroform and their interaction was monitored by ^{1}H NMR spectroscopy. In similar observations to those made by Trapp and co-workers, the amide protons of the selector moiety underwent significant splitting in presence of the chiral additive which is owed to formation of diastereomeric, supramolecular complexes between the diamide and the two enantiomeric rotamers of the complex (see Figure 3-7). The splitting increases at lower temperatures indicating an even stronger differentiation between the two ligand states. Interaction with the chiral additive removes energetic degeneration of the two ligand isomers leading to rotameric enrichment of the energetically favoured S_{ax} species. Assignment of rotamer species was done on the basis of results for the unmethylated catalyst **H-32**, where identical behaviour was assumed. At 22 °C, a distribution of 56:44 (S_{ax}:R_{ax}, 12% *ee*) and a signal splitting of 381 ppb was observed, which is about 80 ppb above of what was observed for **H-32**. A similar result had been obtained with the unmethylated system previously investigated by Trapp *et al.* and cooling the mixture to -38 °C had been found to significantly increase deracemization. Disappointingly, no significant improvement of the enantiomeric excess of complex **32** could be achieved, when the sample was cooled, but signal splitting increased to 510 ppb. Accordingly, hydrogenation of methyl 2-acetamidocinnemate **20** using stereo-enriched complex mixtures at -20 °C gave only a slight enantiomeric excess of 4 % *ee S* for the respective product and a complete racemate was obtained when the reaction was repeated at room temperature.

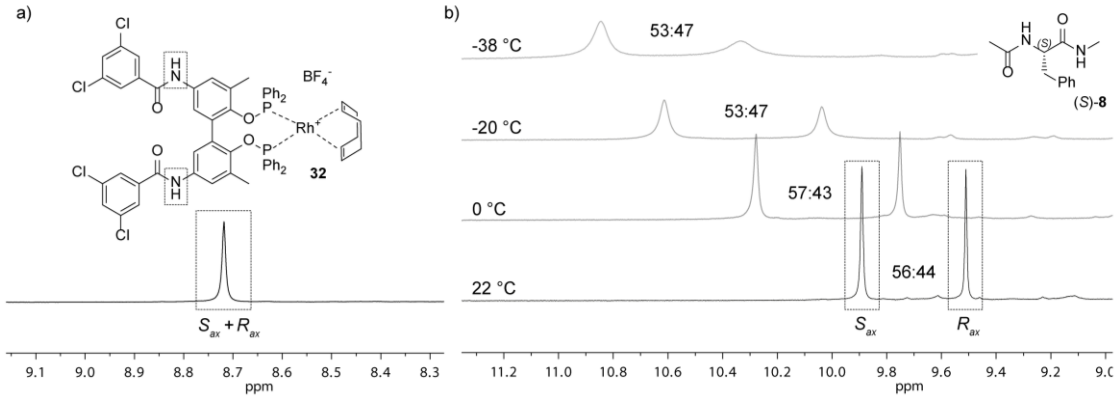

Figure 3-7: a) Section of ^{1}H NMR spectrum of **32** shows superimposed signals of the amide protons of both rotamers. b) Interaction studies with phenylalanine-derived diamide (*S*)-**8** (in dry and degassed $CDCl_3$, 6.5 mM in complex with 5 eq. diamide) show strong signal splitting of the two rotamers for the amide proton due to diastereotopic, non-covalent interaction of additive and selector sites along with minor enrichment of the energetically favoured S_{ax} rotamer.

Since increased signal splitting of the catalyst's amide proton in the ^{1}H NMR spectrum with lower temperature (510 ppb at -38 °C) contradicts a decrease of interaction strength and enantiodifferentiation compared to un-methylated complex **H-32**, the increased rotational barrier was believed to inhibit deracemization at lower temperatures. Consequently, it was attempted to use phosphoramidite ligand **33**, which bears the same ligand backbone, but is believed to have a much lower barrier of inversion. Changing the ligand type, however, did not lead to an improvement of selectivity for the subsequent catalysis. Using catalyst **34** and additive (*S*)-**8** and only

racemates were obtained when hydrogenation reactions were run at room temperature or at -20 °C.

3.4 Investigation of *tropos* ligands with amino acid-based-selector sites

3.4.1 Deracemization and hydrogenation experiments with a glycine-based bisphosphinite ligand

To enlarge the spectrum of investigated racemic, "switchable" ligands, further investigations were performed on ligand **19d**, which has already been introduced in chapter 2.4.1, page 17. As all investigated *tropos* bisphosphinite ligands, compound **19d** undergoes spontaneous, quantitative dimerization yielding a C_2-symmetric, hydrogen bonded complex with unsymmetrical subunits. Since the glycine-based selector sites do not contain a stereochemical bias, a racemic mixture of (S_{ax}/S_{ax})-**19d** and (R_{ax}/R_{ax})-**19d** is formed. Given the high interaction strength of the diamide selectors that is evident from the dimerization, it seemed promising to further investigate, if chirality transfer could be accomplished on this ligand. This seems especially true since NMR data of compound **19d**, unlike those of compounds **19a-c**, show significant line broadening at room temperature and spectra had to be recorded at -20°C to be interpretable, indicating enhanced dynamic and chemical exchange. As stereo-aligning agents, different amino acid derivatives were chosen. In accordance with literature[83] and with previously observed interaction patterns between ligand selector moieties in the dimeric ligand structure, a pincer-like coordination of small diamide derivatives was expected (see Figure 3-8).

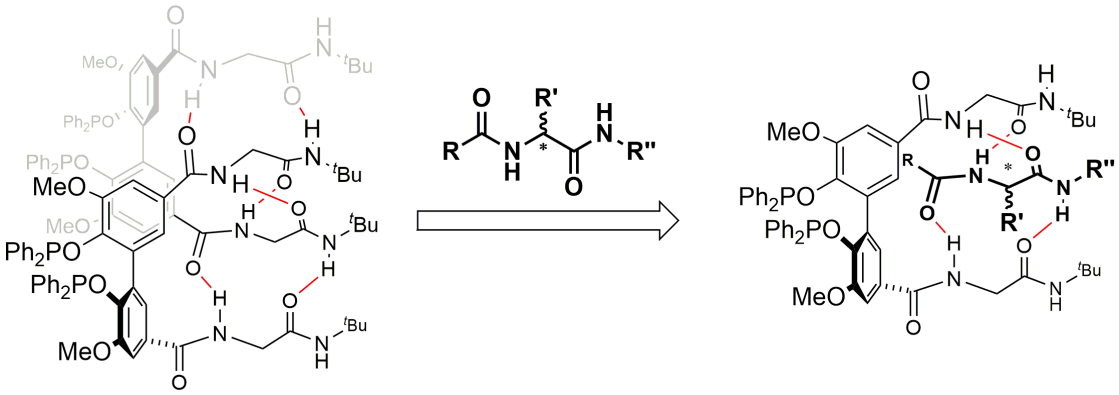

Figure 3-8: Expected interaction pattern between ligand **19d** and chiral, amino acid-derived diamides that can induce ligand deracemization.

When interaction of racemic ligand **19d** with (*S*)-**8** was investigated by ^{31}P NMR spectroscopy in dry and degassed THF-d8, formation of a new singlet signal was observed at -20 °C, which had a relative intensity of 1:8 compared to the dimerized ligand. However, treatment of the ligand with [Rh(COD)$_2$]BF$_4$, before or after alignment, yielded a very unselective catalyst and 5% *ee R* were obtained for product **13** during subsequent hydrogenation of methyl 2-acetamidoacrylate **12** (see Table 3-1, entry 2). Intriguingly, repeating the experiment with selector-like additive (*S*)-**25** yielded intensely broadened, uninterpretable ^{31}P NMR spectra and hydrogenation afforded the product with 14% *ee R* (entry 3). As expected, employment of (*R*)-**25** gave the opposite selectivity (entry 4). Strong dependency of the alignment on additive's substitution pattern was confirmed in following experiments where dichlorophenyl-substituted (*S*)-**9** could induce 34% *ee R* (entry 5), while methyl amide **10** gave a much less selective catalyst (7% *ee R*, entry 6)

and 3-nitrophenyl analogue **35** failed to induce any selectivity at all (entry 8). In a final experiment, the catalyst was treated with tetraamide **24**, which has the ability to undergo the same form of dimerization as the catalyst itself and was thus considered to be a much better competitor to the catalysts self-interaction. Employing this catalytic mixture, prochiral olefin **12** could be hydrogenated with 41% *ee R*.

Table 3-1: Asymmetric hydrogenation of methyl 2-acetamidoacrylate 12 using racemic catalyst with ligand 19d after pre-alignment with different additives.

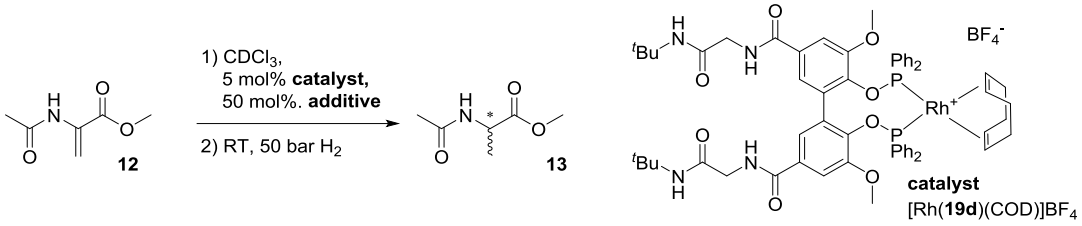

Entry[a]	Additive		ee %[b]	Entry	Additive		ee %
1	-		*rac*	**5**[c]	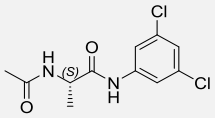	(*S*)-**9**	34 *R*
2	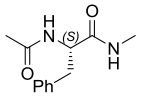	(*S*)-**8**	5 *R*	**6**	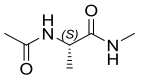	(*S*)-**10**	7 *R*
3	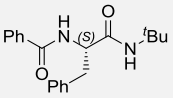	(*S*)-**25**	14 *R*	**7**[c]	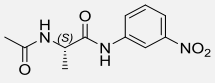	(*S*)-**35**	1 *R*
4	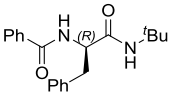	(*R*)-**25**	14 *S*	**8**[d]	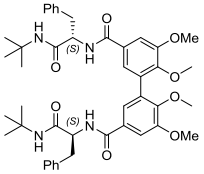	**24**	41 *S*

a) Complex was allowed to equilibrate in presence of additive for 16 hours at room temperature before addition of substrate and subsequent hydrogenation. Detailed experimental protocol can be found in chapter 7.3.11, page 131. All reactions showed full conversion. b) Enantiomeric excess was determined using chiral GC. c) Only 5 eq. of the additive were used and additive did not fully dissolve. d) Only 5 eq. of the additive were used.

3.4.2 Deracemization and hydrogenation experiments with a bisphosphinite ligand bearing racemic phenylalanine selector units

Due to the self-sorting behaviour of the catalyst, it seems plausible to investigate if the ligand's self-interaction adversely affects the level of alignment that is reached using additives mentioned above. Consequently, it was attempted to further destabilize supramolecular catalyst structure in order to enhance competitiveness of these additives over the ligand's interaction sites. To maintain the selectors interaction strength, both secondary amide functionalities were to be preserved. Therefore, the effect of implementing racemic phenylalanine-based selector moieties into the ligand backbone was investigated. This substitution pattern would lead to a formally achiral, racemic ligand *meso*-**19c** and it was expected that opposing chiral information in the ligand selector units would form a "mismatch" during dimerization and destabilize the supramolecular structure.

The desired catalyst could conveniently be synthesized by the same procedure as all previous bisphosphinites of similar structure. Since a stereoselective attachment of selector groups appeared too laborious, the respective diol precursor *meso*-**19c** was synthesized by coupling a racemic mixture of the selector groups. A mixture of stereoisomers (*S,S*)-**19c**:*meso*-**19c**:(*R,R*)-**19c** in a ratio of 1:2:1 was obtained and the desired *meso* diastereomer could be isolated by flash chromatography. Intriguingly, no second set of signals was observed for *meso*-**19c** in the ^{1}H NMR spectrum (see Figure 3-9)

This is a clear sign that the compound does not form the same stable, dimeric structure observed for compounds with homochiral selectors and instead retains a much higher dynamic leading to a C_2-symmetric state in solution. The subsequently formed bisphosphinite ligand *meso*-**19c** exhibited similar characteristics of internal symmetry and signal broadening through increased molecular dynamic as evident from the broad singlet signal observed in the respective ^{31}P NMR spectrum. Complexation of the ligand to a rhodium precursor lead to signal splitting caused by Rh-P coupling, as well as, P-P coupling of non-equivalent halves of the molecule as a result of slower rate of isomerization.

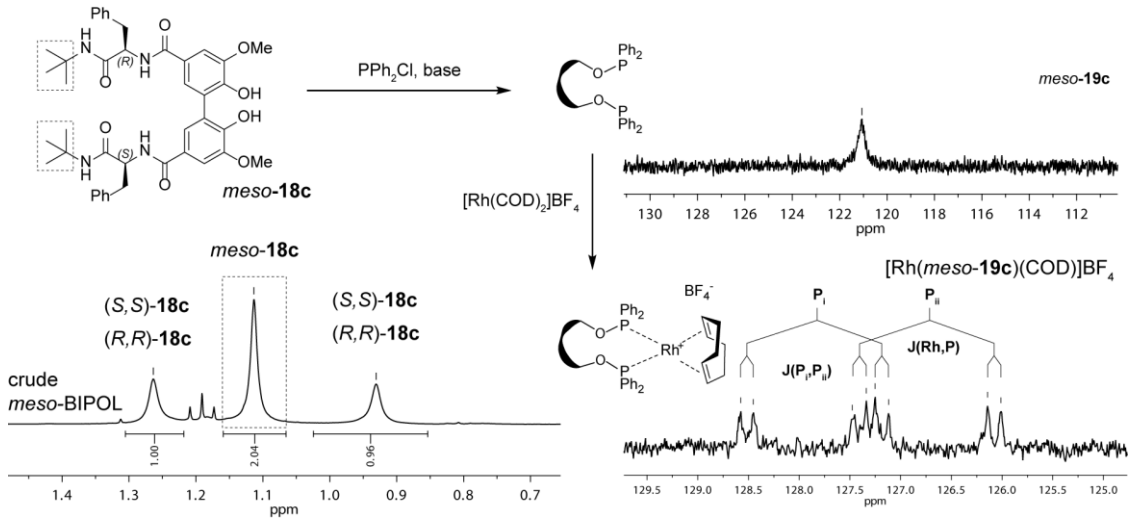

Figure 3-9: *Left*: Section of ^{1}H NMR spectrum showing ^{t}Bu protons of all three stereoisomers of X, which can be separated by flush chromatography. Homochiral diols form dimers represented by two singlet signals. *Meso*-**19c** did not readily dimerize, hence, only one singlet was detected. *Top right*: ^{31}P NMR spectrum of *meso*-**19c** shows a single, broad singlet. *Bottom right*: ^{31}P NMR spectrum of the respective Rh complex.

Addition of chiral diamides to the ligand or its complex did not lead to a visible change in the ^{31}P or ^{1}H NMR spectra and intense line broadening was still observed even at -40 °C. Ligand *meso*-**19c** was subsequently employed in asymmetric hydrogenation reactions of olefin **12** (see Table 3-2). A racemate was obtained, when no chiral additive was present. Once more, pre-aligning the catalyst for 16 hours using a range of chiral diamides gave enantioenriched hydrogenation products. Similar trends and selectivities compared to those previously found for glycine-based compound **19d** were obtained. Among diamide additives, the highest selectivity could be induced with alanine derivative (*S*)-**9** (23% *ee R*, entry 3). When tetraamide **24** was employed as stereoinducing agent, the enantiomeric excess of the reduction could be increased to 46% *ee R* (entry 10).

Table 3-2: Asymmetric hydrogenation of methyl 2-acetamidoacrylate 12 using a racemic catalyst with ligand *meso*-19c after pre-alignment with different additives.

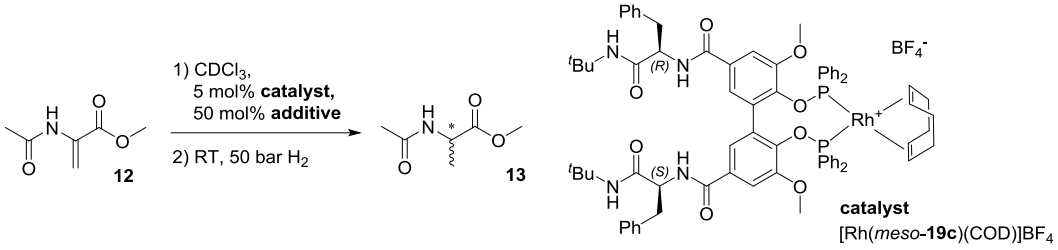

Entry[a]	Additive		*ee* %[b]	Entry	Additive		*ee* %
1	-		*rac*	**6**	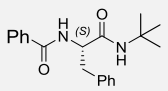	(*S*)-**25**	14 *R*
2	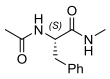	(*S*)-**8**	1 *R*	**7**	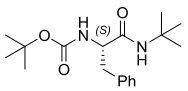	(*S*)-**S5**	3 *R*
3[c]	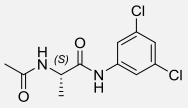	(*S*)-**9**	23 *R*	**8**[c]	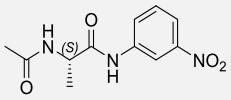	(*S*)-**35**	1 *R*
4	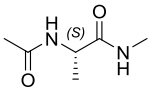	(*S*)-**10**	6 *R*	**9**	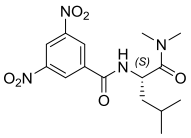	(*S*)-**36**	5 *R*
5	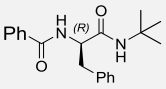	(*R*)-**25**	14 *S*	**10**[d]	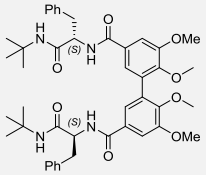	**24**	46 *R*

a) Complex was allowed to equilibrate in presence of additive for 16 hours at room temperature before addition of the substrate and subsequent hydrogenation. Detailed experimental protocol can be found in chapter 7.3.11, page 131. All reactions showed full conversion. b) Enantiomeric excess was determined using chiral GC. c) Additive did not completely dissolve. d) Only 5 eq. of the additive were used.

3.4.3 Ligand comparison

The similar extent of chirality transfer compared to glycine-based ligand **19d** suggests, that ligand dimerization does not adversely affect the level of chiral induction. It can be assumed that fast chemical exchange among supramolecular structures, previously also observed for similar compounds with chiral, enantiopure selectors (see page 20), still allows for chiral additives to intervene and occupy bonding sites. The subtle differences in selectivity that were achieved between both ligand types can be understood by acknowledging that ligand *meso*-**19c** bears additional phenyl groups that might be beneficial for certain non-covalent interaction modes. However, the individual chiral selector sites can be expected to have a greatly reduced level of interaction with additives of the opposite chirality, meaning that only one out of two selectors on each molecule effectively bonds with stereoinducing additives during alignment. This clearly reduces the overall extent of the interaction, something that is not to be expected for ligand **19d** which that bears achiral selector sites.

3.5 Results

In this chapter, a number of different, racemic ligands have been investigated for their potential as switchable catalysts, that deracemize due to non-covalent interactions with chiral amino acid derivatives in solution.

In the first part, a bisphosphinite ligand bearing 3,5-dichlorobenzoyl moieties as selector sites, previously investigated by Trapp *et al*., has been modified with methyl groups in 3,3'-position to investigate potential improvements of chirality transfer onto the ligand and of selectivity in subsequent asymmetric hydrogenation reactions of prochiral substrates. Unfortunately, the substitution was found to inhibit deracemization of the Rh complex of ligand **31** at lower temperatures, presumably due to an increased rotational barrier, and only a maximum deracemization to a *dr* of 57:43 (S_{ax}:R_{ax}) could be achieved.

Based on these results, highly stereodynamic phosphoramidite ligand **33** was subsequently synthesized from the same ligand precursor. Attempts to generate a stereoselective catalyst through non-covalent interaction with chiral additives failed and yet again subsequent hydrogenation reactions gave only racemates.

In the second part of the project, racemic ligands bearing 5,5'-diamido selector moieties were investigated. Self-aggregating ligand **19d** with glycine-derived selector sites could successfully be aligned by allowing the respective Rh complex to interact with different amino acid-derived diamide additives. The switchable nature of the catalyst was verified by employing both enantiomers of phenylalanine derivative **25** separately as aligning agents where subsequent hydrogenation of **12** gave products in 14% *ee S* or *R* when the *R* or the *S* additive was used. Among other diamides, alanine-derived compound (*S*)-**9** showed the biggest alignment potential allowing for reduction to proceed with 34% *ee R*. When ligand-mimicking tetraamide **24** was employed selectivity could be increased further to 41% *ee R* due to a higher stability of the ligand-additive adduct.

To reduce ligand-ligand interaction by employing "mismatching" selector units, bisphosphinite ligand *meso*-**19c** bearing racemic phenylalanine-derived interaction sites was devised. The ligand was found not to form stable supramolecular dimers and again, significant chirality transfer could be achieved. Selectivities were similar to those obtained with catalyst **19d.** Best results using diamide additives were again achieved with alanine-derived compound (*S*)-**9** yielding methyl 2-acetamidoalanate **13** with 23% *ee R*. As with ligand **19d**, selectivity could be further increased by deracemization of *meso*-**19c** with tetraamide **24** where a selectivity of 46% *ee R* was obtained.

The similar extent of alignment found to occur with both achiral ligand types suggests, that ligand dimerization does not adversely affect the degree of chirality transfer, potentially due to fast chemical exchange among supramolecular compounds that allows chiral additives to intervene and occupy bonding sites.

4 Development of a reaction with enantioselective self-inhibiting properties

4.1 State of knowledge

Among the most intriguing phenomena that occurred during the evolution of life is the adaptation of homochirality and nature's ability to maintain this state of enantiopurity. The chemical pathway that led to this state is yet unidentified and various aspects such as the initiating impulse that caused deviation from a racemic state and the subsequent increase of the initial enantiomeric surplus are controversially discussed on a practical[18,161-165] as well as on a theoretical level.[19,20,166-168] An often proposed scenario concerning the augmentation of an enantiomeric excess is a self-reinforcing system, where an initial deviation from a racemic state is sustained and extended by its own involvement. The strive for a better understanding of the various aspects of such systems on a molecular level has sparked great interest in the studies of asymmetric, autoinductive, self-amplifying reactions.

At its core, an *autoinductive* asymmetric reaction is based on the participation of a chiral reaction product in the production of itself. Different scenarios include catalytical activity of the product molecules as such or the incorporation of the product into a more complex catalyst. Considering a *self-amplifying* reaction adds an additional layer of complexity. Long ahead of the first experimental realization of such a reaction, Frank described the crucial, underlying principle of "mutual antagonism".[20] The desired reaction must be assisted by the inducing product species and the undesired reaction must simultaneously be suppressed in order to prevent a drop in selectivity. This fundamental process manifests in the emergence of non-linear effects (NLE) which signify an increased optical purity (*positive* NLE) or a decreased optical purity (*negative* NLE) of the reaction product compared to the purity of the initially employed catalyst. Such non-linearities root in the different properties of racemates compared to optically pure compounds, which is a long known phenomenon that has been studied – *inter alia* – in the context of the NMR spectroscopic non-equivalence of enantiomers,[169-171] the enantiomeric separations in liquid chromatography using an achiral stationary phase[172-174] or other physical properties.[175-177] Non-linear effects in asymmetric catalysis have been intensely studied, among others, by Kagan and Noyori.[23,26,178-180] A famous example is the asymmetric alkylation of aldehydes that is catalysed by 3-exo-(dimethylamino)isoborneol (DAIB) zinc complexes discovered by Noyori *et al*.[181] When a mixture of both ligand enantiomers is employed, formation of catalyst dimers leads to artificial increase in the ligands enantiopurity, which is caused by the higher stability of the inactive *meso* catalyst complex (see Figure 4-1).

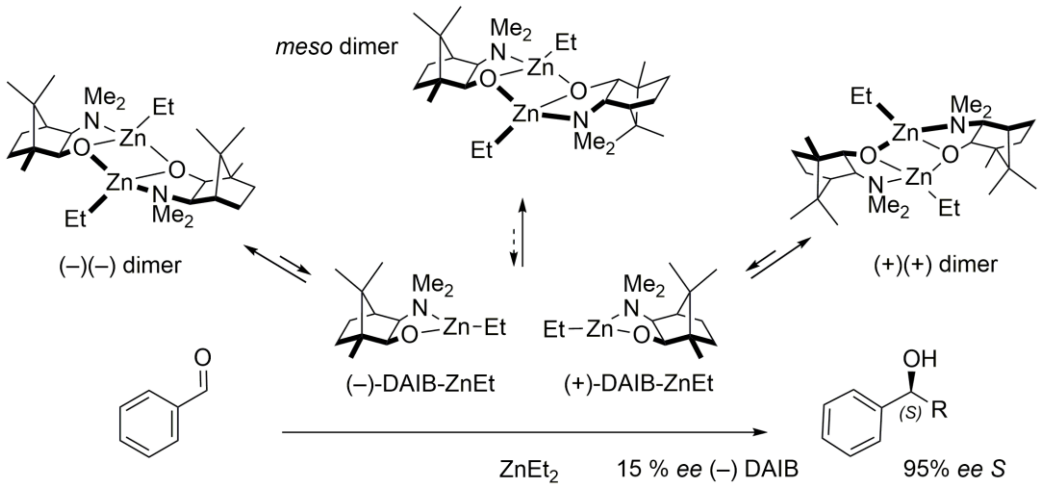

Figure 4-1: Asymmetric alkylation of benzaldehyde with enantioenriched DAIB by Noyori *et al.* shows positive non-linear effects on the enantiomeric distribution of produced benzylic alcohol.[181] Formation of catalyst dimers of which the *meso* form was found to have a greater stability than the two homochiral complexes artificially increases enantiomeric excess of the catalytically active monomer.

The first experimental example that incorporated these principles to achieve a self-amplifying reaction was delivered by Wynberg and Alberts, who demonstrated autoinductive effect during the reaction of benzaldehyde and ethyl lithium by employing deuterated reaction products as chiral initiators.[182] Wynberg and Feringa later took advantage of intermolecular interactions during the oxidative coupling of chiral phenols and camphor to obtain homochiral dimers.[183] Danda *et al*. and Shvo *et al*.[184] reported NLEs and self-amplifying properties during enantioselective hydrocyanation reactions on aldehydes catalysed by cyclic diamides.[185] Similarly, Figadère and co-worker realized an autoinductive aldol reaction where 2-trimethylsilyloxyfuran reacts with prochiral aldehydes in the presence of a BINOL-Ti catalyst that gradually implements generated alcohol molecules into its structure.[186] An electro-cyclic, autoinductive reaction was reported by Wulff *et al*., who employed an aluminium complex of VAPOL ("vaulted biphenanthrol ligand") as catalyst for the Diels-Alder reaction between cyclopentadiene and methyl acrylate (see Figure 4-2).[187]

The most prominent example for a self-amplifying reaction is the Soai reaction in which substituted 5-pyrimidylaldehydes react with diisopropylzinc to form the corresponding pyrimidyl alcohols.[188] The reaction is catalyzed by zinc complexes of the produced pyrimidyl alcohol and governed by a strong positive NLE which is based on the kinetics of the complex reaction network for the formation of the different catalyst stereoisomers. A small initial enantiomeric excess of the pyrimidyl alcohol is sufficient to alkylate aldehydes with high enantioselectivities and re-employment of the enantioenriched product as ligand for following catalytic reaction allows for the generation of enantiopure compounds from almost racemic mixtures in only three consecutive runs (see Figure 4-3).[189] Initial dis-symmetrisation has also been achieved by using other small, chiral molecules or even chiral surfaces of organic or inorganic crystals.[190]

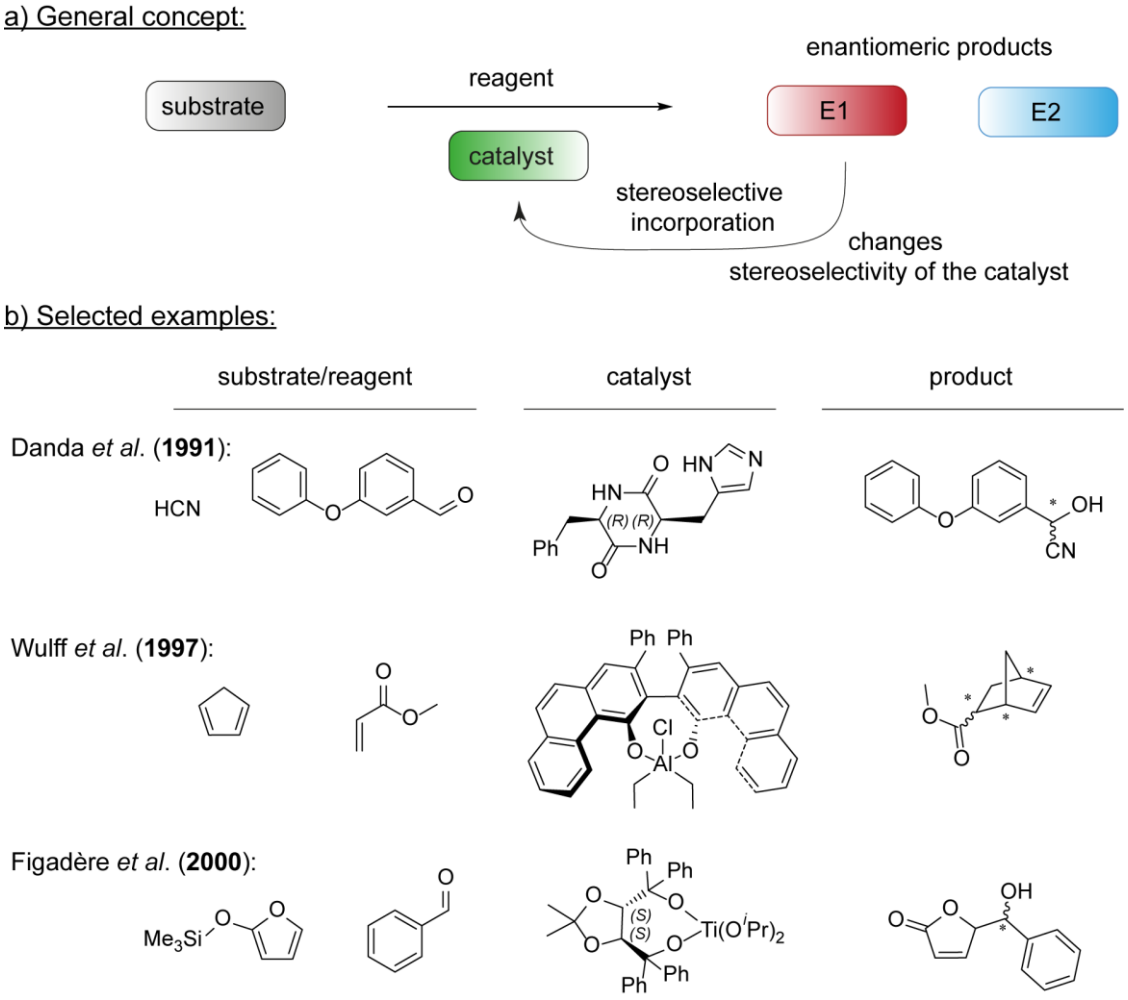

Figure 4-2: a) Concept of autocatalytic, self-amplifying reactions. A substrate is converted in presence of a catalyst, whose selectivity changes upon stereoselective incorporation of product molecules to increase selectivity of the catalyst overtime. b) Examples by Danda,[185] Wulff[187] and Figadère[186] and co-workers are shown.

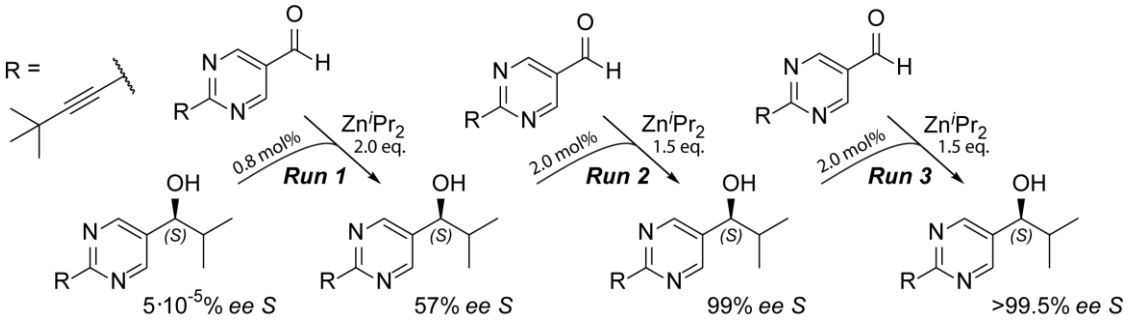

Figure 4-3: Illustration of the potential for self-amplification in the Soai reaction.[189] 5-Pyrimidylaldehyde is alkylated by diisopropylzinc. Addition of the reaction product in very low *ee* and consecutive recovery of newly formed alcohol as initiator for consecutive runs allows to obtain enantiopure product within two repetitions.

Trapp and Storch recently succeeded to develop a "by-design" catalyst system for the self-amplifying, asymmetric hydrogenation of prochiral olefins using a rhodium catalyst bearing *tropos* phosphoramidite ligands (see Figure 4-4).[40] During the hydrogenation reaction, the structure of the rhodium catalyst could be altered by strong, non-covalent interactions between the chiral reaction products and the interaction sites (selectors) on the ligands influencing the selectivity of the catalyst. In order to accomplish this, an interaction motive between (*S*)-*N*-pivaloylproline-3,5-dimethylanilide and (*S*)-*N*-(3,5-dinitrobenzoyl)leucine dimethylamide, developed by Pirkle and Murray,[77,78] was abstracted and structural elements were implemented into the hydrogenation product and the stereodynamic phosphoramidite ligand. During the design of the targeted system a number of crucial requirements were identified: 1) The dynamic nature of non-covalent interaction between the catalyst and the reaction products would allow for a constant adaptation to a changing product distribution, altering the selectivity of the catalyst as the reaction progresses. 2) Rapid chirality transfer from the chiral reaction product to the ligands should occur much faster than the hydrogenation of the substrate. 3) The interaction between the chiral selector sites and product molecules needs to be stereoselective in order to enhance the catalyst's selectivity for one particular product stereoisomer, while simultaneously supressing further formation of the other one ("mutual antagonism"). A number of different designed substrates where hydrogenated. As the catalyst's selectivity was found to be positively correlated to the level of interaction with product molecules, an increased enantiopurity of the reaction product was obtained at lower catalyst loadings.

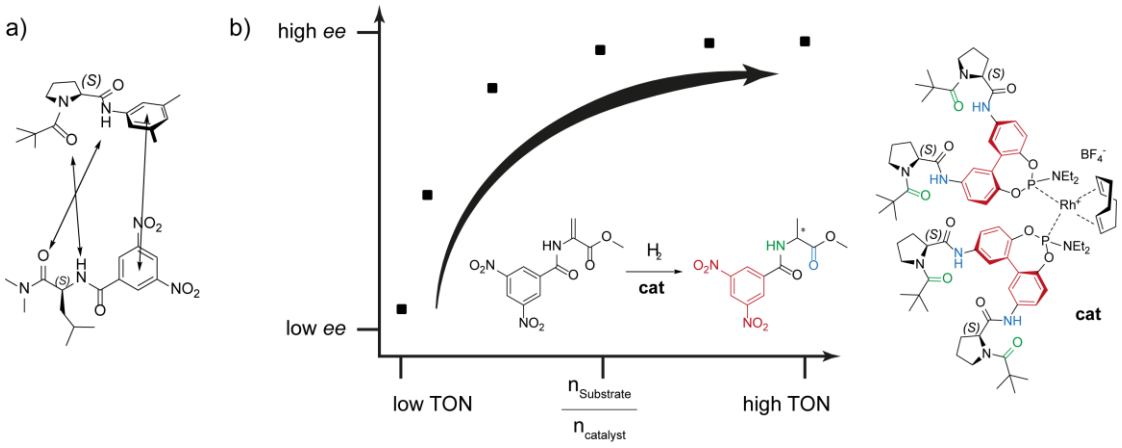

Figure 4-4: a) Chiral recognition model for the interaction pair investigated by Pirkle and Murray.[77,78] b) Illustration of self-amplifying catalysis developed by Trapp and Storch.[40] Stereoselective interaction of the reaction product with the phosphoramidite catalyst changes the selectivity of the reaction affording higher enantiomeric excesses when the turnover number increases.

4.2 Objective

It seems evident that an "inverse" model of an *autoinductive*, *self-inhibiting* reaction could be based on the same prerequisites as the ones identified by Trapp and Storch that were discussed above. Moreover, it would be of interest due to its complementary.
As before, utilizing chiral diamides as stereoinducing agent was believed to be a promising and convenient method, since these can be readily generated from suitable olefinic precursors by asymmetric hydrogenation. Catalyst alignment, driven by non-covalent interaction, and ensuing change of enantioselectivity during the reduction of the olefin would close the loop to an autoinductive cycle.
Studies detailed in chapters 2 have shown that appropriately substituted 2,2'-biphenyl ligands with phenylalanine-derived, diamide-based selectors in the 5,5'-position exhibit strong, enantioselective interaction with chiral amino acid-derived diamide residues or molecules bearing the same chiral information aligning the ligand to induce the opposite stereoinformation during the subsequent asymmetric hydrogenation of substituted olefins. Selectors bearing two secondary amide groups were thereby found to interact in a highly enantioselective manner, but efficient binding and an additional chelate effect led to formation of stable ligand dimers and a loss of the ligand's stereodynamics. Consequently, ligands bearing phenylalanine-derived amidoester selector moieties were chosen to be investigated, which were believed to have better balanced binding strength (see Figure 4-5).

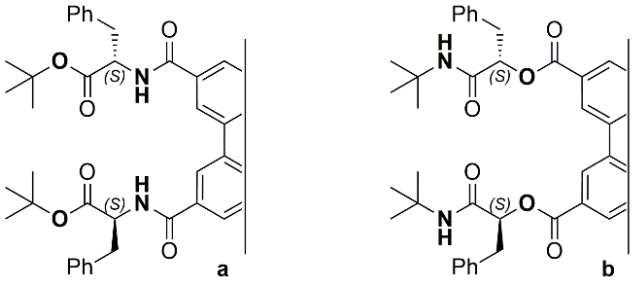

Figure 4-5: Ligands bearing phenylalanine-derived amidoester selectors in 5,5'-position to be investigated for their isomerization dynamics and their potential to align in presence of chiral amino-acid derived diamides.

In a two-step development process (1) interaction studies between each selector type **a** and **b** and different chiral additives were to be conducted in order to evaluate the capability of each selector unit to transfer chiral information from a chiral solute onto the *tropos* ligand and subsequently, (2) these insights were to be utilized to realize an asymmetric hydrogenation reaction that shows chiral, autoinductive self-inhibition, i.e. a reactions where a chiral hydrogenation product supresses its own formation.

4.3 Investigation of amidoester-based selector units for chiral induction

4.3.1 Ligand syntheses

Initial interaction studies on the potency of the selectors were performed on *tropos* bisphosphinite ligands, as their Rh complexes have a rotational barrier high enough to allows for a clear NMR spectroscopic differentiation of the two axial isomers, while equilibration and structural change of the ligand still readily occurs at room temperature. Moreover, the relationship between

the ligand's rotamer distribution and its enantioselectivity in asymmetric hydrogenation reactions is known and can be directly correlated. Syntheses of the ligands is depicted in Figure 4-6. Oxidative dimerization[111] of methyl 4-hydroxy-3-methoxybenzoate **14** and subsequent allyl protection of the hydroxy groups[191] gave diester **37** that was saponificated into dicarboxylic acid **38**. The selector attachment was achieved by two-fold coupling of (*S*)-phenylalanine *tert*-butyl ester hydrochloride to the corresponding bis(acid chloride) (**39a**) or by Steglich esterification of with (*S*)-2-hydroxy-3-phenylpropionic acid *tert*-butyl amide (**39b**). After removal of the phenol protecting groups to obtain BIPOLs **40a** und **40b**, these were treated with chlorodiphenylphosphine to yield the bisphosphinite ligands **41a** and **41b**. The corresponding Rh complexes **42a** and **42b** were prepared by reaction with $[Rh(COD)_2]BF_4$.

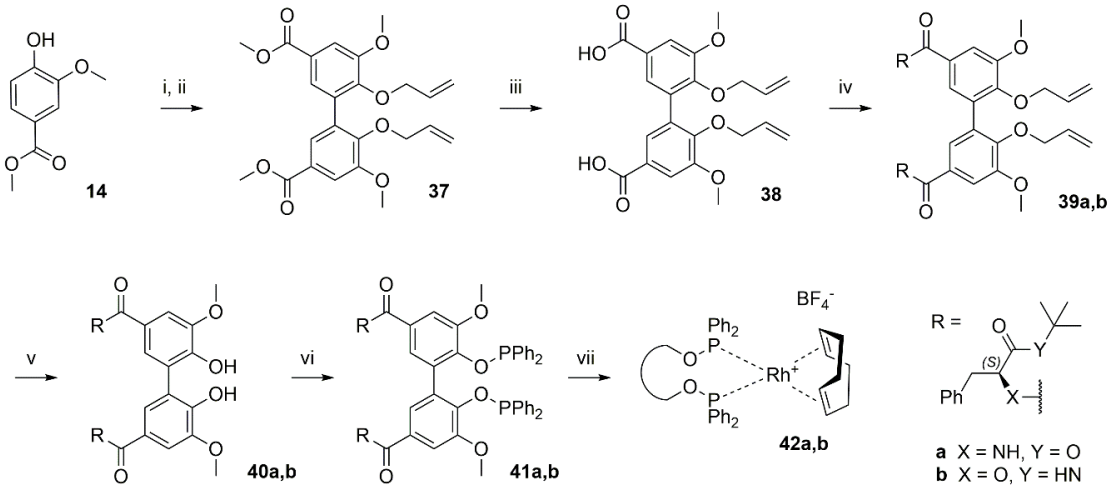

Figure 4-6: Synthesis of bisphosphinite complexes **42a,b** i) $PhI(OAc)_2$, 51%, ii) allyl bromide, K_2CO_3, 97%, iii) KOH, 99%, iv) **39a**: $SOCl_2$, then NH_3Cl-(*S*)Phe-O^{t}Bu, diisopropylethylamine, 91%; **39b**: HO-(*S*)Phe-NH^{t}Bu, DMAP, EDCI·HCl, 50%, v) $Pd(OAc)_2$, $PPh_2(C_6H_4NMe_2)$, HCOOH, **40a**: 71%; **40b**: 93% vi) **41a**: PPh_2Cl, 1,4-diazabicyclo[2.2.2]octane, 20%; **41b**: PPh_2Cl, triethylamine, 69%, vii) **42a,b** $[Rh(COD)_2]BF_4$, *in situ* (EDCI·HCl = 1-ethyl-3-(3-dimethylammoniumpropyl)carbodiimide hydrochloride, DMAP = 4-dimethylaminopyridine, DIPEA= diisopropylethylamine)

4.3.2 Chirality transfer and hydrogenation experiments

Regarding the choice of additives used to influence the stereodynamic behaviour of the ligands, similar concepts to those developed by Trapp and Storch for a self-amplifying hydrogenation reaction were applied.[40] Amide derivatives of different amino acids were chosen, since these were expected to effectively interact with the ligands' amino acid-based selector units through their various hydrogen bond donor and acceptor sites or through π-π interactions. A greater number of attachment points would rigidify the transient adducts and facilitate the transmission of a chiral information onto the ligand backbone. Furthermore, the highly enantioselective nature of interactions between amino acid-derived additives and selector units, which has been established in previous chapters and which is also recorded in literature,[192] is necessary for the observation of non-linear effects. As discussed above, the latter serve as a basis for the envisioned stereoselective, self-inhibiting reaction. Finally, amino acids and their derivatives can conveniently be generated through enantioselective rhodium-catalyzed hydrogenation of suitable olefins which makes them ideal products for an asymmetric, autoinductive reaction.

When the different selector types were compared, a significant difference with regard to the ligand behaviour was observed. Ligand **41b** and its Rh complex **42b** were found to form a close

to racemic mixture. Addition of various chiral additives had negligible influence on the rotamer distribution and employment of those rhodium complex **42b** in hydrogenation reactions of methyl 2-acetamidoacrylate **12** gave exclusively racemates (see chapter 7.4.20, page 149 for spectral data). For compound **41a**, however, the selector moieties evoked a very different behaviour. The $^{31}P\{^{1}H\}$ NMR spectrum of the bisphosphinite contained a sharp singlet representing a minor species, while the major isomer appeared as two broad singlet signals. The two-fold set of signals, also found in corresponding ^{1}H and ^{13}C NMR spectra, is indicative for the dimerization phenomenon which has already been observed for similar diamide selector-modified ligands and has been extensively investigated in chapter 2. It signifies strong, rotamer-specific interaction between selector moieties allowing for retrospective assignment of the minor compound as the S_{ax} rotamer and the major, dimierized compound as the R_{ax} rotamer.
When ligand **41a** was treated with (*S*)-amino acid-derived additive PhCO-(*S*)Phe-NH^{t}Bu **25**, re-symmetrisation along with an rotameric enrichment of R_{ax}-**41a** was observed (see chapter 7.4.18, page 144 for spectral data). The resulting ligand *de* was found to be dependent both on the additive:ligand ratio and the ligand concentration. When ligand **41a** was complexated to form Rh complex **42a**, no dimeric behaviour could be detected any more. Yet again, significant conformational change was observed in presence of chiral diamides (see Figure 4-7).

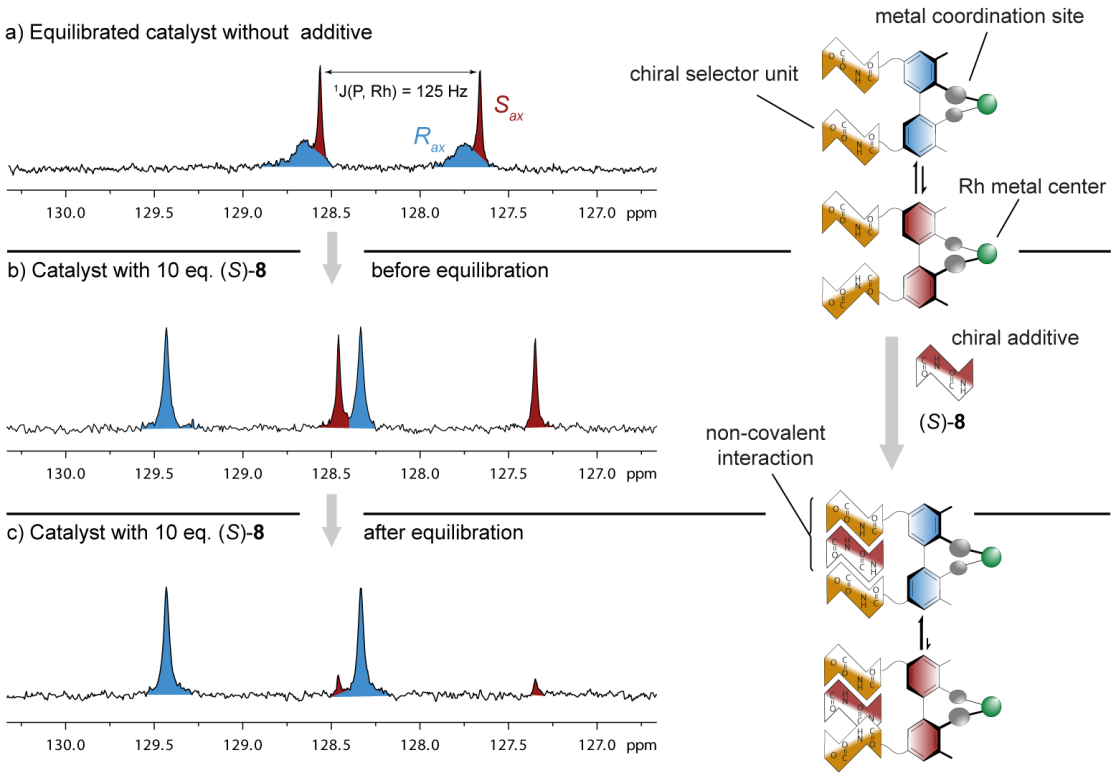

Figure 4-7: Exemplary $^{31}P\{^{1}H\}$ NMR spectra depicting interactions studies between bisphosphinite complex **42a** and amino acid-derived diamides. a) Equilibrated complex shows equilibrium between two rotamers. b) Addition of chiral diamide (*S*)-**8** leads to signal sharpening/broadening and shift of R_{ax}-**42a**, exclusively, indicating stereoselective engagement in non-covalent interaction. c) Ligand-additive interaction results in significant enrichment of the more stabilized isomer R_{ax}-**42a**.

Significant downfield shift, signal sharpening or broadening and a significant rotameric enrichment of R_{ax}-**42a** over a period of several hours was observed by ^{31}P NMR spectroscopy. The minor species S_{ax}-**42a** did not seem to significantly interact with additives and no change signal

shape or position was observed in any case. A comprehensive overview of the spectroscopic data for all interaction experiments can be found in chapter 7.4.19, page 145.

At this point it should be highlighted, that all additives employed for stereoinduction represent potential products of a preceding hydrogenation reaction and are thus candidates for autoinductive hydrogenation experiments. Due to massive signal overlap and broadening in most cases, the degree of enrichment could not unambiguously be determined. Since the ligand rotamer ratio is correlated to the enantiomeric distribution of products from asymmetric hydrogenation experiments, however, those could be used in order to quantitatively asses the structural change of the catalyst. Catalyst mixtures of **42a**, aligned after interaction with various additives, was consequently employed for the reduction of olefin **12** (see Figure 4-8).

The untreated complex was found to hydrogenate the substrate with 27% *ee R*. Almost all additives proved capable of significantly enhancing the catalyst's selectivity. In the presence of AcNH-(*S*)Phe-NHMe (*S*)-**8**, which had evoked a strong ^{31}P NMR signal shift as well as significant enrichment for R_{ax}-**7a**, selectivity of the hydrogenation increased to 56% *ee R* (Δ*ee* = 29%). The enantiomer AcNH-(*R*)Phe-NHMe (*R*)-**8**, however, was unable to significantly align the catalyst to increase its selectivity (29% *ee R*, Δee = 2%). This indicates that the ^{t}BuO-(*S*)Phe-NH selector, just like its diamide analogue, interacts with other amino acid-derived compounds in a highly enantioselective manner. The differentiability of chiral molecules in solution and ensuing selective chirality transfer from one enantiomer is a vital prerequisite for chiral amplification.

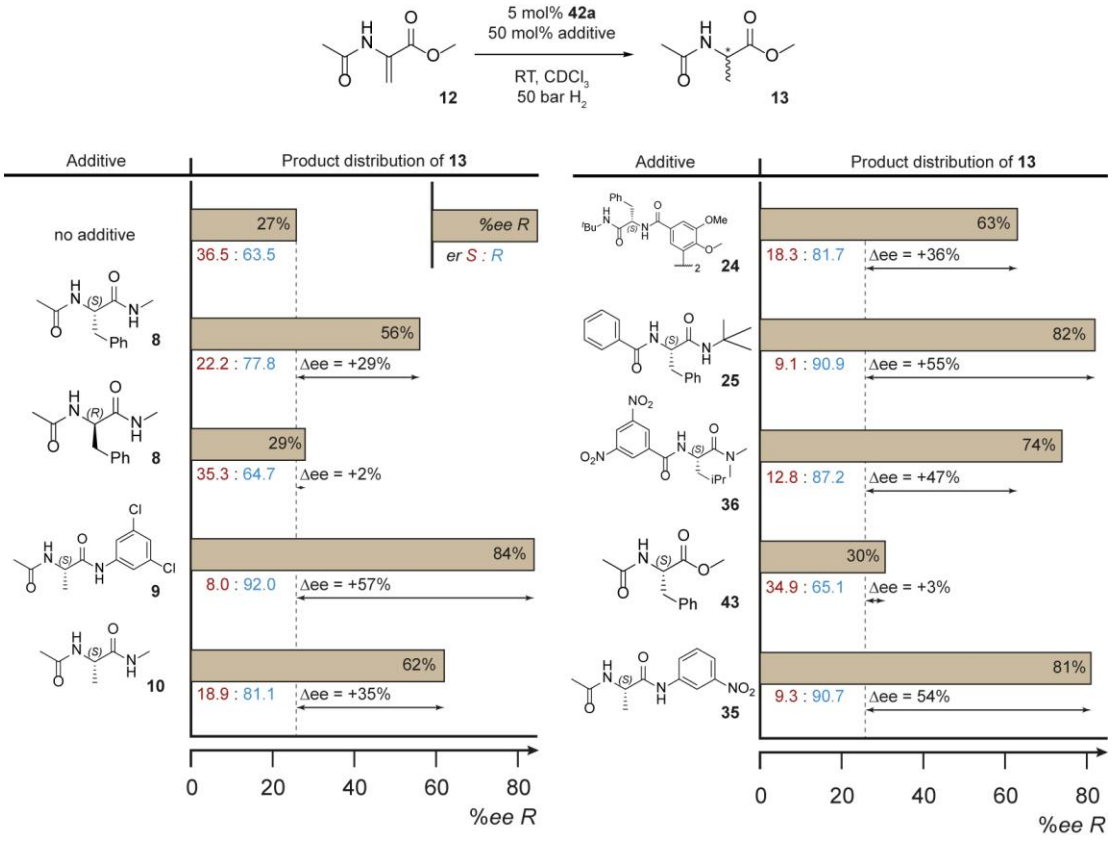

Figure 4-8: Hydrogenation experiments using catalyst **42a** that was pre-aligned using different amino acid-derived additives. Rh complex **42a** and additive where dissolved in dry and degassed $CDCl_3$ (4.3 mM in catalyst) and left standing for 16 hours until re-equilibration was completed. For additive **24** only 25 mol% where used. Compounds (*S*)-**9** and (*S*)-**35** did not fully dissolve. Detailed experimental procedure can be found in chapter 7.4.22, page 150.

The strongest catalyst alignment, observed for those additives that also caused the heaviest signal broadening for the enriched R_{ax} isomer, was achieved with alanine derivatives (*S*)-**9** and (*S*)-**35**, which allowed for reduction of **12** with 84% *ee R* (Δ*ee* = 57%) and 81% *ee R* (Δ*ee* = 54%), respectively, and with selector-imitating diamide (*S*)-**25**, which gave an increase in selectivity to 82% *ee R* (Δ*ee* = 55%).

4.4 Enantioselective self-inhibition in an asymmetric hydrogenation reaction

4.4.1 Concept and syntheses

Based on results from interaction studies with complex **42a**, discussed in chapter 4.3.2, ligand-substrate system was designed that would fulfil all prerequisites necessary to show autoinductive, self-inhibiting properties (see Figure 4-9). The most important ones where 1) a highly stereodynamic catalyst with different, accessible ligand states that is each selective for the formation of one enantiomer, 2) a prochiral substrate that can be converted into a reactions product, which is capable of swiftly altering the catalyst's ligand state through non-covalent interaction and 3) stereoselective interaction between formed reaction product and selector sites of the catalyst.

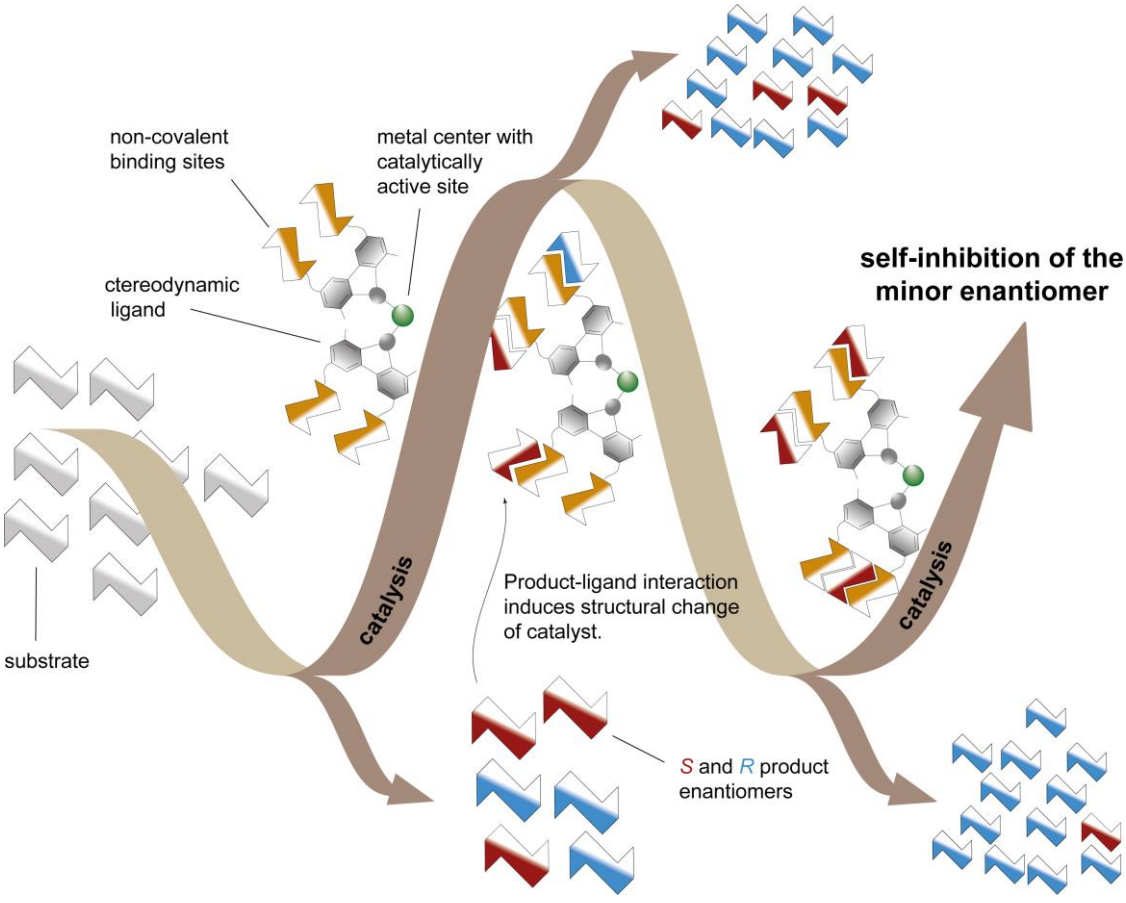

Figure 4-9: Conceptualization for a self-inhibiting reaction. A prochiral substrate is converted by a stereodynamic ligand. Stereoselective incorporation of one product enantiomer into the catalyst through non-covalent interaction changes selectivity of the catalyst and supresses further formation of the same stereoisomer.

Catalyst **42a** bearing amidoester selector sites was found to be most strongly affected by the presence of diamides (*S*)-**9**, (*S*)-**25** and (*S*)-**35**, where over the course of several hours, a strong rotameric enrichment of one catalyst epimer was observed. To decrease the time required for catalyst alignment, it was instead decided to employ corresponding phosphoramidite ligand, as previously done by Trapp and Storch, where a much lower inversion barrier of the ligand would lead to immediate equilibration. As for the substrate design, important qualities include strong, enantioselective interaction capabilities of the hydrogenated product, as well as good solubility of both product and respective substrate. Among the diamides in question, compounds (*S*)-**9** and (*S*)-**35** were only sparingly soluble. Since dehydrogenation generally tends to reduce solubility of diamides even further, it was decided to rely on the substitution pattern of diamide **25** for the substrate design.

Syntheses are shown in Figure 4-10. Treating BIPOL **40a** with diethylphosphoramidous dichloride in presence of triethylamine afforded phosphoramidite ligand **44**, which was added to $[Rh(COD)_2]BF_4$ in two-fold excess to give catalyst **45**. The envisioned substrate could conveniently synthesized through an Erlenmeyer azlactone synthesis by reacting glycine with benzoic acid chloride and benzaldehyde to afford azlactone **46**, from which olefins **47a-c** were obtained through aminolysis.

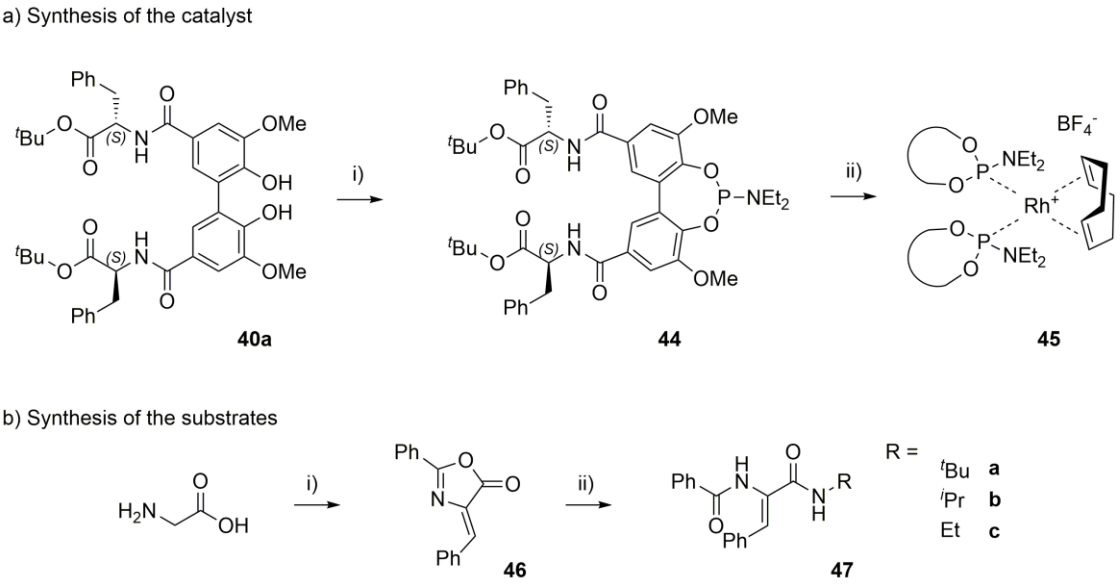

Figure 4-10: a) Synthesis of phosphoramidite complex **45** i) Cl_2PNEt_2, TEA, 77%, ii) $[Rh(COD)_2]BF_4$, quant. b) Synthesis of olefinic substrates **47a-c**: i) PhCOCl, PhCHO, ii) **47a**: $^tBuNH_2$, 68%, **47b**: $^iPrNH_2$, 69%, **47c**: $EtNH_2$, 73%.

4.4.2 Asymmetric hydrogenation and enantioselective self-Inhibition

As previously found for similar compounds, complex **45** produced a complex ^{31}P NMR spectrum comprising various species that presumably form when phosphoramidite ligands rotate around the Rh-P bond (see this reference[40] and supplementary information therein). Testing the stereodynamic behaviour of the catalyst, a notable change in the distribution of species was observed by ^{31}P NMR spectroscopy in presence of (*S*)-**25**, which did not occur when only the enantiomer (*R*)-**25** was present (see Figure 4-11a).

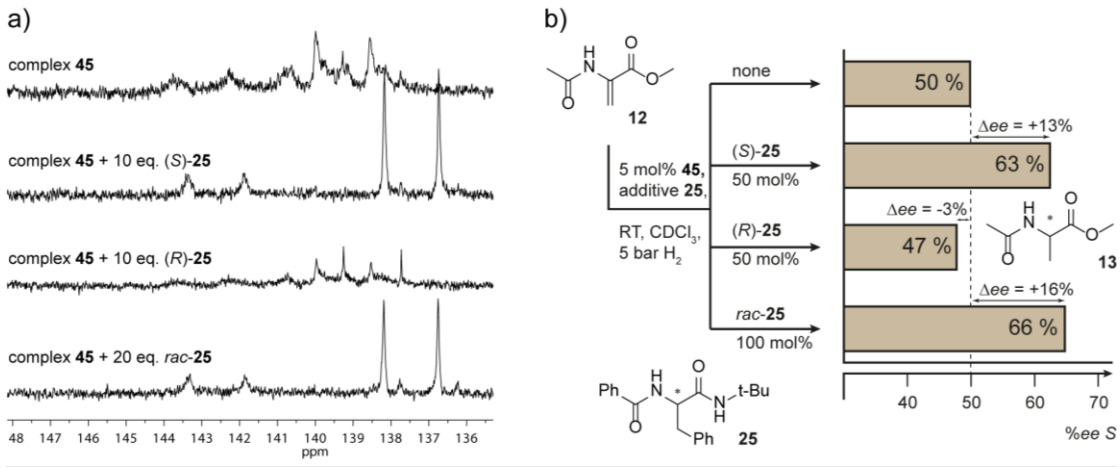

Figure 4-11: a) ^{31}P NMR spectra of phosphoramidite complex **45** depicting structural change of the ligand mixture if the *S* enantiomer of **25** is present. b) Employing mixtures of catalyst **45** and additive **25** during asymmetric hydrogenation of olefin **12** shows that observed structural change is linked to a change in selectivity if the *S* enantiomer of the additive is present. Reactions were run in dry and degassed chloroform with a 3.2 mM solution with respect to the catalyst. Detailed experimental procedures can be found in chapter 7.4.22, page 150.

This change could be linked to a change in selectivity when mixtures of complex and *S* and/or *R* additive were used for the asymmetric hydrogenation of prochiral olefin **12**. A change in product *ee* was found whenever the *S* enantiomer of the additive was present (see Figure 4-11b). These results indicate, that insights about stereoselective interactions and resulting stereoinductions obtained for bisphosphinite ligand **41a** can be transferred to its more dynamic phosphoramidite analog **44**.

In order to investigate autoinductive effects during the hydrogenation of olefin **47**, catalytic runs with different catalyst loadings at the same catalyst concentrations were conducted, which is tantamount to a change of the turnover number (TON) [4]. A decreased catalyst loading leads to an increase in catalytic cycles, eventually resulting in higher levels of interaction between the catalyst and the reaction product by increasing the relative amount of the latter. This consequently causes the catalyst structure to change to a greater extent over time. When olefin **47a** was converted at 3.2 mM catalyst concentration with 5 bar hydrogen and a catalyst loading of 100 mol%, which equates to an average TON of one, the *S* enantiomer of **25** was found to form with 19% *ee*. The same selectivity was found, when the reaction was re-run under the same conditions, but with 100 bar H_2 gas. This affirms that the obtained selectivities are dictated by the specific distribution of the catalyst's different conformers and not by selective catalyst activation, i.e. kinetically favoured hydrogenation of the COD co-ligand for one catalyst species. Increasing the TON led to a significant change in the enantiomeric distribution of the product towards the *R* enantiomer. When experiments were conducted with 10, 2.5 and 1 mol% catalyst (TON of 10, 40 and 100), selectivities of 10% *ee S*, 12% *ee R* and 41% *ee R* were obtained (see Figure 4-12). This accounts for an overall change in enantiomeric excess of $\Delta ee = 60\%$.

Since it has been established that only the *S* product enantiomer is capable of interacting with the catalyst to change its selectivity, the rising formation of (*R*)-**25** with increased turnover number is a clear sign that the initially predominant enantiomer promotes the formation of its mirror image at its own expense, classifying this reaction as autoinductive and self-inhibiting. When

[4] TON is referred to here as the quotient n(substrate)/n(catalyst). Partial catalyst activation was experimentally addressed, but is formally not considered.

similar experiments were performed using weakly interacting substrate **12**, a reaction with 10 mol% catalyst and 100 mol% catalyst had similar outcomes yielding the product with selectivities of 50% *ee* and 49% *ee*. This shows that diamide **25** is vital to change of selectivity that was observed for the reduction of **47a**. Constitution of the substrate was found to have a significant influence on the extent of the autoinductive effect. When substrates **47b** was tested, a much less pronounced change in selectivity was observed and for substrate **47c,** enantiomeric distribution did not change at all, when the catalyst loading was altered.

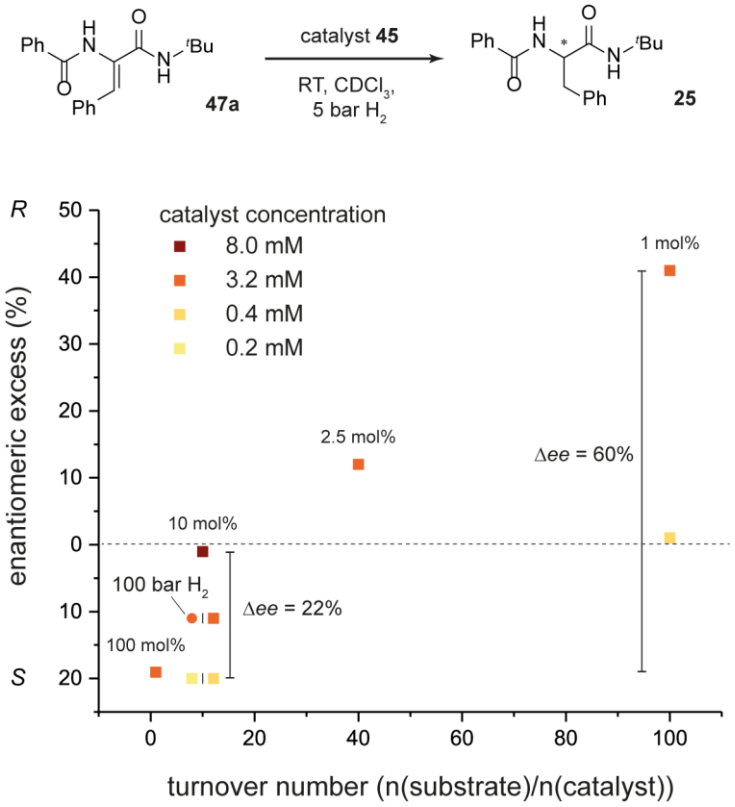

Figure 4-12: Results for the asymmetric hydrogenation of olefin **47a** using phosphoramidite complex **45**. The catalyst's selectivity was found to be dependent on its concentration. Moreover, characteristics of auto induction and self-inhibition for the enantioselective formation of (*S*)-**25** were detected, when the turnover number of the reaction was varied. Increased interaction between the catalyst and formed product led to a reversal of selectivity. A detailed experimental description can be found in chapter 7.4.22, page 150.

Due to the fact that a decreased catalyst loading at constant catalyst concentration is restricted by the solubility of the substrate, it appeared desirable to run reactions with lower catalyst concentrations in order to reach higher turnover numbers. As studies of bisphosphinite ligand **41a** bearing an identical ligand backbone had established that the ligand's rotamer distribution was found out to be concentration dependent, the same was assumed to be true for Rh complex **45**. Consequently, a second set of reactions was carried out, where olefin **47a** was reduced using a constant catalyst loading of 10 mol% and varying concentrations. When reactions were run at 8.0 mM, 3.2 mM, 0.4 mM and 0.2 mM, an increasing selectivity for the *S* enantiomer of **25** (1%, 11%, 23% and, again, 23% *ee S*) was observed accounting for an overall difference of Δ*ee* = 22%. This is in line with previous observations of weak ligand-ligand interaction for ligand **41a** and suggests that an increased presence of the selector moiety influences other catalyst molecules selectivity in favour of (*R*)-**25**. Given the structural similarities between selector and reaction product, it comes to no surprise, that both are similarly capable of exerting influence over

surrounding catalyst molecules and that identical trends of enhanced production of (*R*)-**25** were observed when either the catalyst or the product concentration was increased.
Finally, attempts to run reactions with increased TONs at lower temperatures were found to be limited by catalyst deactivation. Although the presumed trends were identified, reactions at 0.4 mM catalyst concentration and 0.5 mol% catalyst loading repeatedly failed to give full conversion: First run finished with 19% *ee R* and about 25% conversion, second run finished with 4% *ee R* at about 10% conversion. When catalysis was repeated with 1 mol% catalyst at 0.4 mM catalyst concentration, however, full conversion with a selectivity of 1% *ee R* was observed, which is a considerable shift of selectivity towards the *R* enantiomer of diamide **25** and is thus in line with the previously established self-inhibiting nature of the reaction.

4.5 Resume

This chapter describes the development of an asymmetric autoinductive, self-inhibiting hydrogenation reaction. It serves as a complementary system to the self-amplifying hydrogenation reaction recently developed by Trapp and Storch[40] and relies on the same principles: 1) a highly stereodynamic catalyst with different enantioselective states, 2) a chiral reactions product, which is capable of swiftly altering the catalyst's ligand state through strong non-covalent interaction leading to concurrent increase in production of one enantiomer on the expense of the other one and 3) preferential interaction between the selector sites of the catalyst and one enantiomeric reaction product over the other one.
A two-stage process was devised. In the first step, a novel (*S*)-phenylalanine-based amidoester selector was investigated for its ability to serve as coordination site for non-covalent interaction with chiral, amino acid-derived additives. Using a variety of differently substituted (*S*)-amino acid-derived additives as alignment agents, all of them representing potential hydrogenation products, the rotamer ratio of stereodynamic bisphosphinite **41a** and its Rh complex **42a** could successfully be manipulated. In subsequent asymmetric reductions of methyl 2-acetamidoacrylate **12** significantly increase in selectivity for the (R)-product enantiomer was observed. While the untreated complex **42a** converted the substrate with 27% *ee R*, selectivity could be improved to up to 84 % *ee R* (Δee = +57%) after incubating the catalyst with (*S*)-**9** for several hours.
Building on these results, highly dynamic phosphoramidite complex **45** bearing the same amidoester selector sites was synthesized along with the olefins **47a-c**, which constitute the unsaturated analogues of strongly interacting diamide (*S*)-**25**. When olefin **47a** was hydrogenated using phosphoramidite complex **45**, it could be shown that (*S*)-**25**, initially produced in excess, successfully supressed its own production during subsequent catalyst turnovers by altering the catalyst selectivity. When catalyst loadings were decreased, ongoing enantioselective self-inhibition lead to a change in selectivity form 19% *ee S* (100 mol% catalyst) to 41% *ee R* (1 mol% catalyst) which accounts for an overall difference of Δee = 60%. Self-inhibition was found to be strongly affected by the substitution pattern of the substrate and a much weaker autoinductive effect was observed for compounds **47b** and **47c**. Another factor found to influence the product distribution was the concentration of the catalyst. This was linked to previously observed, weak intermolecular interaction of ligand molecules which is an attenuated form of the diastereoselective *narcissistic self-sorting* previously found for ligands with a similar structure (see chapter 2) and that can be understood as a different manifestation of the same in inhibition process when considering the structural similarity between the selector sites and compound (*S*)-**25**.

5 *Tropos* ligands based on *meso*-tartaric acid

5.1 State of knowledge

A number of stereodynamic ligands have been discussed and different pathways outlined, that allow to exert influence over the rotameric distribution of these ligands. These include - among others - use of chiral co-ligands,[193,194] covalently attached chiral auxiliary groups,[52-54] ligand isomerization through light and temperature[146,148,149] and chirality transfer through no-covalent interaction between the stereodynamic ligand and a chiral molecule.[40,41,62,153,154,195]
Most widely applied *tropos* ligands bear a stereochemical axis that allows interconversion between the S_{ax} and the R_{ax} isomer (see Figure 5-1). Prevalent examples are biphenyl-based bidentate ligands, such as BIPOL or BIPHEP. Others include oxazoline based BiphBOX,[196] 2,2'-bipyridyl-based ligands,[197] or corresponding monodentate ligands such biphenol-based phosphoramidites or phosphites. Closely related are compounds with small bridging unit between two backbone aryl rings such as benzophenone (DBPB),[198-200] diaryl ether (DPEPhos)[201] or bisphenylmethane (MBP).[202] A different type of rotation is encountered with ligands based on ferrocene, such as dppf, whose conformers interconvert through rotation of the cyclopentadienyl anion around the cp-Fe-cp axis, or PhanePhos-type ligands,[203] where both aryl groups have to rotate for enantiomeric interconversion. Apart from chiral axes, helicity of polymeric structures can also be influenced under certain conditions forcing them to switch between *M*- and *P*-state.[204]

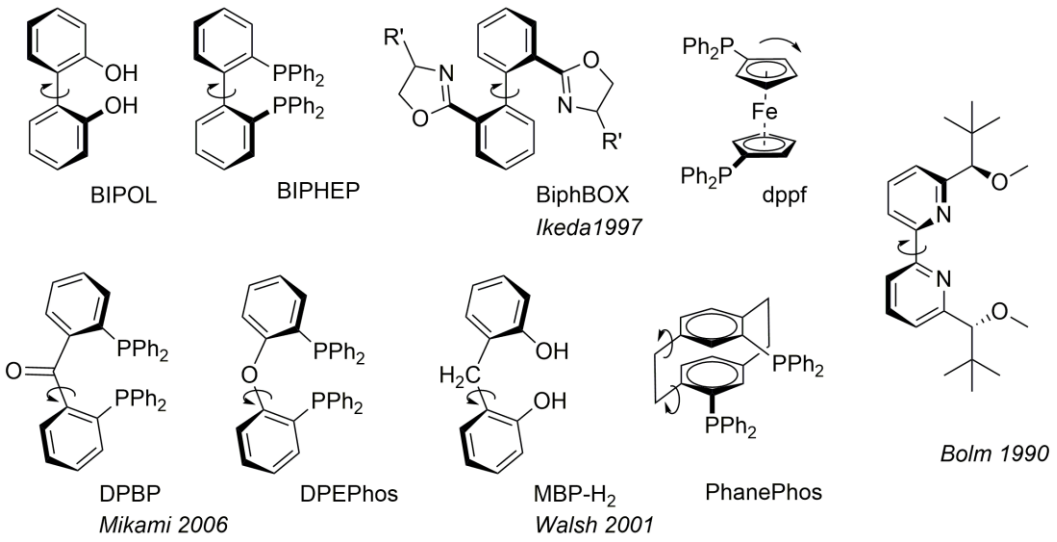

Figure 5-1: A variety of bidentate, stereodynamic ligands with stereodynamic axes is shown.

Examples for *tropos* ligands where interconversion of the two ligands state occurs by rotation around an sp3-sp3 bond, on the other hand, are scarce. Privileged ligands containing a C(sp3)-C(sp3) backbone include DIOP[205] and Chiraphos.[206] Since rotation around an aliphatic C-C single bond is very fast, ethane having a barrier of rotation as low as 12.5 kJ/mol,[207] stabilization of one rotamer needs to be provided by steric repulsion of the backbone substituents in order for the ligands to be selective. For both ligands above, this is caused by the spatial arrangement of the substituents that form two stereocenters. A respective stereodynamic *tropos* ligand with an

aliphatic ligand backbone requires interconversion of two enantiomeric synclinal (gauche) conformations. If the complexity of the ligand backbone exceeds that of simple ethane, substituents have to be attached so that the *meso* compound is formed in order to retain the equivalence of both synclinal (*sc*) conformers. A comparison with the rotamer ligand states of a biaryl ligand is depicted in Figure 5-2. In both cases, two enantiomeric, ligand rotamers (S_{ax} and R_{ax} or +*sc* and –*sc*) can be found that can be interconverted through an achiral planar/synperiplanar state.

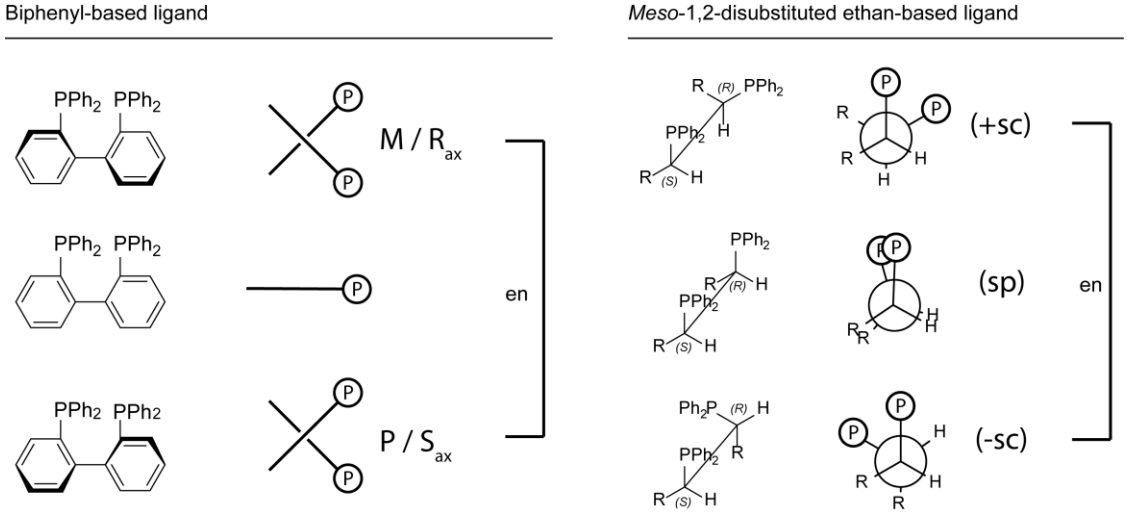

Figure 5-2: Comparison of different rotational states of a biphenyl-based ligand (*left*) to those of a *meso*-1,2-disubstituted DPPE-type ligand (*right*). In both cases, two enantiomorphic rotamers are found, that interconvert through an achiral conformer.

Previously attributed to internal compensation, the optical inactivity of *meso*-tartaric acid was found to be the caused by the existence of a racemic mixture of both enantiomeric *sc* forms.[208] Unlike homochiral (*R*,*R*)- or (*S*,*S*)-tartaric acid, which is known to be predominantly exist in antiperiplanar conformation (*ap*), *meso*-tartaric acid was found to primarily adapt one of these two conformers in both solid and in solution state instead.[209,210]
Walsh and co-workers used *meso*-1,2-diamies and their respective imines as achiral ligands to enhance selectivity in reactions with chiral co-ligands (see Figure 5-3).[211] This can be considered as an inverse analogue of the asymmetric activation strategy developed by Mikami and Noyori, where achiral BIPHEP ligands are stereochemically aligned by chiral diamines.[45]

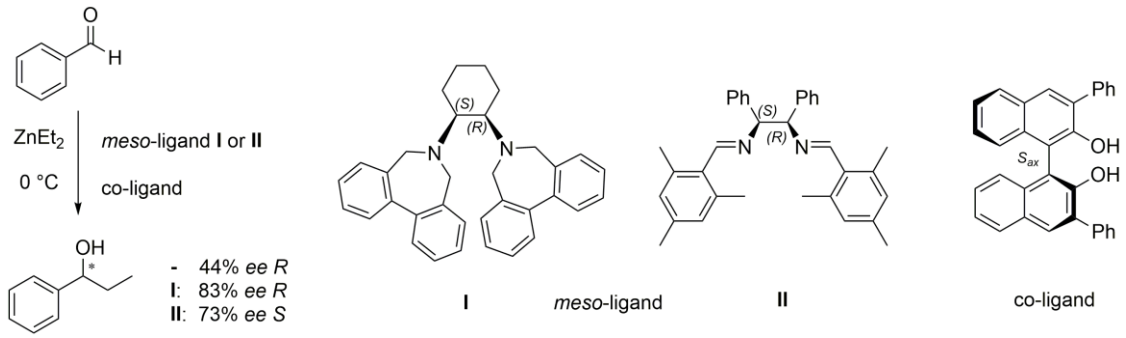

Figure 5-3: Asymmetric alkylation of aromatic aldehydes by Walsh and co-workers.[211] After coordination to a zinc atom, naphthol co-ligand forces the 1,2-diamine- or imine-based *meso* ligands **I** or **II** in one of two possible synclinal conformations, significantly increasing the selectivity of the reaction.

5.2 Objective

Following the trend to build stereodynamic ligand systems with selector sites for non-covalent interaction, synthesis of a novel ligand type with an aliphatic backbone and amino-acid-derived selectors for non-covalent interaction was envisioned. Ease of accessibility with carboxylic acid groups as selector attachment points and stereocenters already in place made *meso*-tartaric acid the most convenient substrate to start from.
Synthesis of a Chiraphos-type ligand and a bisphosphinite analogue was attempted. Focus was on the development of a synthetic strategy for each ligand along with investigation of their stereodynamic behaviour. As selector sites, previously investigated phenylalanine-derived diamide residues were to be implemented. In this context, it was also to be examined, whether this kind of atomic arrangement would prohibit the ligand to form dimers, as previously observed for biaryl compounds that were modified with this type of selector.

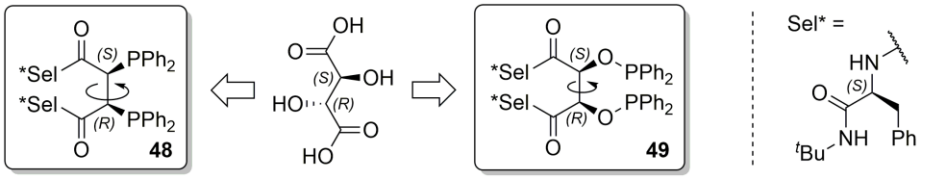

Figure 5-4: Ligands to be synthesized from *meso*-tartaric acid or a derivative include a Chiraphos-type bisphosphine **48** (*left*) and a corresponding bisphosphinite **49** (*right*).

5.3 Synthetic approaches

5.3.1 Bisphosphine ligand

The most common approach for the synthesis of alkylphosphines is treatment of a suitable precursor bearing a leaving group, such as bromine or triflate, with the respective metal phosphanide. Due to the generally observed air sensitivity of phosphines, their introduction in the last stage of the synthesis seemed sensible. The synthetic strategies that were attempted are outlined in Figure 5-5.
Initial attempts to directly couple the hydrochloride of phenylalanine *tert*-butylamide to *meso*-2,3-dibromotartaric acid **50** remained unsuccessful, potentially due to the instability of the activated dicarboxylic acid species. Instead, *trans*-alkene **51** was synthesized from fumaric acid with 75% yield and subsequent stereoselective bromination was achieved at room temperature to afford *meso*-2,3-dibromotetraamide **52** in quantitative yield. Unfortunately, final exchange of the halogen atoms with diphenylphosphine proved to be challenging. Treatment of compound **52** under different conditions with $PHPh_2$ in presence of KO^tBu,[212] with PPh_2Li[213,214] or with $PHPh_2(BH_3)$ and *n*-butyl lithium[215] led to full consumption of the phosphorous reagent, but no product could be isolated in either case. Among a number of different species identified by ^{31}P NMR spectroscopy and HR mass spectrometry, some are believed to be vinyl phosphines suggesting that after the first substitution, elimination of the remaining bromine atom is favoured due to sterical hindrance.

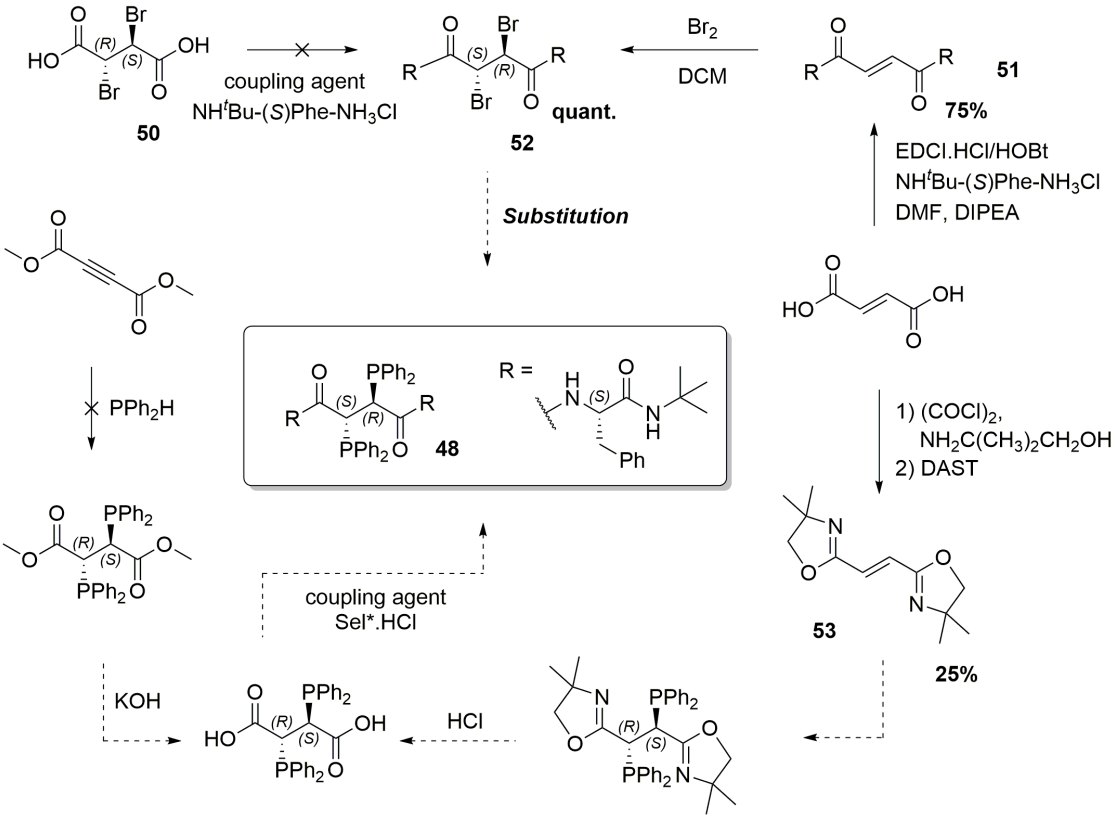

Figure 5-5: Synthetic attempts to synthesized Chiraphos analogue **48**. More detailed experimental data for successfully synthesized compounds can be found in chapter 7.5, page 151.

Consequently, other synthetic routes were tested, where attachment of the selector units would occur after previous introduction of the diphenylphosphine moieties. It was previously reported by Bookham and co-workers, that diarylphosphines add to diphenylacetylene and depending on the type of phosphine, some diphosphines were predominantly formed in *meso*-form.[216] Addition of arylphosphines to dimethyl acetylenedicarboxylate is similarly known.[217] Reaction of alkyne and diphenylphosphine occurred readily, however, no selective formation of the diphosphines could be observed. In a final attempt, the carboxylic acid groups of fumaric acid were transformed into oxazolines, which are known to withstand strongly basic organometallic reagents. Subsequent introduction of leaving groups in *meso*-configuration would potentially allow for the substrate to withstand much harsher conditions during subsequent halogen-phosphine exchange. Fumaric acid was consequently treated with oxalyl chloride and 2,2-dimethylaminoethanol. The resulting dialcohol could successfully be dehydrated using diethylamino sulfurtrifluoride (DAST)[218,219] to give *trans*-bis(oxazoline) alkene **53**. Treatment of this compound with bromine or ^{t}Bu$_4$NBr$_3$ led to decomposition of the substrate, most likely due to faster side reactions with the oxazoline protecting groups. Attempts to use different, less aggressive reagents such as PhI(OAc)$_2$/KBr [220] or CuBr$_2$/LiBr[221] gave no reaction at all. Iodination was found to be equally unsuccessful.

5.3.2 Bisphosphinite ligand

For the potential bisphosphinite ligand it seemed equally sensible to introduce the arylphosphorus groups in the last reaction step of the sequence to avoid having to handle moisture and oxygen sensitive ligand precursors. The most convenient approach thus seemed to be coupling of

the selector moieties to *meso*-tartaric acid and subsequent treatment of the diol with PPh_2Cl. The synthetic strategy for the ligand is outlined in Figure 5-6.

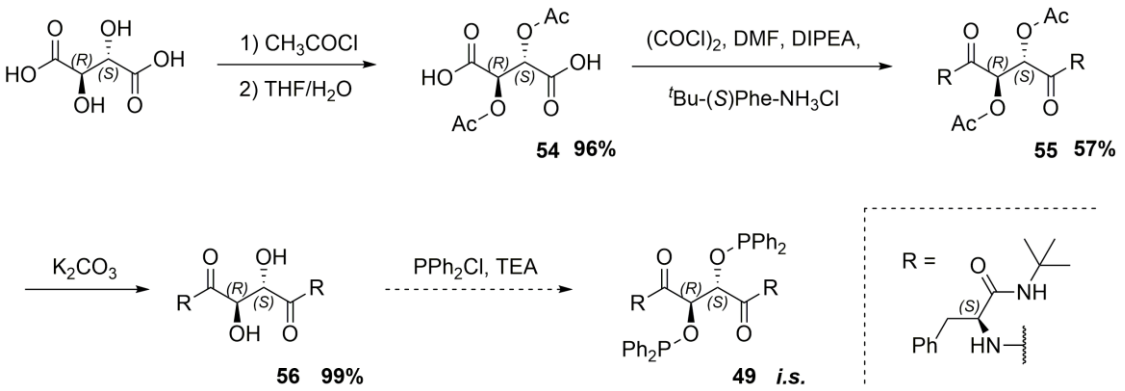

Figure 5-6: Synthetic approach for the synthesis of bisphosphinite ligand **49** from *meso*-tartaric acid. More detailed experimental data can be found in chapter 7.5, page 151.

In the first reaction step, *meso*-tartaric acid was treated with acetyl chloride to protect the hydroxy groups. The resulting anhydride was dissolved in water and THF to yield dicarboxylic acid **54**.[222] Selector moieties could subsequently be introduced by coupling with phenylalanine *tert*-butylamide hydrochloride using oxalyl chloride and DMF as catalyst to give tetraamide **55** in good yield.[223] When compound **55** was subsequently heated in methanol in the presence of potassium carbonate, full deprotection of the hydroxy groups was observed within 90 minutes. Intriguingly, racemization of the stereocenters occurred when the suspension was concentrated in presence of the base during workup. Pure diol **56** could finally be obtained by loading the fully deprotected crude mixture onto a plug of silica and eluating with ethanol. During the last reaction step, test reactions with chlorodiphenylphosphine or diethylamino diphenylphosphine in presence of different bases were conducted to analyse product formation. Reaction of diol **56** with mildly reactive PPh_2NEt_2 in presence of N,N-dimethylaminopyridine at 70 °C was monitored by ^{31}P NMR spectroscopy over several days (see Figure 5-7). Formation of intermediate species represented by two singlet signals of equal size, which was assigned to the two possible mono-phosphorylated compounds, became visible within four hours. After longer reaction times, two additional singlet signals of equal intensity representing the desired bisphosphinite **49** were detected. With longer reaction times, intensity of these signals increased while those assigned to the intermediate structures became weaker. Despite long reaction times, however, full conversion could not be reached.

When **56** was reacted with an excess of highly reactive chlorodiphenylphosphine in presence of triethylamine, however, no intermediate was detected and full conversion to the desired bisphosphinite **49** was reached. Unfortunately, purification of the compound proved to be laborious due to its high solubility and sensitivity towards oxygen and moisture. No pure sample could be obtained within the timeframe of the project

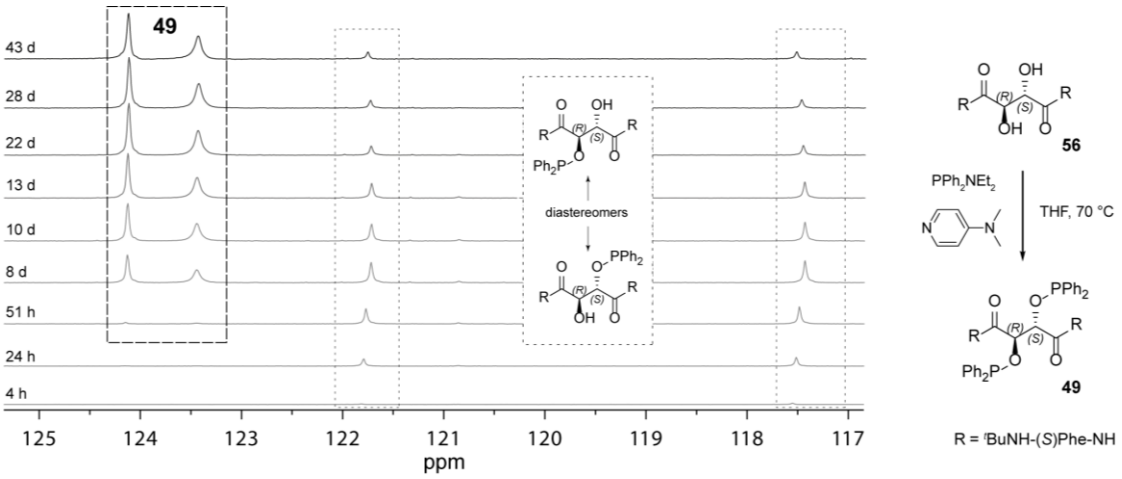

Figure 5-7: Section of ^{31}P NMR spectrum monitoring reaction progress for the synthesis of bisphosphinite **49** from diol **56** and PPh_2NEt_2 . Formation of mono-phosphorylated intermediate was also observed.

5.4 Conformational analysis

Since both desired ligands could not be synthesized in pure form within the timeframe of the project, an analysis of the ligands' stereodynamics seems void. A brief investigation of the NMR data for all obtained ligand precursors, however, might reveal preliminary insights into the general appearance of compounds of this sort.

Compounds **52** (dibromo derivative), **55** (acetyl-protected diol), **56** (diol) and crude **49** (bisphosphinite) were compared. In all cases only one species was observed by NMR spectroscopy which indicates either complete immobilization of one fully enriched rotamer or rapid rotation around the central C-C bond where the NMR spectrum represents a weighted average between the staggered conformers, which are the two synclinal conformers (-*sc* and +*sc*) and the antiperiplanar rotamer (*ap)* shown in Figure 5-8. Presence of additional stereocenters on the selector groups removes the energetic equivalence of the two *sc* conformers. Each of these rotamers are intrinsically diastereotopic, and if stable enough, orientation of both molecular halves can be estimated with help of the Karplus equation, which connects the coupling constants of the two vicinal methin to their dihedral angle.[224] Maximal coupling (8-15 Hz) is observed for dihedral angles of 0° and 180°, where orbital overlap is maximized. A synclinal conformation results in smaller coupling constants (2-5 Hz) and no coupling is observed if a 90° angle is adapted.

The ^1H NMR spectrum of compound **51**, however, exhibits intense line broadening, when collected in $CDCl_3$ suggesting the compound remains highly dynamic in aprotic solvents. Spectra of acetyl-protected diol **55** (collected in $CDCl_3$), of deprotected compound **56** (CD_3OD) and of *in situ*-formed bisphosphinite **49** (THF-d8) gave doublet signals for both methin protons of the tartaric acid moiety and a coupling constant of $^3J(H,H)$ = 2.1 Hz, 2.1 Hz and 1.9 Hz, respectively, was observed which suggests that both compounds retain a synclinal conformation as their most stable form (see Figure 5-8).

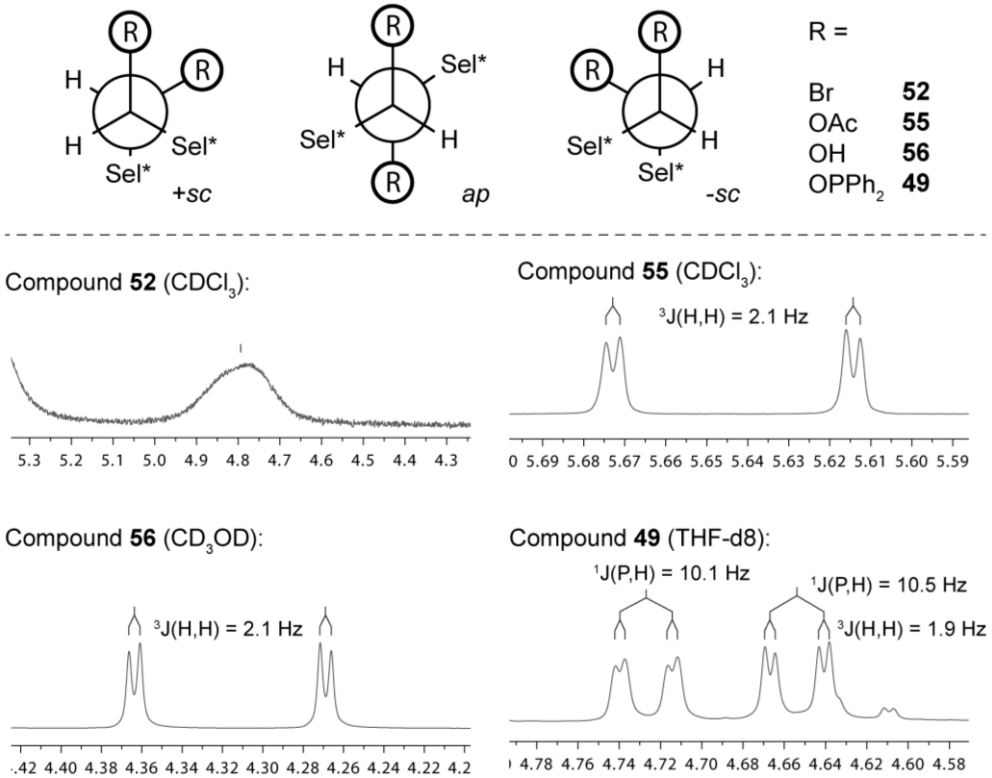

Figure 5-8: *Top*: Schematic illustration of the staggered conformers of meso-tartaric acid derivatives bearing phenylalanine derive selectors (Sel* = ^{t}Bu-(*S*)Phe-NHCO). *Bottom*: Sections of ^{1}H NMR spectra showing signals for methin protons of investigated compounds.

Analysis of the amide protons revealed significant differences compared to those biaryl analogues studied in chapter 2. Dimerization of these compounds led to a strong downfield ^{1}H NMR shifts and signals for these protons were generally found between 10.7 and 7.3 ppm. In contrast, shifts for compound **55** were found to be much higher between 7.45 and 6.90 ppm for the inner and 6.06 and 4.83 ppm for the terminal amide groups. This indicates a much smaller hydrogen bond interaction with surrounding molecules. Also, when a sample of diol **55** was dissolved in deuterated methanol, complete deuteration of all amide protons was observed within a few hours. Unlike for diol **18c**, where strong hydrogen bonding was found to significantly decelerate the exchange speed leading to a half-life of several days, this is another strong indicator, that inter- or intramolecular non-covalent self-interactions between selector moieties is significantly reduced in ligands that bear a backbone based on *meso*-tartaric acid. In conclusion, initial NMR-based analysis of the ligand precursors suggests that changing the ligand backbone from a biaryl-based to an aliphatic, ethane-based system strongly impairs the self-interaction capabilities that were previously observed to occur with this selector type. Further studies are needed to confirm these findings and to gain further insight into the stereodynamic properties of these ligands.

5.5 Resume

In this chapter, synthetic approaches to a new motif for stereodynamic ligands have been investigated. *Meso*-tartaric acid exists in two enantiomeric synclinal conformers (-*sc* and +*sc*), which serve as analogues to axial isomers of established biphenyl-based *tropos* ligands. The modification of the carboxyl groups with previously investigated phenylalanine-based diamide selector moieties was pursued to yield a ligand motif for highly dynamic *tropos* ligands that could be

used as a blueprint for different ligand types. The geometric arrangement of selector and ligand backbone in this ligand type was also thought to inhibit ligand dimerization that was previously observed for biaryl-based ligands bearing the same selector sites.
Different strategies for the synthesis bisphosphine **48** were attempted and synthesis of dibromo precursor **52** could be achieved, but the subsequent substitution reaction turned out to be problematic and the desired compound could not be obtained.
Similarly, a synthetic strategy for the respective bisphosphinite **49** was devised. Starting from *meso*-tartaric acid, synthesis of respective diol precursor **56** could be achieved in three steps. Reaction to the bisphosphinite was also successful, full purification of the ligand, however, proved difficult and no pure ligand sample was obtained within the timeframe of the project.
Conclusive NMR-assisted investigations of intermediates suggest that, unlike respective biaryl analogues, no ligand dimerization occurs. As with *meso*-tartaric acid, compounds **55**, **56** and **49** were found to adapt a synclinal arrangement as their predominant conformation, when dissolved in $CDCl_3$ or CD_3OD, respectively. Additional experiments, such as DHPCL- or NMR-based interaction studies are necessary to gain a deeper understanding for the stereodynamic behaviour of these types of compounds.

6 Summary and outlook

In this dissertation, the synthesis and study of different stereodynamic ligands and complexes as well as their application in asymmetric reactions have been described. Investigations followed the intent to modify rotational behaviour of compounds through non-covalent interaction of ligand-bound interaction sites with other chiral molecules in order to alter selectivity in enantioselective transformations.

Chapter 2 describes investigations on chiral (*S*)-amino acid-based selector sites, derived from selector sites of high-performance gas chromatography CSP CHIRASIL VAL. Different 2,2'-biphenol-based BIPOL, bisphosphine, bisphosphinite and phosphoramidite ligands with interaction sites in 5,5'-position were devised and it was found that such a substitution entails spontaneous enrichment of the R_{ax} ligand rotamer (see Figure 6-1). Detailed investigations, *inter alia*, by NMR spectroscopy, X-ray structure analysis and HD exchange experiments revealed that intermolecular non-covalent interactions of the selector units lead to formation of well-ordered ligand dimers. The chiral information of the amino acid-based selector groups dictates the axial chirality of the ligand's biphenyl backbones within the supramolecular structure through cooperative chiral induction, allowing only for R_{ax} rotamers to dimierise. This causes selective stabilization of one rotamer and drives the rotameric enrichment. The process can be described as a form of stereoselective, *narcissistic self-sorting* and the state of rotameric enrichment is self-reinforced by dynamic exchange among the complex subunits, which is a form of stereocontrol that resembles that found in *sergeant-soldier*-type self-organizing, supramolecular systems. For selector-modified bisphosphine **7**, a strongly weighted equilibrium between a monomeric S_{ax} rotamer and a dimeric R_{ax} rotamer with a ratio of 16:84 (S_{ax}:R_{ax}) was observed, which could be influenced by adding different chiral or achiral hydrogen bond donors and acceptors that would occupy the interaction sites. BIPOL ligands **18a-c**, phosphinite ligands **19a-c** and phosphoramidite ligands **23a-b**, on the other hand, were found to undergo complete transformation into one diastereomerically pure R_{ax} species each.

BIPOL ligands were used in titanium-mediated enantioselective alkylation reactions of aromatic aldehydes. A variety of different alcohols could be generated with selectivities of up to 79.8% *ee* of the *R* enantiomer.

All phosphorus-based ligands were employed in asymmetric, rhodium-catalyzed hydrogenation reactions. Methyl 2-acetamidoacrylate **12** was reduced using bisphosphine **7** to give the product with an *er* of 17.4:82.6 (*S*:*R*), which indicates high selectivity for each individual ligand rotamer. The enantiomeric excess of the product could be influenced by employing ligand mixtures whose rotameric distribution had previously been adapted by equilibration in presence of chiral or achiral additives and selectivity could be enhanced to an *er* of 8.6:91.4 (*S*:*R*, Δee = +18%, additive Ac-(*S*)Ala-NH(3,5-dichlorophenyl) (*S*)-**9**). Diastereomerically pure bisphosphinite ligands **19a-c** were used for the hydrogenation of benchmark substrates **12** and **20**-**22** where all ligands were found to exhibit high to very high selectivities. Best results were obtained with the phenylalanine-based ligand **19c**, which reduced olefin **12** with a selectivity of 4.0:96.0 (*S*:*R*).

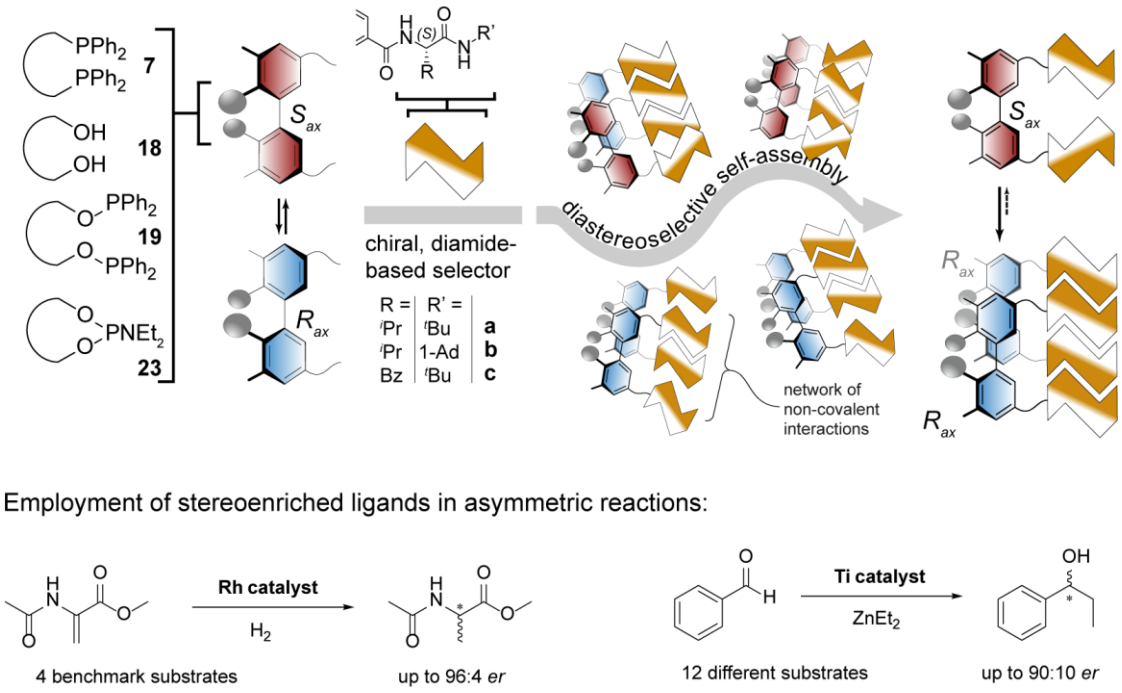

Figure 6-1: Illustration of the diastereoselective self-interaction process. Modifying *tropos* biaryl ligands in 5,5'-position with chiral diamide selectors induces formation of homochiral, energetically favoured dimers, which can be employed as ligands in asymmetric transformations.

Phosphoramidite ligands **23a** and **23b** performed less selectively and the highest enantiomeric ratio of 73.2:26.8 (*S*:*R*) was achieved with ligand **23a** in the reduction of **12**. Interestingly, a reversal in selectivity was observed when the valine-based selector was replaced by a phenylalanine-based one indicating a more complex path of stereoinduction for this ligand type.
With regard to future research, it should be highlighted that this ligand motive yields a predictable structure that can be used to design of self-recognizing enantioselective catalysts for a wide range of reactions. The question arises whether self-assembly-driven enrichment of this type of *tropos* ligands can be realized with other ligand structures. Different interaction modes should be tested in order to identify more specific prerequisites for this process to occur.

In chapter 3, investigations were extended to achiral binding sites for non-covalent interaction. Inspired by the model of "switchable" catalysts, hydrogen-bond driven deracemization of racemic catalysts was examined (see Figure 6-2). A bisphosphinite ligand with 3,5-dichlorobenzoyl selector moieties, previously investigated by Trapp *et al.*[41], was modified with stereodirecting groups in 3,3'-position in order to analyze potential improvement of catalyst selectivity. However, decreased deracemization at lower temperatures was observed and no improvement in selectivity could be achieved. In addition, racemic ligands with 5,5'-diamido selector moieties were investigated. The rhodium complex of dimerizing ligand **19d** with glycine-derived selector sites could successfully be deracemized in presence of different amino acid-derived diamide additives. The switchable nature of the catalyst was verified by employing both enantiomers of compound PhCO-Phe-NH^{t}Bu **25** separately as aligning agents. Subsequent hydrogenation of **12** gave products in 14% *ee S* or *R* when the *R* or the *S* additive was used. Ac-(*S*)Ala-NH(3,5-dichlorophenyl) (*S*)-**9** showed the biggest alignment potential among employed diamides allowing for the reduction to proceed with 34% *ee R*. When ligand-mimicking tetraamide **24** was employed, selectivity could be further increased to 41% *ee R*. In order to investigate adverse

effects of ligand dimerization on the deracemization process, ligand interaction was reduced by employing racemic phenylalanine-derived interaction sites as "mismatching" selector units. The ligand *meso*-**19c** was found not to form stable supramolecular dimers and again, significant chirality transfer was observed. As with ligand **19d**, best selectivities were achieved with diamide (*S*)-**9**, which induced a selectivity of 23% *ee R* for the reduction of **12** and with tetraamide **24** where a selectivity of 46% *ee R* was obtained. Similar selectivities for both catalysts **19d** and *meso*-**19c** in combination with different aligning agents indicate that ligand self-assembly has no adverse effect on the deracemization process, most likely due to fast molecular exchange between ligand subunits, which allows for stereoinducing additives to compete for the interaction sites.

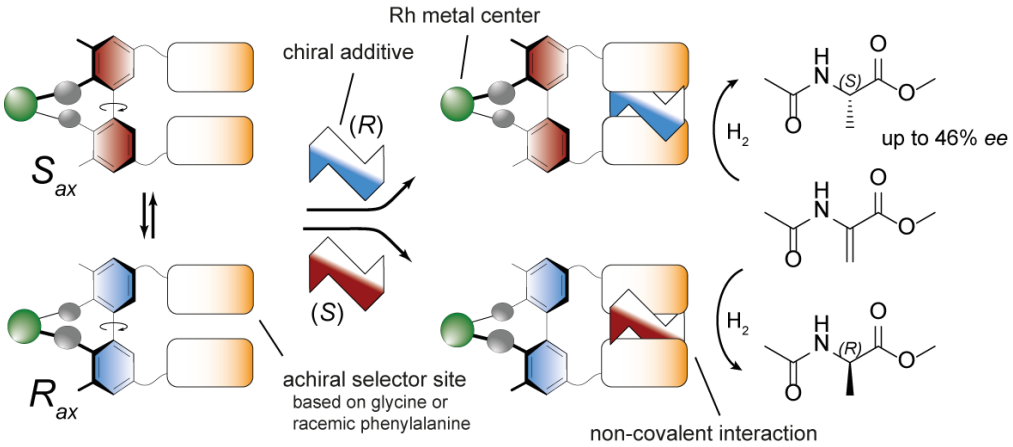

Figure 6-2: Simplified illustration of racemic bisphosphinite catalyst systems described in chapter 3. Deracemization was achieved through non-covalent interactions between the ligands and chiral amino acid derivatives yielding a catalyst for enantioselective hydrogenation.

Prospective research should focus on extending the library of investigated chiral additives in order to correlate substitution patterns to increased ligand deracemization. Detailed mechanistic studies would permit a more directed improvement of the systems. Moreover, it seems desirable to transfer the design to other racemic stereodynamic catalysts to access a wider range of reaction types.

Chapter 4 covers the development of an autoinductive catalyst system. Based on a "by design" self-amplifying reaction previously described by Trapp *et al.*,[40] a complementary system was developed in which the selectivity of a hydrogenation reaction is based on self-inhibiting properties. In a two-stage process, a novel, (*S*)-phenylalanine-based amidoester selector motif was first investigated for its potential to interact with chiral additives. Using a variety of differently substituted (*S*)-amino acid-derived additives as alignment agents, all of them representing potential hydrogenation products, the rotamer ratio of stereodynamic rhodium complex **42** could successfully be manipulated. In subsequent asymmetric reductions of **12** significantly increase in selectivity for the (*R*)-product enantiomer was achieved from 27% *ee R* with the untreated complex to up to 84 % *ee R* (Δee = +57%), after incubating the catalyst with PHCO-(*S*)Phe-NH^{t}Bu (*S*)-**25** for several hours (see Figure 6-3a).

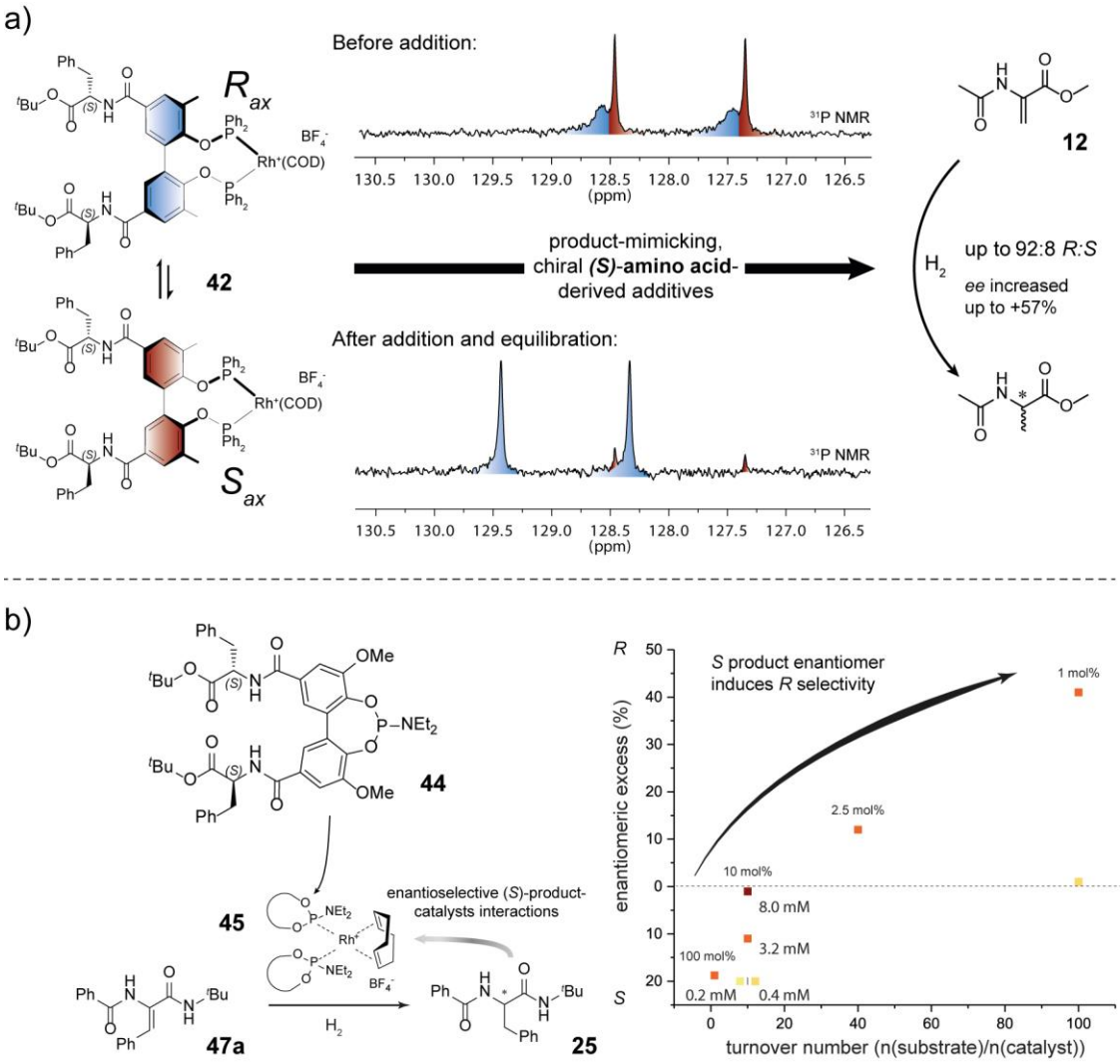

Figure 6-3: Illustration of the two-stage process for the development of an autoinductive, self-inhibition reaction described in chapter 4. a) Investigation of chiral induction between potential hydrogenation products and phenylalanine-derived selector sites. b) Findings were used to devise a system that shows self-inhibiting properties.

Building on these results in the second stage of the project, highly dynamic phosphoramidite complex **45** bearing the same amidoester selector sites was synthesized along with olefin **47a**, among others, which constitutes the unsaturated analogue of strongly interacting diamide (*S*)-**25**. When olefin **47a** was hydrogenated using phosphoramidite complex **45**, it could be shown that (*S*)-**25**, initially produced in excess, successfully supressed its own production during subsequent catalyst turnovers by altering the catalyst selectivity (see Figure 6-3b). When catalyst loadings were decreased, ongoing chiral self-inhibition lead to a reversal in selectivity from 19% *ee S* (100 mol% catalyst) to 41% *ee R* (1 mol% catalyst). The catalyst concentration was found to be another important factor and increasing the catalyst concentration at constant catalyst loadings led to a selectivity shift from 23% *ee S* (0.2 mM in catalyst) to 1% *ee S* (8 mM in catalyst). This was linked to weak intermolecular interaction of ligand molecules, which is an attenuated form of the stereoselective self-sorting process previously found for ligands of similar structure. Considering the structural similarities between the selector sites of catalyst **45** and (*S*)-**25**, this concentration dependency can also be understood as a different manifestation of the enantioselective self-inhibition process. Ultimately, these findings illustrate how the process of self-inhibition, a mechanism prevalent in nature, can be recreated on a molecular level. The process also

forms a complementary addition to the previously published example of chiral self-amplification and can be used as foundation to device new concepts for enantioselective transformations. It also demonstrates how a small deviation from the racemic state can transform into a state of high enantiomeric enrichment as it is presumed to have happened during the emergence of homochirality.

In the last part of the dissertation in Chapter 5 initial studies concerning a novel ligand motive for selector-modified *tropos* ligands with an aliphatic ligand backbone derived from *meso*-tartaric acid are presented. *Meso*-tartaric acid predominantly exists in two enantiomeric synclinal conformers (-*sc* and +*sc*), which serve as analogues to axial isomers of biphenyl-based *tropos* ligands and modification with selector sites for non-covalent interaction was believed to yield a novel motif for highly dynamic *tropos* ligands that could be used as a blueprint for different ligand types (see Figure 6-4). Strategies for the synthesis of a bisphosphine were attempted and different precursor compounds could be obtained.

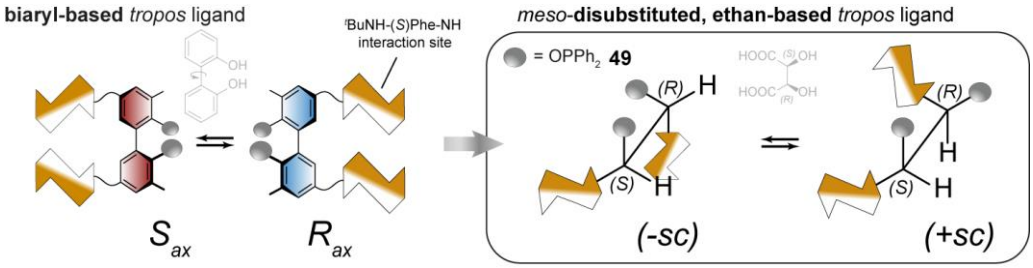

Figure 6-4: Illustration of the conceptual similarity between rotamer species from biphenyl-based *tropos* ligands to ones that are based on *meso*-tartaric acid.

Similarly, a synthetic strategy for the respective bisphosphinite was devised. Starting from *meso*-tartaric acid, synthesis of the diol precursor could be achieved in three steps and reaction to bisphosphinite ligand **49** could successfully be conducted *in situ*. Conclusive NMR-assisted investigations of the ligand and different precursors suggest that no ligand dimerization occurs and compounds were found to adapt a synclinal arrangement as their predominant conformation. Aside from improvement of the synthetic protocols, additional experiments will be necessary to gain a deeper understanding of the stereodynamic behaviour of these types of compounds, which will determine their applicability in subsequent enantioselective reactions.

In conclusion, this dissertation describes a variety of different stereodynamic catalysts, whose selectivity in asymmetric transformations can be manipulated by enantioselective hydrogen bonding. These examples illustrate how non-covalent interactions can become a strong driving force for the transmission of a chiral bias and they can serve as starting points for the investigation of other stereodynamic systems. Moreover, these findings can be used to understand pathways for the transfer of chiral information in nature, which is particularly interesting in the context of auto induction and homochirality. They can also be a basis for the development of novel catalyst systems.

7 Experimental section

7.1 General remarks

Materials:
All reactions involving the use of oxygen or moisture sensitive substances were carried out in dried glassware under an atmosphere of nitrogen or argon using standard Schlenk techniques. All chemicals were used as received from suppliers without further purification. Column chromatography was done using silica gel (technical grade, pore size 60 Å, 70-230 mesh, 63-200 µm) produced by Sigma-Aldrich Chemie GmbH. Thin layer chromatography was performed on coated aluminium sheets (Machery-Nagel POLYGRAM ® SIL G/UV 254). Components were visualized by fluorescence quenching during irradiation with UV light (254 nm) or by using appropriate staining agents. Dry solvents were taped from solvent purification system MB SPS-800 and used immediately. Manual degassing of solvents, if needed, was done by performing three consecutive freeze-pump-thaw cycles. Dry, oxygen-free solvents were then stored in J. Young ampules over molecular sieves and under an atmosphere of argon. Dry and degassed THF was purchased containing 250 ppm BHT as stabilizer.

Analytics:
NMR spectra were recorded at the NMR Spectroscopy Facilities of the Institute of Organic Chemistry, University of Heidelberg (Head: Dr. Jürgen Graf) and of the Faculty of Chemistry and Pharmacy, LMU Munich (Head: Dr. David Stephenson) on Varian NMR-Systems (300, 400 and 600 MHz) and Bruker Avance III HD and DRX (300, 400, 600 and 800 MHz). NMR shifts are given in parts per million (ppm) and are referenced to the residual proton or carbon solvent signals.[225] Couplings are termed as follows: s (singlet), bs (broad singlet), d (doublet), t (triplet), sept (septet), dd (doublet of a doublet), dt (doublet of triplet) and tt (triplet of triplet), m (multiplet). Assignment was done by means of two-dimensional experiments (^{1}H-^{1}H-COSY, ^{1}H-^{13}C-HSQC, ^{1}H-^{13}C-HMBC). The numbering is depicted in the respective figure shown above each procedure. If two halves of a formally symmetric molecule are represented by different signal sets, respective atoms are denoted with numbers X and X'.
Mass spectra were acquired at the Mass Spectrometry Facilities of the Institute of Organic Chemistry, University of Heidelberg (Head: Dr. Jürgen H. Gross) and of the Faculty of Chemistry and Pharmacy, LMU Munich (Head: Dr. Werner Spahl) on JEOL JMS-700 magnetic sector (EI), Thermo Finnigan MAT 95/Jeol MStation sector field (FAB), Bruker ApexQe hybrid 9.4 T FT-ICR (DART), Thermo Q Exactive Hybrid Quadrupole Orbitrap and on Thermo Finnigan LTQ FT Ultra FT-ICR (ESI).
For solid state IR analysis, Thermo Fisher Nicolet 6700 FT-IR-Spectrometer was employed and the wavenumber of reflectance was measured with signals being denoted as s (strong), m (medium), w (weak) and b (broad signal).
Crystallographic data was collected at the X-Ray Crystallography Laboratories of the Institute of Organic Chemistry, University of Heidelberg (Head: Dr. Frank Rominger) and of the Faculty of Chemistry and Pharmacy, LMU Munich (Head: Dr. Peter Mayer) on Bruker APEX-II Quazar area detector and on a STOE-IPDS system with Mo Kα radiation (λ = 0.71073 Å).

Elemental analysis was conducted at the combustion analysis laboratories of the Faculty of Chemistry and Pharmacy, LMU Munich (Head: Dr. Bernhard Kempf) on a Elementar vario micro cube equipped with a thermal conductivity detector.
UPLC-MS analysis was conducted on Waters UPLC-SQD2 (DAD/APCI-MS) equipped with reversed-phase BEH C18 using different gradients of acetonitrile and water as mobile phase. HPLC and HPLC-MS measurements were performed on Agilent Technologies 1200 HPLC machines equipped with DAD and quadrupole mass spectrometer. All columns with chiral stationary phases were obtained from Chiral Technologies. HPLC-grade solvents were obtained for Sigma-Aldrich.
GC analysis was done on Thermo Trace GC ULTRA, equipped with autosampler, split/splitless injector (20 mL/min splitflow, 250 °C injector temperature) and FID detector. Chiral columns (25 m, i.d. 250 µm, film thickness 250 nm) were prepared and coated in the Trapp group.
In order to improve comprehensibility, most compounds are described with simplified names instead of IUPAC names.

7.2 Experimental data for chapter 2

1.1.1 Methyl-3-bromo-5-hydroxybenzoate (1i)

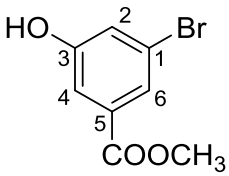

3-Bromo-5-hydroxybenzoic acid (2.90 g, 13.4 mmol, 1.00 eq.) was dissolved in methanol (25.0 mL). Concentrated sulfuric acid (3.54 g, 1.92 mL, 36.1 mmol, 2.70 eq.) was added and the clear solution was refluxed for five hours. The solution was then allowed to cool to room temperature and sodium hydroxide solution (2M, 20.0 mL) was added until pH 8 was reached. Water (40.0 mL) was added and white solids precipitated. The suspension was stirred for 15 min to complete the crystallization. Afterwards, solids were filtered off, washed with cold water and dried in vacuo yielding the product **1i** as white crystals (2.60 g, 11.2 mmol, 84%).
^{1}**H-NMR** ($CDCl_3$, 600.24 MHz, 300 K): δ = 3.92 (s, 3H, CH_3), 6.14 (s, 1H, OH), 7.24 (s, 1H, H2), 7.51 (s, 1H, H4), 7.73 (s, 1H, H6) ppm.
^{13}C{^{1}H}-NMR ($CDCl_3$, 150.93 MHz, 300 K): δ = 52.9 (CH_3), 115.6 (C4), 123.0 (C1), 123.6 (C2), 125.0 (C6), 132.7 (C5), 156.8 (C3), 166.3 (C=O) ppm.
HRMS (EI): m/z calcd. for $C_8H_7BrO_3$ where Br is ^{79}Br $[M]^+$: 229.9579; found: 229.9563.
FTIR: $\tilde{\nu}$ = 763 (s), 1271 (s), 1425 (s), 1591 (s), 1706 (s), 2841 (w), 2958 (m), 3044 (w), 3096 (m), 3392 (b) cm^{-1}.

1.1.2 Methyl-5-bromo-3-(diphenylphosphinoyl)benzoate (2)

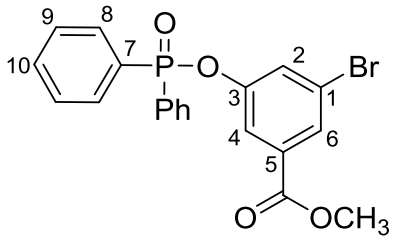

An adaptation of the procedure published by Keay et al. was applied.[96] Phenol derivative **1i** (3.34 g, 14.5 mmol, 1.00 eq.) and 4-(dimethylamino)pyridine (88.3 mg, 733 µmol, 0.05 eq.) were stirred in dry dichloromethane (40.0 mL). Solids dissolved upon addition of dry triethylamine (2.05 g, 2.82 mL, 20.2 mmol, 1.40 eq.) and the clear solution was cooled in an ice bath. Diphenylphosphinic chloride (4.79 g, 3.86 mL, 20.2 mmol, 1.40 eq.) was added dropwise at 0 °C. After warming to room temperature, the resulting orange solution was stirred for 20 hours. Upon subsequent addition of n-hexane, triethylammonium chloride precipitated and stirring was resumed for 15 min. The solids were filtered off and washed with more n-hexane. The combined organic layer was evaporated to give the crude mix as a clear oil, which was purified using column chromatography (silica, petrol ether: ethyl acetate 10:1 → 1:1, R_f = 0.49 in 2:1 petrol ether: ethyl acetate). The product **2** could be obtained as a white solid (5.17 g, 12.0 mmol, 83%).
^{1}H-NMR (CD_2Cl_2, 600.24 MHz, 300 K): δ = 3.87 (s, 3H, CH_3), 7.51 (dt, 4H, ^{3}J(H,H) = 5.00 Hz, ^{4}J(P,H) = 3.48 Hz, H9), 7.59 (t, 2H, ^{3}J(H,H) = 7.43 Hz, H10), 7.63 (s, 1H, H2), 7.79 (s, 1H, H4), 7.88 (dd, 4H, ^{3}J(H,H) = 7.72, ^{3}J(P,H) = 12.67 Hz, H8), 7.91 (s, 1H, H6) ppm.
^{13}C{^{1}H}-NMR (CD_2Cl_2, 150.93 MHz, 300 K): δ = 52.9 (s, 1C, CH_3), 121.0 (d, 1C, ^{3}J(C,P) = 5.16 Hz, C4), 122.9 (s, 1C, C1), 128.5 (d, 1C, ^{3}J(C,P) = 4.78 Hz, C2), 129.1 (s, 1C, C6), 129.2 (d, 4C, ^{3}J(C,P) = 13.51 Hz, C9), 130.7 (d, 2C, ^{1}J(C,P) = 137.59 Hz, C7), 132.0 (d, 4C, ^{2}J(C,P) = 10.42 Hz, C8), 133.2 (d, 2C, ^{4}J(C,P) = 2.82 Hz, C10), 133.5 (s, 1C, C5), 151.9 (d, 1C, ^{2}J(C,P) = 7.92 Hz, C3), 165.1 (s, 1C, C=O) ppm.
^{31}P{^{1}H}-NMR (CD_2Cl_2, 242.98 MHz, 300 K): δ = 31.84 (s) ppm.
HRMS (ESI): m/z calcd. for $C_{20}H_{17}BrO_4P$ where Br is ^{79}Br $[M+H]^+$: 431.0042; found: 431.0042.
FTIR: $\tilde{\nu}$ = 724 (s), 1204 (s), 1428 (s), 1573 (s), 1725 (s), 2946 (w), 2993 (w), 3051 (m) cm^{-1}.

1.1.3 Methyl-3-bromo-4-(diphenylphosphoryl)-5-hydroxy (3)

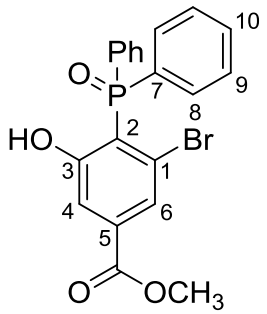

Phosphoric acid ester **2** (1.25 g, 2.90 mmol, 1.00 eq.) was dissolved in dry THF (25.0 mL) and the flask was placed in an acetone/dry ice cooling bath. LDA solution (342 mg, 1.59 mL, 3.19 mmol, 1.10 eq.; 2M in THF/n-heptane/ethylbenzene) was added dropwise at -78 °C and the yellow solution was kept stirring in the cooling bath to warm to room temperature overnight.

After 15 hours, the solution was quenched with saturated ammonium chloride solution (25.0 mL). The layers were separated and the aqueous layer was washed twice with ethyl acetate. Combined organic layers were washed with HCl solution (1M) and brine, dried over sodium sulfate and evaporated to afford the crude product as a yellow oil. Purification by column chromatography (silica, PE:EE 15:1 → 8:1, R_f = 0.46 in 4:1 PE:EE) gave a yellow solid. Washing with a mixture of petrol ether and ethyl acetate (20:1 v/v) removed the impurities and after drying in vacuo, the pure compound **3** was obtained as a white solid (360 mg, 835 µmol, 29%).
^{1}H-NMR ($CDCl_3$, 600.24 MHz, 300 K): δ = 3.92 (s, 3H, CH_3), 7.53 (dt, 4H, ^{3}J(H,H) = 7.56 Hz, ^{4}J(P,H) = 2.76 Hz, H9), 7.61-7.62 (m, 1H, H4), 7.63 (t, 2H, ^{3}J(H,H) = 7.32 Hz, H10), 7.66-7.68 (m, 1H, H6), 7.85 (dd, 4H, ^{3}J(H,H) = 7.68 Hz, ^{3}J(P,H) = 12.93 Hz, H8), 13.12 (s, 1H, OH) ppm.
^{13}C{^{1}H}-NMR ($CDCl_3$, 150.93 MHz, 300 K): δ = 52.9 (s, 1C, CH_3), 114.7 (d, 1C, ^{1}J(C,P) = 102.50 Hz, C2), 119.9 (d, 1C, ^{3}J(C,P) = 6.82 Hz, C4), 125.2 (d, 1C, ^{3}J(C,P) = 7.50 Hz, C6), 125.3 (d, 1C, ^{2}J(C,P) = 5.52 Hz, C1), 128.8 (d, 4C, ^{3}J(C,P) = 13.10 Hz, C9), 130.2 (d, 2C, ^{1}J(C,P) = 110.01 Hz, C7), 132.7 (d, 4C, ^{2}J(C,P) = 10.85 Hz, C8), 133.0 (d, 2C, ^{4}J(C,P) = 2.78 Hz, C10), 136.4 (d, 1C, ^{4}J(C,P) = 1.63 Hz, C5), 165.2 (s, 1C, C=O), 167.7 (d, 1C, ^{2}J(C,P) = 3.52 Hz, C3) ppm.
^{31}P{^{1}H}-NMR ($CDCl_3$, 242.98 MHz, 300 K): δ = 45.07 ppm.
HRMS (ESI): m/z calcd. for $C_{20}H_{14}BrO_4P$ where Br is ^{79}Br $[M-H]^-$: 429.9897; found: 428.9888.
FTIR: $\tilde{\nu}$ = 694 (s), 1118 (s), 1398 (s), 1551 (s), 1722 (s), 2653 (b), 2955 (w), 3062 (w) cm^{-1}.

1.1.4 Methyl-3-bromo-4-(diphenylphosphoryl)-5-methoxy benzoate (4)

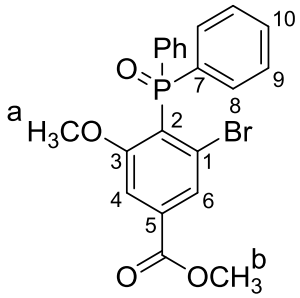

A slightly adapted procedure introduced by Brown et al. was employed.[49] Phosphine oxide **3** (360 mg, 835 µmol, 1.00 eq.) was suspended in acetone (15.0 mL) at 0 °C. After adding caesium carbonate (544 mg, 1.67 mmol, 2.00 eq.) the suspension became highly viscous and turned yellow. Iodomethane (1.18 g, 510 µL, 8.34 mmol, 10.0 eq.) was added dropwise via syringe and after warming to room temperature, the mixture was stirred for nine hours. Subsequently, evaporation of the colorless suspension yielded a white solid residue which was dissolved in a mixture of water and dichloromethane (20.0 mL, 1:1 v/v). The layers were separated, the aqueous phase was extracted with dichloromethane twice more and the combined organic layer was washed with water and brine. Drying over sodium sulfate and evaporation of the solvent gave the pure product **4** as a white solid (362 mg, 835 µmol, 98%).
^{1}H-NMR (CD_2Cl_2, 600.24 MHz, 300 K): δ = 3.25 (s, 3H, CH_3^a), 3.91 (s, 3H, CH_3^b), 7.43-7.48 (m, 5H, H6 and H9), 7.53 (t, 2H, ^{3}J(H,H) = 7.38 Hz, H10), 7.66 (dd, 4H, ^{3}J(H,H) = 7.50 Hz, ^{3}J(P,H) = 12.93 Hz, H8), 7.95 (s, 1H, H4) ppm.
^{13}C{^{1}H}-NMR (CD_2Cl_2, 150.93 MHz, 300 K): δ = 53.0 (s, 1C, CH_3^b), 55.9 (s, 1C, CH_3^a), 112.1 (d, 1C, ^{2}J(C,P) = 5.30 Hz, C6), 125.9 (d, 1C, ^{1}J(C,P) = 98.4 Hz, C2), 128.7 (d, 4C, ^{3}J(C,P) = 12.7 Hz, C9), 128.7 (s, 1C, C1), 129.2 (d, 1C, ^{3}J(C,P) = 7.83 Hz, C4), 131.3 (d, 4C, ^{2}J(C,P) = 10.17 Hz, C8), 131.8 (d, 2C, ^{4}J(C,P) = 2.79 Hz, C10), 134.1 (d, 2C, ^{1}J(C,P) = 110.20 Hz, C7),

135.7 (d, 1C, ^{4}J(C,P) = 1.71 Hz, C5), 162.6 (d, 1C, ^{2}J(C,P) = 3.26 Hz, C3), 165.3 (s, 1C, C=O) ppm.

$^{31}P\{^{1}H\}$-NMR (CD_2Cl_2, 242.98 MHz, 300 K): δ = 25.72 ppm.

HRMS (ESI): m/z calcd. for $C_{21}H_{19}BrO_4P$ where Br is ^{79}Br $[M+H]^+$: 445.0199; found: 445.0199.

FTIR: $\tilde{\nu}$ = 698 (s), 1240 (s), 1546 (s), 1717 (s), 2953 (w), 2984 (w), 3048 (w) cm^{-1}.

1.1.5 3,3′-Dimethoxy-5,5′-bis(methoxycarbonyl)-[1,1′-biphenyl]-2,2′-bis(diphenylphosphine oxide) (5)

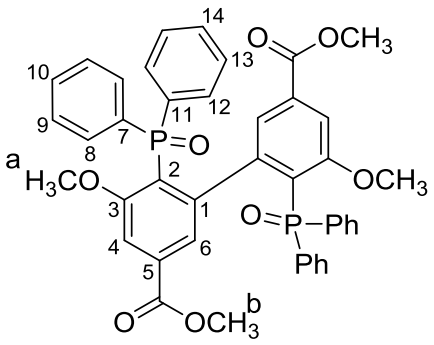

Phosphine oxide **4** (350 mg, 786 µmol, 1.00 eq.) was stirred in dry dimethylformamide (6 mL). Copper powder (125 mg, 1.97 mmol, 2.50 eq.) was added at once and the mixture was heated to 80 °C. After two hours, the mixture was filtrated and the remaining solids were washed with dichloromethane. The organic layer was collected and the green solution was washed with saturated ammonium chloride solution to remove copper salts. It was then washed with water and brine, dried over sodium sulfate and evaporated to give the crude product as a white foam. Purification by column chromatography (silica, dichloromethane:methanol 200:1 → 50:1, R_f = 0.05 in 100:1 dichloromethane:methanol) gave the pure bis(phosphine oxide) **5** as a white solid (262 mg, 358 µmol, 91%).

^{1}H-NMR (CD_3OD, 600.24 MHz, 300 K): δ = 3.41 (s, 6H, CH_3^a), 3.81 (s, 6H, CH_3^b), 7.30-7.35 (m, 6H, H6 and H9), 7.43 (dt, 2H, ^{3}J(H,H) = 7.44 Hz, ^{5}J(P,H) = 0.96 Hz, H10), 7.55 (dd, 2H, ^{4}J(H,H) = 4.56 Hz, ^{4}J(P,H) = 0.90 Hz, H4), 7.58 (dt, 4H, ^{3}J(H,H) = 7.65 Hz, ^{4}J(P,H) = 2.88 Hz, H13), 7.64-7.72 (m, 6H, H8 and H14), 7.85 (dd, 4H, ^{3}J(H,H) = 8.18 Hz, ^{3}J(P,H) = 12.26 Hz, H12) ppm.

$^{13}C\{^{1}H\}$-NMR (CD_3OD, 150.93 MHz, 300 K): δ = 52.9 (s, 2C, CH_3^b), 55.8 (s, 2C, CH_3^a), 112.4 (d, 2C, ^{3}J(C,P) = 6.10 Hz, C4), 123.5 (d, 2C, ^{1}J(C,P) = 102.10 Hz, C2), 126.8 (d, 2C, ^{3}J(C,P) = 10.00 Hz, C6), 129.0 (d, 4C, ^{3}J(C,P) = 13.08 Hz, C9), 129.6 (d, 4C, ^{3}J(C,P) = 12.61 Hz, C13), 132.3 (d, 2C, ^{4}J(C,P) = 2.62 Hz, C10), 132.4 (d, 4C, ^{2}J(C,P) = 11.19 Hz, C8), 133.2 (s, 2C, C14), 133.8 (d, 2C, ^{1}J(C,P) = 106.37 Hz, C11), 134.7 (d, 2C, ^{4}J(C,P) = 1.66 Hz, C5), 136.4 (d, 2C, ^{1}J(C,P) = 112.32 Hz, C7), 150.3 (t, 2C, ^{2}J(C,P) = 3.95 Hz, C1), 162.1 (d, 2C, ^{2}J(C,P) = 5.81 Hz, C3), 167.2 (s, 2C, C=O) ppm.

$^{31}P\{^{1}H\}$-NMR (CD_3OD, 121.65 MHz, 300 K): δ = 30.61 ppm.

HRMS (ESI): m/z calcd. for $C_{42}H_{37}O_8P_2$ $[M+H]^+$: 731.1958; found: 731.1962.

FTIR: $\tilde{\nu}$ = 693 (s), 1280 (s), 1384 (s), 1433 (s), 1558 (s), 1715 (s), 2851 (w), 2925 (m), 3051 (w) cm^{-1}.

1.1.6 3,3′-Dimethoxy-5,5′-bis(methoxycarbonyl)-[1,1′-biphenyl]-2,2′-bis(diphenylphosphine) (6)

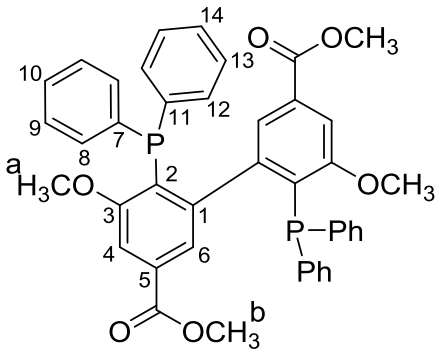

Diphenylphosphine oxide **5** (52.0 mg, 71.2 µmol, 1.00 eq.) was placed under an atmosphere of nitrogen, and phenylsilane (0.50 mL) was added. The suspension was heated to 120 °C and stirred for 40 hours. After cooling to room temperature, the crude mix was directly placed on a short pad of silica under an inert atmosphere. Silanes were removed first by washing with dry and degassed n-pentane (50.0 mL). Subsequently, the product was eluated using dry and degassed dichloromethane (70.0 mL). Upon removal of the solvent in vacuo, bisphosphine **6** could be obtained as a waxy white solid. (47.0 mg, 67.3 µmol, 95%). The compound is oxygen-sensitive and must be stored under argon.

Enantiomeric separation of a sample for subsequent hydrogenation experiments was performed on Chiralpak® IA (250 mm, i.d. 20 mm, particle size 5 µm) using n-hexane and 2-propanol (95:5) as eluent with a solvent flow of 19.7 mL/min. Fractions of the pure enantiomers, collected automatically by slope analysis, were immediately combined and cooled to -10 °C to avoid racemization. Removal of solvent afforded the separated enantiomers as white solids with an enantiomeric excess of 91% *ee*, as determined by HPLC.

Note: Due to the complexity of the phosphorous coupling, only phosphorous decoupled spectra are being reported. Signals are denoted as multiplets if coupling occurs.

^{1}H-NMR ($CDCl_3$, 600.24 MHz, 300 K): δ = 3.36 (2, 6H, CH_3^a), 3.79 (s, 6H, CH_3^b), 7.05-7.10 (m, 6H, H9 and H10), 7.14-7.17 (m, 4H, H8), 7.30-7.33 (m, 6H, H13 and H14), 7.44-7.45 (m, 2H, H6), 7.47-7.50 (m, 6H, H4 and H12) ppm.

^{13}C{^{1}H}-NMR ($CDCl_3$, 150.93 MHz, 300 K): δ = 52.3 (s, 2C, CH_3^b), 55.3 (s, 2C, CH_3^a), 111.8 (s, 2C, C4), 124.7 (m, 2C, C6), 127.0 (s, 2C, C10), 127.6 (m, 4C, C9), 128.1 (m, 4C, C13), 128.3 (s, 2C, C14), 129.0 (m, 2C, C2), 131.7 (m, 4C, C8), 131.8 (s, 2C, C5), 133.8 (m, 4C, C12), 136.0 (m, 2C, C11), 137.4 (m, 2C, C7), 151.7 (m, 2C, C1), 162.2 (s, 2C, C3), 166.8 (s, 2C, C=O) ppm.

^{31}P{^{1}H}-NMR ($CDCl_3$, 242.98 MHz, 300 K): δ = -15.47 ppm.

HRMS (ESI): m/z calcd. for $C_{42}H_{37}O_6P_2$ $[M+H]^+$: 699.2060; found: 699.2063.

FTIR: $\tilde{\nu}$ = 689 (s), 790.4 (s), 1259 (s), 1553 (s), 1717 (s), 2962 (m), 3036 (w) cm^{-1}.

1.1.7 6,6'-bis(diphenylphosphaneyl)-5,5'-dimethoxy-[1,1'-biphenyl]-3,3'-dicarboxylic acid (6i)

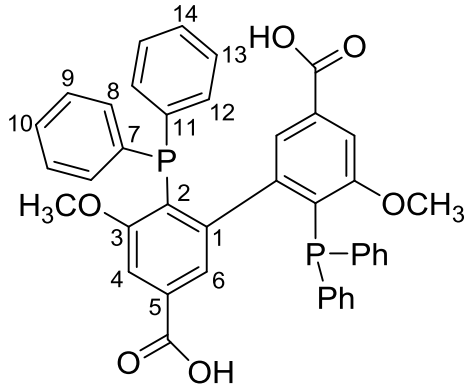

Compound **6** (10.0 mg, 14.3 µmol, 1.00 eq.) was placed under an atmosphere of nitrogen. A degassed solution of potassium hydroxide in water and THF (12.1 mg, 2145 µmol, 10.0 eq.; 3.00 mL solvent, 4:1 v/v) was added by syringe and the resulting clear solution was stirred vigorously at 55 °C for 5 hours. THF was then removed under reduced pressure and the aqueous layer was washed twice with degassed water (1.50 mL). Subsequent addition of hydrochloric acid in diethyl ether (0.45 mL, 0.45 mmol; 1M) and evaporation of all solvents gave yellow solids. They were slurried twice in water (1.50 mL each) to remove inorganic salts. Final extraction with methanol gave an orange solution. Its evaporation afforded the free acid **6i** as a yellow solid (9.50 mg, 14.2 µmol, 99%). The compound is oxygen-sensitive and must be stored under argon.

Note: Due to the complexity of the phosphorous coupling, only phosphorous decoupled spectra are being reported. Signals are denoted as multiplets if coupling occurs.

^{1}H-NMR (CD_3OD, 600.24 MHz, 300 K): δ = 3.36 (s, 6H, CH_3), 7.04-7.09 (m, 6H, H9 and H10), 7.12-7.15 (m, 4H, H8), 7.30-7.34 (m, 6H, H13 and H14), 7.38 (s, 2H, H6), 7.45-7.47 (m, 4H, H12), 7.53 (s, 2H, H4) ppm. No COOH signal was observed due to rapid HD exchange.

^{13}C{^{1}H}-NMR (CD_3OD, 150.93 MHz, 300 K): δ = 55.5 (s, 2C, CH_3), 112.7 (s, 2C, C4), 125.7 (m, 2C, C6), 128.0 (s, 2C, C10), 128.5 (m, 4C, C9), 129.2 (m, 4C, C13), 129.5 (s, 2C, C14), 129.9 (s, 2C, C5), 130.1 (m, 2C, C2), 132.4 (m, 4C, C8), 134.8 (m, 4C, C12), 137.0 (m, 2C, C11), 138.9 (m, 2C, C7), 153.1 (m, 2C, C1), 163.5 (m, 2C, C3), 169.2 (s, 2C, C=O) ppm.

^{31}P{^{1}H}-NMR (CD_3OD, 242.98 MHz, 300 K): δ = -15.99 ppm.

HRMS (ESI): m/z calcd. for $C_{40}H_{31}O_6P_2$ $[M-H]^-$: 669.1601; found: 669.1598.

FTIR: $\tilde{\nu}$ = 691 (s), 1034 (s), 1247 (s), 1552 (s), 1685 (s), 2552 (b), 2849 (w), 2933 (w), 2961 (w) cm^{-1}.

7.2.1 ^{t}BuNH-(*S*)Val-NH bisphosphine (7)

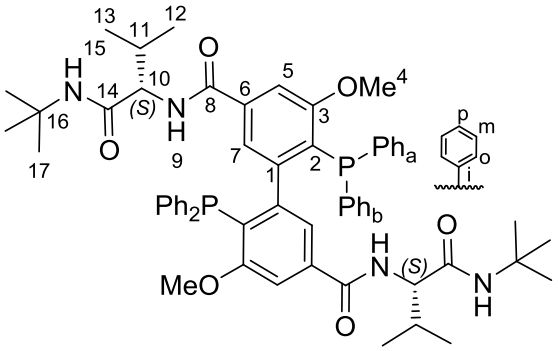

Deprotected bisphosphine precursor **6i** (119 mg, 177 µmol, 1.00 eq.) and HOBt (47.9 mg, 354 µmol, 2.00 eq.) were placed in a dried Schlenk flask and stirred in dry and degassed DCM (3 ml). In a separate flask, the amine hydrochloride **S2** (81.5 mg, 390 µmol, 2.20 eq.) was stirred in dry and degassed DCM and DIPEA (68.0 µl, 390 µmol, 2.20 eq.) was added. Both mixtures were cooled in an ice bath. Subsequently, EDCI.HCl (74.8 mg, 390 µmol, 2.20 eq.) was added to the suspended bisphosphine. Within 15 min, a bright yellow solution had formed, the deprotonated amine from the second flask was added dropwise using a syringe and its flask rinsed twice (1 ml solvent each). The mixture was kept stirring at low temperatures for one hour and then at room temperature for another 17 hours. For workup, the resulting turbid solution was stirred vigorously after addition of hydrochloric acid in diethyl ether (1 ml, 2 M) and degassed water (8 ml) for several minutes. The aqueous layer was subsequently removed via syringe. This was repeated twice. The organic layer was finally washed with water (3 ml) and evaporated to give the crude as a white solid. It was further purified by inert column chromatography (neutral alumina, DCM as forerunning, DCM:MeOH 125:1 as eluent) to give the product **7** as a white solids (110 mg, 112 µmol, 63%). The compound is oxygen-sensitive and has to be stored under argon.

The product was obtained as a mixture of a minor and a major diastereomer **A** and **B**, which was heated in dry and degassed $CDCl_3$ for 16 hours to ensure equilibration. For analytic purposes, pure samples of both rotamers were prepared and individually analysed (see page 100).
Note: Due to the complexity of the phosphorus coupling, only phosphorus decoupled spectra are being reported. Signals are denoted as multiplets if coupling occurs.

^{31}P{^{1}H}-NMR ($CDCl_3$, 242.98 MHz, 300 K): δ = -15.85 (s, A), -17.80 (d, ^{TS}J(P,P) = 9.7 Hz, B1), -18.24 (d, ^{TS}J(P,P) = 9.7 Hz, B2) ppm.
^{1}H-NMR ($CDCl_3$, 600.24 MHz, 300 K): δ = 0.70 (s, H9, B/H16'), 0.83 (d, 6H, ^{3}J(H,H) = 6.66 Hz, A/H11), 0.94 (d, 6H, ^{3}J(H,H) = 6.75 Hz, A/H12), 0.96 (d, 3H, ^{3}J(H,H) = 6.50 Hz, B/H11'), 1.07 (d, 6H, ^{3}J(H,H) = 6.5 Hz, B/H11 and H12'), 1.33 (d, 3H, ^{3}J(H,H) = 6.5 Hz, B/H12), 1.35 (s, 18H, A/H16), 1.41 (s, 9H, B/H16), 1.99-2.06 (m, 2H, ^{3}J(H,H) = 6.94 Hz, A/H10), 2.21 (s, 3H, B/H17'), 2.29-2.39 (m, 1H, B/H10), 2.41-2.51 (m, 1H, B/H10'), 3.38 (s, 3H, B/H17), 3.93 (dd, 1H, ^{3}J(H,H) = 6.6 Hz, ^{3}J(H,H) = 9.7 Hz, B/H9), 4.43 (s, 6H, A/H17), 4.13 (t, 2H, ^{3}J(H,H) = 8.00 Hz, A/H9), 5.22 (dd, 1H, ^{3}J(H,H) = 5.04 Hz, ^{3}J(H,H) = 9.78 Hz, B/H9'), 5.75 (s, 1H, B/H14), 5.84 (bs, 2H, A/H14), 6.38 (d, 2H, ^{3}J(H,H) = 7.8 Hz, A/H8), 6.51 (s, 1H, B/H4'), 6.79-6.91 (m, 6H, B/H$^{m}_{Ph,c}$ and H$^{m}_{Ph,d}$ and H$^{p}_{Ph,c}$ and H$^{p}_{Ph,d}$), 6.96 (s, 1H, B/H14'), 6.96-7.07 (m, 5H, B/H$^{o}_{Ph,c}$ and H$^{o}_{Ph,d}$ and H$^{p}_{Ph,b}$), 6.97-7.00 (m, 2H, A/H6), 7.07-7.18 (m, 5H, B/H$^{m}_{Ph,b}$ and H$^{m}_{Ph,a}$

and $H^{p}_{Ph,a}$), 7.08-7.10 (m, 6H, A/$H^{m}_{Ph,a}$ and $H^{p}_{Ph,a}$), 7.16 (m, 4H, A/$H^{o}_{Ph,a}$), 7.287.32 (m, 4H, A/H4 and $H^{p}_{Ph,b}$), 7.33-7.37 (m, 4H, A/$H^{m}_{Ph,b}$), 7.34-7.40 (m, 2H, B/$H^{o}_{Ph,a}$), 7.41-7.47 (m, 2H, B/$H^{o}_{Ph,b}$), 7.45-7.49 (m, 4H, A/$H^{o}_{Ph,b}$), 7.57 (s, 1H, B/H4), 7.60 (bs, 1H, B/H6'), 7.87 (bs, 1H, B/H6) 8.34 (d, 1H, ^{3}J(H,H) = 6.6 Hz, B/H8), 9.05 (d, 1H, ^{3}J(H,H) = 10.05 Hz, B/H8') ppm.
^{13}C{^{1}H}-NMR ($CDCl_3$, 150.93 MHz, 300 K): δ = 17.6 (s, 1C, B/C11' or C12'), 18.7 (s, 2C, A/C12), 19.6 (s, 2C, A/C11), 19.8 (s, 1C, B/C11' or C12'), 20.0 (s, 1C, B/C11 or C12), 20.5 (s, 1C, B/C11 or C12), 28.5 (s, 1C, B/C16'), 29.0 (s, 1C, B/C16), 29.0 (s, 6C, A/C16), 30.3 (s, 1C, B/C10), 31.4 (s, 2C, A/C10), 33.0 (s, 1C, B/C10'), 50.6 (s, 1C, B/C15'), 51.8 (s,2C, A/C15), 51.8 (s, 1C, B/C15), 53.4 (s, 1C, B/C17'), 55.2 (s, 1C, B/C17), 55.4 (s, 2C, A/C17), 57.7 (s, 1C, B/C9'), 60.0 (s, 2C, A/C9), 62.9 (s, 1C, B/C9), 110.0 (s, 1C, B/C4'), 110.6 (s, 1C, B/C4), 110.8 (s, 2C, A/C4), 120.7 (m, 1C, B/C6'), 121.1 (m, 2C, A/C6), 121.3 (m, 1C, B/C6), 125.4 (m, 1C, B/C2'), 126.4 (s, 1C, B/$C^{p}_{Ph,c}$ or $C^{p}_{Ph,d}$), 126.5 (s, 1C, B/$C^{p}_{Ph,c}$ or $C^{p}_{Ph,d}$), 127.0 126.4 (m, 1C, B/$C^{m}_{Ph,c}$), 127.1 (s, 2C, A/$C^{p}_{Ph,a}$), 127.1 (m, 1C, B/$C^{m}_{Ph,d}$), 127.3 (m, 2C, A/C2), 127.3 (s, 1C, B/$C^{p}_{Ph,b}$), 127.5 (m, 1C, B/$C^{m}_{Ph,a}$), 127.6 (m, 4C, A/$C^{m}_{Ph,a}$), 127.7 (s, 1C, B/$C^{p}_{Ph,a}$), 127.8 (m, 1C, B/$C^{m}_{Ph,b}$), 127.9 (m, 1C, B/C2), 128.4 (m, 4C, A/$C^{m}_{Ph,b}$), 128.5 (s, 2C, A/$C^{p}_{Ph,b}$), 131.6 (m, 4C, A/$C^{o}_{Ph,a}$), 131.6 (m, 1C, B/$C^{o}_{Ph,c}$), 132.0 (m, 1C, B/$C^{o}_{Ph,d}$), 132.9 (m, 1C, B/$C^{o}_{Ph,b}$), 133.7 (m, 4C, A/$C^{o}_{Ph,b}$), 133.9 (m, 1C, B/$C^{o}_{Ph,a}$), 134.0 (m, 1C, B/$C^{i}_{Ph,d}$), 134.7 (s, 1C, B/C5), 135.3 (m, 1C, B/$C^{i}_{Ph,c}$), 135.8 (m, 2C, A/$C^{i}_{Ph,b}$), 136.2 (s, 1C, B/C5'), 136.5 (s, 2C, A/C5), 137.2 (m, 1C, B/$C^{i}_{Ph,a}$), 137.7 (m, 2C, A/$C^{i}_{Ph,a}$), 138.4 (m, 1C, B/$C^{i}_{Ph,b}$), 151.7 (m, 2C, A/C1), 162.6 (m, 2C, A/C3), 151.9 (m, 1C, B/C1), 153.1 (m, 1C, B/C1'), 161.6 (m, 1C, B/C3'), 162.5 (m, 1C, B/C3), 166.2 (s, 1C, B/C7), 166.5 (s, 1C, B/C7'), 167.4 (s, 2C, A/C7), 170.1 (s, 2C, A/C13), 171.6 (s, 1C, B/C13'), 172.1 (s, 1C, B/C13) ppm.
HRMS (DART): m/z calcd. for $C_{58}H_{68}N_4O_6P_2$ $[M^+H]^+$: 979.4687; found: 979.4666 (A), 979.4656 (B).
FTIR: $\tilde{\nu}$ = 692 (s), 1026 (s), 1533 (b), 1632 (s), 2961 (m), 3053 (w), 3070 (w), 3307 (b) cm^{-1}.

7.2.2 Dimethyl 6,6'-dihydroxy-5,5'-dimethoxy-[1,1'-biphenyl]-3,3'-dicarboxylate (15)

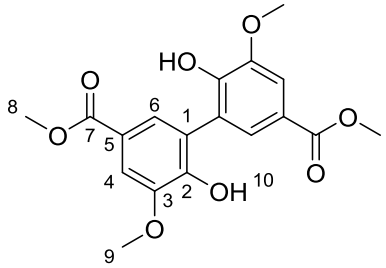

This compound was synthesized according to a known protocol.[111] Methyl vanillate **14** (7.65 g, 42.0 mmol, 1.00 eq.) was dissolved in acetonitrile (150.0 mL) and the solution was cooled in an ice bath. (Diacetoxyiodo)benzene (6.83 g, 21.2 mmol, 0.51 eq.) was added in portions. The mixture was warmed to room temperature and stirred for 18 hours in the dark. Subsequently, all solids were filtered off , washed with fresh, cool acetonitrile (3 x 30 ml) and dried *in vacuo* to yield the product **15** as a white, fluff y solid (3.89 g, 21.0 mmol, 51%).

^{1}H-NMR (DMSO-d6, 400.33 MHz, 300 K): δ = 3.81 (s, 6H, H8), 3.90 (s, 6H, H9), 7.45 (d, 2H, ^{4}J(H,H) = 1.54 Hz, H6), 7.47 (d, 2H, ^{4}J(H,H) = 1.54 Hz, H4), 9.49 (bs, 2H, H10) ppm.
^{13}C{^{1}H}-NMR (DMSO-d6, 100.66 MHz, 300 K): δ = 51.7 (C8), 56.0 (C9), 111.0 (C4), 119.5 (C5), 124.4 (C1), 125.4 (C6), 147.5 (C3), 148.9 (C2), 166.1 (C7) ppm.

HRMS (ESI): m/z calcd. for $C_{18}H_{19}O_8$ $[M+H]^+$: 363.1074; found: 363.1074.
FTIR: $\tilde{\nu}$ = 1420 (s), 1587 (s), 1706 (s), 2960 (w), 3011 (w), 3067.2 (w), 3404 (b) cm^{-1}.

7.2.3 6,6'-Dihydroxy-5,5'-dimethoxy-[1,1'-biphenyl]-3,3'-dicarboxylic acid (16)

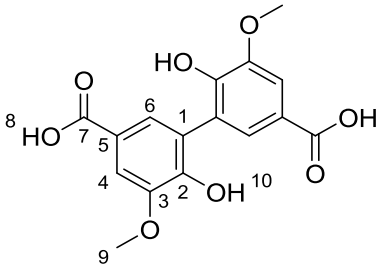

Diester **15** (4.97 g, 13.7 mmol, 1.00 eq.) was suspended in a mixture of THF and water (150 ml, 1:1 v:v) and KOH pellets (7.70 g, 137 mmol, 10.0 eq.) were added in portions. The resulting clear, two-phased solution was heated to 70°C and stirred vigorously for 16 hours. After cooling to room temperature, the organic layer was removed and the aqueous layer was acidified with HCl solution (6M) until pH 1 was reached and white solids formed. The precipitate was collected and washed with water to neutrality. Subsequent lyophilisation gave product **16** as a white solid (4.45 g, 13.7 mmol, 97%).

^{1}H-NMR (DMSO-d6, 400.33 MHz, 300 K): δ = 3.90 (s, 6H, H9), 7.42 (d, 2H, ^{4}J(H,H) = 2.00 Hz, H6), 7.46 (2, 2H, ^{4}J(H,H) = 2.00 Hz, H4), 9.37 (bs, 2H, H10), 12.5 (bs, 2H, H8) ppm.
^{13}C{^{1}H}-NMR (DMSO- d6, 100.66 MHz, 300 K): δ = 56.0 (C9), 111.2 (C4), 120.6 (C1), 124.4 (C5), 125.5 (C6), 147.3 (C2), 148.5 (C3), 167.3 (C7) ppm.
HRMS (ESI): m/z calcd. for $C_{16}H_{13}O_8$ $[M-H]^+$: 333.0616; found: 333.0616.
FTIR: $\tilde{\nu}$ = 768 (s), 1046 (s), 1202 (s), 1591 (s), 1685 (s), 1711 (m), 2839 (w), 2939 (w), 2972 (w), 3245 (bs) cm^{-1}.

7.2.4 General procedure for peptide couplings to diamido-modified BIPOLs

Dicarboxylic acid **16** (1.00 eq.) and HOBt (85%, 2.50 eq.) were placed in a heat-gun dried Schlenk tube and dry DMF (10 ml/mmol acid) was added. Addition of DIPEA (2.50 eq.) gave a slightly yellow solution. The mixture was cooled in an ice bath and EDCI.HCl (2.50 eq.) was added. After 15 min of incubation, the amine hydrochloride (2.50 eq.) was added as a solid, the mixture was slowly warmed to room temperature and stirring was continued for 16 hours. To quench existing O-isoaryl urea side product **17**, *N*,*N*-dimethylethylenediamine (50.0 eq.) was added in portions and stirring was continued for another six hours. For work-up, the solution was diluted with ethyl acetate (20 times the volume of DMF), washed with HCl solution (3M, three times, careful when quenching excess of diamine), saturated $NaHCO_3$ solution (three times) and brine (once). The organic layer was finally dried over sodium sulfate and evaporated to give the BIPOL **18** as an amorphous solid.

7.2.4.1 ^{t}BuNH-(*S*)Val-NH diol (18a)

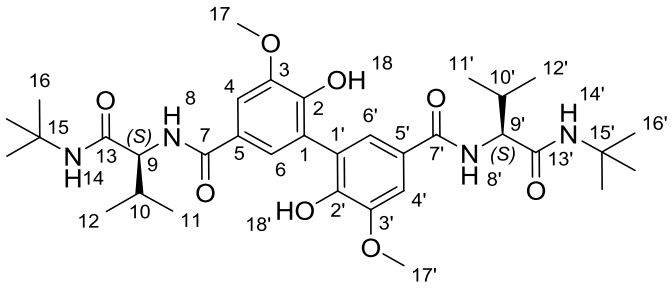

The compound was synthesized according to the procedure described above using dicarboxylic acid 1**6** (800 mg, 2.39 mmol) and valine-based amine hydrochloride (*S*)-**S2a** (1.25 g, 5.98 mmol) to give the product as an off-white solid (1.37 g, 2.13 mmol, 90%).

^{1}H-NMR ($CDCl_3$, 600.243 MHz, 253 K): δ = 0.84 (s, 9H, H16), 1.00 (m, 6H, H12 and H12'), 1.05 (d, 3H, ^{3}J(H,H) = 5.9 Hz, H11'), 1.11 (d, 3H, ^{3}J(H,H) = 5.9 Hz, H11), 1.40 (s, 9H, H16'), 2.23-2.34 (m, 1H, H10'), 2.34-2.46 (m, 1H, H10), 3.67 (s, 3H, H17), 3.95 (s, 3H, H17'), 4.04 (m, 1H, H9'), 4.72 (m, 1H, H9), 5.90 (s, 1H, H18), 6.00 (s, 1H, H18'), 6.37 (bs, 1H, H14'), 7.07 (s, 1H, H4), 7.23 (s, 1H, H6), 7.76 (s, 1H, H4'), 8.04 (s, 1H, H6'), 8.09 (s, 1H, H14), 9.36 (d, 1H, ^{3}J(H,H) = 5.1 Hz, H8'), 10.02 (d, 1H, ^{3}J(H,H) = 7.9 Hz, H8) ppm.
^{13}C{^{1}H}-NMR ($CDCl_3$, 150.93 MHz, 253 K): δ = 19.9 (2C, C11 and C11'), 20.5 (C12'), 20.6 (C12), 27.9 (C16), 28.9 (C16'), 30.0 (C10), 30.1 (C10'), 51.0 (C15), 51.5 (C15'), 55.7 (C17), 56.3 (C17'), 60.4 (C9), 62.5 (C9'), 109.9 (C4), 110.9 (C4'), 120.4 (C6), 122.3 (C1), 123.1 (C1'), 123.4 (C6'), 125.3 (C5'), 126.3 (C5), 144.5 (C2), 145.4 (C3), 145.9 (C3'), 146.2 (C2'), 165.1 (C7), 166.3 (C7'), 145.9 (C13') 146.2 (C13) ppm.
HRMS (ESI): m/z calcd. for $C_{34}H_{49}N_4O_8$ $[M-H]^-$: 641.3556; found: 641.3554.
FTIR: $\tilde{\nu}$ = 679 (m), 1044 (m), 1221 (s), 1488 (m) 1624 (m), 2873 (w), 2930 (w), 2961 (w), 3077 (bw), 3275 (bs), 3535 (bw) cm^{-1}.

7.2.4.2 1-AdNH-(*S*)Val-NH diol (18b)

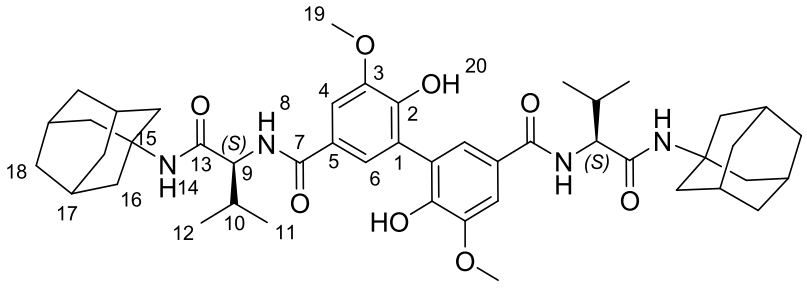

The compound was synthesized according to the procedure described above using dicarboxylic acid **16** (200 mg, 0.60 mmol) and valine-based amine hydrochloride (*S*)-**S2b** (429 mg, 1.50 mmol) to give the product as an off -white solid (246 mg, 0.31 mmol, 51%).

^{1}H-NMR ($CDCl_3$, 600.24 MHz, 253 K): δ = 0.90-1.06 (m, 9H, H12 and H11' and H12'), 1.09 (d, 3H, ^{3}J(H,H) = 4.5 Hz, H11), 1.16-1.30 (m, 3H, H16), 1.30-1.41 (m, 3H, H18), 1.41-1.51 (m, 3H, H18), 1.67 (s, 9H, H16 and H18'), 1.73 (s, 3H, H17), 2.08 (s, 9H, H16' and H17'), 2.20-2.30 (m, 1H, H10'), 2.30-2.43 (m, 1H, H10), 3.68 (s, 3H, H19), 3.95 (s, 3H, H19'), 4.02-4.18 (m, 1H, H9'), 4.55-4.65 (m, 1H, H9), 5.83 (s, 1H, H20), 5.91 (s, 1H, H20'), 6.22 (bs, 1H, H14'),

7.12 (s, 1H, H4), 7.21 (1H, H6), 7.79 (s, 1H, H4'), 7.88 (s, 1H, H14), 8.11 (s, 1H, H6'), 9.38 (d, 1H, ^{3}J(H,H) = 4.5 Hz, H8'), 10.03 (d, 1H, ^{3}J(H,H) = 6.8 Hz, H8) ppm.

^{13}C{^{1}H}-NMR ($CDCl_3$, 150.93 MHz, 253 K): δ = 19.9 (C12'), 20.0 (C11), 20.1 (C11'), 20.6 (C12), 29.3 (C17'), 29.4 (C17), 29.7 (C10), 29.9 (C16), 30.1 (C10'), 36.3 (C18), 36.5 (C16'), 40.1 (C16), 41.6 (C16'), 51.7 (C15), 52.2 (C15'), 55.7 (C16), 56.2 (C16'), 60.8 (C9), 62.3 (C9'), 110.1 (C4), 110.9 (C4'), 120.5 (C6), 122.3 (C1), 123.2 (C1'), 123.5 (C6'), 125.6 (C5'), 126.3 (C5), 144.5 (C2), 15.3 (C3), 146.0 (C2'), 146.1 (C3'), 164.9 (C7), 166.3 (C7'), 172.2 (C13'), 173.2 (13) ppm.

HRMS (ESI): m/z calcd. for $C_{46}H_{61}N_4O_8$ $[M-H]^-$: 797.4495; found: 797.4497.

FTIR: $\tilde{\nu}$ = 758 (m), 1043 (s), 1223 (s), 1486 (s), 1534 (s), 1590 (s), 1628 (s), 2848 (s), 2904 (s), 3077 (bw), 3277 (bs), 3525 (bw) cm^{-1}.

7.2.4.3 ^{t}BuNH-(*S*)PheNH diol (18c)

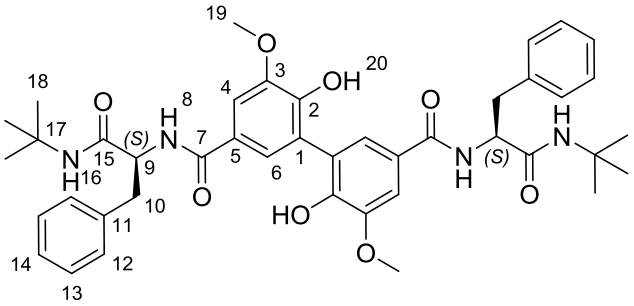

The compound was synthesized according to the procedure described above using dicarboxylic acid **16 (**500 mg, 1.50 mmol) and phenylalanine-based amine hydrochloride (*S*)-**S2c** (960 mg, 3.74 mmol) to give the product as an off-white solid (1.00 g, 1.36 mmol, 91%).

^{1}H-NMR ($CDCl_3$, 600.24 MHz, 298 K): δ = 1.01 (s, 9H, H18), 1.32 (s, 9H, H18'), 3.02 (dd, 1H, ^{2}J(H,H) = 13.7 Hz, ^{3}J(H,H) = 8.9 Hz, H10a'), 3.15-3.28 (m, 2H, H10b and H10b'), 3.52 (dd, 1H, ^{2}J(H,H) = 12.5 Hz, ^{3}J(H,H) = 12.4 Hz, H10a), 3.67 (s, 3H, H19), 3.97 (s, 3H, H19'), 4.50-4.59 (m, 1H, H9'), 5.34 (s, 1H, H16'), 5.58-5.68 (m, 1H, H9), 5.79 (s, 1H, H20), 5.89 (s, 1H, H20'), 6.99 (s, 1H, H4'), 7.09-7.16 (m, 1H, H14), 7.17-7.24 (m, 3H, 4H, H13 and H13'), 7.26-7.31 (m, 2H, H12'), 7.35 (d, 1H, ^{4}J(H,H) = 1.1 Hz, H6), 7.66-7.68 (m, 2H, H12), 7.77 (s, 1H, H4'), 7.85 (s, 1H, H6'), 8.33 (s, 1H, H16), 9.42 (d, 1H, ^{3}J(H,H) = 5.6 Hz, H8'), 10.10 (d, 1H, ^{3}J(H,H) = 8.77 Hz, H8) ppm.

^{13}C{^{1}H}-NMR ($CDCl_3$, 150.93 MHz, 289 K): δ = 28.1 (C18), 28.9 (C18'), 38.3 (C10'), 39.0 (C10), 51.1 (C17), 51.6 (C17'), 55.8 (C19), 56.5 (C9), 56.6 (C19'), 58.5 (C9'), 110.3 (C4), 111.3 (C4'), 121.0 (C6), 122.9 (C1), 123.5 (C1'), 123.5 (C6'), 125.4 (C5'), 126.0 (C14), 126.3 (C5), 126.8 (C14'), 128.1 (C13'), 128.5 (C13), 129.7 (C12'), 130.1 (C12), 138.1 (C11'), 139.3 (C11), 145.2 (C2), 145.8 (C3), 146.5 (C2'), 146.7 (C3'), 166.2 (C7), 166.5 (C7'), 172.8 (C15'), 174.0 (C15) ppm.

HRMS (ESI): m/z calcd. for $C_{42}H_{49}N_4O_8$ $[M-H]^-$: 737.3556; found: 737.3546.

FTIR: $\tilde{\nu}$ = 697 (s), 1042 (m), 1220 (s), 1487 (s), 1487 (s), 1547 (s), 1627 (m), 2929 (w) 2965 (w), 3064 (w), 3276 (bs), 3502 (bw) cm^{-1}.

7.2.4.4 ^{t}BuNH-Gly-NH diol (18d)

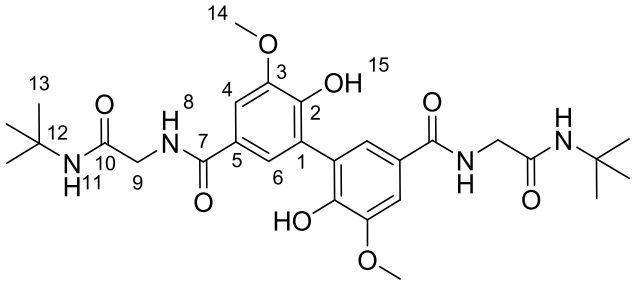

The compound was synthesized using dicarboxylic acid **16** (500 mg, 1.50 mmol) and glycine-based amine hydrochloride **S2d** (623 mg, 3.74 mmol) according to the procedure described above, but with a modified work-up procedure: After *N*,*N*-dimethylethylenediamine had been added and the mixture had been stirred of another 18 hours, it was diluted with DCM (120 ml) and HCl solution (6M, 40 ml) was added carefully under formation of fumes. Subsequent addition of deionized water (80 ml) gave a white precipitate that was filtered off. The solids were washed with water (2x10 ml) and DCM (2x 10 ml) and finally dried *in vacuo* to give the product as an off -white solid (666 mg, 1.19 mmol, 80%).

^{1}H-NMR (DMSO-d6, 600.24 MHz, 295 K): δ = 1.25 (s, 9H, H13), 3.77 (d, 2H, ^{3}J(H,H) = 5.8 Hz, H9), 3.88 (s, 3H, H14), 7.37 (d, d, ^{4}J(H,H) = 2.0 Hz, H6), 7.44 (s, 1H, H11), 7.47 (d, 1H, ^{4}J(H,H) = 1.9 Hz, H4), 8.41 (t, 1H, ^{3}J(H,H) = 5.9 Hz, H8), 9.09 (s, 1H, H15) ppm.
^{13}C{^{1}H}-NMR (DMSO-d6, 150.93 MHz, 295 K): δ = 28.6 (C13), 42.8 (C9), 50.1 (C12) 56.0 (C14), 109.8 (C4), 123.0 (C6), 124.1 (C5), 124.9 (C1), 147.1 (C3), 147.2 (C2), 166.0 (C7), 168.4 (C10) ppm.
HRMS (ESI): m/z calcd. for $C_{28}H_{37}N_4O_8$ [M-H]$^{-}$: 557.26169; found: 557.26229.
FTIR: $\tilde{\nu}$ = 673 (m), 1043 (m), 1219 (s), 1486 (s), 1543 (s), 1584 (s), 2872 (w), 2934 (w) 2967 (bm), 3076 (bm), 3235 (bs) cm^{-1}.

7.2.5 General procedure for bisphosphinite syntheses

The compounds were synthesized according to a known protocol, which was slightly modified.[112] The respective biphenol **18a-d** (1.00 eq.) and DABCO (4.00 eq., freshly sublimated) were placed in a heat-gun dried Schlenk and suspended in dry and degassed DCM (10ml/mmol biphenol). The mixture was cooled in an ice bath and PPh_2Cl (4.00 eq.) was added dropwise yielding a clear solution. The ice bath was removed after 15 min and stirring was continued at room temperature for another three hours. The solvent was then removed and the residue diluted with dry, degassed and stabilized THF (about 1/4 of the original volume). The suspension was passed through a pad of dry, neutral alumina under inert conditions and was eluated with more THF (4x, same volume). Combined fractions were evaporated *in vacuo* using an external cooling trap. The resulting residue was re-precipitated three times from dry DCM/*n*-pentane (1:10 ml) and the supernatant solution removed using a filter-tipped cannula. Finally, drying *in vacuo* gave the desired bisphosphinite as a white solid.

7.2.5.1 ^{t}BuNH-(*S*)Val-NH bisphosphinite (19a)

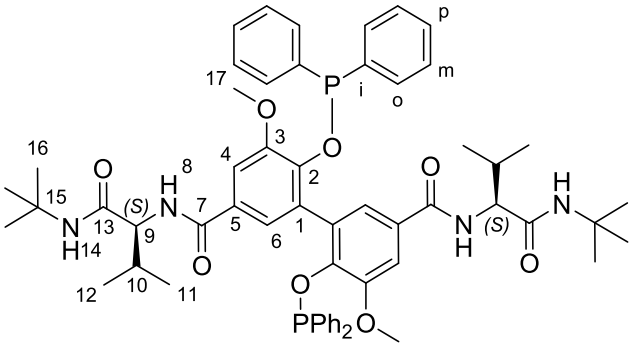

The compound was synthesized according to the procedure described above using biphenol **18a** (300 mg, 0.47 mmol) and was obtained as a white solid (230 mg, 0.23 mmol, 49%).

^{1}H-NMR (THF−d8, 600.24 MHz, 295 K): δ = 0.85 (s, 9H, H16), 1.01 (d, 3H, ^{3}J(H,H) = 6.5 Hz, H12), 1.11 (d, 3H, ^{3}J(H,H) = 6.8 Hz, H11), 1.19 (d, 3H, ^{3}J(H,H) = 6.8 Hz, H12'), 1.35 (d, 3H, ^{3}J(H,H) = 6.6 Hz, H11'), 1.44 (s, 9H, H16'), 2.36-2.45 (m, 1H, H10), 2.48-2.56 (m, 1H, H10'), 3.06 (s, 3H, H17), 3.64 (s, 3H, H17'), 4.27 (dd, 1H, ^{3}J(H,H) = 9.3, ^{3}J(H,H) = 7.4 Hz, H9'), 4.71 (dd, 1H, ^{3}J(H,H) = 10.3, ^{3}J(H,H) = 8.7 Hz, H9), 6.60 (d, 1H, ^{4}J(H,H) = 1.6 Hz, H6), 6.78-6.82 (m, 2H, H_m^d), 6.83 (d, 1H, ^{4}J(H,H) = 1.6 Hz, H4), 6.87-6.91 (m, 1H, H_p^d), 6.92-7.00 (m, 4H, H_o^c and H_o^d), 7.03-7.10 (m, 5H, H_m^c and H_o^b and H_p^c), 7.10-7.16 (m, 4H, H_m^b and H_m^a), 7.17-7.21 (m, 1H, H_p^b), 7.22-7.26 (m, 1H, Hp^a), 7.29-7.35 (m, 2H, H_o^a), 7.56 (s, 1H, H14'), 7.74 (d, 1H, ^{4}J(H,H) = 1.8 Hz, H4'), 7.97 (d, 1H, ^{4}J(H,H) = 1.8, H6'), 8.11 (s, 1H, H14), 9.12 (d, 1H, ^{3}J(H,H) = 7.4 Hz, H8'), 9.43 (d, 1H, ^{3}J(H,H) = 8.7 Hz, H8) ppm.

^{13}C{^{1}H}-NMR (THF-d8, 150.93 MHz, 295 K): δ = 20.4 (s, C11), 20.5 (s, C11'), 21.5 (s, C12), 21.5 (s, C12'), 28.6 (s, C16), 29.3 (s, C16'), 31.0 (s, C10), 31.2 (s, C10'), 51.8 (s, C15'), 51.9 (s, C15), 55.4 (s, C17), 55.7 (s, C17'), 61.3 (s, C9), 62.3 (s, C9'), 112.7 (s, C4'), 112.9 (s, C4), 120.6 (s, C6), 122.6 (s, C6'), 128.1 (d, ^{3}J(C,P) = 5.1 Hz, C_m^C), 128.2 (d, ^{3}J(C,P) = 8.4 Hz, C_m^d), 128.3 (s, C_p^c), 128.4 (d, ^{3}J(C,P) = 7.4 Hz, C_m^a), 128.4 (d, ^{3}J(C,P) = 7.1 Hz, C_m^b), 128.6 (s, C_p^b), 129.4 (s, C5), 129.7 (s, C_p^a), 129.7 (d, ^{2}J(C,P) = 22.0 Hz, C_o^b), 129.8 (s, C_p^d), 130.2 (d, ^{2}J(C,P) = 19.0 Hz, C_o^c), 130.3 (s, C5'), 131.3 (d, ^{2}J(C,P) = 2.3 Hz, C1), 131.9 (d, ^{2}J(C,P) = 24.2 Hz, C_o^a), 132.3 (d, ^{2}J(C,P) = 26.5 Hz, C_o^d), 133.2 (d, ^{3}J(C,P) = 2.2 Hz, C1'), 143.2 (d, ^{1}J(C,P) = 23.3 Hz, C_i^d), 144.3 (d, ^{1}J(C,P) = 16.2 Hz, C_i^c), 144.3 (d, ^{1}J(C,P) = 15.2 Hz, C_i^b), 145.0 (d, ^{1}J(C,P) = 21.1 Hz, C_i^a), 147.6 (d, ^{2}J(C,P) = 8.4 Hz, C2), 148.8 (d, ^{2}J(C,P) = 7.6 Hz, C2'), 150.8 (d, ^{4}J(C,P) = 1.9 Hz, C3), 152.9 (d, ^{4}J(C,P) = 2.4 Hz, C3'), 165.7 (s, C7), 166.4 (s, C7'), 174.3 (s, C13), 174.4 (s, C13') ppm.

^{31}P{^{1}H}-NMR (THF-d8, 202.47 MHz, 295 K): δ = 112.8 (s, 1P), 122.5 (s, 1P) ppm.

HRMS (ESI): m/z calcd. for $C_{58}H_{69}N_4O_8P_2$ $[M+H]^+$: 101.4585; found: 1011.4619.

FTIR: $\tilde{\nu}$ = 691 (s), 847 (m), 1093 (m), 1217 (s), 1433 (m), 1534 (m), 1624 (s), 1653 (s), 2838 (w), 2962 (w), 3055 (w), 3286 (bm), 3417 (bw) cm^{-1}.

7.2.5.2 1-AdNH-(*S*)Val-NH bisphosphinite (19b)

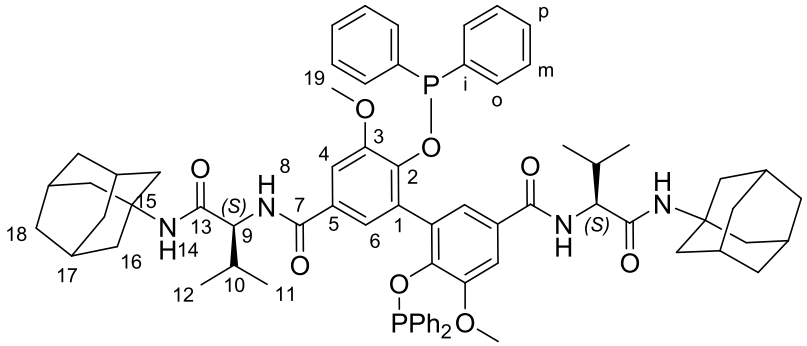

The compound was synthesized according to the procedure described above using biphenol **18b** (300 mg, 0.38 mmol) and was obtained as a white solid (234 mg, 0.20 mmol, 53%).

^{1}H-NMR (THF-d8, 600.24 MHz, 295 K): δ = 1.03 (d, 3H, ^{3}J(H,H) = 6.6 Hz, H11), 1.14 (d, 3H, ^{3}J(H,H) = 6.8 Hz, H12), 1.21 (d, 3H, ^{3}(H,H) = 6.8 Hz, H11'), 1.28-1.35 (m, 3H, H16), 1.35 (d, 3H, ^{3}J(H,H) = 6.5 Hz, H12'), 1.45-1.57 (m, 6H, H18), 1.66-1.71 (m, 3H, H16), 1.75-1.79 (m, 6H, H18'), 1.91-2.00 (m, 3H, H17), 2.06-2.13 (m, 3H, H17'), 2.14-2.26 (m, 6H, H16'), 2.33-2.41 (m, 1H, H10), 2.49-2.56 (m, 1H, H10'), 3.05 (s, 3H, H19), 3.69 (s, 3H, H19'), 4.27 (dd, 1H, ^{3}J(H,H) = 8.8 Hz, ^{3}J(H,H) = 8.1 Hz, H9'), 4.64 (dd, 1H, ^{3}J(H,H) = 9.8 Hz, ^{3}J(H,H) = 9.1 Hz, H9), 6.54 (d, 1H, ^{4}J(H,H) = 1.5 Hz, H6), 6.78-6.82 (m, 2H, H_m^d), 6.83 (d, 1H, ^{4}J(H,H) = 1.6 Hz, H4), 6.86-6.92 (m, 3H, H_o^c and H_p^d), 6.95-7.00 (m, 2H, H_o^d), 7.01-7.10 (m, 5H, H_o^b and H_m^c and H_p^c), 7.12-7.16 (m, 4H, H_m^b and H_m^a), 7.19-7.23 (m, 1H, H_p^b), 7.23-7.27 (m, 1H, H_p^a), 7.30-7.35 (m, 2H, H_o^a), 7.44 (s, 1H, H14'), 7.79 (d, 1H, ^{3}J(H,H) = 1.7 Hz, H4'), 7.95 (s, 1H, H14), 7.98 (d, 1H, ^{4}J(H,H) = 1.7 Hz, H6'), 9.11 (d, ^{3}J(H,H) = 7.5 Hz, H8'), 9.46 (d, 1H, ^{3}J(H,H) = 8.6 Hz, H8) ppm.

^{13}C{^{1}H}-NMR (THF-d8, 150.93 MHz, 295 K): δ = 20.5 (s, C12), 20.5 (s, C12'), 21.5 (s, C11), 21.6 (s, C11'), 30.4 (s, C17), 30.8 (s, C17'), 30.9 (s, C10) 31.1 (s, C10'), 37.4 (s, C18), 37.5 (s, C18'), 41.3 (s, C16), 42.6 (s, C16'), 52.7 (s, C15'), 52.7 (s, C15), 55.3 (s, C19'), 55.4 (s, C19), 61.4 (s, C9), 62.4 (s, C9'), 112.2 (s, C4'), 112.8 (s, C4) 120.6 (s, C6), 122.5 (C6'), 128.1 (d, ^{3}J(C,P) = 4.6 Hz, C_m^c), 128.3 (s, C_p^c), 128.3 (d, ^{3}J(C,P) = 7.6 Hz, C_m^d), 128.4 (d, ^{3}J(C,P) = 7.4 Hz), C_m^a), 128.5 (s, C_p^b), 129.5 (s, C5), 129.6 (d, ^{2}J(C,P) = 23.5 Hz, C_o^b), 129.7 (s, C_p^a), 129.9 (s, C_p^d), 130.2 (d, ^{2}J(C,P) = 18.2 Hz, C_o^c), 130.5(s, C5'), 131.3 (d, ^{4}J(C,P) = 1.7 Hz, C1), 131.9 (d, ^{2}J(C,P) = 24.1 Hz, C_o^a), 132.5 (d, ^{2}J(C,P) = 26.6 Hz, C_o^d), 133.4 (d, ^{3}J(C,P) = 2.1 Hz, C1'), 143.1 (d, ^{1}J(C,P) = 24.2 Hz, C_i^d), 144.3 (d, ^{1}J(C,P) = 14.1 Hz, C_i^c), 144.4 (d, ^{1}J(C,P) = 16.0 Hz, C_i^b), 145.0 (d, ^{1}J(C,P) = 21.3 Hz, C_i^a), 147.5 (d, ^{2}J(C,P) = 8.9 Hz, C2), 148.4 (d, ^{2}J(C,P) = 7.8 Hz, C2'), 150.7 (d, ^{3}J(C,P) = 2.2 Hz, C3), 152.6 (d, ^{3}J(C,P) = 2.3 Hz, C3'), 165.6 (s, C7), 166.4 (s, C7'), 174.0 (s, C13), 174.1 (s, C13') ppm.

^{31}P{^{1}H}-NMR (THF-d8, 202.47 MHz, 295 K): δ = 114.5 (s, 1P), 125.2 (s, 1P) ppm.

HRMS (MALDI): m/z calcd. for $C_{70}H_{81}N_4O_8P_2$ $[M+H]^+$: 1167.5524; found: 1167.5569.

FTIR: $\tilde{\nu}$ = 693 (s), 1092 (s), 1217 (s), 1458 (s), 1627 (s), 2848 (m), 2904 (s), 3002 (w), 2053 (w), 3282 (bm), 3416 (bw) cm^{-1}.

7.2.5.3 ^{t}BuNH-(*S*)Phe-NH bisphosphinite (19c)

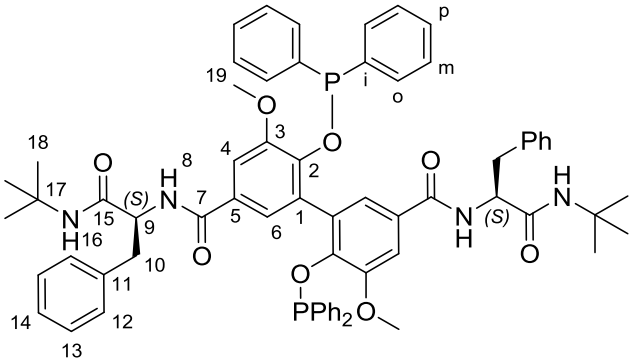

The compound was synthesized according to the procedure described above using biphenol **18c** (100 mg, 0.13 mmol) and was obtained as a white solid (125 mg, 0.11 mmol, 83%).

^{1}H-NMR (THF-d8, 600.24 MHz, 300 K): δ = 1.07 (s, 9H, H18), 1.47 (s, 9H, H18'), 3.04 (s, 3H, H19), 3.21-3.30 (m, 2H, H10a and H10'b), 3.41 (dd, 1H, ^{2}J(H,H) = 14.1 Hz, ^{3}J(H,H) = 8.9 Hz, H10'a), 3.58 (dd, 1H, ^{2}J(H,H) = 25.0 Hz, ^{3}J(H,H) = 11.9 Hz, H10b), 3.64 (s, 3H, H19') 4.79-4.84 (m, 1H, H9'), 5.70-5.77 (m, 1H, H9), 6.18-6.23 (m, 2H, H_m^d), 6.45-6.50 (m, 1H, H_p^d), 6.60 (d, 1H, ^{4}J(H,H) = 2.0 Hz, H4), 6.72-6.78 (m, 2H, H_o^d), 6.82 (d, 1H, ^{4}J(H,H) = 2.0 Hz, H6), 6.97-7.02 (m, 2H, H_o^a), 7.03-7.09 (m, 5H, H_m^a and H_m^b and H_p^c), 7.09-7.16 (m, 5H, H14 and H_o^c and H_m^c), 7.16-7.21 (m, 3H, H14' and H_p^a and H_p^b), 7.21-7.26 (m, 2H, H_o^b), 7.28-7.35 (m, 4H, H13 and H13'), 7.59 (s, 1H, H16'), 7.61-7.64 (m, 2H, H12'), 7.68 (d, 1H, ^{4}J(H,H) = 1.8 Hz, H4'), 7.86-7.92 (m, 3H, H12 and H6'), 8.52 (s, 1H, H16), 9.28 (d, 1H, ^{3}J(H,H) = 7.0 Hz, H8'), 9.75 (d, 1H, ^{3}J(H,H) = 8.7 Hz, H8') ppm.

^{13}C{^{1}H}-NMR (THF-d8, 150.93 MHz, 300 K): δ = 28.4 (s, C18), 29.1 (s, C18'), 39.2 (s, C10'), 39.6 (s, C10), 51.6 (s, C17), 51.6 (s, C17'), 55.1 (s, C19), 55.6 (s, C19'), 57.3 (s, C9), 58.2 (s, C9'), 112.4 (s, C4), 112.4 (s, C4'), 121.0 (s, C6), 122.7 (C6'), 126.9 (s, C14), 127.1 (s, C14'), 127.7 (d, ^{3}J(C,P) = 8.0 Hz, C_m^d), 127.9 (d, ^{3}J(C,P) = 5.0 Hz, C_m^b), 128.0 (s, C_p^c), 128.2 (d, ^{3}J(C,P) = 8.7 Hz, C_m^a), 128.2 (d, ^{3}J(C,P) = 8.8 Hz, C_m^c), 128.4 (s, C_p^b), 128.6 (s, C5), 128.6 (s, C13'), 128.8 (s, C13), 129.5 (s, C_p^a), 129.6 (s, C5'), 129.7 (d, ^{2}J(C,P) = 23.0 Hz, C_o^c), 129.7 (s, C_p^d), 129.9 (d, ^{2}J(C,P) = 19.3 Hz, C_o^a), 130.7 (s, C12'), 130.9 (d, ^{3}J(C,P) = 2.1 Hz, C1'), 131.0 (s, C12), 131.9 (d, ^{2}J(C,P) = 24.3 Hz, C_o^b), 132.6 (d, ^{2}J(C,P) = 25.8 Hz, C_o^d), 133.3 (d, ^{3}J(C,P) = 2.9 Hz, C1), 139.7 (s, C11'), 140.5 (s, C11), 142.4 (d, ^{1}J(C,P) = 21.3 Hz, C_i^d), 144.1 (d, ^{3}J(C,P) = 16.1 Hz, C_i^c), 144.3 (d, ^{3}J(C,P) = 15.0 Hz, C_i^b), 144.4 (d, ^{3}J(C,P) = 20.9 Hz, C_i^a), 147.1 (d, ^{2}J(C,P) = 8.4 Hz, C2), 149.1 (d, ^{2}J(C,P) = 7.7 Hz, C2'), 150.4 (d, ^{3}J(C,P) = 1.8 Hz, C3), 152.9 (d, ^{3}J(C,P) = 2.6 Hz, C3'), 165.9 (s, C7'), 166.4 (s, C7), 174.8 (s, C15'), 175.0 (C15) ppm.

^{31}P{^{1}H}-NMR (THF-d8, 202.47 MHz, 295 K): δ = 114.8 (s, 1P), 124.7 (s, 1P) ppm.

HRMS (ESI): m/z calcd. for $C_{66}H_{69}N_4O_8P_2$ $[M+H]^+$: 1107.4585; found: 1107.4564.

FTIR: $\tilde{\nu}$ = 692 (s), 860 (m), 1219 (s), 1360 (m), 1545 (m), 1626 (s), 2930 (w), 2966 (w) 3058 (w), 3280 (bm) cm^{-1}.

7.2.5.4 ^{t}BuNH-Gly-NH bisphosphinite (19d)

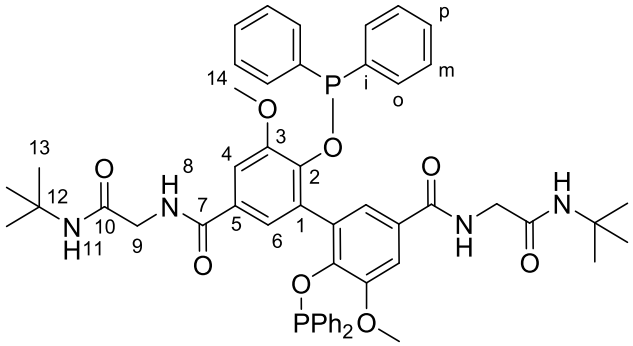

The compound was synthesized according to the procedure described above using biphenol **18d** (300 mg, 0.54 mmol) and was obtained as a white solid (261 mg, 0.28 mmol, 53%).

^{1}H-NMR (THF-d8, 600.24 MHz, 300 K): δ = 0.89 (s, 9H, H13), 1.40 (s, 9H, H13'), 3.02 (s, 3H, H14), 3.48 (dd, 1H, ^{2}J(H,H) = 15.9 Hz, ^{3}J(H,H) = 4.4 Hz, H9$_{b}$), 3.54 (s, 3H, H14'), 3.70 (dd, 1H, ^{2}J(H,H) = 15.9 Hz, ^{3}J(H,H) = 5.3 Hz, H9'$_{b}$), 4.51 (dd, 1H, ^{2}J(H,H) = 15.9 Hz, ^{3}J(H,H) = 6.8 Hz, H9'$_{a}$), 4.88 (dd, 1H, ^{3}J(H,H) = 15.9 Hz, ^{3}J(H,H) = 8.8 Hz, H9$_{a}$), 6.79 (d, 1H, ^{4}J(H,H) = 1.7 Hz, H4), 6.84-6.94 (m, 4H, H$_{m}^{Ar}$ and H$_{o}^{Ar}$), 6.95 (d, 1H, ^{4}J(H,H) = 1.6 Hz, H6), 6.96-7.02 (m, 1H, H$_{p}^{Ar}$), 7.05-7.20 (m, 12H, 2xH$_{o}^{Ar}$ and 3xH$_{m}^{Ar}$ and 2xH$_{p}^{Ar}$), 7.21-7.30 (m, 3H, H$_{o}^{Ar}$ and H$_{p}^{Ar}$), 7.66 (s, 1H, H11), 7.70 (d, 1H, ^{4}J(H,H) = 1.5 Hz, H4'), 7.75 (d, 1H, ^{4}J(H,H) = 1.55 Hz, H6'), 8.82 (s, 1H, H11), 9.36 (dd, 1H, ^{3}J(H,H) = 6.5 Hz, ^{3}J(H,H) = 5.3 Hz, H8'), 10.20 (dd, 1H, ^{3}J(H,H) = 9.1 Hz, ^{3}J(H,H) = 4.3 Hz, H8).

^{13}C{^{1}H}-NMR (THF-d8, 150.93 MHz, 300 K): δ = 27.3 (s, C13), 28.0 (s, C13'), 42.3 (s, C9), 42.9 (s, C9'), 50.6 (s, C12), 50.7 (s, C12'), 54.3 (d, ^{5}J(C,P) = 6.0 Hz, C14), 54.5 (s, C14'), 110.9 (s, C4), 111.4 (s, C4'), 120.1 (s, C6), 121.7 (C6'), 127.2 (s, C$_{m}^{Ar}$), 127.3 (s, C$_{p}^{Ar}$), 127.3 (s, C$_{p}^{Ar}$), 127.4 (s, C$_{m}^{Ar}$), 127.5 (s, C$_{m}^{Ar}$), 127.8 (s, C$_{m}^{Ar}$), 128.4 (s, C5), 128.6 (s, C$_{p}^{Ar}$), 128.7 (s, C5'), 128.8 (d, ^{2}J(C,P) = 24.1 Hz, C$_{o}^{Ar}$), 128.9 (s, C$_{p}^{Ar}$), 129.5 (d, ^{2}J(C,P) = 21.4 Hz, C$_{o}^{Ar}$), 130.5 (d, ^{3}J(C,P) = 2.8 Hz, C1'), 130.7 (d, ^{2}J(C,P) = 24.6 Hz, C$_{o}^{Ar}$), 131.2 (d, ^{2}J(C,P) = 24.6 Hz, C$_{o}^{Ar}$), 131.8 (d, ^{3}J(C,P) = 3.2 Hz, C1), 142.3 (d, ^{1}J(C,P) = 21.3 Hz, C$_{i}^{Ar}$), 143.1 (d, ^{1}J(C,P) = 15.3 Hz, C$_{i}^{Ar}$), 143.2 (d, ^{1}J(C,P) = 16.9 Hz, C$_{i}^{Ar}$), 143.3 (d, ^{1}J(C,P) = 20.5 Hz, C$_{i}^{Ar}$), 146.7 (d, ^{3}J(C,P) = 8.9 Hz, C2), 147.4 (d, ^{3}J(C,P) = 7.9 Hz, C2'), 150.1 (d, ^{3}J(C,P) = 2.1 Hz, C3), 151.7 (d, ^{3}J(C,P) = 2.6 Hz, C3'), 165.1 (s, C7'), 166.0 (s, C7), 170.5 (s, C10), 170.7 (C10') ppm.

^{31}P{^{1}H}-NMR (THF-d8, 202.47 MHz, 295 K): δ = 115.1 (s, 1P), 123.0 (s, 1P) ppm.

HRMS (ESI): m/z calcd. for $C_{52}H_{57}N_4O_8P_2$ $[M+H]^+$: 927.36461; found: 927.3672.

FTIR: $\tilde{\nu}$ = 693 (s), 851 (s), 1219 (s), 1361 (m), 1477 (m), 1555 (m), 1627 (m), 2928 (w) 2967 (w), 3073 (bw), 3267 (bm), 3336 (w), 3370 (w), 3392 (w) cm^{-1}.

7.2.6 ^{t}BuNH-(*S*)Val-NH phosphoramidite (23a)

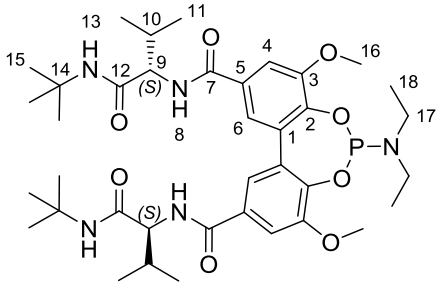

Diol **18a** (100 mg, 0.16 mmol, 1.00 eq.) was suspended in dry and degassed toluene (1.5 ml) and $P(NEt_2)_3$ (85.2 µl, 311 µmol, 2.00 eq.) was added. The suspension was refluxed for three hours and after all solids had dissolved, a thick gel formed. After cooling to room temperature, 5 ml dry and degassed *n*-pentane was added to achieve full precipitation and all solvents were removed using a filter-tipped cannula. The crude product was subsequently slurried in dry and degassed DCM (1 ml), re-precipitated with *n*-pentane (5 ml) and the solvent was removed again. This was repeated another two times. Obtained solids were finally dried *in vacuo* to yield the product **23a** as a white powder (65.0 mg, 87.4 µmol, 56%). The compound is oxygen-sensitive and has to be stored under argon.

Note: The large number of species with very similar NMR shifts, due to dimer formation and the chirality of phosphorus atoms, made an exact assignment of all signal unreasonable. Therefore, no distinction is made between molecules with different chirality of phosphorus atoms.

^{1}H-NMR (THF-d4, 400.22 MHz, 300 K): δ = 0.97-1.26 (m, 104 H, H11/H11’ and H15/H15’ and H18/H18’), 1.39-1.50 (m, 40H, H15/H15’), 2.31-2.46 (m, 4H, H10’), 2.53-2.69 (m, 4H, H10), 2.72-2.94 (m, 8H, H17/H17’), 3.00-3.19 (m, 8H, H17/H17’), 3.48-3.51 (m, 6H, H16/H16’), 3.55 (s, 3H, H16/H16’), 3.61 (s, 3H, H16/H16’), 3.85-3.88 (m, 6H, H16/H16’), 3.88-3.91 (m, 6H, H16/H16’), 4.15-4.28 (m, 4H, H9’), 4.97-5.13 (m, 4H, H9), 7.13 (s, 1H, H4/H4’), 7.27 (s, 1H, H4/H4’), 7.29 (s, 1H, H4/H4’), 7.36 (s, 1H, H6/H6’), 7.41-7.43 (m, 2H, H6/H6’), 7.45 (s, 1H, H6/H6’), 7.49 (s, 1H, H4/H4’), 7.61-7.70 (m, 4H, H13’), 7.80-7.87 (m, 5H, H6/H6’ and H4/H4’), 7.90 (s, 1H, H6/H6’), 7.95 (s, 1H, H6/H6’), 8.04 (s, 1H, H6/H6’), 8.60-8.81 (m, 4H, H13), 9.16-9.49 (m, 4H, H8’), 10.43-10.57 (m, 4H, H8) ppm.
^{13}C{^{1}H}-NMR (THF-d4, 201.24 MHz, 300 K): δ = 14.4-14.7 (C8/C8’), 20.2-21.3 (C11/C11’), 28.6-29.4 (C15/C15’), 31.0-31.3 (C10/C10’), 38.4-38.8 (C17/C17’), 51.9-52.2 (C14/C14’), 55.5-56.2 (C16/C16’), 61.8-63.2 (C9/C9’), 112.9-113.9 (C4/C4’), 118.6-119.1 (C6/C6’), 121.7-122.1 (C6/C6’), 130.4-131.9 (C5/C5’ and C1/C1’), 133.0-133.5 (C1/C1’), 142.7-143.2 (C2/C2’), 151.9-153.1 (C3/C3’), 166.1-16.7 (C7/C7’), 174.4-174.8 (C12/C12’) ppm.
^{31}P{^{1}H}-NMR (THF-d4, 161.98 MHz, 300 K): δ = 147.2 (s), 147.3 (s), 147.4 (s), 147.8 (s) ppm.
HRMS (ESI): m/z calcd. for $C_{38}H_{59}N_5O_8P$ $[M+H]^+$: 744.4095; found: 744.4091.
FTIR: $\tilde{\nu}$ = 668 (s), 826 (s), 1023 (s), 1176 (s), 1361 (s), 1458 (s), 1542 (s), 1624 (s), 2870 (w), 2934 (w), 2966 (m), 3077 (bw), 3270 (bm) cm^{-1}.

7.2.7 ^{t}BuNH-(*S*)Phe-NH phosphoramidite (23b)

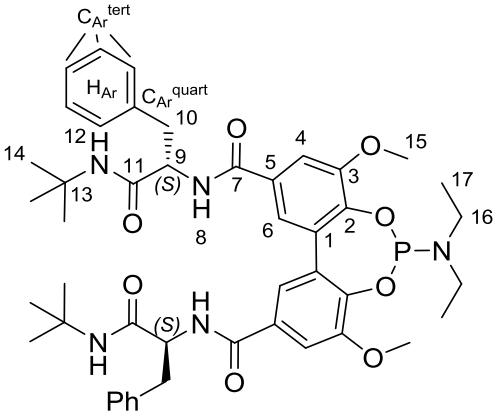

Diol **18c** (150 mg, 0.20 mmol, 1.00 eq.) and triethylamine (70.7 µl, 507 µmol, 2.50 eq.) were mixed in dry, degassed and stabilized THF (5 ml). The mixture was cooled in an ice bath and a thick gel formed. NEt_2PCl_2 (32.5 µl, 223 µmol, 1.10 eq.) was added dropwise and stirring was continued at room temperature for 16 hours. All volatiles were evaporated and the residue was stirred again in THF (2 ml). The mixture was passed through a short, inert column of neutral alumina and eluted with more THF (30 ml). The collected fraction was evaporated, the white residue dissolved in dry and degassed DCM (1 ml) and the product was precipitated by adding dry and degassed *n*-pentane (10 ml). The supernatant solution was removed using a filter-tipped cannula. Re-precipitation was repeated another three times. Obtained solids were finally dried *in vacuo* to yield the product **23b** as a white powder (54.1 mg, 64.4 µmol, 32%). The compound is oxygen-sensitive and has to be stored under argon.

Note: The large number of species with very similar, overlapping NMR shifts, due to dimer formation and the chirality of phosphorus atoms, made an exact assignment of all signal unreasonable. Therefore, no distinction is made between molecules with different chirality of phosphorus atoms.

^{1}H-NMR (THF-d4, 400.22 MHz, 300 K): δ = 0.94-1.00 (m, 12H, H17/H17'), 1.02-1.08 (m, 12H, H17/H17'), 1.22 (s, 18H, H14/H14'), 1.27 (s, 9H, H14/14'), 1.28 (s, 9H, H14/H14'), 1.43 (s, 18H, H14/H14'), 1.49 (s, 9H, H14/H14'), 1.50 (s, 9H, H14/H14'), 2.70-2.93 (m, 8H, H16 and H16'), 3.00-3.23 (m, 16H, H10a' and H10b' and H16 and H16'), 3.54 (s, 3H, H15/H15'), 3.56 (s, 3H, H15/H15'), 3.58 (s, 3H, H15/H15'), 3.60 (s, 3H, H15/H15'), 3.61 (s, 3H, H15/H15'), 3.89 (s, 3H, H15/H15'), 3.90 (s, 3H, H15/H15'), 3.91 (s, 3H, H15/H15'), 3.93 (s, 3H, H15/H15'), 4.55 (m, 4H, H9'), 5.85-6.25 (m, 4H, H9), 7.10 (s 1H, H4/H4'), 7.12-7.30 (m, 28H, H4/H4' and H_{Ar}), 7.32-7.42 (m, 10H, H_{Ar} and H12'), 7.49-7.52 (m, 1H, H12'), 7.54-7.64 (m, 4H, H6/H6'), 7.71-7.78 (m, 6H, H4/H4' and H6/H6'), 7.79-7.88 (m, 10H, H6/H6' and H_{Ar}), 9.10 (s, 1H, H12), 9.12 (s, 1H, H12), 9.14 (s, 1H, H12), 9.20 (s, 1H, H12), 9.20-9.24 (m, 2H, H8'), 9.32-9.35 (m, 2H, H8'), 10.58-10.72 (m, 4H, H8) ppm.
^{13}C{^{1}H}-NMR (THF-d4, 100.65 MHz, 300 K): δ = 13.4-13.6 (C17/C17'), 27.8-28.3 (C14/C14'), 37.4-37.8 (C16/C16'), 38.3-38.7 (C10/C10'), 50.8-51.0 (C13/C13'), 54.4-55.3 (C15/C15'), 56.9-57.0 (C9/C9'), 58.1-58.2 (C9/C9'), 111.6-112.1 (C4/C4'), 117.7-117.9 (C6/C6'), 120.7-120.9 (C6/C6'), 126.0-126.1 (C_{Ar}^{tert}), 127.6-127.7 (C_{Ar}^{tert}), 128.9 (C1/C1' or C5/C5'), 129.5-130.0 (C_{Ar}^{tert} and C1/C1' and C5/C5'), 130.1-132.6 (C1/C1' and C5/C5'), 138.2-

139.2 (C_{Ar}^{quart}), 141.5-142.1 (C2/C2'), 143.3-144.0 (C2/C2'), 150.8-152.1 (C3/C3'), 165.6-166.0 (C7/C7'), 173.5-174.4 /C11/C11') ppm.
$^{31}P\{^{1}H\}$-NMR (THF-d4, 161.98 MHz, 300 K): δ = 148.1 (s), 148.2 (s), 148.2 (s), 148.3 (s) ppm.
HRMS (ESI): m/z calcd. for $C_{46}H_{59}N_5O_8P$ $[M+H]^+$: 840.40958; found: 840.40831.
FTIR: $\tilde{\nu}$ = 698 (s), 860 (s), 1023 (s), 1090 (s), 1176 (s), 1362 (s), 1455 (s), 1541 (s), 1626 (s), 2870 (w), 2931 (w), 3063 (w), 3081 (w), 3277 (bw) cm^{-1}.

7.2.8 Inversion barrier of compound 6

Stereodynamics of BIPHEP **6** were investigated using dynamic HPLC measurements. Elution profiles were measured between 35 and 70 °C and evaluated using the Unified Equation which allows the determination of rate constants from first order reactions taking place in chromatographic systems.[109] The Unified Equation was solved using the program DCXplorer.[226] Preparation of the Eyring plot was done with Microsoft Excel 2013 and ChemOrganizer.[227]

7.2.8.1 Chromatograms

Conditions: Chiralpak® IA (250 mm, i.d. 4.6 mm, particle size 5 µm); 1,0 ml/min; n-hexane:2-propanol 95:5 (v/v); 35 °C bis 70 °C with 5 °C interval, three measurements per temperature.

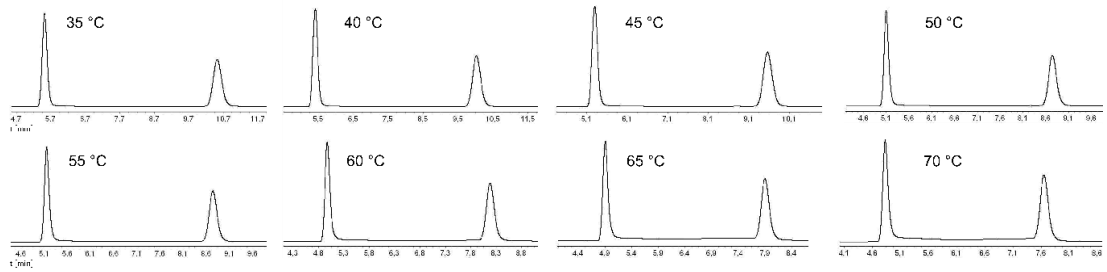

Figure 7-1: Elution profiles for the inversion barrier determination of compound **6**.

7.2.8.2 Chromatographic data Eyring plot

Table 7-1: Raw data of elution plots

	Retention time [min]		FDHM [s]		Height [%]			# of theoretical plates	
T [°C]	**t1**	**t2**	**w1**	**w2**	**Peak 1**	**Plateau**	**Peak 2**	**N1**	**N2**
35,0	5,522	10,529	9,4	17,3	100,00	0,13	50,44	4620	6056
35,0	5,519	10,512	9,4	17,2	100,00	0,10	50,47	4614	6105
35,0	5,517	10,502	9,4	17,3	100,00	0,10	50,57	4609	6022
40,0	5,393	10,009	9,2	16,1	100,00	0,19	52,21	4551	6250
40,0	5,389	9,995	9,2	16,1	100,00	0,19	52,27	4543	6231
40,0	5,389	9,987	9,4	16,2	100,00	0,18	52,40	4352	6143
45,0	5,281	9,561	9,2	15,3	100,00	0,30	54,47	4322	6250
45,0	5,276	9,540	9,1	15,2	100,00	0,28	54,50	4408	6301
45,0	5,277	9,535	9,2	15,2	100,00	0,28	54,60	4314	6294
50,0	5,183	9,156	9,1	14,6	100,00	0,42	57,61	4218	6229
50,0	5,180	9,144	9,1	14,6	100,00	0,43	57,63	4212	6211
50,0	5,128	8,776	6,3	12,1	100,00	0,38	52,77	8570	8244

55,0	5,111	8,712	6,4	11,9	100,00	0,53	53,83	8236	8384
55,0	5,110	8,702	6,4	11,9	100,00	0,53	53,27	8232	8362
55,0	5,113	8,705	6,4	12,0	100,00	0,52	53,62	8244	8230
60,0	4,981	8,208	6	10,9	100,00	0,80	58,75	8788	8729
60,0	4,979	8,189	6	11,0	100,00	0,84	58,92	8779	8526
60,0	4,981	8,19	6,1	10,9	100,00	0,83	58,99	8502	8686
65,0	4,919	7,931	6	10,5	100,00	1,24	62,65	8516	8698
65,0	4,919	7,921	6	10,5	100,00	1,55	62,28	8516	8673
65,0	4,917	7,912	5,9	10,4	100,00	1,56	62,38	8798	8817
70,0	4,866	7,689	5,9	10,2	100,00	1,92	65,32	8571	8585
70,0	4,863	7,669	5,9	10,1	100,00	2,11	64,54	8558	8703
70,0	4,863	7,657	5,9	10,0	100,00	2,08	64,54	8558	8846

Table 7-2 Kinetic data

T [°C]	k_1^{UE} [1/s]	G_{app} [kJ/mol]	1/T [1/K]	$\ln(k_1^{UE}/T)$
35,0	6,6470E-05	100,20	3,2452E-03	-15,3493
35,0	5,1120E-05	100,87	3,2452E-03	-15,6119
35,0	5,0920E-05	100,88	3,2452E-03	-15,6158
40,0	9,3550E-05	100,98	3,1934E-03	-15,0237
40,0	9,3390E-05	100,98	3,1934E-03	-15,0254
40,0	8,6350E-05	101,19	3,1934E-03	-15,1038
45,0	1,3860E-04	101,59	3,1432E-03	-14,6464
45,0	1,3030E-04	101,76	3,1432E-03	-14,7082
45,0	1,2890E-04	101,79	3,1432E-03	-14,7190
50,0	1,8290E-04	102,49	3,0945E-03	-14,3847
50,0	1,8630E-04	102,44	3,0945E-03	-14,3663
50,0	2,1830E-04	102,01	3,0945E-03	-14,2078
55,0	2,9560E-04	102,80	3,0474E-03	-13,9200
55,0	2,9580E-04	102,80	3,0474E-03	-13,9193
55,0	2,9080E-04	102,85	3,0474E-03	-13,9363
60,0	4,1910E-04	103,45	3,0017E-03	-13,5860
60,0	4,2890E-04	103,38	3,0017E-03	-13,5629
60,0	4,1770E-04	103,46	3,0017E-03	-13,5893
65,0	5,8830E-04	104,09	2,9573E-03	-13,2618
65,0	7,1150E-04	103,55	2,9573E-03	-13,0716
65,0	7,2120E-04	103,51	2,9573E-03	-13,0581
70,0	8,4130E-04	104,65	2,9142E-03	-12,9187
70,0	9,3080E-04	104,36	2,9142E-03	-12,8176
70,0	9,2010E-04	104,39	2,9142E-03	-12,8292

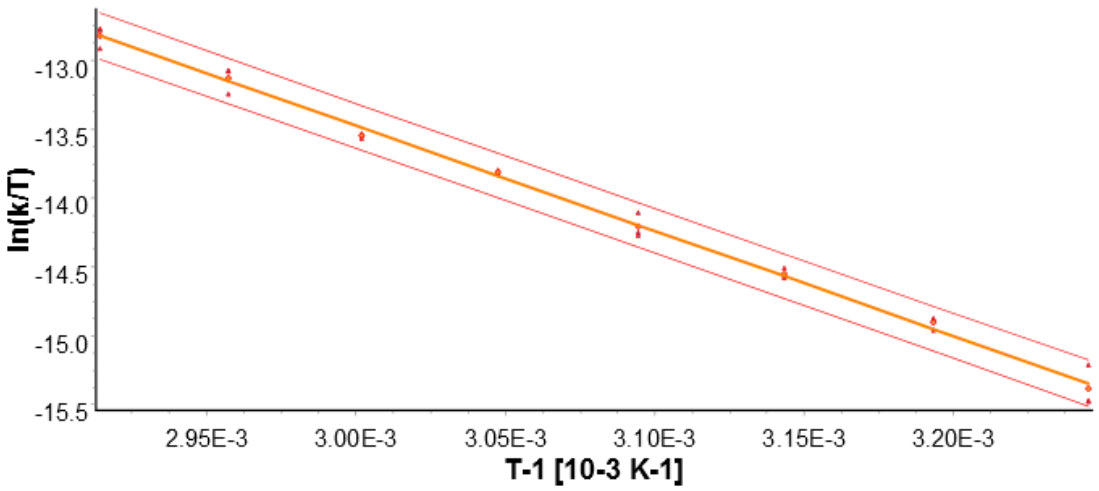

Figure 7-2: Eyring plot for the determination of thermodynamic parameters.

$$Y = -8.06738 \cdot 10^3 x + 1.06694$$

$\Delta G^{\ddagger}_{298}$ = 97,81 kJ·mol^{-1}, $\Delta H^{\ddagger}$ = 67,08 ± 0,50 kJ·mol^{-1}, $\Delta S^{\ddagger}$ = -103,10 ± 1,8 J·K^{-1}·mol^{-1}

7.2.9 Determination of the inversion barrier of compound 7

Pure samples of each rotamer were prepared by dissolving each compound in dry and degassed $CDCl_3$ to give a 5.1 mM solution. Samples were heated to 60 °C and spectra were collected periodically until equilibrium was reached (for spectral data see page 100).

Kinetic data and thermodynamic calculations

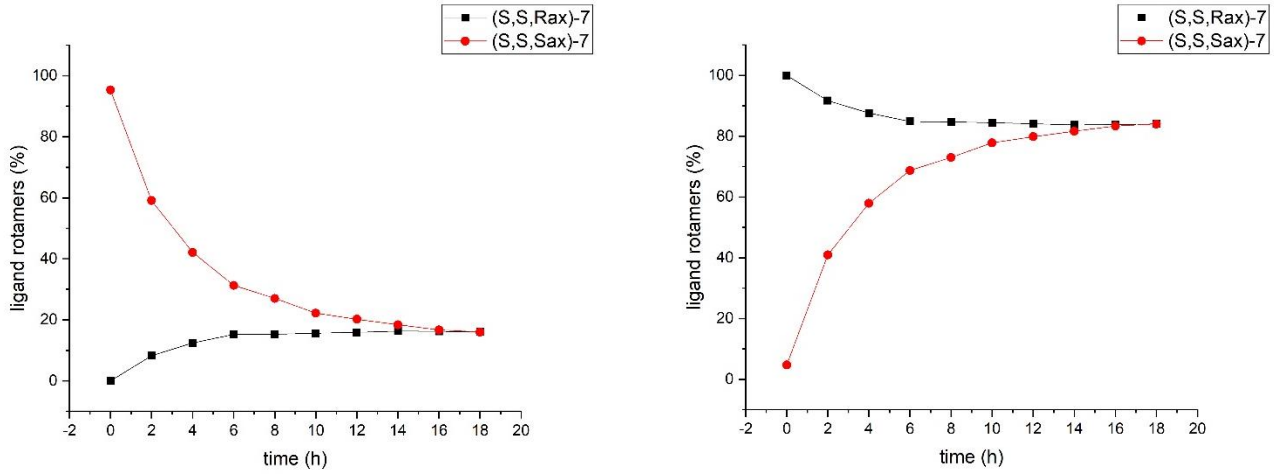

Figure 7-3: NMR-based kinetic measurements for the interconversion of bisphosphine **7**.

For thermodynamic calculations, a model of *first order kinetics* with *opposing reactions* was assumed:

$$A \underset{k_{-1}}{\overset{k_1}{\rightleftharpoons}} B$$

$$[A(t)] = A_e + x_e\, exp[-(k_1 + k_{-1})t]$$

$$y\,(t) = \ ln\left(\frac{A(t) - A_e}{x_e}\right) = \ -(k_1 + \ k_{-1})t = \ \ a * t$$

$$a \ = \ -(k_1 + k_{-1}) \qquad B_e/A_e \ = \ k_1/k_{-1} \ = \ K_e$$

$$k_{-1} \ = \ -\frac{a}{K_e + 1}$$

$$k_1 \ = \ k - 1 \ * \ K_e$$

time			***R*ax**	***S*ax**	***de***	**A(t)-Ae**	**(A(t)-Ae)/xe**	**ln((A(t)-Ae)/xe)**
h	min	sec	%	%	%			
0	0	0	100	0	100	16.4	1	0
2	120	7200	91.7	8.2	83.5	8.1	0.493902439	-0.705417273
4	240	14400	87.6	12.4	75.2	4	0.243902439	-1.410986974
6	360	21600	84.8	15.2	69.6	1.2	0.073170732	-2.614959778
8	480	28800	84.7	15.3	69.4	1.1	0.067073171	-2.701971155
10	600	36000	84.4	15.6	68.8	0.8	0.048780488	-3.020424886
12	720	43200	84.1	15.9	68.2	0.5	0.030487805	-3.490428515
14	840	50400	83.8	16.2	67.6	0.2	0.012195122	-4.406719247
16	960	57600	83.7	16.3	67.4	0.1	0.006097561	-5.099866428
18	1080	64800	83.6	16.4	67.2	0	0	-

A_e = 83.6 x_e = 16.4 a = -8.35E-05 s^{-1}

K_e = 0.19617225

k_{-1} = 6,97977E-05 s^{-1} k_1 = 1,36924E-05 s^{-1}

$$k(T) = \frac{kT}{h} exp\left(-\frac{\Delta G^{\ddagger}}{RT}\right) \quad \rightarrow \quad \Delta G^{\ddagger} \ = \ -RT * ln\left(\frac{(k(T)h)}{k * T}\right)$$

$k = 1.3806 * 10^{-23}\frac{J}{K}$ $h = \ 6.62607 * 10^{-34} J * \sec$ $R = 8.314\frac{J}{mol*K}$ $T = 333.15\ ^{\circ}C$

$\Delta G_{333K}^{\ddagger}$ ($R_{ax} \rightarrow S_{ax}$) =112.9 kJ/mol $\Delta G_{333K}^{\ddagger}$($S_{ax} \rightarrow R_{ax}$) =108.4 kJ/mol

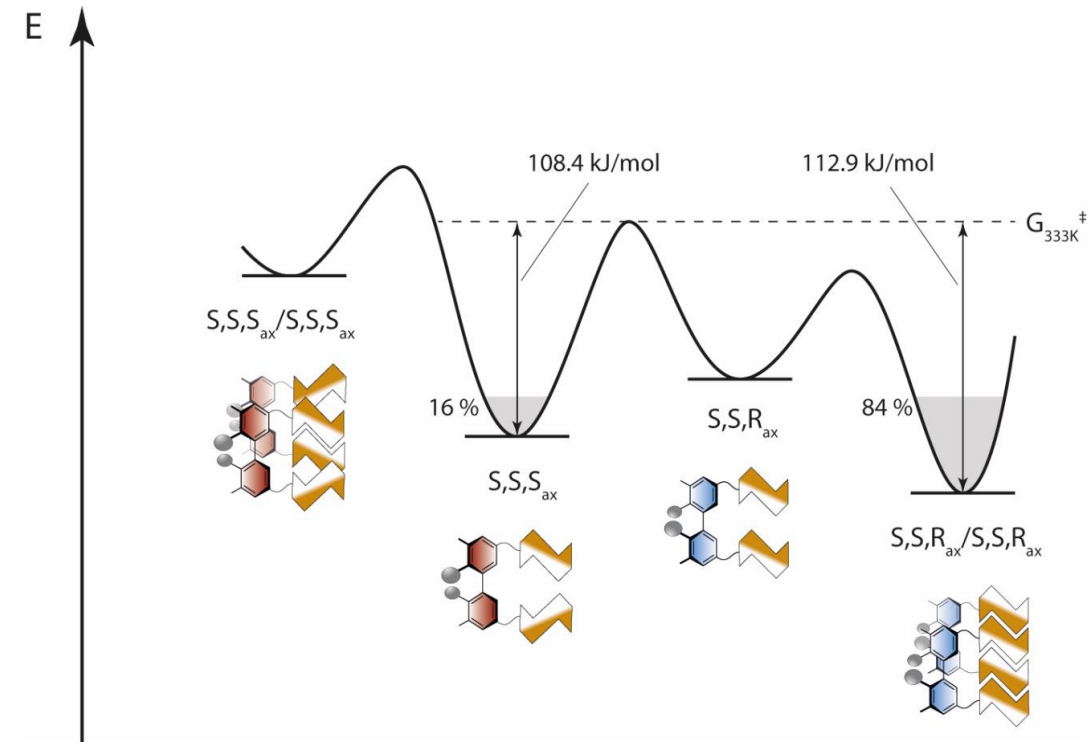

Figure 7-4: Schematic energy profile of interconverting species of ligand **7**.

7.2.10 Ligand equilibration and seeding experiments of bisphosphine 7

7.2.10.1 Ligand isomerization

A mixture of both ligand diastereomers was precipitated from dry and degassed DCM/*n*-pentane (1:5, *v*:*v*) and the solids were collected and dried to give highly enriched **(*R*$_{ax}$)-7**. The filtrate was evaporated and residual solids re-precipitated from dry and degassed diethyl ether/pentane (1:5, *v*:*v*) to obtain the respective rotamer **(*S*$_{ax}$)-7**. Solutions in $CDCl_3$ (5.1 mM) were prepared and heated to 60 °C. Spectra were collected periodically until equilibrium was reached.

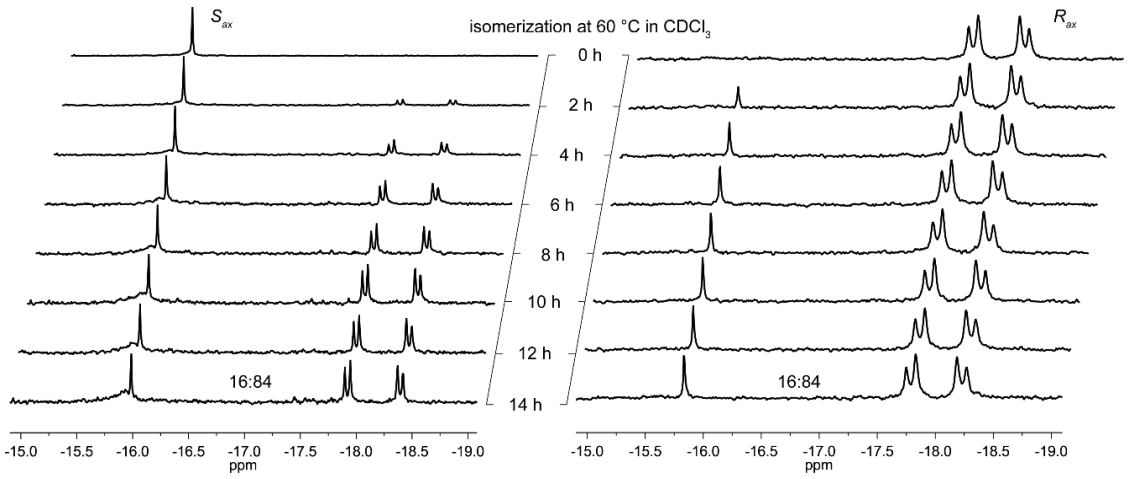

Figure 7-5: Equilibration of (*S*$_{ax}$)- and (*R*$_{ax}$)-**7** at elevated temperatures leads to the same equilibrium distribution of rotamer species.

7.2.10.2 Re-symmetrization

Strong hydrogen bond donors induce re-symmetrization the major rotamer (R_{ax})-**7**^{C1} to form a new species (R_{ax})-**7**^{C2}.

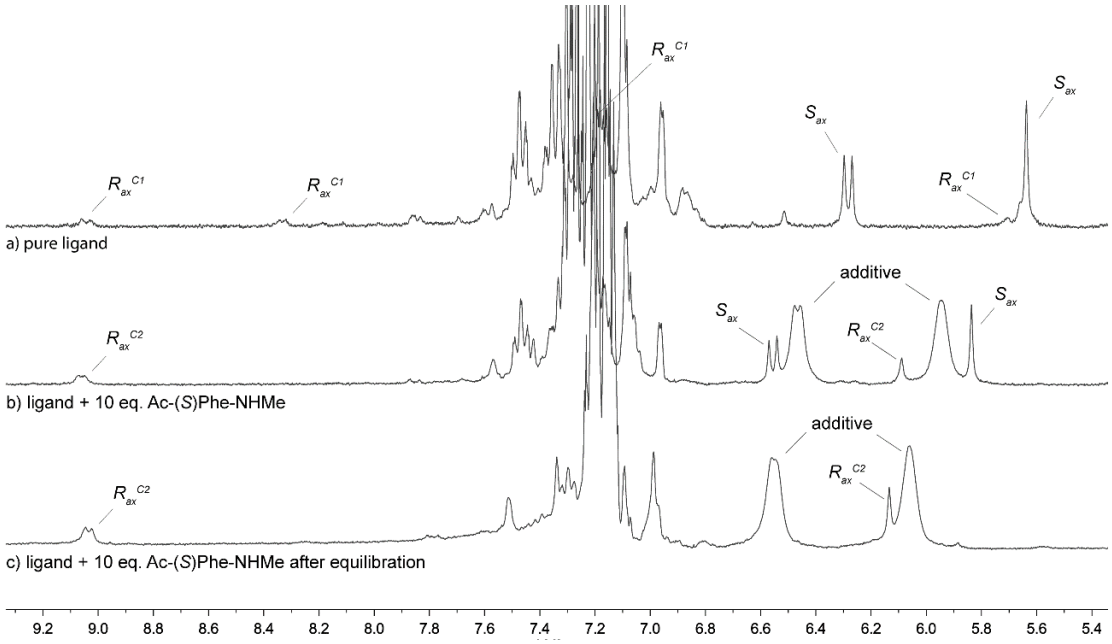

Figure 7-6: (a) Employing an un-equilibrated sample of the ligand with **(*S*$_{ax}$)-7** in excess. (b) Addition of the additive (*S*)-**8** converts (R_{ax})-**7**^{asym} into its symmetric equivalent. (c) Equilibration of the solution leads to significant enrichment of the newly formed species at the expense of the less stable S_{ax} rotamer due to thermal isomerization.

7.2.10.3 Solute-dependent equilibrium distribution

Ligand equilibrium distribution was found to be depending on the chemical environment. Ligand **7** was equilibrated in the presence of different chiral and achiral additives. For all experiments, the ligand (2 mg) was placed in a J.Young-NMR tube and dissolved in dry and degassed $CDCl_3$ (0.4 ml) to give a 5.1 mM solution. After addition of 10 equivalents of the respective additive, the mixture was equilibrated at 60 °C and the progress monitored by $^{31}P\{^1H\}$-NMR spectroscopy.

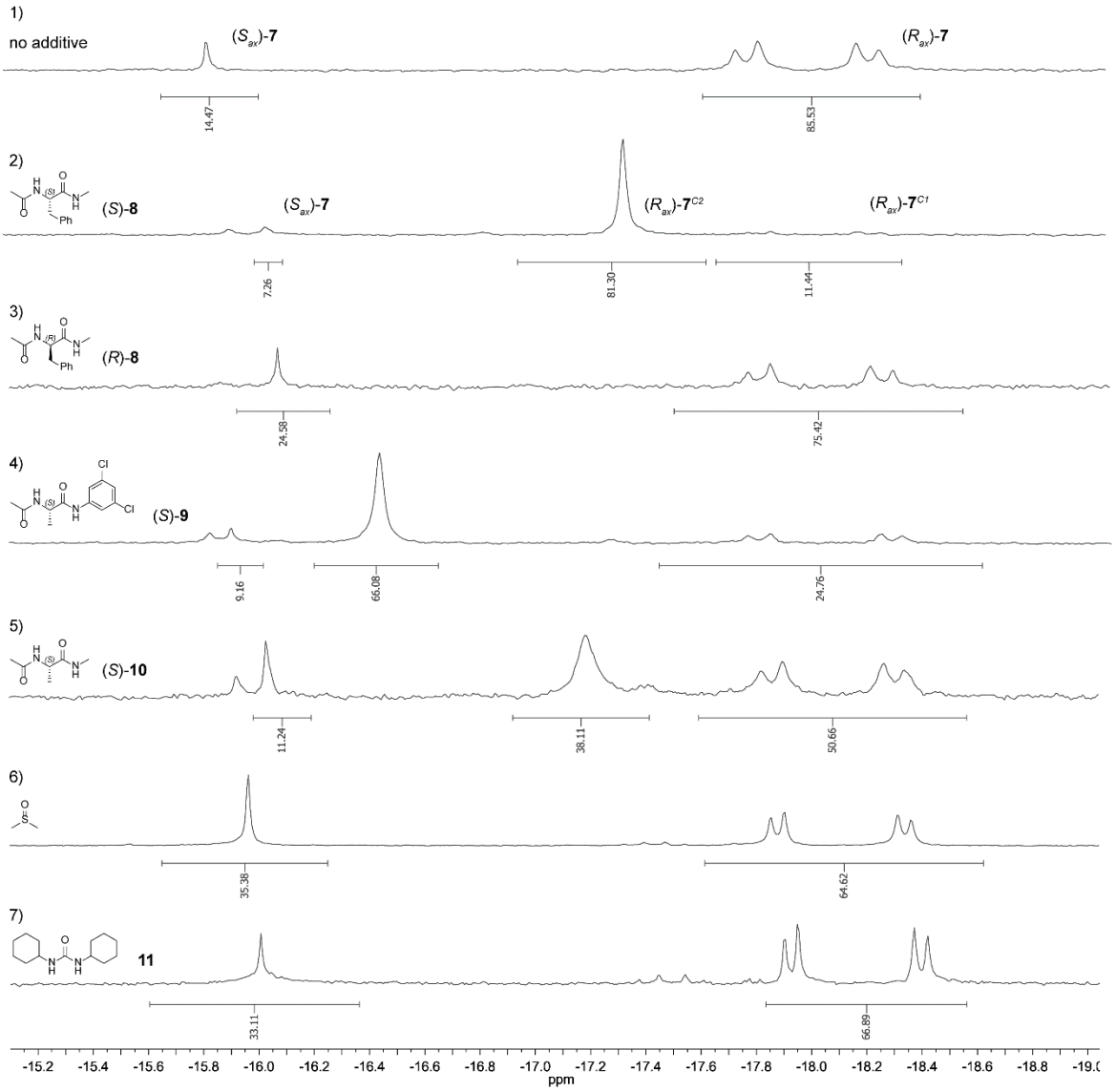

Figure 7-7: Equilibrium distribution for ligand **7** under different conditions. Procedure as described above with exceptions as follows*: Spectrum 4*: Only 5 eq. Ac-(*S*)Ala-NH(3,5-dichlorophenyl) **9** were used and not all solids dissolved. *Spectrum 6*: For DMSO, ligand was equilibrated in pure and degassed DMSO-d6. Due to line broadening, final compound distribution was determined by evaporating the sample and measuring it in $CDCl_3$ where (R_{ax})-**7**^{C2} could not be determined. *Spectrum 7*: 10 eq. dicyclohexyl urea **11** were used, but not all solids dissolved.

7.2.11 HMBC correlation data

Two-dimensional ^{1}H-^{13}C-HMBC NMR data of ligand precursors **18a-c** and ligand **19a** show cross peaks between protons belonging to the two diff erent signal sets and quaternary carbons of the respective other set linking all signals in the spectrum to the same molecular scaffold.

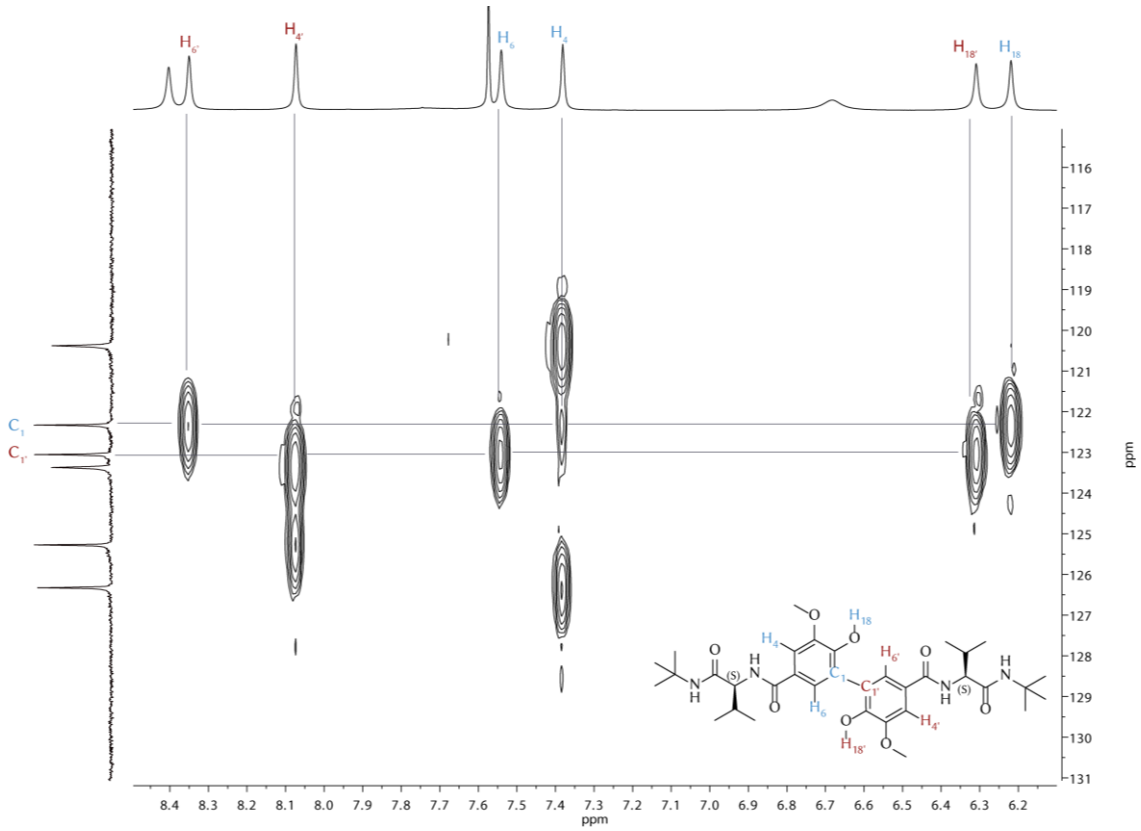

Figure 7-8**:** Section of ^{1}H-^{13}C-HMBC spectrum of ligand precursor **18a** with annotated cross peaks.

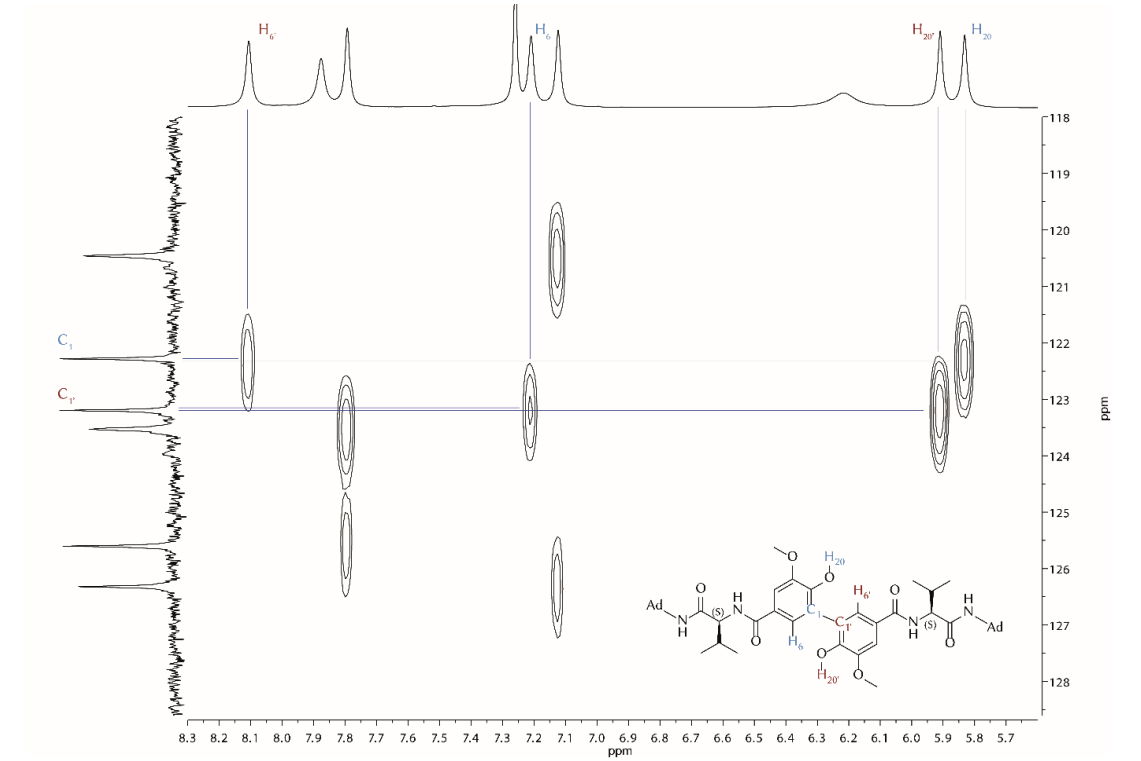

Figure 7-9: Section of ^{1}H-^{13}C-HMBC spectrum of ligand precursor **18b** with annotated cross peaks.

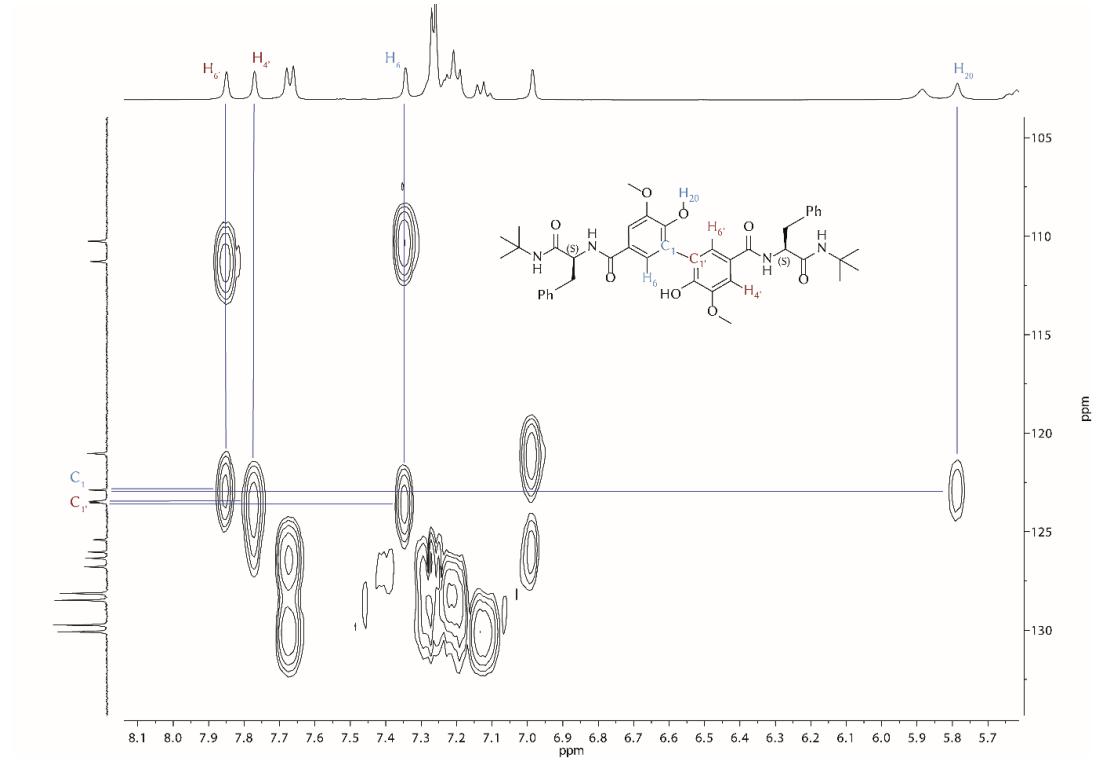

Figure 7-10: Section of ^{1}H-^{13}C-HMBC spectrum of ligand precursor **18c** with annotated cross peaks.

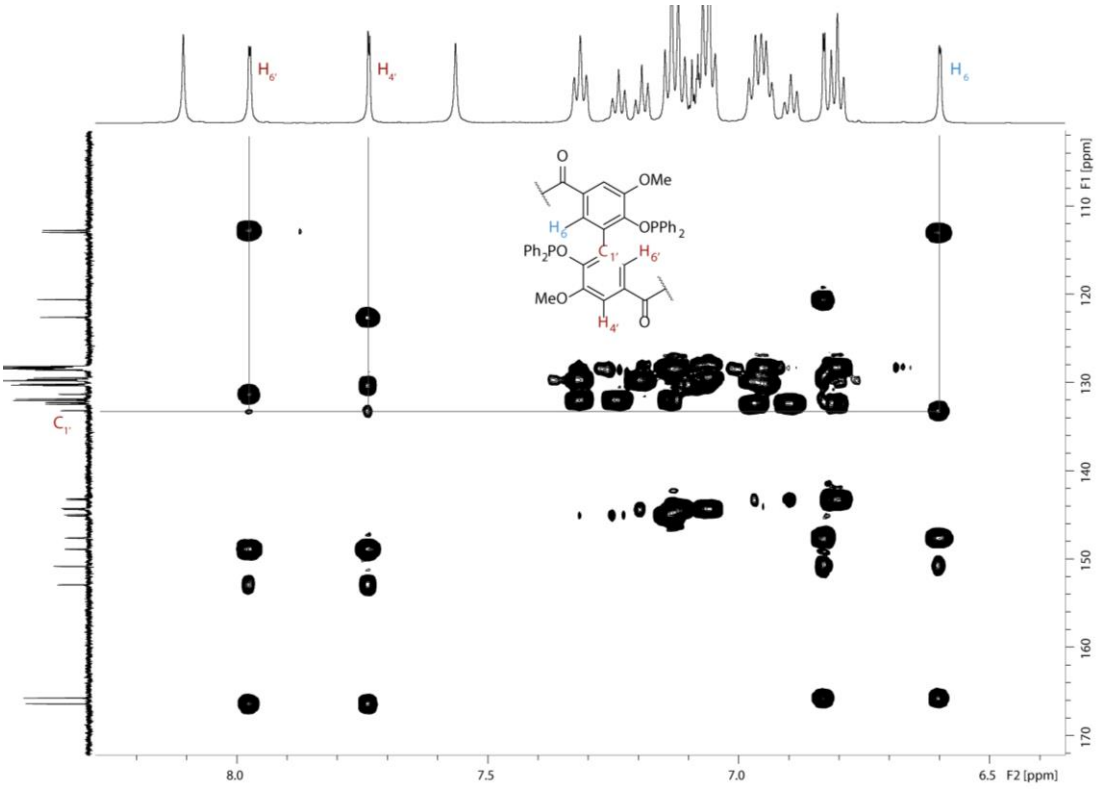

Figure 7-11**:** Section of ^{1}H-^{13}C-HMBC spectrum of ligand **19a** with annotated cross peaks.

7.2.12 Crossover experiments

7.2.12.1 Bisphosphinite ligands 19a and 19b

From a stock solution in THF-d8, 2.55 mg **19a** and 2.95 mg **19b** were placed in a J.Young tube to give a 5 mM solution in each component. After the first measurement, the solution was evaporated and another equivalent of **19a** in 0.5 ml solvent was added.

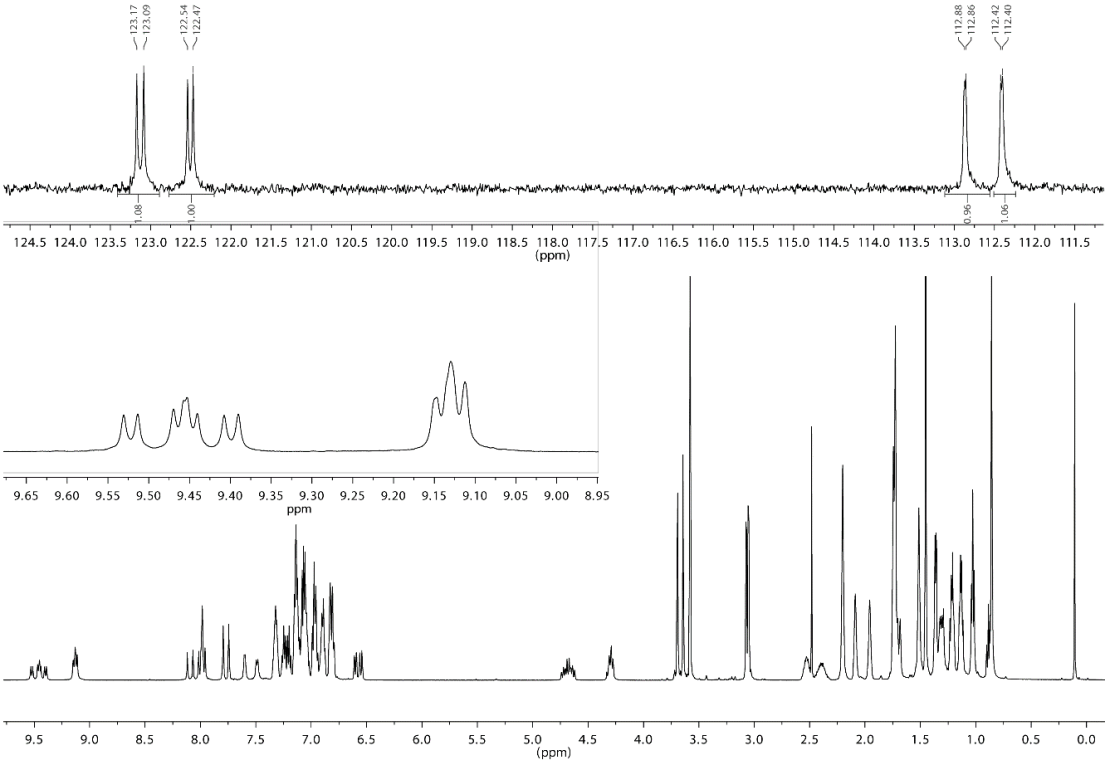

Figure 7-12**:** Crossover experiment using ligands **19a** and **19b** in equimolar amounts. *Top*: $^{31}P\{^{1}H\}$-NMR spectrum. *Bottom*: ^{1}H-NMR spectrum with expansion of area of amide protons.

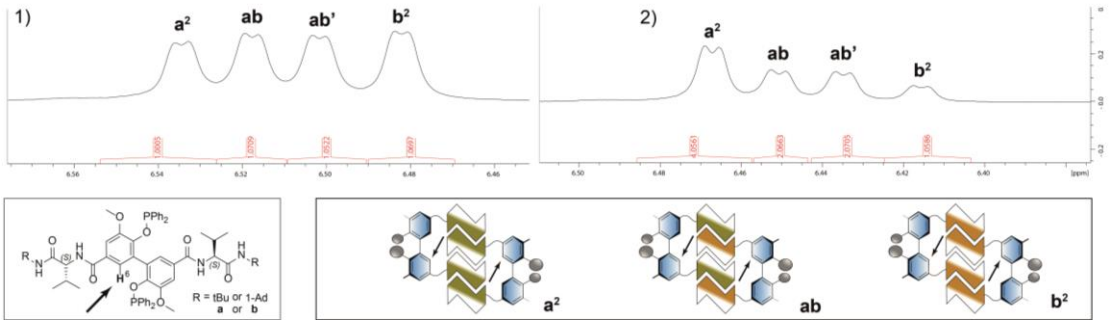

Figure 7-13**:** ^{1}H-NMR segment of proton H6. 1) 1:1 mixture of **19a** and **19b** gives **a^2:ab:b^2** dimers in a ratio of 1:2:1 with the mixed dimer bearing two diastereotopic protons H6 and H6', thus yielding four signals of identical intensity. 2) 2:1 mixture (**a**:**b**) gives dimers in 4:4:1 distribution, thus yielding four signals with 4:2:2:1 intensity (see below for kinetic considerations).

Assuming a similar behaviour of both compounds in terms of interaction, the dimerization behaviour can be described as follows:

$$k_{AA} \sim [A]^2 \qquad k_{BB} \sim [B]^2 \qquad k_{AB} = k_{BA} \sim 2[A][B]$$

$$\text{If } [A] = [B] \rightarrow k_{AA} = k_{BB} = ½\ k_{AB} = ½\ k_{BA}$$

$$\text{If } [A] = 2[B] \rightarrow k_{AA} = 4[B]^2 \qquad k_{BB} = [B]^2 \qquad k_{AB} = k_{BA} = 4[B]^2$$

7.2.12.2 BIPOL ligands 18a and 18b

Diols **18a** and **18b** were mixed in dry $CDCl_3$ to give a 5 mM in each component. NMR spectra were collected at -38 °C and compared to those of the isolated compounds under identical conditions. Mixing the ligands gives rise to a variety of new (partially overlapping) signals that can be attributed to the formation of the heterodimeric compound.

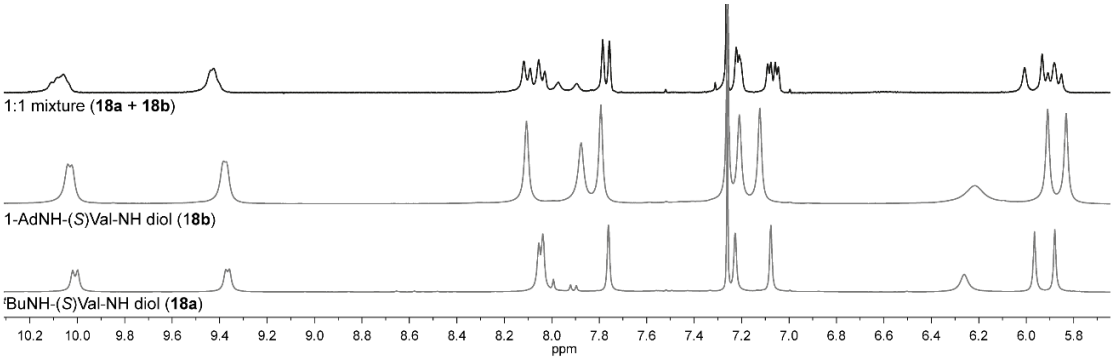

Figure 7-14: Section of ^{1}H NMR spectra of diols **18a**, **18b** and their respective 1:1 mixture in $CDCl_3$

7.2.13 Temperature-dependent NMR measurements

A sample of bisphosphine **7** (8 mM in dry and degassed $CDCl_3$ or $CDCl_2CDCl_2$) was measured at different temperatures from -38 to 80 °C. Strong line broadening was observed for the dimerized ligand species with increasing temperature.

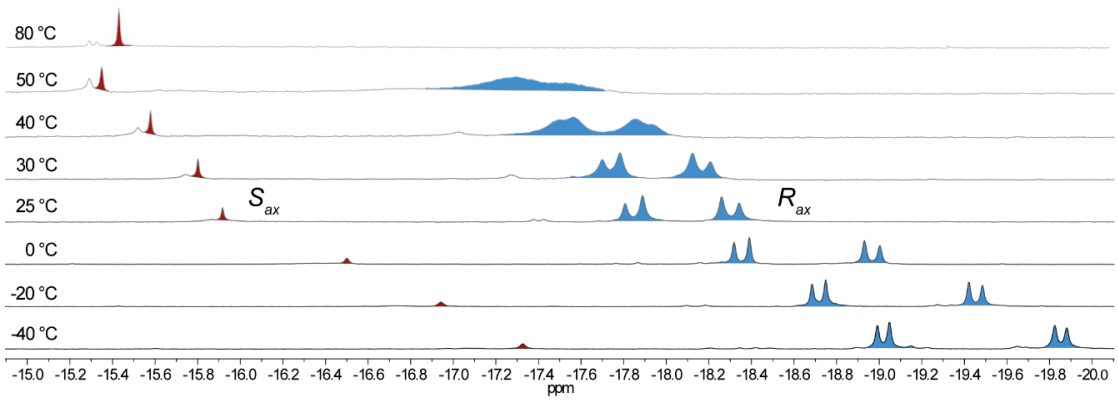

Figure 7-15**:** Temperature-dependent $^{31}P\{^1H\}$ NMR spectra of bisphosphine **7** in $CDCl_3$ (-40 °C – 50 °C) and $CDCl_2CDCl_2$ (80 °C).

Samples of bisphosphinite **19a** (8 mM in dry and degassed NMR solvent) were measured at different temperatures from -38 to 50 °C (THF-d8) and from 20 to 100 °C ($CDCl_2CDCl_2$).

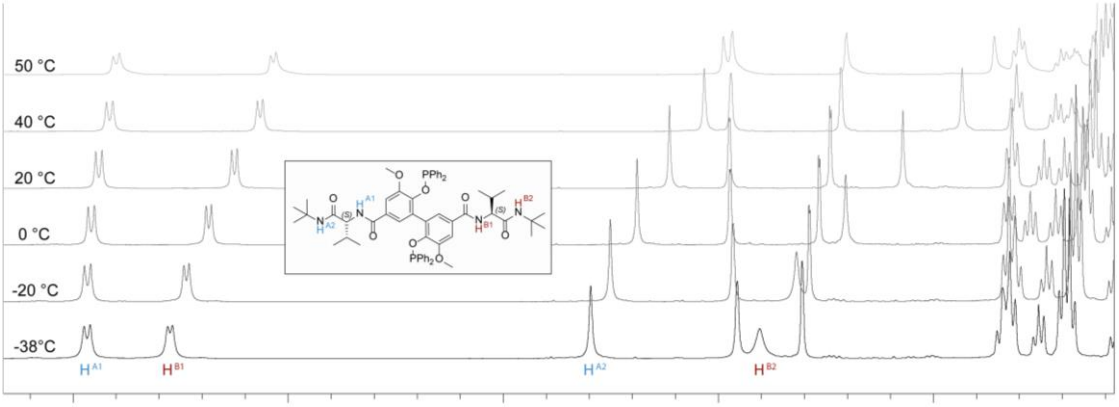

Δδ [ppm]	ΔT [K]	ppb/K	Δδ [ppm]	ΔT [K]	ppb/K	Δδ [ppm]	ΔT [K]	ppb/K	Δδ [ppm]	ΔT [K]	ppb/K
-0.0016	18	-0.0889	-0.0388	18	-2.1556	-0.0455	18	-2.5278	-0.0860	18	-4.7778
-0.0080	20	-0.4000	-0.0517	20	-2.5850	-0.0623	20	-3.1150	-0.1142	20	-5.7100
-0.0181	20	-0.9050	-0.0596	20	-2.9800	-0.0755	20	-3.7750	-0.1300	20	-6.5000
-0.0250	20	-1.2500	-0.0600	20	-3.0000	-0.0813	20	-4.0650	-0.1375	20	-6.8750
-0.0155	10	-1.5500	-0.0310	10	-3.1000	-0.0440	10	-4.4000	-0.0740	10	-7.4000
	H^{A1}	**-0.8388**		H^{B1}	**-2.7641**		H^{A2}	**-3.5766**		H^{B2}	**-6.2526**

Figure 7-16: Temperature-dependent shifts of amid protons of **19a** are used to qualitatively asses binding strength on non-covalent interactions.

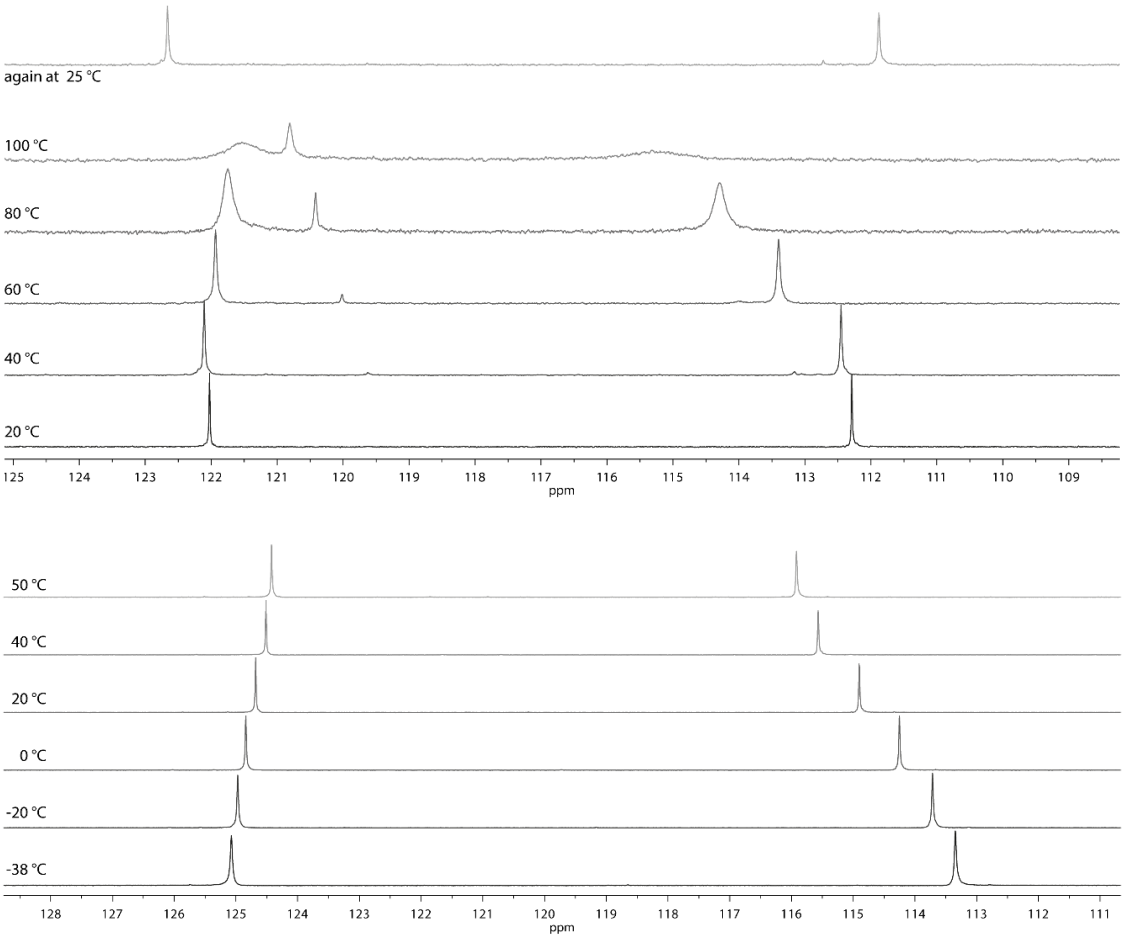

Figure 7-17**:** Temperature-dependent $^{31}P\{^{1}H\}$ NMR spectra of **19a** in THF-d8 (bottom) and in $CDCl_2CDCl_2$ (top). New singlet species forms at 40 °C and above that vanishes when sample is measured again at room temperature afterwards.

Samples from crossover experiments exhibited a similar behaviour to samples containing one single ligand. A mixture of compounds **19a** and **19b** (5 mM solution in each compound in dry and degassed NMR solvent) were measured at diff erent temperatures from -38 to 50 °C (THF-d8) and from 20 to 100 °C ($CDCl_2CDCl_2$).

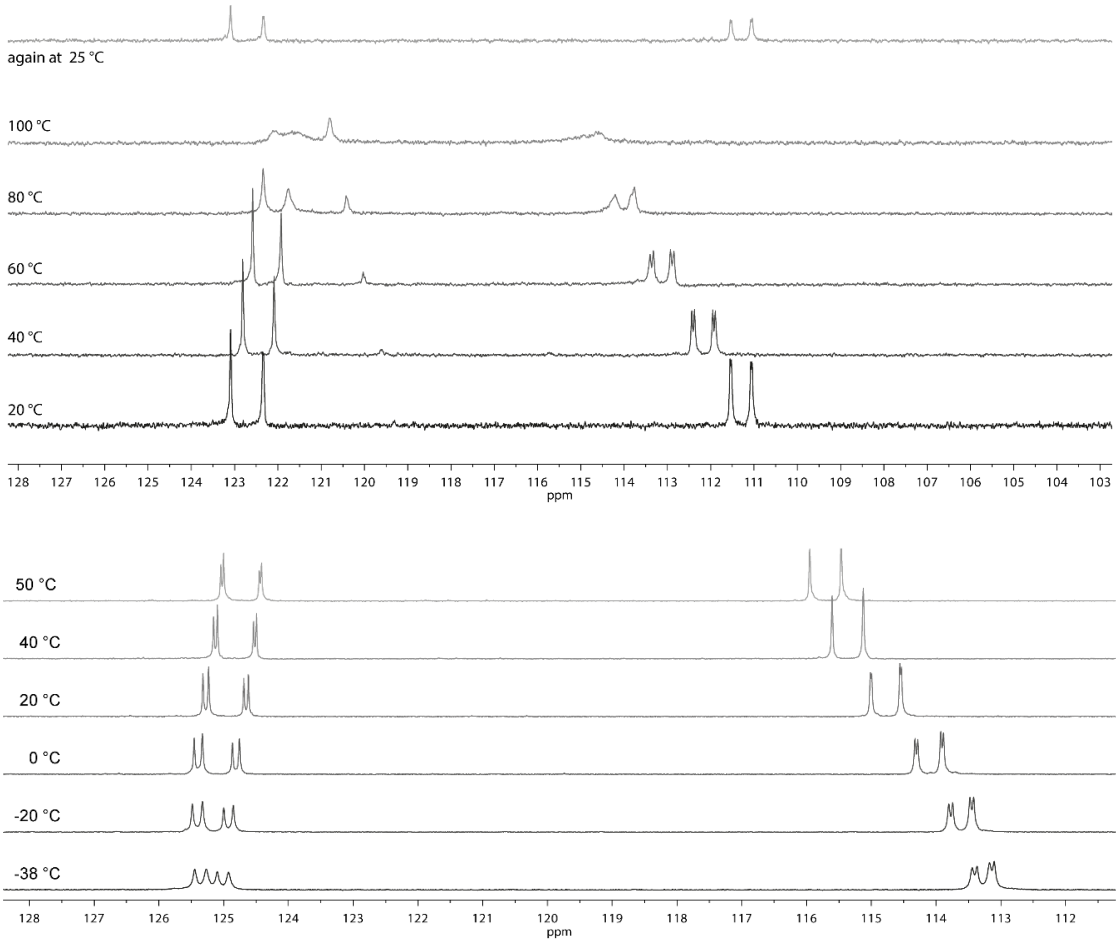

Figure 7-18**:** Temperature-dependent $^{31}P\{^1H\}$ NMR spectra of **19a** and **19b** in THF-d8 (bottom) and in $CDCl_2CDCl_2$ (top). New singlet species forms at 40 °C and above that vanishes when sample is measured again at room temperature afterwards.

7.2.14 Model structure model-19a and NOESY spectra of 19a

7.2.14.1 Structure optimization

The model structure **model-19a** for an illustrative analysis of NOESY spectra was generated with Gaussian 16, Revision A.03.[228] using the B3LYP functional[229] with Grimme's D3BJ dispersion correction[230] and Dunning's cc-pVDZ basis set[231] with additional diff use functions[232] on hetero atoms and on amide protons. The initial structure was based on the crystallographic data obtained for glycine-based phosphinite compound **19d** and a variety of conformers were optimized to find the one of lowest energy. No imaginary frequencies were observed for the ground state and Gibbs free energies refer to standard temperature (298.15 K) and pressure (1 atm).

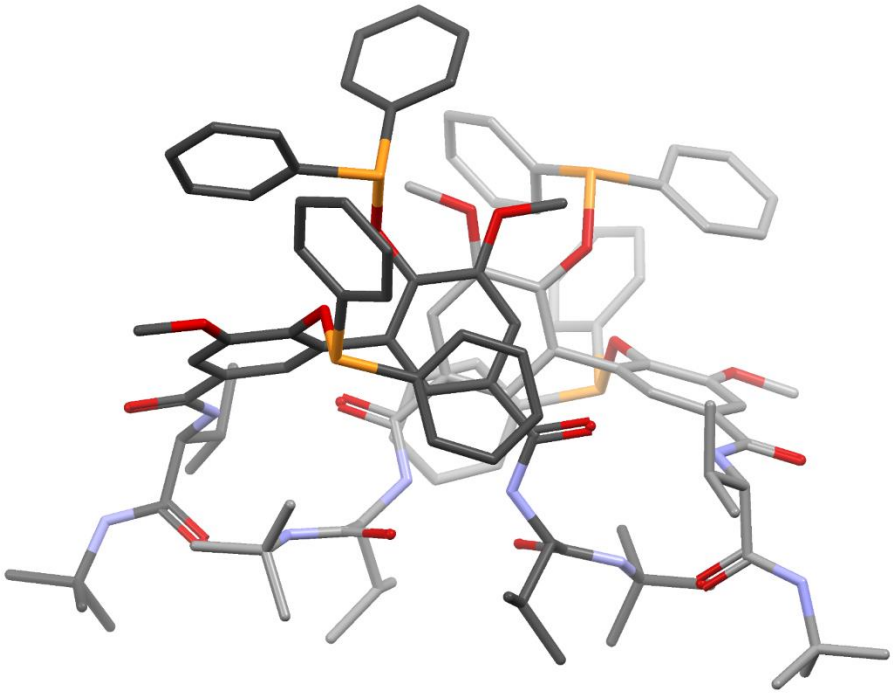

Figure 7-19**:** Front view of calculated structure **model-19a**. The two molecular subunits of the dimer are coloured in light and dark grey. Protons are omitted for clarity. Nitrogen = blue, oxygen = red, phosphorus = orange.

Energy: HF= -7510.9041682

Cartesian coordinates (in Å):

Center Number	Atomic Number	Atomic Type	Atomic Coordinates (Angstroms) X	Y	Z
1	15	0	-5.379776	2.849292	-2.373805
2	15	0	-3.827478	-1.224812	-4.337429
3	8	0	-5.048477	1.142272	-2.299531
4	8	0	-7.414509	0.735718	-1.123386
5	8	0	-6.339024	-1.577080	3.316897
6	8	0	-3.125379	-1.282688	-2.753965
7	8	0	-0.797245	-0.838158	-4.070001
8	8	0	1.582826	2.737845	-1.422793
9	8	0	2.056704	1.970292	2.716085
10	7	0	-4.087312	-1.824043	3.315696
11	1	0	-3.179175	-1.625501	2.895978
12	7	0	0.495408	2.881041	0.562448
13	1	0	-0.286541	2.604634	1.161800
14	7	0	3.779181	3.185518	1.847619
15	1	0	4.000417	3.971503	1.234524
16	6	0	-6.026994	2.803766	-4.098241
17	6	0	-6.951567	1.803813	-4.443170
18	1	0	-7.199993	1.029439	-3.717994
19	6	0	-7.526947	1.791000	-5.714602
20	1	0	-8.232497	0.999419	-5.976487
21	6	0	-7.201877	2.780747	-6.647843
22	1	0	-7.654951	2.768503	-7.641597
23	6	0	-6.292367	3.784740	-6.304259
24	1	0	-6.028944	4.557667	-7.029779

25	6	0	-5.705312	3.796788	-5.036075
26	1	0	-4.980473	4.572516	-4.781734
27	6	0	-3.668787	3.479292	-2.640892
28	6	0	-2.792413	2.932808	-3.594459
29	1	0	-3.128656	2.112138	-4.230511
30	6	0	-1.493184	3.422948	-3.707579
31	1	0	-0.806688	2.982435	-4.432569
32	6	0	-1.056794	4.464863	-2.879993
33	1	0	-0.032502	4.829065	-2.960928
34	6	0	-1.922484	5.015107	-1.934581
35	1	0	-1.582953	5.823873	-1.286712
36	6	0	-3.223115	4.515719	-1.808177
37	1	0	-3.896552	4.925305	-1.051187
38	6	0	-5.079882	0.542530	-1.071720
39	6	0	-6.318882	0.302183	-0.438147
40	6	0	-6.352970	-0.345428	0.795511
41	1	0	-7.284038	-0.540070	1.323112
42	6	0	-5.156554	-0.767958	1.398463
43	6	0	-3.936704	-0.538842	0.757388
44	1	0	-2.997314	-0.859810	1.196094
45	6	0	-3.888503	0.123340	-0.474226
46	6	0	-8.687038	0.535846	-0.525220
47	1	0	-9.416766	0.951574	-1.230784
48	1	0	-8.763322	1.062602	0.440718
49	1	0	-8.892135	-0.536588	-0.372492
50	6	0	-5.250956	-1.420752	2.744149
51	8	0	-3.764388	-0.263913	5.706357
52	7	0	-5.307942	-1.677541	6.614235
53	1	0	-5.835777	-2.516411	6.419618
54	6	0	-4.089731	-2.410992	4.637669
55	1	0	-4.885044	-3.172510	4.679133
56	6	0	-4.386865	-1.334481	5.693053
57	6	0	-5.717528	-0.887461	7.796752
58	6	0	-2.579096	0.374016	-1.135799
59	6	0	-2.258718	-0.320795	-2.306894
60	6	0	-1.014357	-0.115884	-2.936543
61	6	0	-0.102584	0.775444	-2.380127
62	1	0	0.865424	0.957499	-2.838029
63	6	0	-0.416187	1.470192	-1.202940
64	6	0	-1.651745	1.266241	-0.582312
65	1	0	-1.928038	1.809538	0.318278
66	6	0	-3.229622	-2.881433	-4.929369
67	6	0	-2.186092	-2.893938	-5.867452
68	1	0	-1.802871	-1.946583	-6.248918
69	6	0	-1.628416	-4.100237	-6.298298
70	1	0	-0.810239	-4.095053	-7.021711
71	6	0	-2.118280	-5.311704	-5.801561
72	1	0	-1.684572	-6.256259	-6.137512
73	6	0	-3.173445	-5.310890	-4.882907
74	1	0	-3.567311	-6.255653	-4.501111
75	6	0	-3.728046	-4.103751	-4.451763
76	1	0	-4.550334	-4.111657	-3.735270
77	6	0	-5.543520	-1.687463	-3.839543
78	6	0	-5.882062	-2.146551	-2.559252
79	1	0	-5.108214	-2.238466	-1.798633

80	6	0	-7.208955	-2.461488	-2.255112
81	1	0	-7.460795	-2.805487	-1.249615
82	6	0	-8.206128	-2.328747	-3.224865
83	1	0	-9.242835	-2.573433	-2.983227
84	6	0	-7.872460	-1.876689	-4.506030
85	1	0	-8.647289	-1.766657	-5.268199
86	6	0	-6.548974	-1.551131	-4.808399
87	1	0	-6.295901	-1.170426	-5.801253
88	6	0	0.491591	-0.755301	-4.671349
89	1	0	0.488117	-1.488519	-5.486279
90	1	0	1.283077	-1.020210	-3.956490
91	1	0	0.674318	0.254121	-5.077186
92	6	0	0.622023	2.414145	-0.691806
93	6	0	1.498876	3.738212	1.173524
94	1	0	2.037998	4.263238	0.377131
95	6	0	2.482651	2.873163	1.974560
96	6	0	4.876283	2.637472	2.683743
97	15	0	5.394851	-2.818108	1.953285
98	15	0	2.879471	-3.647448	-3.327182
99	8	0	4.860952	-2.512408	0.328150
100	8	0	7.328561	-1.523554	-0.066044
101	8	0	6.584169	3.274138	-1.736549
102	8	0	4.203016	5.594879	0.213096
103	8	0	2.709571	-2.172535	-2.417058
104	8	0	0.193317	-3.146956	-2.224391
105	8	0	-1.439635	-1.583441	2.334150
106	8	0	-1.622646	2.664545	2.407774
107	7	0	4.328862	3.515096	-1.760025
108	1	0	3.405717	3.150571	-1.527729
109	7	0	5.774217	6.648669	-1.061175
110	1	0	6.259819	6.592029	-1.945098
111	7	0	-0.196736	0.269315	2.752892
112	1	0	0.603359	0.863264	2.518909
113	7	0	-3.325501	1.708029	3.581833
114	1	0	-3.545518	0.977426	4.261224
115	6	0	5.762695	-4.600460	1.641232
116	6	0	6.411144	-4.969991	0.450654
117	1	0	6.625578	-4.215278	-0.306383
118	6	0	6.743845	-6.305862	0.221310
119	1	0	7.221195	-6.583107	-0.720522
120	6	0	6.459883	-7.280973	1.182300
121	1	0	6.721463	-8.325201	0.998558
122	6	0	5.833442	-6.914644	2.377071
123	1	0	5.602952	-7.671543	3.130211
124	6	0	5.480623	-5.581482	2.604605
125	1	0	4.964393	-5.306354	3.526705
126	6	0	3.773041	-2.949231	2.827097
127	6	0	2.614449	-3.485657	2.244254
128	1	0	2.632968	-3.824871	1.211220
129	6	0	1.425661	-3.545949	2.970415
130	1	0	0.521581	-3.934564	2.500123
131	6	0	1.382480	-3.078591	4.288153
132	1	0	0.445054	-3.111933	4.846237
133	6	0	2.530344	-2.543351	4.877386
134	1	0	2.496290	-2.165127	5.900648

135	6	0	3.718800	-2.467054	4.144313
136	1	0	4.610189	-2.020797	4.592849
137	6	0	5.001984	-1.247244	-0.174948
138	6	0	6.288097	-0.698972	-0.379284
139	6	0	6.418118	0.602307	-0.861153
140	1	0	7.387890	1.075928	-0.997817
141	6	0	5.271301	1.354098	-1.167231
142	6	0	4.007404	0.779952	-1.021789
143	1	0	3.100664	1.325108	-1.267417
144	6	0	3.864236	-0.515818	-0.516960
145	6	0	8.641993	-0.991568	-0.156547
146	1	0	9.313699	-1.798544	0.160819
147	1	0	8.767722	-0.120529	0.507981
148	1	0	8.885090	-0.694978	-1.190808
149	6	0	5.458337	2.780734	-1.582911
150	6	0	4.413300	4.917325	-2.101678
151	1	0	5.199315	5.036983	-2.863354
152	6	0	4.799052	5.740381	-0.862824
153	6	0	6.266925	7.648802	-0.087311
154	6	0	2.498480	-1.077085	-0.330305
155	6	0	1.966579	-1.935545	-1.301108
156	6	0	0.647647	-2.417959	-1.170769
157	6	0	-0.099244	-2.083484	-0.044377
158	1	0	-1.113544	-2.450594	0.087678
159	6	0	0.425073	-1.204954	0.917312
160	6	0	1.716357	-0.695068	0.764265
161	1	0	2.148692	-0.025328	1.504598
162	6	0	2.520227	-5.007323	-2.133665
163	6	0	3.200592	-5.152375	-0.916590
164	1	0	3.961738	-4.426887	-0.635614
165	6	0	2.910401	-6.226494	-0.073055
166	1	0	3.450171	-6.330809	0.868910
167	6	0	1.939924	-7.163195	-0.442374
168	1	0	1.717382	-8.005604	0.216552
169	6	0	1.257678	-7.026105	-1.655681
170	1	0	0.500041	-7.757434	-1.945857
171	6	0	1.545264	-5.948955	-2.497336
172	1	0	1.006361	-5.828260	-3.439859
173	6	0	4.735480	-3.667353	-3.239462
174	6	0	5.461414	-2.466489	-3.210857
175	1	0	4.933242	-1.515324	-3.157269
176	6	0	6.857907	-2.486468	-3.213850
177	1	0	7.405247	-1.542941	-3.172629
178	6	0	7.547880	-3.700267	-3.263005
179	1	0	8.639912	-3.712381	-3.262412
180	6	0	6.830951	-4.899730	-3.312842
181	1	0	7.360662	-5.854367	-3.353232
182	6	0	5.434405	-4.884258	-3.301064
183	1	0	4.886395	-5.828616	-3.314033
184	6	0	-1.054298	-3.823437	-2.090183
185	1	0	-1.206607	-4.352568	-3.036486
186	1	0	-1.879437	-3.112673	-1.947919
187	1	0	-1.015001	-4.543114	-1.256036
188	6	0	-0.461974	-0.853928	2.062358
189	6	0	-1.079622	0.768886	3.796600

190	1	0	-1.648106	-0.073919	4.204625
191	6	0	-2.048562	1.794696	3.188712
192	6	0	-4.377983	2.715991	3.294042
193	6	0	-2.727012	-3.086416	4.920466
194	1	0	-1.951507	-2.321752	4.753041
195	6	0	-0.255687	1.424920	4.931628
196	1	0	0.342820	2.226356	4.470988
197	6	0	3.065272	5.402893	-2.683676
198	1	0	2.291339	5.173541	-1.932964
199	6	0	7.382233	8.418783	-0.803099
200	1	0	7.002329	8.907183	-1.715059
201	1	0	7.788406	9.199010	-0.143610
202	1	0	8.208040	7.744970	-1.082871
203	6	0	5.122663	8.600692	0.290814
204	1	0	4.744611	9.126108	-0.599655
205	1	0	4.294072	8.045364	0.750153
206	1	0	5.480881	9.352673	1.010567
207	6	0	6.826632	6.951593	1.160746
208	1	0	6.025567	6.433346	1.701890
209	1	0	7.594151	6.214371	0.881838
210	1	0	7.280634	7.696369	1.832538
211	6	0	6.175906	3.208888	2.107677
212	1	0	6.164147	4.307783	2.125585
213	1	0	7.032599	2.864310	2.704882
214	1	0	6.327661	2.886619	1.068153
215	6	0	4.685737	3.107278	4.134488
216	1	0	4.712247	4.206343	4.195816
217	1	0	3.723205	2.753735	4.529914
218	1	0	5.490600	2.706319	4.769899
219	6	0	4.913026	1.104188	2.619897
220	1	0	4.034401	0.659890	3.101799
221	1	0	4.947717	0.765580	1.579084
222	1	0	5.817485	0.736797	3.128624
223	6	0	-6.287478	0.470464	7.363089
224	1	0	-5.504220	1.084467	6.902411
225	1	0	-7.099058	0.335380	6.632758
226	1	0	-6.685245	1.006093	8.238910
227	6	0	-6.802058	-1.712372	8.498671
228	1	0	-6.416233	-2.701271	8.794862
229	1	0	-7.144584	-1.194851	9.406151
230	1	0	-7.673538	-1.857465	7.839983
231	6	0	-4.510377	-0.697563	8.726723
232	1	0	-4.806135	-0.115578	9.613097
233	1	0	-4.123872	-1.671421	9.064627
234	1	0	-3.705081	-0.159657	8.209046
235	6	0	-5.674963	2.160123	3.890351
236	1	0	-5.571358	1.997673	4.972350
237	1	0	-6.496199	2.872663	3.725892
238	1	0	-5.950531	1.202343	3.427157
239	6	0	-4.005139	4.041130	3.977670
240	1	0	-4.779680	4.798130	3.779815
241	1	0	-3.923575	3.907539	5.067539
242	1	0	-3.046256	4.416825	3.594361
243	6	0	-4.553702	2.926187	1.783407
244	1	0	-3.652058	3.356112	1.331789

245	1	0	-4.777266	1.977639	1.283389
246	1	0	-5.396695	3.611805	1.606650
247	6	0	0.825556	4.776469	2.104372
248	1	0	0.260941	4.211089	2.862264
249	6	0	1.862962	5.656207	2.809151
250	1	0	1.355848	6.425900	3.411054
251	1	0	2.504019	5.074941	3.486964
252	1	0	2.517193	6.161240	2.080693
253	6	0	-0.169028	5.624785	1.309310
254	1	0	0.346148	6.187670	0.511944
255	1	0	-0.944220	5.000731	0.846189
256	1	0	-0.667469	6.351592	1.969730
257	6	0	3.066763	6.912998	-2.936135
258	1	0	2.111784	7.222256	-3.387298
259	1	0	3.200099	7.489978	-2.009617
260	1	0	3.871643	7.201164	-3.634336
261	6	0	2.735742	4.630026	-3.965087
262	1	0	3.514014	4.790321	-4.730227
263	1	0	2.649727	3.552228	-3.774301
264	1	0	1.778236	4.974930	-4.385601
265	6	0	-2.485104	-4.234974	3.935883
266	1	0	-3.246022	-5.023853	4.060790
267	1	0	-2.507470	-3.886384	2.895369
268	1	0	-1.497708	-4.688623	4.114722
269	6	0	-2.622334	-3.574117	6.368079
270	1	0	-2.678406	-2.747942	7.091382
271	1	0	-3.426120	-4.291087	6.608631
272	1	0	-1.662799	-4.090468	6.524029
273	6	0	0.707744	0.401250	5.533817
274	1	0	0.153958	-0.438779	5.987181
275	1	0	1.385797	-0.007935	4.774634
276	1	0	1.320332	0.867535	6.321496
277	6	0	-1.160584	2.034008	6.007205
278	1	0	-1.765200	2.864536	5.616143
279	1	0	-1.851958	1.281863	6.419366
280	1	0	-0.547834	2.429740	6.831794

7.2.14.2 NOESY spectra

Spectra obtained for **19a** (8 mM in THF-d8) show cross peaks between the ligand monomers in the hydrogen bond complex. Atoms X and X' refer to *inner* and *outer sphere* atoms of the complex.

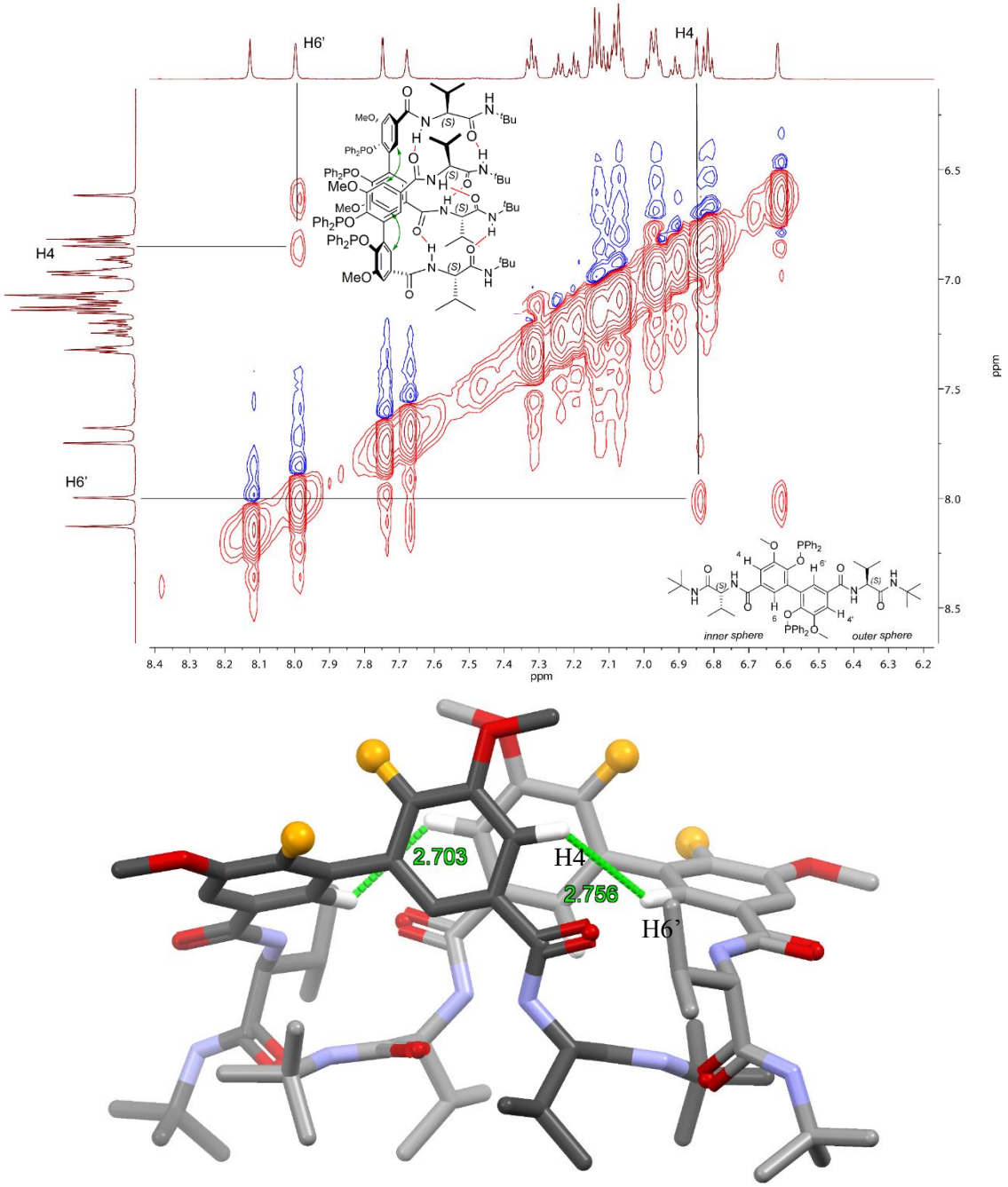

Figure 7-20**:** NOESY spectrum of **19a** with annotated cross signals depicting vicinity of protons H4 and H6' shown in the calculated structure **model-19a** below. For clarity reasons, irrelevant hydrogen atoms were omitted and $OPPh_2$ groups are represented by placeholder atoms. The two molecular subunits of the dimer are coloured in light and dark grey. Nitrogen = blue, oxygen = red, $OPPh_2$ moiety = orange.

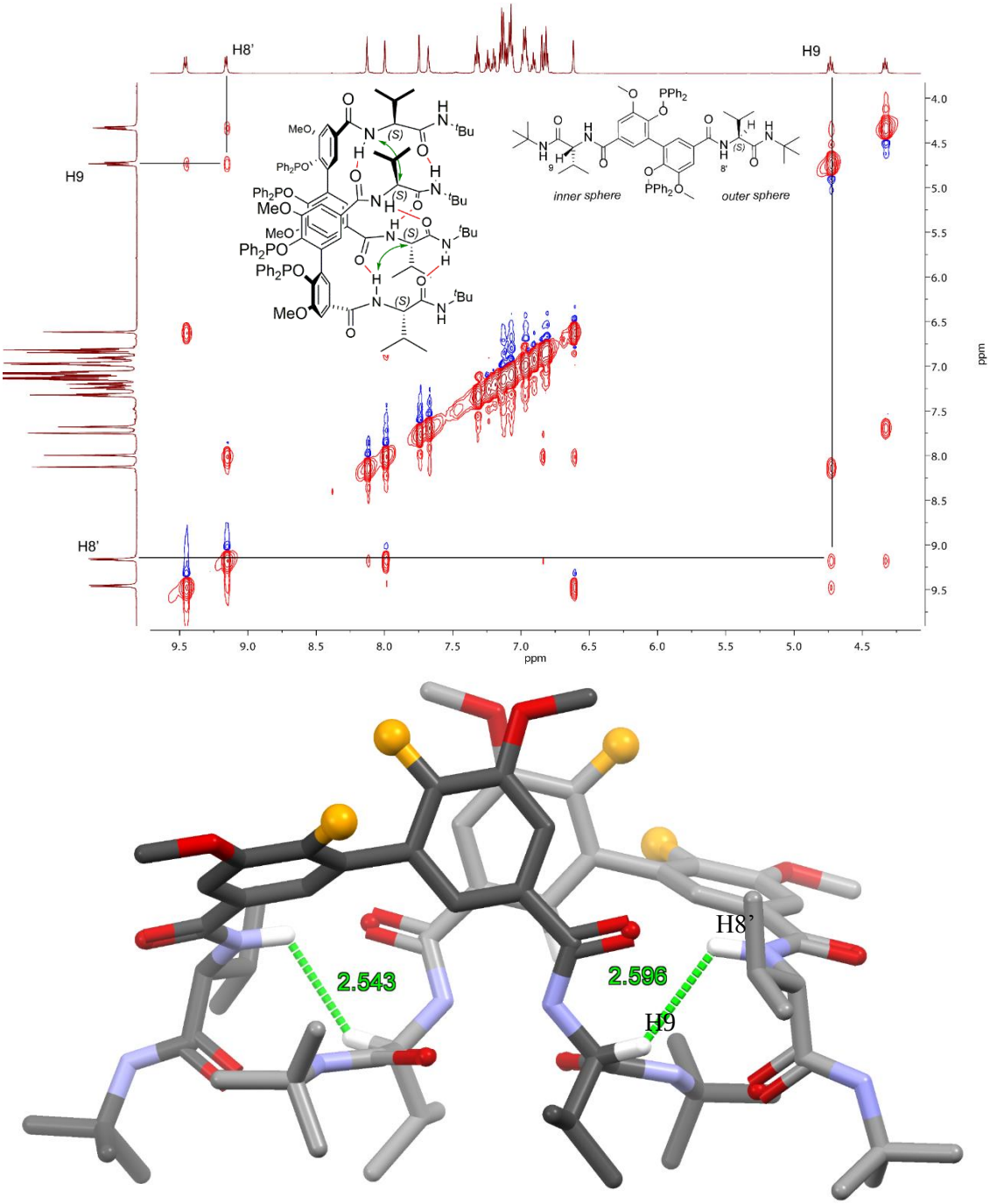

Figure 7-21**:** NOESY spectrum of **19a** with annotated cross signals depicting vicinity of *inner* and *outer sphere* selectors shown in structure **model-19a** below. For clarity reasons, irrelevant hydrogen atoms were omitted and $OPPh_2$ groups are represented by placeholder atoms. The two molecular subunits of the dimer are coloured in light and dark grey. Nitrogen = blue, oxygen = red, $OPPh_2$ moiety = orange.

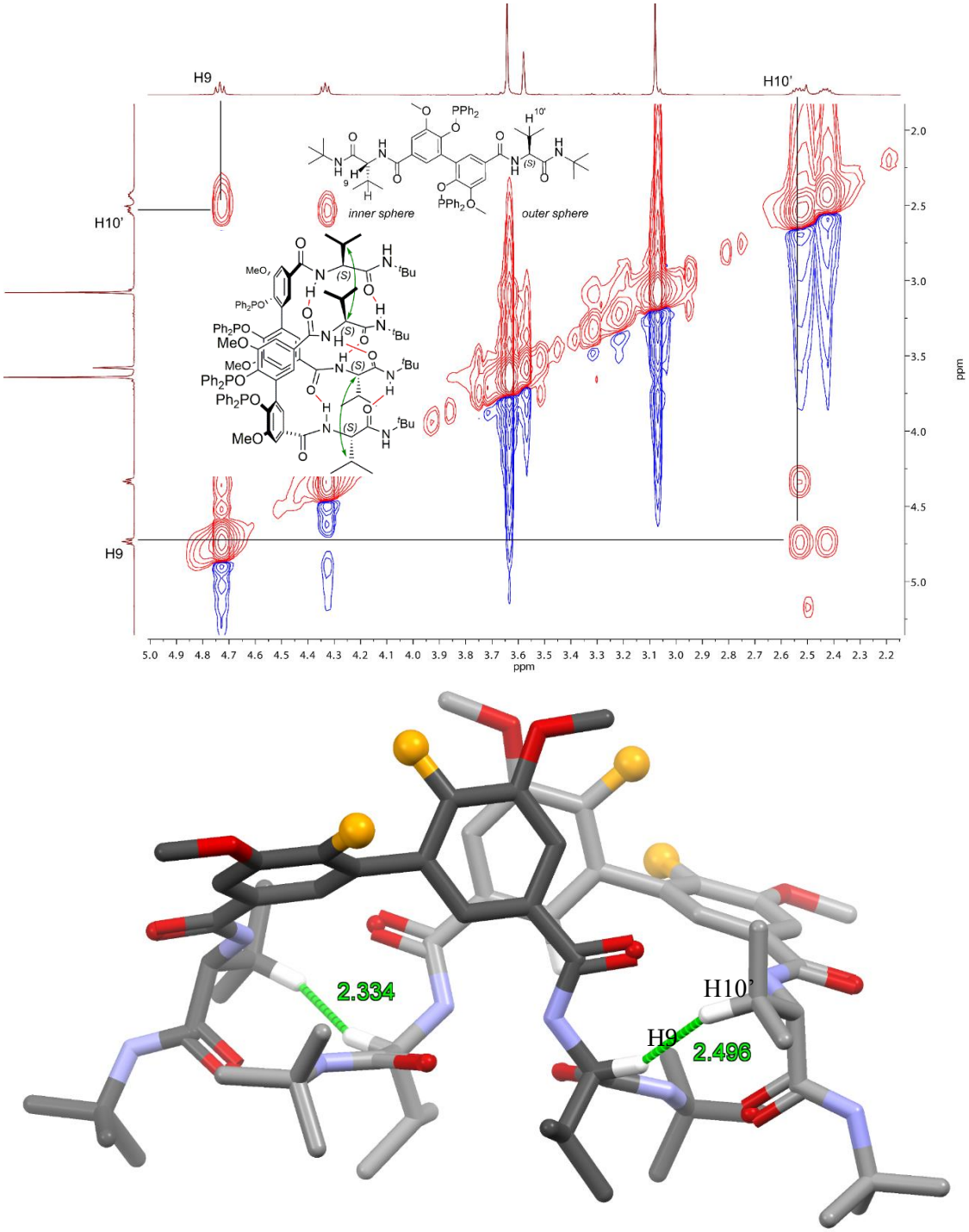

Figure 7-22**:** NOESY spectrum of **19a** with annotated cross signals depicting vicinity of *inner* and *outer sphere* selectors shown in the structure **model-19a** below. For clarity reasons, irrelevant hydrogen atoms were omitted and $OPPh_2$ groups are represented by placeholder atoms. The two molecular subunits of the dimer are coloured in light and dark grey. Nitrogen = blue, oxygen = red, $OPPh_2$ moiety = orange.

7.2.15 CD_3OD titration experiments with BIPOL 18c

Analyte solutions of compound **18c** (20 mM) were prepared in solvent mixtures of $CDCl_3$ and CD_3OD with ratios 99:1, 90:10, 50:50 and 0:100 (v:v). Both methanol and chloroform was taken from a freshly opened bottle and the latter was passed twice through a plug of dry, basic alumina to remove traces of acid. Spectra were calibrated to the terminal ^{t}Bu group at 0.94 ppm, which showed a negligible shift difference in all four spectra.

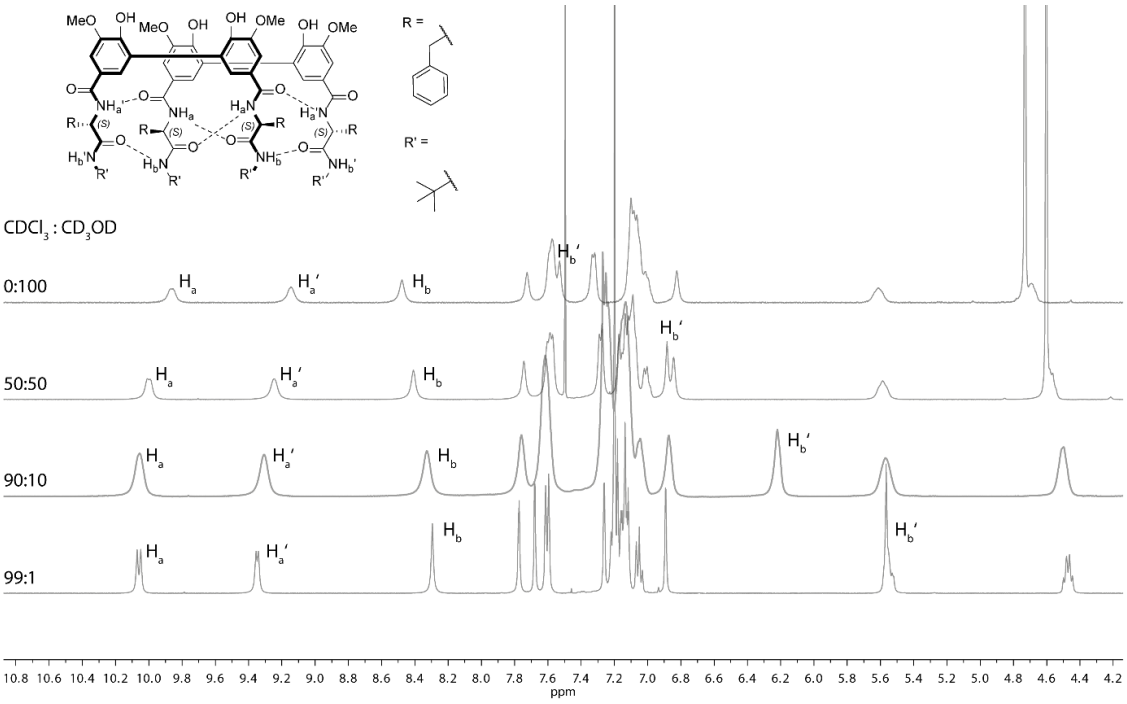

Figure 7-23: Diol **18c** in different mixtures of deuterated chloroform and methanol.

7.2.16 HD exchange kinetics of BIPOL 18c

Analyte solutions of **18c** and (*S*)-**25** with a concentration of 20 mM and 40 mM, respectively, in freshly opened methanol-d4 were prepared. With a final methanol concentration of 24.6 M, HD exchange was considered to proceed with pseudo-first-order kinetics. Spectra were collected periodically with intervals suitable for the speed of exchange. All acquired spectra were baseline and phase corrected. The decay of the signal was evaluated relatively to the non-exchanging methin proton in the chiral center, H9. Regression curves were generated using Origin 16's quick fit functionality with the exponential decay function:

$$y = y0 + A1 * exp(-(x - x0)/t1)$$

The y-intercept is taken to normalize the final data to start from 100%. For proton H_a**4**, full signal decay was observed within 30 sec when the first spectrum was measured. Half-life is thus estimated based on a signal decay to 1% within 30 sec (equal to 6.65 half-lives): $t_{1/2}$(H_a**4**) = 4.5 sec. Half-lives were read out and kinetic constants calculated according to first-order-kinetics:

$$t_{0.5} = \ln(2)\,/k_{ex}$$

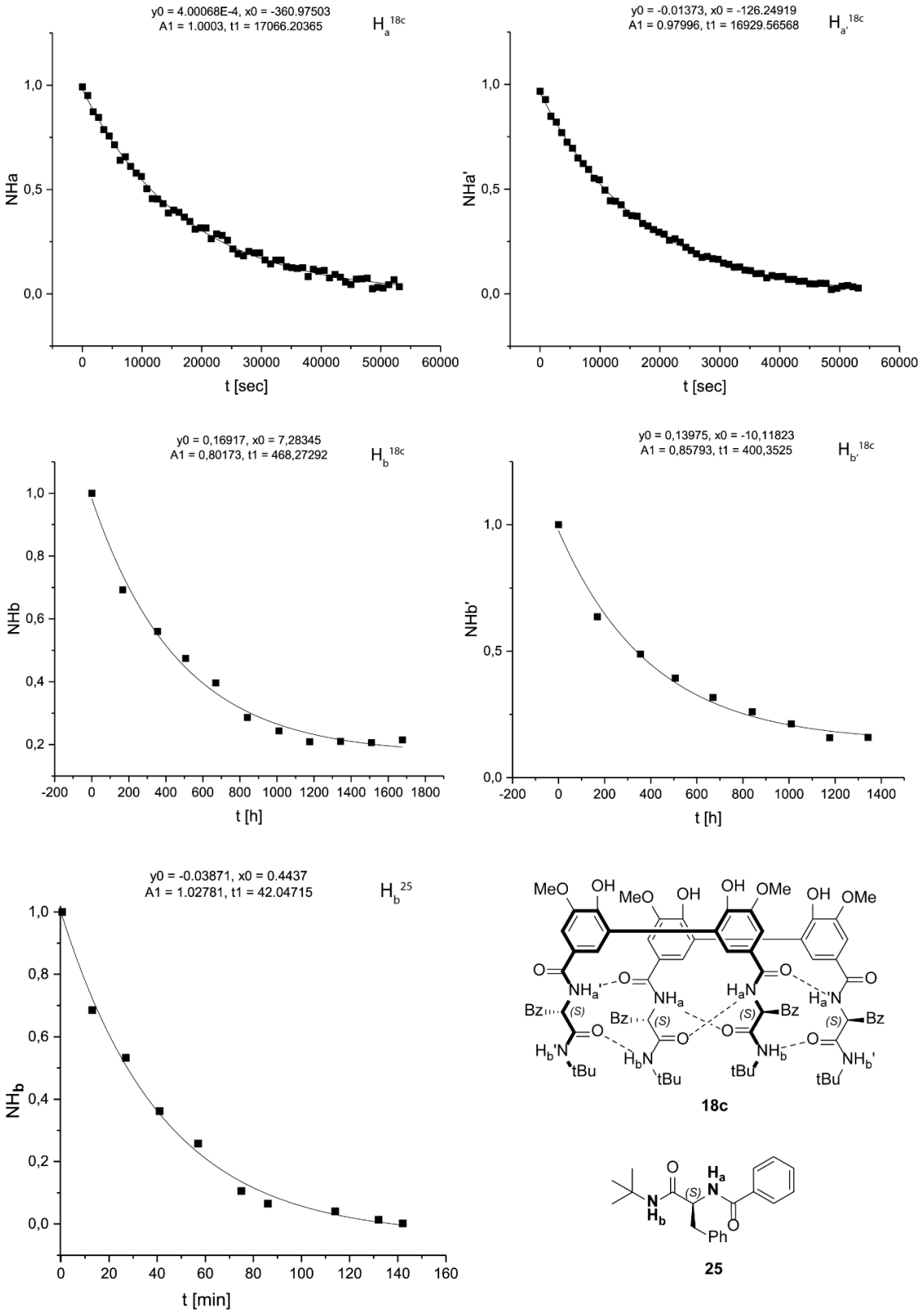

Figure 7-24: Deuterium exchange for amide protons of compounds **18c** and **25**.

Retardation factors describe slowdown of amide proton exchange compared to the model compound.

Table 7-3: Estimated half-life and exchange rates for HD exchange in methanol

	Diol **18c**				Diamide **25**	
	H_a	H_b	H_a'	H_b'	H_a	H_b
$t_{1/2}$ [10^2 min]	1.91	253.3	1.80	201.6	0.0008[a)]	0.28
k_{ex} [sec^{-1}]	$6.03 \cdot 10^{-5}$	$4.56 \cdot 10^{-7}$	$6.41 \cdot 10^{-5}$	$5.72 \cdot 10^{-7}$	$1.54 \cdot 10^{-1}$	$4.18 \cdot 10^{-4}$
Retardation Factor[b)]	2554	-	2402	-	1	-
	-	917	-	731	-	1

a) Complete exchange was observed before after 30 second. Half-life time was estimated (see above). b) Retardation Factor = $k_{ex}(H_X^{25})$ / $k_{ex}(H_X^{18c})$

7.2.17 Hydrogenation experiments

To evaluate the enantioselectivity of the ligand structure, enantiomers of precursor ligand **5** were separated using preparative HPLC and the Rh complex was generated *in situ*.
As for ligand **7**, samples of the equilibrated compound (2.00 mg, 2.04 µm) were placed in J.Young NMR tubes. Where the effect of additives was investigated, these and 0.4 ml dry and degassed $CDCl_3$ were added. The mixture was re-equilibrated at 60 °C for 16 hours and the solvent subsequently removed under reduced pressure after determination of the ligand's *dr* via $^{31}P\{^1H\}$-NMR spectroscopy. The Rh catalyst was generated *in situ* by evaporating the solution and adding equal amounts of Rh precursor $[Rh(COD)_2]BF_4$ in 0.5 ml dry and degassed $CDCl_3$ to the prepared ligand sample to give a clear yellow solution. Finally, methyl 2-acetamido acrylate (20 eq.) was added.
For ligands 1**9a-c** and **23a-b**, Rh complexes were prepared by adding equimolar amounts of $[Rh(COD)_2]BF_4$ to a solution of the ligand in dry and degassed DCM. After stirring the mixture for three hours, the solution was concentrated and addition of *n*-pentane gave yellow solids. The supernatant solution was removed using a filter-tipped cannula and precipitation was repeated another two times. Yellow solids were dried and 3.2 mM stock solutions in DCM were prepared from which 0.5 ml were taken and substrate (10 eq. for ligands 1**9a-c** and 20 eq. for ligands **23a-b**) was added.
The prepared solution was transferred into a nitrogen-filled stainless steel reactor loaded with a standard NMR tube and a small stirring bar and cooled in a bath of 2-propanol utilizing a cryostatic temperature regulator, if necessary. The reactor was pressurized with hydrogen gas (20 bar for the phosphine ligands, 95 bar for phosphinite ligands and 35 bar for the phosphoramidite ligands) to initiate the catalysis.
The autoclave was re-opened after one or two days and the solution was passed through a short pipet filled with silica (ca. 3 cm) using ethyl acetate as eluent. Evaporation gave the hydrogenation product as a yellow oil. Enantiomeric ratio was determined by chiral GC (compound **12**:

Chirasil Val-C5: 110 °C, k_{subst} = 1.53, k_R = 2.21, k_S = 2.35, α = 1.06 or (6-TBDMS-2,3-Ac)-β-CD: 130 °C, k_R = 6.84, k_S = 9.07, α = 1.33, both 25 m, i.d. 250 µm, film thickness 250 nm, prepared and coated in the Trapp group, 100 kPa helium; compound **22**: (6-TBDMS-2,3-dimethyl)-β-CD, 120 °C, k_R = 27.6, k_R = 30.3, α = 1.10, 13 m, i.d. 250 µm, film thickness 250 nm, prepared and coated in the Trapp group, 100 kPa helium) or chiral HPLC (compound **20**: Chiralpak ODH, hexane:isopropanol:methanol 97:1.5:1.5, 1.5 ml/min, 20 °C, t_R = 17.0 min and t_S = 19.9 min; compound **21**: Chiralpak IB, hexane:isopropanol 95:5, 1.0 ml/min, 20 °C, t_R = 5.4 min and t_S = 6.3 min). Assignment of absolute configuration was accomplished by comparison of the elution order to known standards or literature values. All reactions showed full conversion.

7.2.18 Enantioselective alkylation of aromatic aldehydes.

7.2.18.1 Investigation of the Ti complex

BIPOL **18c** (10 mg, 13.5 µmol, 1.00 eq.) was dissolved in 0.5 ml dry and degassed DCM-d2 (^{1}H NMR spectrum 1). Addition of Ti(O^{i}Pr)$_4$ (4.1 µl, 13.5 µmol, 1.00 eq.) gave a yellow precipitate (spectrum 2). When another charge of Ti(O^{i}Pr)$_4$ (24.6 µl, 81.0 µmol, 6.00 eq.) was added, solids re-dissolved and a clear, yellow solution formed (spectrum 3) Finally, Zn(Et)$_2$ (135 µl, 1 M in hexane, 135 µmol, 10.0 eq.) was added (spectrum 4).

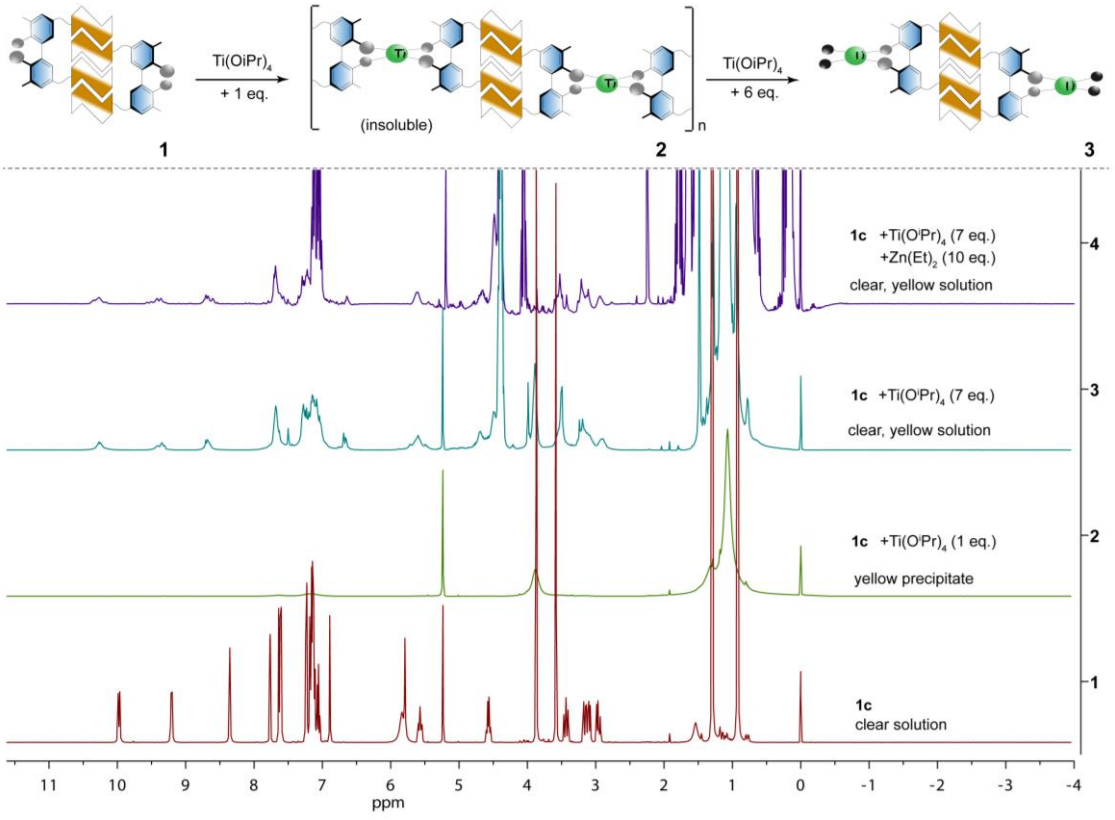

Figure 7-25: Investigation of the interplay of BIPOL ligand **18c**, titanium precursor Ti(O^{i}Pr)$_4$ and Zn(Et)$_2$. Structures on top are suggestions. To improve clarity, a different representation is chosen for ligand dimer **18c**.

7.2.18.2 Reaction setup

In a typical procedure, a heat-gun dried Schlenk flask equipped with a magnetic stirring bar was charged with ligand (25 µmol) and titanium tetraisopropoxide (175 µmol). Dry and degassed solvent (1 ml) was added and the mixture was stirred for 10 min. Diethylzinc (375 µmol from a

1M solution in toluene) was added and stirring was continued for another 10 min. The temperature of the mixture was subsequently adjusted, the substrate (125 µmol) was added and stirring was continued for 16 hours. The reaction was stopped by addition of saturated ammonium chloride solution (3 ml) and the product was extracted with ethyl acetate (2 x 3 ml).
Combined organic layers were dried over sodium sulfate and conversion and enantioselectivity were determined by chiral GC (Chirasil-β-Dex, 25 m, i.d. 250 µm, film thickness 250 nm, prepared and coated in the Trapp group, Reactions with benzaldehyde: 100 °C, 80 kPa He, k_{subst} = 2.78, k_R = 25.8, k_S = 28.7, α = 1.11)) or HPLC (Chiralcel OD-H). Retention times and absolute configuration were assigned by comparison with GC traces in literature, of known compounds or by identification with GC-MS.

7.3 Experimental data for chapter 3

7.3.1 MOM-protected 2,2'-biphenol (27i)

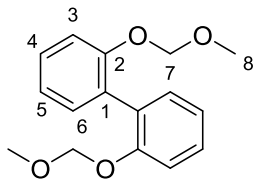

This compound was synthesized according to a known procedure.[159] 2,2'-biphenol (5.00 g, 26.9 mmol, 1.00 equiv.) was dissolved in dry THF (40 ml). The solution was added to a stirred suspension of sodium hydride (1.42 g, 59.1 mmol, 2.20 eq.) in THF (90 ml) at 5 °C over 30 minutes. The resulting mixture was kept stirring at low temperatures for one hour, warmed to room temperature for 15 minutes and cooled again in an ice bath. Chloromethyl methyl ether (4.28 ml, 56.4 mmol, 2.10 eq.) was added dropwise. The mixture turned yellow and solids formed. After warming to room temperature, the suspension was kept stirring overnight. For work-up, the mixture was quenched with saturated ammonium chloride (100 ml) and all volatiles were removed under reduced pressure. The residue was extracted with DCM (3 x 100 ml), combined organic layers were washed with brine (1 x 100 ml), dried over sodium sulfate, filtered and evaporated to give the crude product as a yellow oil. Purification by column chromatography (silica, petrol ether:ethyl acetate 20:1 to 10:1, R_f = 0.38 in petrol ether:ethyl acetate 10:1) gave a colourless oil that transformed into a waxy solid after prolonged drying under high vacuum (4.50 g, 16.4 mmol, 61%).

^{1}H-NMR ($CDCl_3$, 400.33 MHz, 298 K): δ = 3.34 (s, 3H, H8), 5.07 (s, 2H, H7), 7.06-7.10 (m, 1H, H4/H5), 7.21-7.34 (m, 3H, H3 and H4/H5 and H6) ppm.
^{13}C{^{1}H}-NMR ($CDCl_3$, 100.66 MHz, 289 K): δ = 56.0 (C8), 95.4 (C7), 115.8 (C3/C4/C5), 122.0 (C4/C5), 128.8 (C3/C4/C5/C6), 129.4 (C1), 131.7 (C3/C4/C5/C6), 155.1 (C2) ppm.
HRMS (ESI): m/z calcd. for $C_{16}H_{22}NO_4$ $[M+NH_4]^+$: 292.15433; found: 292.15456.
FTIR: $\tilde{\nu}$ = 750 (s), 920 (s), 984 (s), 1079 (s), 1149 (s), 1475 (s), 1593 (s), 2788 (w), 2823 (m), 2903 (m), 2950 (m), 2973 (w), 2994 (w) cm^{-1}.

7.3.2 3,3'-Dimethyl-2,2'-biphenol (28)

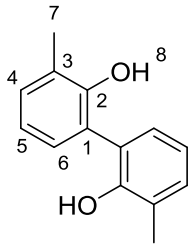

This compound was synthesized according to a known procedure.[159] Methoxy methyl-protected biphenol **27i** (5.00 g, 18.2 mmol, 1.00 eq.) was dissolved in dry THF (130 ml). Butyl lithium (1.6 M in hexane, 34.2 ml, 54.7 mmol, 3.00 eq.) was slowly added at room temperature and the resulting brown suspension warmed up slightly. Stirring was continued for one hour and the flask was subsequently placed in a water bath. Iodomethane (3.40 ml, 54.7 mmol, 3.00 eq.) was added and a clear, yellow solution formed, which was stirred for another hour. The mixture was subsequently quenched wit saturated Na_2SO_3 solution (130 ml) and ethyl acetate (180 ml) was added. Layers were separated and the aqueous layer was extracted twice more with ethyl acetate (150 ml each). Combined organic layers were dried over sodium sulfate, filtered and evaporated to give a yellow oil. Hydrochloric acid in isopropanol (5-6 M, 30 ml) was added and the solution instantly turned black. After 18 hours of stirring, the mixture was concentrated and the residue diluted with DCM (150 ml). The organic layer was washed sodium bicarbonate solution and brine. Evaporation gave a brown oil. Further purification by column chromatography (silica, petrol ether:ethyl acetate 20:1 to 10:1, R_f = 0.5 in petrol ether:ethyl acetate 10:1) gave an off-white, crystalline solid that was washed with little *n*-pentane and finally dried *in vacuo* (1.5 g, 7.00 mmol, 38%).

^{1}H-NMR ($CDCl_3$, 400.33 MHz, 298 K): δ = 2.33 (s, 3H, H7), 5.20 (s, 1H, H8), 6.92-6.96 (m, 1H, H5), 7.07-7.09 (m, 1H, H4/H6), 7.20-7.22 (m, 1H, H4/H6) ppm.
^{13}C{^{1}H}-NMR ($CDCl_3$, 100.66 MHz, 289 K): δ = 16.3 (C7), 121.4 (C5), 122.3 (C1), 125.7 (C3), 128.5 (C4/C6), 131.6 (C4/C6), 151.7 (C2) ppm.
HRMS (EI): m/z calcd. for $C_{14}H_{14}O_2$ $[M]^+$: 214.09938; found: 214.0989.
FTIR: $\tilde{\nu}$ = 758 (s), 839 (m), 1087 (s), 1198 (s), 1239 (s), 1322 (s), 1450 (s), 1587 (w), 2520 (w), 2579 (bw), 2921 (w), 2952 (bs), 3022(w) cm^{-1}.

7.3.3 3,3'-Dimethyl-5,5'-dinitro-2,2'-biphenol (29)

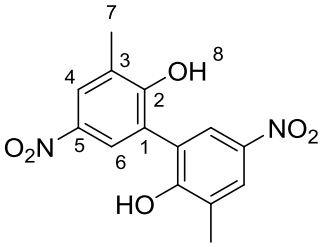

This compound was synthesized according to a known procedure, which was slightly modified.[160] Biphenol **28** (400 mg, 1.87 mmol, 1.00 eq.) and sodium nitrate (476 mg, 5.60 mmol, 3.00 eq.) were placed in a flask and dissolved in water:diethyl ether (50ml, 1:1 v:v). Concentrated hydrochloric acid (6.8 ml) was added and the mixture was stirred vigorously. After 16

hours, the etheric layer had turned slightly yellow while the aqueous layer remained clear. Another charge of hydrochloric acid (4 ml) was added in portions (0.8 ml each) over 10 hours, the mixture was kept stirring overnight and brown solid precipitated. The etheric layer was subsequently evaporated and the solids were filtered off. They were suspended in acetonitrile (5 ml) and the mixture was stirred for one hour. After placing the flask in the fridge for several hours to reduce loss of product, the product was filtered off, rinsed with small amounts of fresh acetonitrile and dried *in vacuo* to yield the pure product as a brown powder (365 mg, 1.20 mmol, 64%).

^{1}H-NMR (DMSO-d6, 300.18 MHz, 298 K): δ = 2.31 (s, 3H, H7), 7.91 (d, 1H, ^{4}J(H,H) = 2.6 Hz, H6), 8.10 (d, 1H, ^{4}J(H,H) = 2.6 Hz, H4), ppm.
^{13}C{^{1}H}-NMR (DMSO-d6, 75.49 MHz, 289 K): δ = 16.8 (C7), 124.3 (C1), 125.2 (C6), 125.9 (C4), 126.6 (C3), 139.2 (C5), 160.0 (C2) ppm.
HRMS (ESI): m/z calcd. for $C_{14}H_{11}N_2O_6$ [M-H]$^-$: 303.06226; found 303.06214.
FTIR: $\tilde{\nu}$ = 651 (s), 746 (s), 904 (s), 1097 (s), 1189 (s), 1231 (s), 1322 (s), 1422 (s), 1502 (s), 1583 (m), 2922 (w), 3084 (w), 3106 (w), 3446 (bs) cm^{-1}.

7.3.4 5,5'-DClB-selector modified 3,3'-dimethyl-2,2'-biphenol (30)

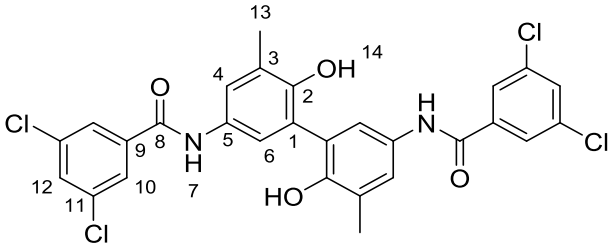

This compound was synthesized according to a known procedure, which was slightly modified.[41] Substrate **29** (970 mg, 3.19 mmol, 1.00 eq.) and tin(II) chloride (6.04 g, 31.9 mmol, 10.0 eq.) were placed in a Schlenk flask. Ethanol (24 ml) and hydrochloric acid (5-6 M in isopropanol, 12 ml, 15.0 eq.) were added and the mixture was refluxed for seven hours. To the clear, yellow solution, DCM (30 ml) was added. It was cooled in an ice bath and subsequently treated first with triethylamine (7.11 ml, 51.0 mmol, 16.0 eq.) and then with dichlorobenzoyl chloride (2.67 g, 12.75 mmol, 4.00 eq.) The ice bath was removed after 45 minutes and stirring was continued at room temperature for another five hours, then *N*,*N*-dimethylethylenediamine was added (13.9 ml, 128 mmol, 40.0 eq.) and the mixture was kept stirring for yet another 16 hours. For work-up, the clear solution was diluted with ethyl acetate (400 ml) and cautiously acidified with hydrochloric acid (3 M, 150 ml). Layers were separated and the organic layer was washed twice more with hydrochloric acid (3 M, 150 ml each), then with saturated sodium bicarbonate solution (2 x 150 ml) and finally with brine (1 x 150 ml). Any solids that formed during the washing process were discarded. The organic layer was finally dried over sodium sulfate and evaporated to give orange, waxy solids. Further purification by column chromatography (silica, DCM to ethyl acetate, R_f = 0.8 in ethyl acetate) gave yellow solids that were washed with little acetone and finally dried *in vacuo* at 60 °C to give the pure product **30** as an off-white solid (1.56 g, 2.64 mmol, 83%).

^{1}H-NMR (DMSO-d6, 400.33 MHz, 298 K): δ = 2.26 (s, 3H, H13), 7.47 (d, 1H, ^{4}J(H,H) = 2.4 Hz, H6), 7.53 (d, 1H, ^{4}J(H,H) = 2.4 Hz, H4), 7.84 (t, 1H, ^{4}J(H,H) = 1.9 Hz, H12), 7.97 (d, 2H, ^{4}J(H,H) = 1.9 Hz, H10), 10.23 (s, 1H, H7) ppm.
^{13}C{^{1}H}-NMR (DMSO-d6, 100.66 MHz, 289 K): δ = 117.1 (C13), 121.5 (C6), 122.5 (C4), 125.6 (C3), 126.4 (C10), 126.7 (C1), 130.6 (C5), 130.8 (C13), 134.4 (C11), 138.3 (C9), 149.1 (C2), 162.1 (C9) ppm.
HRMS (ESI): m/z calcd. for $C_{28}H_{19}Cl_4N_2O_4$ [M-H]$^-$: 587.01044; found: 587.01059.
FTIR: $\tilde{\nu}$ = 803 (s), 864 (s), 1022 (m), 1108 (m), 1211 (bm), 1415 (m), 1477 (s), 1564 (s), 1647 (s), 2918 (w), 2962 (w), 3078 (w), 3156 (bm), 3525 (bm) cm^{-1}.

7.3.5 3,5-Dichlorobenzoyl-selector modified 3,3'-dimethyl-2,2'-bisphosphinite (31)

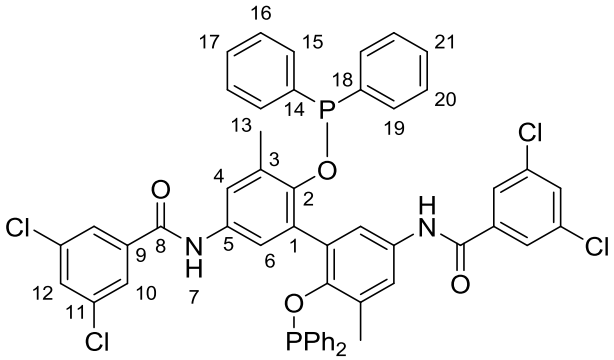

Selector-modified biphenol **30** (300 mg, 0.51 mmol, 1.00 eq.) and DABCO (228 mg, 2.03 mmol, 4.00 eq.) were placed in a heat-gun dried Schlenk flask and dry, degassed and stabilized THF (10 ml) was added to give a clear, yellow solution. After cooling in an ice bath, chlorodiphenylphosphine (0.35 ml, 2.03 mmol, 4.00 eq.) was added dropwise, during which the solution became colorless and white solids precipitated. Stirring was continued for 30 minutes at low temperatures and the for another two hours at room temperature. For work-up, the mixture was passed through a short pad of neutral alumina under inert conditions using THF as eluent (3 x 10 ml). Evaporation gave amorphous solids that were re-precipitated three times from dry and degassed DCM/*n*-pentane (1:10 ml). Final drying gave the compound as a white solid (256 mg, 0.37 mmol, 73%). The product decomposes in presence of air or moisture and should be stored in the freezer under an atmosphere of argon.

^{1}H-NMR (THF-d8, 400.33 MHz, 298 K): δ = 1.81 (s, 3H, H13), 7.15-7.19 (m, 3H, H21 and H19), 7.24-7.28 (m, 3H, H15 and H17), 7.29 (d, 1H, ^{4}J(H,H) = 2.7 Hz, H6), 7.36 (d, 1H, ^{4}J(H,H) = 2.7 Hz, H4), 7.36-7.40 (m, 2H, H20), 7.48-7.51 (m, 2H, H16), 7.66 (t, 1H, ^{4}J(H,H) = 1.9 Hz, H12), 7.88 (d, 2H, ^{4}J(H,H) = 1.9 Hz, H10), 9.25 (s, 1H, H7) ppm.
^{13}C{^{1}H, ^{31}P}-NMR (THF-d8, 150.93 MHz, 289 K): δ = 18.7 (C13), 122.1 (C6), 123.0 (C4), 127.1 (C10), 128.5 (C19), 128.8 (C15), 129.7 (C21), 130.0 (C17), 131.0 (C20), 131.2 (C3), 131.3 (C16), 131.6 (C12), 132.8 (C1), 134.9 (C5), 135.9 (C11), 140.0 (C9), 143.2 (C18), 144.0 (C14), 151.3 (C2), 162.7 (C7) ppm.
^{31}P{^{1}H}-NMR (THF-d8, 243.00 MHz, 289 K): δ = 114.0 (s) ppm.
MS (MALDI): Anthracene matrix, m/z calcd. for $C_{52}H_{37}Cl_4N_2O_4P_2$ [M-H]$^-$: 955.1; found: 955.1.
FTIR: $\tilde{\nu}$ = 690 (s), 856 (s)m 1097 (s), 1201 (s), 1266 (s), 1434 (s), 1541 (s), 1644 (s), 2919 (w), 2964 (w), 3016 (w), 3053 (w), 3068 (w), 3348 (bm) cm^{-1}.

7.3.6 Rh complex of 3,5-dichlorobenzoyl selector-modified 3,3'-dimethyl-2,2'-bisphosphinite (32)

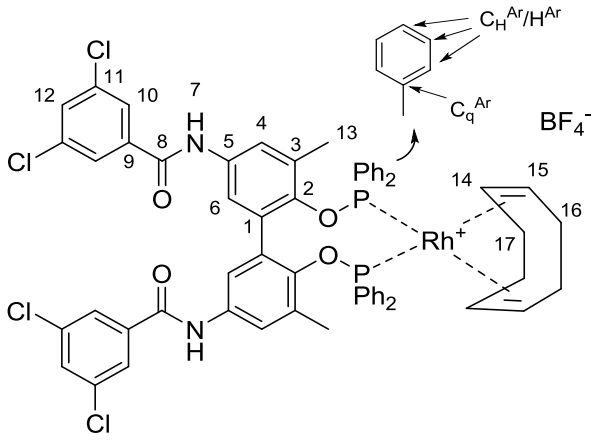

The ligand **31** (100 mg, 104 µmol, 1.00 eq.) and $[Rh(COD)_2]BF_4$ (42.3 mg, 104 µmol, 1.00 eq.) were placed in a heat-gun dried Schlenk flask and dry and degassed DCM (8 ml) were added. The orange solution was stirred for 3 hours and subsequently concentrated. Addition of dry and degassed *n*-pentane (10 ml) produced yellow solids. The supernatant solution was removed using a filter-tipped cannula and re-precipitation was repeated twice. The solids were finally dried *in vacuo* to yield the complex as a yellow powder (93.0 mg, 74.0 µmol, 71%). The product decomposes in presence of air or moisture and should be stored in the freezer under an atmosphere of argon.

^{1}H-NMR ($CDCl_3$, 600.25 MHz, 298 K): δ = 1.97 (s, 3H, H13), 2.30-2.50 (m, 4H, H16 and H17), 4.58-4.59 (m, 1H, H15), 5.41-5.42 (m, 1H, H14), 6.71 (d, 1H, ^{4}J(H,H) = 0.9 Hz, H6), 7.28-7.45 (m, 10H, H^{Ar}), 7.46-7.48 (t, 1H, ^{4}J(H,H) = 1.5 Hz, H12), 7.89 (d, 1H, ^{4}J(H,H) = 0.9 Hz, H4), 7.92 (d, 1H, ^{4}J(H,H) = 1.5 Hz, H10), 8.79 (s, 1H, H7) ppm.
^{13}C{^{1}H, ^{31}P}-NMR ($CDCl_3$, 150.93 MHz, 289 K): δ = 14.4 (C13), 30.2 (C16/C17), 30.3 (C16/C17), 101.5 (C14), 106.7 (C15), 123.7 (C6), 124.3 (C4), 126.4 (C10), 129.0 (C_H^{Ar}), 129.0 (C_H^{Ar}), 129.4 (C_H^{Ar}), 130.0 (C_H^{Ar}), 130.1 (C3), 130.6 (C_H^{Ar}), 131.3 (C1/C5/C9), 131.4 (C1/C5/C9), 131.9 (C_H^{Ar}), 132.0 (C12), 135.5 (C1/C5/C9), 135.9 (C11), 137.4 (C_q^{Ar}), 137.9 (C_q^{Ar}), 146.2 (C2), 163.3 (C8) ppm.
^{31}P{^{1}H}-NMR ($CDCl_3$, 243.00 MHz, 289 K): δ = 122.9 (d, ^{1}J(P,Rh) = 178 Hz) ppm.
HRMS (ESI): m/z calcd. for $C_{60}H_{50}Cl_4N_2O_4P_2Rh$ $[M\text{-}BF_4]^+$: 1167.10495; found: 1167.1057.
FTIR: $\tilde{\nu}$ = 692 (s), 867 (s), 1094 (s), 1200 (s), 1405 (m), 1435 (s), 1541 (s), 1564 (m), 1670 (m), 2836 (w), 2881 (w), 2925 (w), 3076 (w), 3333 (bm) cm^{-1}.

7.3.7 3,5-dichlorobenzoyl selector-modified 3,3'-dimethylphosphoramidite (33)

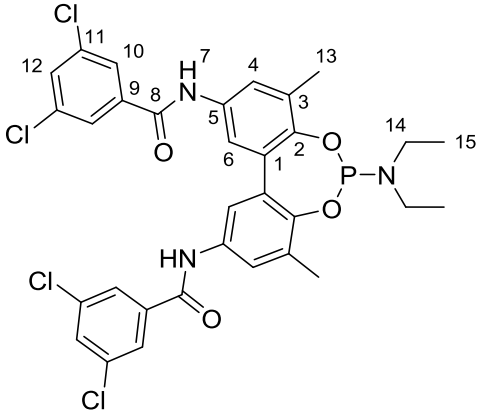

Selector-modified biphenol **30** (400 mg, 678 µmol, 1.00 eq.) was suspended in dry and degassed toluene (5 ml). Tris(diethylamino)phosphine (370 µl, 1.36 mmol, 2.00 eq.) was added and the mixture was refluxed for three hours. All volatiles were subsequently removed and the residue was slurried in dry and degassed DCM (4 ml). After addition of dry and degassed *n*-pentane (15 ml), stirring was continued to complete precipitation and the supernatant solution was subsequently removed using a filter-tipped cannula. Re-precipitation was repeated one more time and obtained solids were dried *in vacuo* yielding product **33** as a white powder (427 mg, 618 µmol, 91%). The product decomposes in presence of air or moisture and should be stored in the freezer under an atmosphere of argon.

For some atoms an additional signal splitting was observed. This is caused by the non-equivalence of the two halves in the BIPOL-phosphoramidite, which has been previously observed for other chiral phosphoramidites.[233,234] Those signals are marked X and X'.

^{1}H-NMR (THF-d8, 400.22 MHz, 298 K): δ = 1.09 (t, 3H, ^{3}J(H,H) = 7.0 Hz, H15), 2.36 (s, 3H, H13), 3.13 (dq, 2H, ^{3}J(H,P) = 7.0 Hz, ^{3}J(H,H) = 9.6 Hz, H14), 7.66 (t, 1H, ^{4}J(H,H) = 1.9 Hz, H12), 7.68 (d, 1H, ^{4}J(H,H) = 2.6 Hz, H4), 7.80 (d, 1H, ^{4}J(H,H) = 2.6 Hz, H6), 7.93 (d, 1H, ^{4}J(H,H) = 2.6 Hz, H10) ppm.

^{13}C{^{1}H}-NMR (THF-d8, 100.65 MHz, 289 K): δ = 15.4 (C15), 15.4 (C15'), 17.1 (C13), 39.3 (C14), 39.5 (C14'), 119.8 (C6), 122.9 (C4), 127.1 (C10), 131.2 (C3), 131.7 (C12), 132.0 (C1), 132.1 (C1'), 135.9 (C11), 139.8 (C9), 147.2 (C2), 147.3 (C2'), 163.2 (C8) ppm. No signal for C5 was observed.

^{31}P{^{1}H}-NMR (THF-d8, 162.00 MHz, 289 K): δ = 146.5 (quint, ^{3}J(P,H) = 10.3 Hz) ppm.

HRMS (ESI), m/z calcd. for $C_{32}H_{32}Cl_4N_4O_4P$ $[M+NH_4]^+$: 707.09098; found: 707.09230.

FTIR: $\tilde{\nu}$ = 668 (s), 752 (s), 833 (s), 851 (s), 1023 (s), 1203 (s), 1417 (s), 1507 (s), 1567 (s), 1652 (s); 2869 (w), 2933 (w), 2971 (m), 3068 (m), 3347 (m), 3396 (m) cm^{-1}.

7.3.8 *rac*-^{t}BuNH-Phe-NH diol (*meso*-18c)

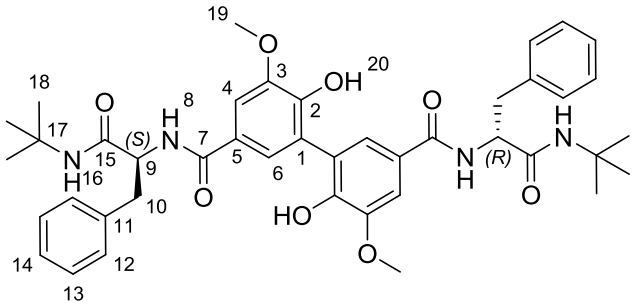

Compound **16** (1.00 g, 2.99 mmol, 1.00 equiv.) and HOBt (1.01 g, 7.48 mmol, 2.50 equiv.) were placed in a heat-gun dried round-bottom flask and dissolved in dry DMF (35 ml) giving a clear solution. DIPEA (1.30 ml, 7.48 mmol, 2.50 equiv.) was added and the resulting slightly yellow solution was cooled in an ice bath. EDCI·HCl (1.43 g, 7.48 mmol, 2.50 equiv.) was added. After 15 min, an equimolar mixture of selector hydrochlorides (*R*)-**S2c** and (*S*)- **S2c** (1.92 g, 7.48 mmol, 2.50 equiv. in total) was added. The reaction mixture was stirred at 0 °C for 30 min, afterwards overnight at room temperature. Subsequently, N,N-dimethylethylenediamine (13.2 g, 16.3 ml, 0.15 mmol, 50.0 equiv.) was added slowly and the mixture was stirred at room temperature for another 6.5 hours. For work-up, the reaction mixture was diluted with ethyl acetate (250 ml) and washed with HCl solution (2M, 3 x 250 ml), sat. $NaHCO_3$ solution (3 x 50 ml) and brine (3 x 50 ml), during which some precipitate formed. The solids were filtered off and the organic phase was dried over Na_2SO_4, filtered again and concentrated under reduced pressure. The resulting crude product (separated solids and residue from organic phase) was purified by flash column chromatography (silica, DCM:acetone:ethyl acetate = 3:1:1 to pure acetone, R_f = 0.34 DCM:acetone:ethyl acetate 2:1:1) to separate the diastereomers. Relevant fractions were combined and evaporated. Prolonged drying under high vacuum gave an off-white solid (716 mg, 0.97 mmol, 65%).

Due to molecular dynamic, the two sides of the molecule are represented by one single set of NMR signals.

^{1}H-NMR (DMSO-d6, 400.22 MHz, 298 K): δ = 1.23 (s, 9H, H18), 2.89-3.08 (m, 2H, H10), 3.84 (s, 3H, H19), 4.67 (dt, 1H, ^{3}J(H,H) = 8.9 Hz, ^{3}J(H,H) = 5.5 Hz, H9), 7.11-7.15 (m, 1H, H14), 7.21-7.25 (m, 2H, H13), 7.31-7.34 (m, 2H, H12), 7.35-7.38 (m, 2H, H4 and H6), 7.57 (m, 1H, H16), 8.19 (d, 1H, ^{3}J(H,H) = 8.4 Hz, H8) ppm.
^{13}C{^{1}H}-NMR (DMSO-d6, 100.65 MHz, 289 K): δ = 28.5 (C18), 37.9 (C10), 50.2 (C17), 55.0 (C9), 56.0 (C19), 109.7 (C4), 123.1 (C6), 125.6 (C5), 126.2 (C14), 128.0 (C13), 129.4 (C12), 138.4 (C11), 147.7 (C3), 149.0 (C2), 166.0 (C7), 171.0 (C15) ppm.
HRMS (ESI): m/z calcd. for $C_{42}H_{51}N_4O_8$ $[M-H]^+$: 739.37014; found: 739.35975.
FTIR: $\tilde{\nu}$ = 3368 (w), 3298 (s), 3083 (w), 3065 (w), 3030 (w), 2933 (w), 2870 (w), 1661 (w), 1639 (s), 1596 (m), 1541 (s), 1486 (s), 1453 (s), 1414 (m), 1392 (w), 1320 (w), 1365 (s), 1303 (m), 1287 (w), 1263 (w), 1246 (w), 1216 (s), 1192 (w), 1152 (m), 1130 (m), 1085 (w), 1067 (m), 1044 (s), 1003 (w), 986 (w), 955 (w), 940 (w), 922 (m), 909 (w), 886 (m), 846 (w), 800 (m), 758(w), 742(m), 698(s) cm^{-1}.

7.3.9 *rac*-^{t}BuNH-Phe-NH bisphosphinite (*meso*-19c)

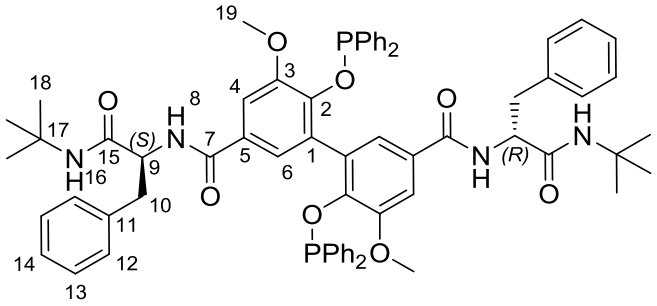

Compound *meso*-**18c** (300 mg, 0.41 mmol, 1.00 equiv.) was dissolved in dry and degassed THF (4 ml, stabilized with 250 ppm BHT) to give a yellow suspension and NEt_3 (185 mg, 0.26 ml, 18.3 µmol, 4.50 equiv.) was added. The reaction mixture was cooled to 0 °C, PPh_2Cl (296 mg, 0.23 ml, 13.4 µmol, 3.30 equiv.) was added dropwise and the resulting solution was stirred at 0 °C for 15 min, afterwards at room temperature for two hours. Precipitated NEt_3·HCl was subsequently filtered off using a filter-tipped cannula. The solvent was removed in high vacuum, the resulting residue was dissolved in dry and degassed DCM (2 ml) and the product precipitated by addition of dry and degassed *n*-pentane (20 ml). After removing the solution via filter-tipped cannula, the precipitation was repeated two times. The resulting solid was dried in high vacuum giving a white powder (302 mg, 0.27 mmol, 67%).

Due to residual molecular dynamic, significant line broadening was observed in ^{1}H and ^{13}C spectra rendering them uninterpretable even at lower temperatures.

^{31}P-NMR (THF-d_8, 161.98 MHz, 295.0 K) δ = 120.6 (bs) ppm.

HR-MS (ESI): m/z calcd. For $C_{66}H_{69}N_4O_8P_2$ $[M+H]^+$: 1107.45851; found: 1107.45756.

IR (FT-ATR, cm^{-1}) ν = 3406 (m), 3298 (s), 3058 (m), 3028 (w), 3002 (w), 2967 (m), 2930 (w), 2865 (w), 1660 (m), 1628 (vs), 1081 (s), 1542 (s), 1507 (w), 1498 (w), 1471 (w), 1459 (w), 1436 (w), 1418 (w), 1392 (m), 1359 (m), 1312 (m), 1279 (w), 1129 (m), 1091 (s), 1046 (m), 1029 (w), 999 (w), 957 (w), 937 (w), 911 (w), 860 (vs), 827 (w), 809 (m), 782 (w), 776 (w), 762 (w), 749 (m), 736 (s), 692 (vs), 664 (w) cm^{-1}.

7.3.10 Rh-complex of *rac*-^{t}BuNH-Phe-NH bisphosphinite (Rh-*meso*-19c)

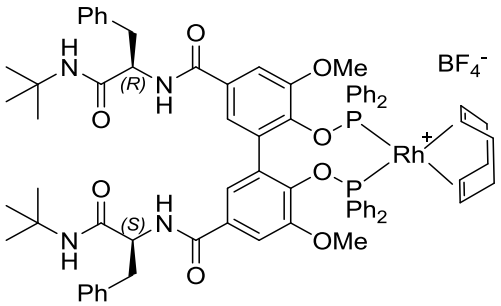

Compound *meso*-**19c** (150.0 mg, 135.5 mmol, 1.00 equiv.) and $[Rh(COD)_2]BF_4$ (55.0 mg, 136 mmol, 1.00 equiv.) were dissolved in DCM (1.5 ml, dry and degassed) and stirred overnight at room temperature. The solvent was removed in high vacuum and the residue was dissolved in DCM (2 ml, dry and degassed) and the complex precipitated with pentane (15 ml, dry and degassed). The solvent was removed *via* filter-tipped cannula and the procedure was repeated

three times. The obtained yellow powder was dried for 2 days and gave the catalyst complex in quantitative yield.

^{31}P-NMR ($CDCl_3$, 162 MHz, $CDCl_3$, 293 K) δ = 126.8 (d, ^{1}J(P,Rh) = 187.4 Hz), 127.9 (d, ^{1}J(P,Rh) = 187.4 Hz) ppm. ($CDCl_3$, 162 MHz, $CDCl_3$, 293 K) δ = 126.47 (dd, ^{1}J(P,Rh) = 178.2, ^{2}J(P,P) = 19.8 Hz), 128.29 (dd, ^{1}J(P,P) = 180.3, ^{2}J(P,P) = 20.9 Hz) ppm.
HR-MS (ESI$^+$): m/z calcd. for $C_{74}H_{80}N_4O_8P_2Rh$, $[M-BF_4^-]^+$: 1317.45009; found: 1317.45416.

7.3.11 Seeding and hydrogenation experiments

For catalysts **32**, complex, substrate **20** and AcNH-(*S*)Phe- NHMe (*S*)-**8** (5 eq.) were dissolved in dry and degassed $CDCl_3$ to give a 3.2 mM catalyst solution. For the respective phosphoramidite complex, ligand **33**, $[Rh(COD)_2]BF_4$ (1 eq.), substrate **20** and AcNH-(*S*)Phe- NHMe (*S*)-**8** (5 eq.) were dissolved in dry and degassed THF-d8 to give a 3.2 mM catalyst solution. The yellow solution was subsequently transferred into a stainless steel reactor loaded with a standard NMR tube and a small stirring bar and cooled to -20°C in a cooling bath. After an equilibration time of 15 min, 95 bar hydrogen was applied.

For ligands **19d** and *meso*-**19c**, stock solutions (4.9 mM) in dry and degassed $CDCl_3$ of the complex were prepared or a stock solution of the ligand was treated with $[Rh(COD)_2]BF_4$ from which 0.5 ml were added to a J. Young NMR tube that had been placed under an atmosphere of argon and charged with a chiral additive. The solution was left standing at room temperature for 16 hours to complete re-equilibration and afterwards, substrate **12** (20 eq. to catalyst) was added. The resulting mixture was transferred into a nitrogen-filled stainless steel reactor and cooled in a bath of 2-propanol utilizing a cryostatic temperature regulator, if necessary. The reactor was pressurized with hydrogen gas (20 bar for the phosphine ligands, 50 bar for catalyst 32) to initiate the catalysis.

The autoclave was reopened after one day and the solution was passed through a short pipet filled with silica (ca. 3 cm) using ethyl acetate as eluent. Evaporation gave the hydrogenation product as a yellow oil. Enantiomeric ratio was determined by chiral GC (compound **13**: (6-TBDMS-2,3-Ac)-β-CD, 25 m, i.d. 250 μm, film thickness 250 nm, prepared and coated in the Trapp group, 100 kPa helium, 130 °C, k_R = 6.84, k_S = 9.07, α = 1.33). Assignment of absolute configuration was accomplished by comparison of the elution order to known standards or literature values. All reactions showed full conversion.

7.4 Experimental data for chapter 4

7.4.1 Allyl-protected 3,3'-methoxy-5,5'-bis(methyloxycarbonyl)-2,2'-biphenol (37)

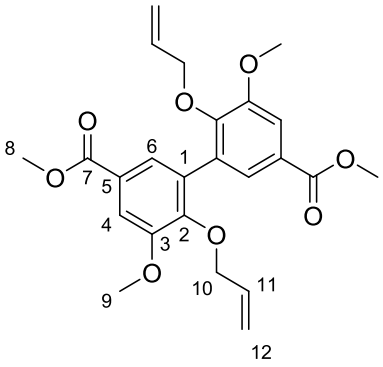

This compound was prepared according to a known procedure.[191] Diol **15** (8.00 g, 22.1 mmol, 1.00 eq.) and potassium carbonate (30.5 g, 221 mmol, 10.0 eq.) were suspended in 2-butanone (250 ml). Allyl bromide (9.55 ml, 110 mmol, 5.00 eq.) was added and the mixture was refluxed for 24 hours. All volatiles were subsequently evaporated and the solid residue was heated to 70 °C for one hour under vacuum to remove residual allyl bromide. Solids were then partitioned between ethyl acetate (200 ml) and water (200 ml), layers were separated and the aqueous layer was re-extracted with more ethyl acetate (twice with 100 ml each). Combined organic layers were washed with brine (100 ml), dried over sodium sulfate and evaporated to give a yellow oil, which crystallized into an off-white solid upon prolonged drying in high vacuum (9.46 g, 22.1 mmol, 97%).

^{1}H NMR ($CDCl_3$, 598.76 MHz, 300 K): δ = 3.88 (s, 3H, H8), 3.93 (s, 6H, H9), 4.43-4.45 (m, 2H, H10), 4.99-5.02 (m, 1H, H12), 5.05-5.09 (m, 1H, H12'), 5.71-5.79 (m, 1H, H11), 7.60 (d, 1H, ^{4}J(H,H) = 2.0 Hz, H6), 7.61 (d, 1H, ^{4}J(H,H) = 2.0 Hz, H4) ppm.
^{13}C{^{1}H} NMR ($CDCl_3$, 150.57 MHz, 300 K): δ = 52.2 (C8), 56.2 (C9), 74.1 (C10), 113.0 (C4), 117.5 (C12), 125.2 (C1), 125.3 (C6), 132.3 (C5), 134.0 (C11), 150.1 (C2), 152.6 (C3), 166.8 (C7) ppm.
HRMS (ESI): m/z calcd. for $C_{24}H_{30}N_1O_8$ $[M+NH_4]^+$: 460.19659; found: 460.19712.
FTIR: $\tilde{\nu}$ = 761 (s), 981 (s), 1042 (s), 1173 (s), 1222 (s), 1286 (s), 1714 (s), 2845 (w), 2870 (w), 2951 (m), 3015 (w), 3090 (w) cm^{-1}.

7.4.2 Allyl-protected dicarboxylic acid (38)

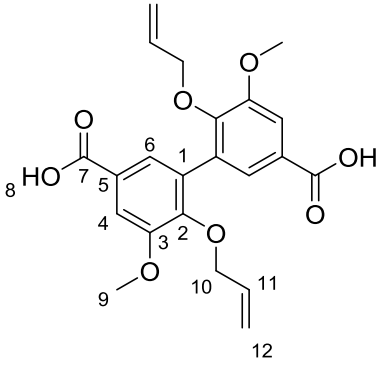

Diester **37** (9.40g, 21.2 mmol, 1.00 eq.) and sodium hydroxide (8.50 g, 212 mmol, 10.0 eq.) were dissolved in a mixture of water (110 ml) and THF (110 ml) and the biphasic system was refluxed under vigorous stirring for 14 hours. For work-up, THF was evaporated and the aqueous orange solution was acidified with conc. HCl solution (6 M) until pH 1 was reached and a thick, white precipitate formed. The solids were filtered off and washed with more water to neutrality. Freeze-drying afforded product **38** as a white powder (8.80 g, 21.2 mmol, 99%).

^{1}H NMR ($CDCl_3$, 800.34 MHz, 300 K): δ = 3.90 (s, 3H, H9), 4.37-4.38 (m, 2H, H10), 4.99-5.01 (m, 1H, H12), 5.04-5.06 (m, 1H, H12'), 5.68-5.73 (m, 1H, H11), 7.41 (d, 1H, ^{4}J(H,H) = 2.0 Hz, H6), 7.57 (d, 1H, ^{4}J(H,H) = 2.0 Hz, H4), 12.91 (bs, 1H, H8) ppm.
^{13}C{^{1}H} NMR ($CDCl_3$, 201.24 MHz, 300 K): δ = 55.9 (C9), 73.2 (C10), 112.8 (C4), 117.1 (C12), 124.3 (C6), 125.7 (C5), 131.5 (C1), 134.1 (C11), 149.0 (C2), 152.1 (C3), 166.8 (C7) ppm.
HRMS (ESI): m/z calcd. for $C_{22}H_{26}NO_8$ $[M+NH_4]^+$: 432.16529; found: 432.16564.
FTIR: $\tilde{\nu}$ = 759 (s), 980 (s), 1040 (s), 1179 (s), 1218 (s), 1285 (s), 1404 (s), 1577 (s), 1677 (s), 2519 (bm), 2837 (bm), 2970 (bm), 3063 (w) cm^{-1}.

7.4.3 Allyl-protected dicarboxylic acid chloride (38i)

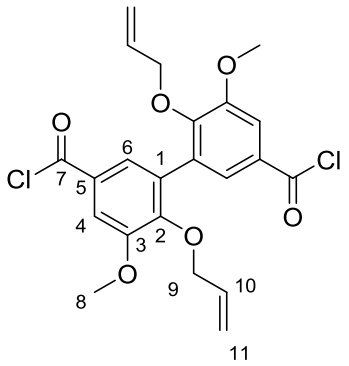

Dicarboxylic acid **38** (4.00 g, 9.65 mmol, 1.00 eq.) was placed in a dried Schlenk flask with reflux condenser and overpressure ventilation and thionyl chloride (30 ml) was added. The mixture was refluxed for seven hours and turned unto a clear, brown solution within minutes. Subsequently, thionyl chloride was removed *in vacuo*, residual solids were suspended in dry toluene (15 ml) and all volatiles were removed again. The last two steps were repeated another two times and after drying, the product was obtained as a grey solid (4.36 g, 9.65 mmol, 99%).

^{1}H NMR ($CDCl_3$, 598.76 MHz, 300 K): δ = 3.96 (s, 3H, H9), 4.50-4.54 (m, 2H, H9), 4.05-5.12 (m, 2H, H11 and H11') 5.73-5.79 (m, 1H, H10), 7.64 (d, 1H, ^{4}J(H,H) = 2.2 Hz, H6), 7.73 (d, 1H, ^{4}J(H,H) = 2.2 Hz, H4) ppm.
^{13}C{^{1}H} NMR ($CDCl_3$, 150.57 MHz, 300 K): δ = 56.3 (C8), 74.4 (C9), 114.2 (C6), 118.2 (C11), 128.0 (C1), 128.1 (C4), 131.9 (C5), 133.5 (C10), 152.2 (C2), 152.8 (C3), 167.6 (C7) ppm.

7.4.4 Allyl–protected tBuO-(*S*)Phe-NH biphenol (39a)

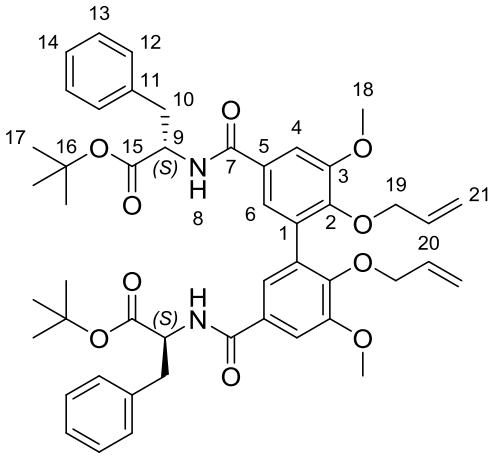

Allyl-protected acid chloride **38i** (800 mg, 4.43 mmol, 2.50 eq.) was dissolved in dry DCM (4 ml). In a separate flask, phenylalanine *tert*-butyl ester hydrochloride (1.14 g, 4.43 mmol, 2.50 eq.) was mixed with DIPEA (1.54 ml, 8.86 mmol, 5.00 eq.) in dry DCM (10 ml) to give a clear solution. Both mixtures were cooled in an ice bath and the acid chloride was subsequently added dropwise to the selector solution. The resulting orange solution was slowly warmed to room temperature and stirring was continued for 18 hours. For work-up, the mixture was diluted with ethyl acetate (120 ml) and subsequently washed with HCl solution (2M, 3 x 120 ml), saturated bicarbonate solution (2 x 120 ml) and brine (120 ml), dried over sodium sulfate and evaporated to yield the product as a brown powder (1.33 g, 1.62 mmol, 91%).

^{1}H NMR ($CDCl_3$, 598.47 MHz, 300 K): δ = 1.39 (s, 9H, H17), 3.14-3.26 (m, 2H, H10 and H10'), 3.89 (s, 3H, H18), 4.35-4.36 (m, 2H, H19), 4.96-5.05 (m, 2H, H21 and H21'), 5.05 (s, 1H, H9), 5.70-5.77 (m, 1H, H20), 7.16-7.28 (m, 6H, H6 and H12 and H13 and H14), 7.43 (s, 1H, H4) ppm. The NH proton was not observed.
^{13}C{^{1}H} NMR ($CDCl_3$, 150.57 MHz, 300 K): δ = 28.1 (C17), 28.3 (C10), 54.5 (C9), 56.1 (C18), 74.1 (C19), 82.3 (C16), 111.7 (C4), 117.5 (C21), 121.2 (C6), 127.0 (14), 128.3 (C13), 128.8 (C5), 129.5 (C12), 132.1 (C1), 134.0 (C20), 136.7 (C11), 148.7 (C2), 152.9 (C3), 166.2 (C7), 171.6 (C15) ppm.
HRMS (ESI): m/z calcd. for $C_{48}H_{57}N_2O_{10}$ $[M+H]^+$: 821.4008; found: 821.40258.
FTIR: $\tilde{\nu}$ = 698 (s), 982 (s), 1151 (s), 1219 (s), 1366 (s), 1537 (s), 1639 (s), 1706 (s), 2867 (w), 2935 (w), 2978 (w), 3029 (w), 3062 (w), 3344 (bm) cm^{-1}.

7.4.5 ^{t}BuO-(*S*)Phe-NH biphenol (40a)

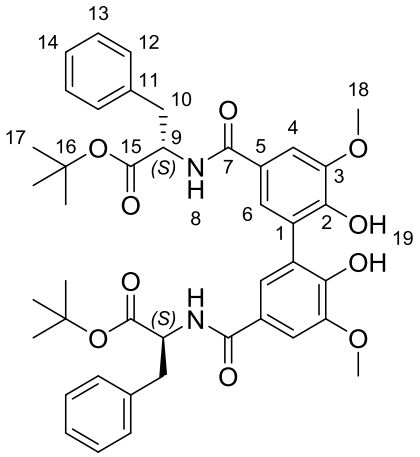

The deprotection was done by a known procedure, which was slightly modified.[235] To remove the allyl groups, substrate **39a** (750 mg, 914 mmol, 1.00 eq.), palladium acetate (10.2 mg, 45.7 µmol, 0.05 eq.) and (4-dimethylaminophenyl)diphenylphosphine (140 mg, 457 µmol, 0.50 eq.) were dissolved in dry ethyl acetate (18 ml) and the suspension was stirred for 15 min. The resulting solution was treated with formic acid (0.20 ml, 5.30 mmol, 5.80 eq.) and the orange mixture was subsequently refluxed. It quickly turned brown and gas evolved. After two hours, the mixture was cooled to room temperature and diluted with ethyl acetate (80 ml). The organic layer was washed with HCl solution (2M, 4 x 100 ml), saturated bicarbonate solution (3 x 100 ml) and brine (1 x 100 ml), dried over sodium sulfate and evaporated. Purification by column chromatography (silica, *n*-pentane:ethyl acetate 1:2, R_f = 0.4). Appropriate fractions were evaporated and the residue precipitated from ethyl acetate:*n*-pentane to yield the desired diol **40a** as an off-white powder (481 mg, 649 µmol, 71%).

^{1}H NMR (CDCl3, 598.74 MHz, 300 K): δ = 1.39 (s, 9H, H9), 3.13-3.23 (m, 2H, H10 and H10'), 3.90 (s, 3H, H18), 5.03-5.04 (m, 1H, H9), 6.20 (bs, 1H, H19), 7.17-7.23 (m, 5H, H12 and H13 and H14), 7.27 (s, 1H, H8), 7.30 (s, 1H, H6), 7.39 (s, 1H, H4) ppm.
^{13}C{^{1}H} NMR ($CDCl_3$, 150.57 MHz, 300 K): δ = 55.9 (C9), 73.2 (C10), 112.8 (C4), 117.1 (C12), 124.3 (C6), 125.7 (C5), 131.5 (C1), 134.1 (C11), 149.0 (C2), 152.1 (C3), 166.8 (C7) ppm.
HRMS (ESI): m/z calcd. for $C_{42}H_{49}N_2O_{10}$ $[M+H]^+$: 741.3382; found: 741.33910.
FTIR: $\tilde{\nu}$ = 698 (s), 1042 (s), 1086 (s), 1150 (s), 1220 (s), 1366 (s), 1487 (s), 1593 (s), 1636 (s), 1710 (s), 2933 (m), 2977 (m), 3029 (w), 3330 (bm), 3508 (bw) cm^{-1}.

7.4.6 ^{t}BuO-(*S*)Phe-NH bisphosphinite (41a)

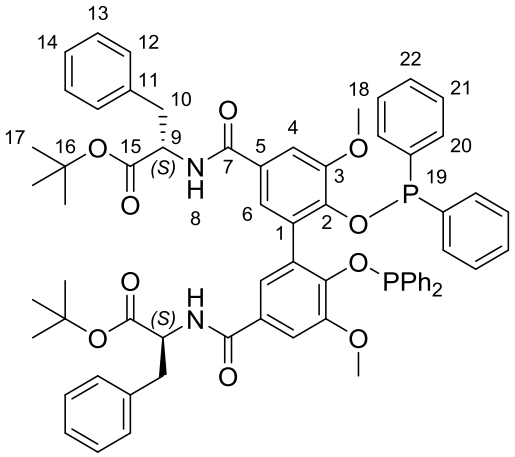

Selector-modified diol **40a** (350 mg, 472 µmol, 1.00 eq.) and DABCO (212 mg, 1.89 mmol, 4.00 eq.) were placed in a dried Schlenk flask and dissolved in dry and degassed DCM (10 ml). The solution was cooled in an ice bath and PPh_2Cl (326 µl, 1.89 mmol, 4.00 eq.) was added. After 15 minutes, the ice bath was removed and stirring was continued at room temperature for another two hours. For work-up, all volatiles were removed and the off-white residue was suspended in dry, degassed and stabilized THF (5 ml). The suspension was filtered through an inert pad of neutral alumina and the product was eluated with more THF. Combined fractions were evaporated to give a white foam. Re-precipitation from DCM:*n*-pentane (4x 1:10 ml) gave the desired phosphinite **41a** as a white powder (105 mg, 94.8 mmol, 20%).

The compound exists as two interconverting rotamers. The minor isomer (A, S_{ax}) shows sharp NMR signals in ^{31}P, ^{1}H and ^{13}C NMR spectra. For the major rotamer (B, R_{ax}), significant line broadening was detected in ^{31}P and ^{1}H NMR spectra and even with concentrated samples, almost no peaks could be detected in the $^{13}C\{^{1}H\}$ NMR spectrum.

^{1}H NMR (THF-d8, 400.22 MHz, 300 K): δ = 1.37 (s, H17, B), 1.39 (s, H17, A), 3.04-3.09 (m, H10, A), 3.12 (bs, H10, B), 3.14-3.19 (m, H10', A), 3.27 (bs, H10', B), 3.53 (bs, H18', B), 3.59 (s, H18, A), 4.75-4.81 (m, H9, A) 4.86 (bs, H9, B), 6.91 (bs, H_{Ar} B), 7.04-7.26 (m, HAr, A and B), 7.12 (m, H6, A), 7.28-7.35 (m, H_{Ar}, A), 7.35 (d, ^{4}J(H,H) = 1.9 Hz, H4, A), 7.40 (d, ^{3}J(H,H) = 7.7 Hz, H8, A), 7.48 (bs, H_{Ar}, B), 8.47 (bs, H8, B) ppm.

^{13}C{^{1}H} NMR (THF-d8, 100.54 MHz, 300 K): δ = 27.2 (C17, A), 37.5 (C10), 54.4 (C9, A), 54.7 (C18, A), 54.9 (C18, B), 80.5 (C16, A), 111.8 (C4, A), 121.1 (C6, A), 120.8 (C6, B), 126.3 (C_{Ar}), 126.2 (C_{Ar}), 127.3 (C_{Ar}), 127.3 (C_{Ar}), 127.4 (C_{Ar}), 127.5 (C_{Ar}), 127.5 (C_{Ar}), 127.5 (C_{Ar}), 127.9 (C_{Ar}), 129.1 (C12, A), 129.2 (C_{Ar}), 129.3 (C_{Ar}), 129.5 (C_{Ar}), 129.5 (C13, A), 129.7 (C_{Ar}), 130.3 (C_{Ar}), 130.5 (C_{Ar}), 130.6 (C_{Ar}), 130.7 (C_{Ar}), 131.3 (C1, A), 137.7 (C11, A), 138.0 (C_{Ar}^{q}, B), 142.5 (C_{Ar}^{q}, B), 142.7 (C_{Ar}^{q}, B), 143.0 (C_{Ar}^{q}, A), 143.1 (C_{Ar}^{q}, A), 147.5 (C2, A), 151.2 (C3, A), 165.0 (C7, A), 165.1 (C7, B), 170.8 (C14, A) ppm.

^{31}P{^{1}H} NMR (THF-d8, 161.85 MHz, 300K): δ = 118.4 (bs, 1P, B), 121.1 (s, 1P, A), 121.1 (bs, 1P, B) ppm.

HRMS (ESI): m/z calcd. for $C_{66}H_{67}N_2O_{10}P_2$ $[M+H]^+$: 1109.4271; found: 1109.42863.

FTIR: $\tilde{\nu}$ = 694 (s), 863 (m), 1094 (s), 1152 (s), 1367 (s), 1476 (s), 1642 (s), 1707 (s), 2859 (w), 1933 (w), 2977 (w), 3054 (w), 3349 (bm) cm^{-1}.

7.4.7 Rh complex of ^{t}BuO-(*S*)Phe-NH bisphosphinite (42a)

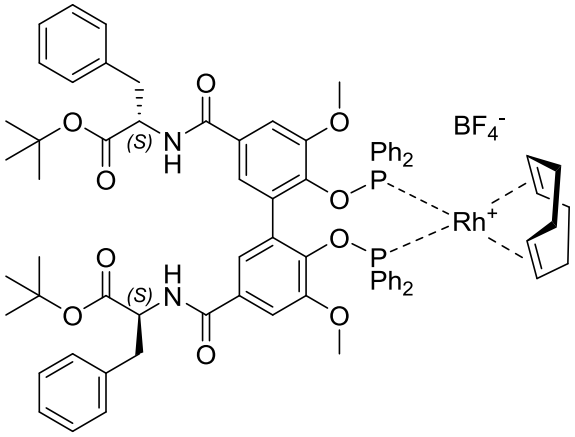

Bisphosphinite **41a** (53 mg, 47.8 µmol, 1.00 eq.) and $[Rh(COD)_2]BF_4$ (19.4 mg, 47.8 µmol, 1.00 eq.) were placed in a dried Schlenk flask and dissolved in dry and degassed DCM (3.5 ml). The clear orange solution was stirred for two hours at room temperature and then concentrated to 1.0 ml. Addition of dry and degassed pentane (10 ml) gave an orange precipitate. The supernatant solution was removed using a filter-tipped cannula and re-precipitation was repeated another two times. The solids were finally dried in high vacuum to give the desired Rh complex as a yellow powder (61.0 mg, 43.4 µmol, 91%).

The compound exists as two interconverting rotamers.
^{31}P{^{1}H} NMR ($CDCl_3$, 161.98 MHz, 300K): δ = 127.91 (d, ^{1}J(P,Rh) = 179.9 Hz, S_{ax}), 128.02 (d, ^{1}J(P,Rh) = 181.3 Hz, R_{ax}) ppm.
EA (CHNS): calcd. for $C_{74}H_{78}N_2O_{10}P_2RhBF_4$: C: 63.17, H: 5.59, N: 1.99; found: C: 61.24, H: 5.48, N: 1.93.
HRMS (ESI): m/z calcd. for $C_{74}H_{78}N_2O_{10}P_2Rh$ $[M\text{-}BF_4]^+$: 1319.41813; found: 1319.41751.

7.4.8 Allyl-protected ^{t}BuNH-(*S*)Phe-O biphenol (39b)

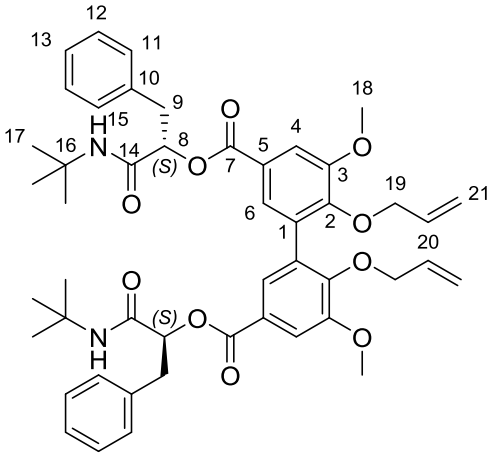

Dicarboxylic acid **38** (1.00 g, 2.41 mmol, 1.00 eq.), amido alcohol **S3** (2.14 g, 9.56 mmol, 4.00 eq.) and dimethylaminopyridine (59.0 mg, 482 µmol, 0.20 eq.) were mixed in dry DCM (40 ml) and cooled in an ice bath. EDCI.HCl (1.16 g, 6.03 mmol, 2.50 eq.) was added and the yellow solution was left stirring to warm to room temperature overnight. After 18 hours, the mixture was diluted with ethyl acetate (200 ml) and subsequently washed with HCl solution (2 M, 3 x

180 ml), saturated bicarbonate solution (2 x 180 ml) and brine (180 ml), dried over sodium sulfate and evaporated. Purification by column chromatography (neutral alumina, diethyl ether:toluene 3:1, R_f = 0.6) yielded the product as a white solid (1.00 g, 1.22 mmol, 50%).

^{1}H NMR ($CDCl_3$, 598.74 MHz, 300 K): δ = 1.24 (s, 9H, H17), 3.26-3.28 (m, 2H, H9), 3.92 (s, 3H, H18), 4.42-4.43 (m, 2H, H19), 4.99-5.08 (m, 2H, H21 and H21'), 5.43-5.45 (m, 1H, H8), 5.58 (s, 1H, H15), 5.71-5.77 (m, 1H, H20), 7.19-7.22 (m, 1H, H13), 7.22-7.29 (m, 4H, H11 and H12), 7.53 (d, 1H, ^{4}J(H,H) = 2.0 Hz, H4), 7.55 (d, 1H, ^{4}J(H,H) = 2.0 Hz, H6) ppm.
^{13}C{^{1}H} NMR ($CDCl_3$, 150.57 MHz, 300 K): δ = 28.7 (C17), 38.0 (C9), 51.3 (C16), 56.2 (C18), 74.2 (C19), 75.3 (C8), 113.2 (C4), 117.7 (C21), 124.3 (C5), 125.4 (C6), 127.1 (C13), 128.5 (C12), 130.0 (C11), 132.3 (C1), 133.9 (C20), 136.2 (C10), 150.6 (C2), 152.7 (C3), 164.9 (C7), 168.0 (C14) ppm.
HRMS (ESI): m/z calcd. for $C_{48}H_{60}N_3O_{10}$ $[M+NH_4]^+$: 838.4273; found: 838.42788.
FTIR: $\tilde{\nu}$ = 696 (s), 979 (s), 1169 (s), 1217 (s), 1657 (s), 1711 (s), 2867 (w), 2966 (w), 3029 (w), 3088 (w), 3291 (bm) cm^{-1}.

7.4.9 ^{t}BuNH-(*S*)Phe-O biphenol (40b)

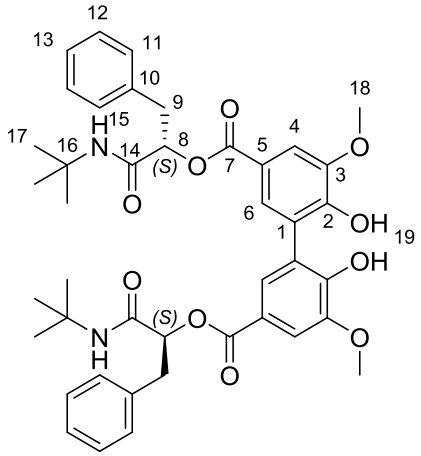

The deprotection was done by a known procedure, which was slightly modified.[235] To remove the allyl groups, substrate **39b** (890 mg, 1.08 mmol, 1.00 eq.), palladium acetate (12.2 mg, 54.2 µmol, 0.05 eq.) and (4-dimethylaminophenyl)diphenylphosphine (166 mg, 542 µmol, 0.50 eq.) were dissolved in dry ethyl acetate (18 ml) and the suspension was stirred for 15 min. The resulting solution was treated with formic acid (0.24 ml, 6.29 mmol, 5.80 eq.) and the orange mixture was subsequently refluxed. It quickly lost its colour and gas evolved. After one hours, the mixture was cooled to room temperature and diluted with ethyl acetate (100 ml). The organic layer was washed with HCl solution (2 M, 4 x 100 ml), saturated bicarbonate solution (2 x 100 ml) and brine (1 x 100 ml), dried over sodium sulfate and evaporated. The residue was precipitated from ethyl acetate:*n*-pentane to yield the desired diol **40b** as an off-white powder (745 mg, 1.01 mmol , 93%).

^{1}H NMR ($CDCl_3$, 598.47 MHz, 300 K): δ = 1.25 (s, 9H, H17), 3.27 (d, 2H, ^{3}J(H,H) = 5.9 Hz, H9), 3.98 (s, 3H, H18), 5.46 (t, 1H, ^{3}J(H,H) = 5.9 Hz, H8), 5.63 (s, 1H, H15), 6.39 (s, 1H, H19), 7.19-7.21 (m, 1H, H13), 7.23-7.26 (m, 4H, H11 and H12), 7.49 (d, 1H, ^{4}J(H,H) = 1.9 Hz, H4), 7.71 (d, 1H, ^{4}J(H,H) = 1.9 Hz, H6) ppm.

$^{13}C\{^1H\}$ NMR ($CDCl_3$, 150.57 MHz, 300 K): δ = 28.7 (C17), 38.00 (C9), 51.4 (C16), 56.5 (C18), 75.0 (C8), 111.2 (C4), 121.0 (C5), 122.8 (C1), 126.4 (C6), 127.0 (C13), 128.4 (C12/C13), 130.0 (C12/C13), 136.3 (C10), 146.8 (C3), 148.0 (C2), 164.9 (C7), 168.2 (C14) ppm.
HRMS (ESI): m/z calcd. for $C_{42}H_{52}N_3O_{10}$ $[M+NH_4]^+$: 758.3647; found: 758.36497.
FTIR: $\tilde{\nu}$ = 699 (s), 740 (m), 1039 (m), 1208 (s), 1277 (s), 1454 (m), 1669 (s), 2868 (w), 2933 (w), 2965 (m), 3027 (w), 3065 (w), 3317 (bm), 3407 (w) cm^{-1}.

7.4.10 ^{t}BuNH-(*S*)Phe-O bisphosphinite (41b)

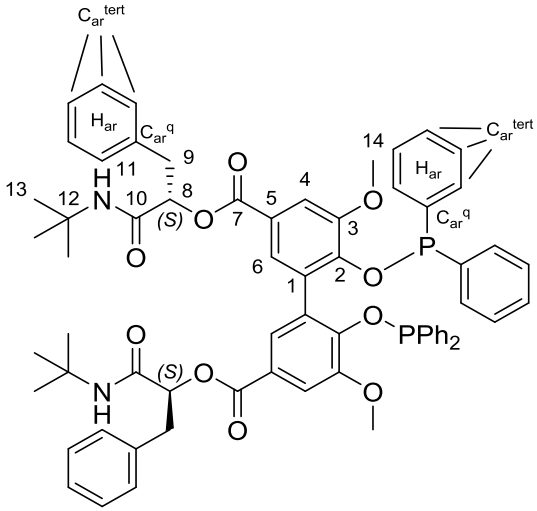

Selector-modified diol **40b** (50.0 mg, 67.5 µmol, 1.00 eq.) was dissolved in dry, degassed and stabilized THF (2 ml) and triethylamine (23.5 µl, 168 µmol, 2.50 eq.) was added. The mixture was cooled in an ice bath and chlorodiphenylphosphine (24.2 µl, 142 µmol, 2.10 eq.) was added. After two hours, the mixture was filtered through a filter-tipped cannula and residual solids rinsed with more THF (2 x 2 ml). Combined organic washings were evaporated and the resulting white crude product was washed with *n*-pentane (5 x 2 ml) to give the product as a white solid (52.0 mg, 46.9 µmol, 69%). Traces of $Ph_2P(O)PPh_2$ (side product) still remained and could not be removed without significant loss of product.

For some atoms an additional signal splitting was observed. Those signals are marked X and X'.
^1H NMR (THF-d8, 399.78 MHz, 300 K): δ = 1.25 (s, 9H, H13), 3.17 (dd, 2H, ^2J(H,H) = 14.8 Hz, ^3J(H,H) =, 6.6 Hz, H9), 3.63 (s, 3H, H18), 5.20 (q, ^3J(H,H) = 6.3 Hz, H8), 6.53 (s, 1H, H11), 7.03-7.32 (m, 15H, H_{ar}), 7.30 (s, 1H, H6), 7.38 (d, 1H, ^4J(H,H) = 2.0 Hz, H4) ppm.
$^{13}C\{^1H\}$ NMR (THF-d8, 100.54 MHz, 300 K): δ = 27.8 (C13), 37.8 (C9/C9'), 50.3 (C12), 54.9 (C14), 75.1 (C8), 75.2 (C8'), 112.9 (C4), 124.4 (C6), 124.7 (^3J(C,P) = 4.6 Hz, C1), 126.3 (J(C,P) = 11.4 Hz, C_{ar}^{tert}), 127.4 (J(C,P) = 7.4 Hz, C_{ar}^{tert}), 127.6 (J(C,P) = 8.3 Hz, C_{ar}^{tert}), 127.9 (J(C,P) = 4.6 Hz, C_{ar}^{tert}), 128.3 (J(C,P) = 7.4 Hz, C_{ar}^{tert}), 128.8 (J(C,P) = 5.5 Hz, C_{ar}^{tert}), 129.4 (C5), 129.5 (J(C,P) = 5.8 Hz, C_{ar}^{tert}), 129.7 (J(C,P) = 11.5 Hz, C_{ar}^{tert}), 130.3 (J(C,P) = 12.9 Hz, C_{ar}^{tert}), 130.5 (J(C,P) = 12.9 Hz, C_{ar}^{tert}), 131.3 (C5), 137.0 ((J(C,P) = 11.4 Hz, C_{ar}^{q}/ $C_{ar}^{q'}$), 142.5 (J(C,P) = 17.8 Hz, C_{ar}^{q}), 142.7 (J(C,P) = 16.6 Hz, C_{ar}^{q}), 149.0 (J(C,P) = 7.3 Hz, C2/C2'), 151.1 (J(C,P) = 7.4 Hz, C3), 164.2 (C7), 167.5 (C10), 167.6 (C10') ppm.
$^{31}P\{^1H\}$ NMR (THF-d8, 161.85 MHz, 300 K): δ = 122.4 (s, 1P), 122.5 (s, 1P) ppm.
HRMS (ESI): m/z calcd. for $C_{66}H_{67}N_2O_{10}P_2$ $[M+H]^+$: 1109.42655; found: 1109.42479.

FTIR: $\tilde{\nu}$ = 692 (s), 1166 (s), 1211 (m), 1453 (m), 1657 (s), 1723 (m), 2867 (w), 2930 (m), 2965 (m), 3002 (w), 3056 (w), 3291 (bm) cm^{-1}.

7.4.11 Rh complex of ^{t}BuNH-(*S*)Phe-O bisphosphinite (42b)

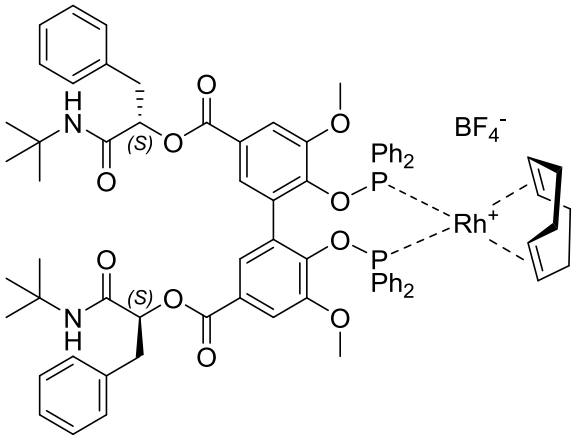

Bisphosphinite **41b** (33.0 mg, 29.8 µmol, 1.00 eq.) and $[Rh(COD)_2]BF_4$ (9.10 mg, 22.3 µmol, 1.00 eq.) were placed in a dried Schlenk flask and dissolved in dry and degassed DCM (2.0 ml). The clear orange solution was stirred for two hours at room temperature and then concentrated to 0.5 ml. Addition of dry and degassed *n*-pentane (5.0 ml) gave an orange precipitate. The supernatant solution was removed using a filter-tipped cannula and re-precipitation was repeated another two times. The solids were finally dried in high vacuum to give the desired Rh complex as a yellow powder (23.3 mg, 16.6 µmol, 74%).

The compound exists as two rotamers A and B.
^{31}P{^{1}H} NMR ($CDCl_3$, 161.98 MHz, 300K): δ = 129.00 (d, ^{1}J(P,Rh) = 179.9 Hz, A), 129.19 (d, ^{1}J(P,Rh) = 179.8 Hz, B) ppm.
HRMS (ESI): m/z calcd. for $C_{68}H_{69}N_3O_{10}P_2Rh$ $[M\text{-}COD\text{-}BF_4+CH_3CN]^+$: 1252.35077; found: 1252.34933.

7.4.12 ^{t}BuO-(*S*)Phe-NH phosphoramidite (44)

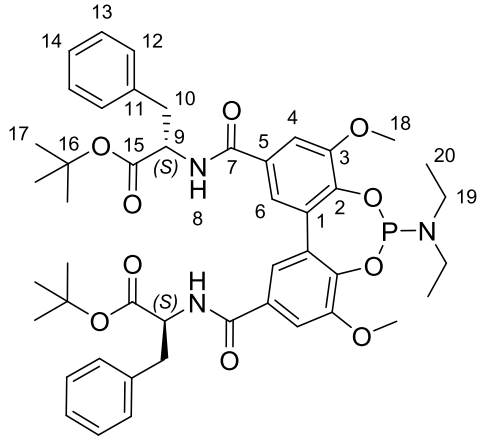

Selector-modified diol **40a** (100 mg, 135 µmol, 1.00 eq.) was dissolved in dry, degassed and stabilized THF (2 ml) and triethylamine (54.6 µl, 391 µmol, 2.90 eq.) was added. The mixture

was cooled in an ice bath and diethylaminophosphoramidous dichloride (22.5 µl, 155 µmol, 1.15 eq.) was added dropwise. The mixture was warmed to room temperature and stirred for 18 hours. For work-up, the mixture was filtered through a filter-tipped cannula and residual solids were rinsed with more THF (2 x 2 ml). Combined organic washings were evaporated and the crude product was washed with *n*-pentane (3 x3 ml) to give complex **44** as a white solid (87.0 mg, 103 µmol, 77%).

For some atoms an additional signal splitting was observed. This is caused by the non-equivalence of the two halves in the BIPOL-phosphoramidite, which has been previously observed for other chiral phosphoramidites.[233,234] Those signals are marked X and X'.
^{1}H NMR (THF-d8, 400.22 MHz, 300 K): δ = 1.05 (t, 3H, ^{3}J(H,H) = 7.0 Hz, H20), 1.40 (s, 9H, H17), 3.05 (dd, 2H, ^{3}J(P,H) = 10.8 Hz, ^{3}J(H,H) = 7.0 Hz, H19), 3.10 (dd, 1H, ^{2}J(H,H) = 13.8 Hz, ^{3}J(H,H) = 8.2 Hz, H10), 3.18 (dd, 1H, ^{2}J(H,H) = 13.8 Hz, ^{3}J(H,H) = 6.5 Hz, H10'), 3.87 (s, 3H, H18), 4.78-4.84 (m, 1H, H9), 7.14-7.18 (m, 1H, H14), 7.23-7.29 (m, 4H, H12 and H13), 7.48-7.49 (m, 1H, H4/H4'), 7.58-7.59 (m, 1H, H6), 7.81-7.84 (m, 1H, H8/H8') ppm.
^{13}C{^{1}H} NMR (THF-d8, 100.65 MHz, 300 K): δ = 14.7 (C20), 28.1 (C17), 38.6 (C10), 38.8 (C16), 55.7 (C9), 56.2 (C18), 81.5 (C16), 111.9 (d, ^{4}J(P,C) = 9.6 Hz, C4), 121.0 (d, ^{4}J(P,C) = 12.4 Hz, C6), 127.3 (C14), 129.0 (C13), 130.2 (C12), 131.8 (C5), 132.0 (m, C1/C1'), 138.6 (C11), 144.3 (m, C2/C2') 152.9 (C3), 166.6 (C7), 171.8 (C15) ppm.
^{31}P{^{1}H} NMR (THF-d8, 162.00 MHz, 300 K): δ = 150.9 (quint, ^{3}J(P,H) = 10.8 Hz) ppm.
HRMS (ESI): m/z calcd. for $C_{46}H_{57}N_3O_{10}P$ $[M+H]^+$: 842.37761; found: 842.37727.
FTIR: $\tilde{\nu}$ = 697 (s), 740 (s), 843 (s), 1022 (s), 1089 (s), 1151 (s), 1366 (s), 1456 (s), 1533 (m), 1585 (m), 1640 (m), 1733 (m), 2868 (w), 2933 (w), 2974 (m), 3028 (w), 3064 (w), 3088 (w), 3330 (bm) cm^{-1}.

7.4.13 Rh complex of ^{t}BuO-(*S*)Phe-NH phosphoramidite (45)

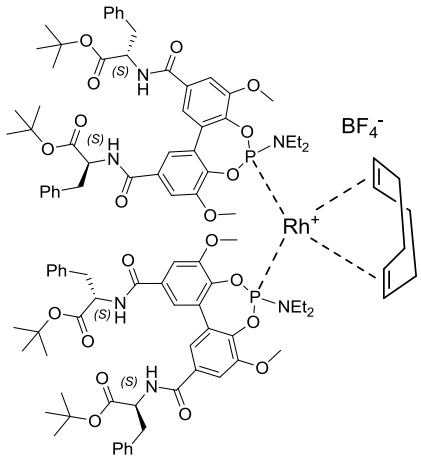

Phosphoramidite **44** (150 mg, 178 µmol, 1.00 eq.) and $[Rh(COD)_2]BF_4$ (36.2 mg, 89.1 µmol, 0.50 eq.) were dissolved in dry and degassed DCM (5 ml). The orange solution was stirred for 18 hours and subsequently concentrated to 0.5 ml. Addition of *n*-pentane (4 ml) gave the complex as a yellow precipitated. The supernatant solution was removed using a filter-tipped cannula and the product was re-precipitated another two times. Subsequent drying gave the product as a yellow powder. (141 mg, 71.1 µmol, 80%).

Due to high molecular dynamics, very broad signals where observed in ^{1}H, $^{13}C\{^{1}H\}$ NMR spectra which made peak assignment impossible. $^{31}P\{^{1}H\}$ NMR spectrum shows various signals which is in line with the nature of previously investigated Rh complexes of similar nature.[40]

$^{31}P\{^{1}H\}$ NMR ($CDCl_3$, 162.00 MHz, 300 K): δ = 137.6, 138.2, 138.6. 139.3, 140.6, 142.3, 143.7 ppm.

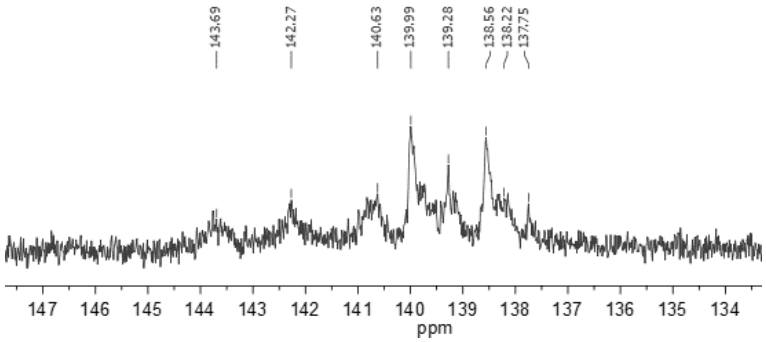

HRMS (ESI): m/z calcd. for $C_{100}H_{124}N_6O_{20}P_2Rh$ $[M\text{-}BF_4^-]^+$: 1894.74287; found: 1894.74635.

EA (CHNS): calcd. for $C_{100}H_{124}N_6O_{20}P_2RhBF_4$: C: 60.61, H: 6.31, N: 4.24; found: C: 58.42, H: 6.13, N: 4.23.

FTIR: $\tilde{\nu}$ = 697 (s), 879 (m), 1022 (s), 1153 (s), 1367 (s), 1456 (m), 1527 (m), 1663 (m), 1728 (m), 2872 (w), 2933 (w), 2975 (w), 3314 (bw) cm^{-1}.

7.4.14 (Z)-4-benzylidene-2-phenyloxazol-5(4H)-one (46)

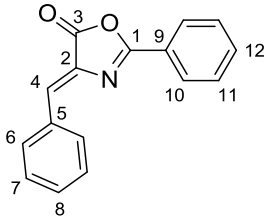

Hippuric acid (25 g, 139 mmol, 1 eq.), benzaldehyde (21.9 g, 2.07 mmol, 1.48 eq.), sodium acetate (8.47 g, 103 mmol, 0.74 eq.) and acetic anhydride (33.0 ml, 349 mmol, 2.50 eq.) were mixed and heated to 140 °C for two hours and yellow solid formed. The product was filtered off, washed with water (3 x 75 ml) and recrystallized from methanol to yield the product as a yellow solid (21.5 g, 86.3 mmol, 62 %).

^{1}H NMR ($CDCl_3$, 400.22 MHz, 300 K): δ = 7.25 (s, 1H, H4), 7.46-7.55 (m, 5H, H7 and H8 and H11), 7.60-7.64 (m, 1H, H12), 8.18-8.22 (m, 4H, H6 and H10) ppm.

$^{13}C\{^{1}H\}$ NMR ($CDCl_3$, 100.65 MHz, 300 K): δ = 125.7 (C2), 128.5 (C10), 129.0 (C11/C7), 129.1 (C11/C7), 131.4 (C8), 131.9 (C4), 132.6 (C6), 133.4 (C5), 133.5 (C12), 133.6 (C9), 163.6 (C1), 167.8 (C3) ppm.

HRMS (ESI): m/z calcd. for $C_{16}H_{12}NO_2$ $[M+H]^+$: 250.08626; found: 250.08642.

FTIR: $\tilde{\nu}$ = 684 (s), 766 (s), 983 (s), 1294 (s), 1448 (s), 1651 (s), 1791 (s), 3028 (w), 3242 (w) cm^{-1}.

7.4.15 PhCO-ΔPhe-NH^{t}Bu (47a)

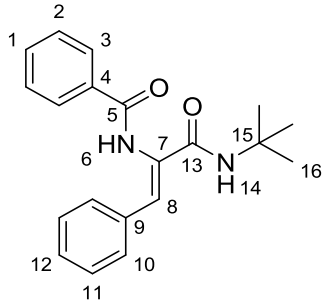

Azlactone **46** (800 mg, 3.21 mmol, 1.00 eq.) was dissolved in chloroform (20 ml). The clear solution was cooled in an ice bath and treated with *tert*-butylamine (3.37 ml, 32.1 mmol, 10.0 eq.). The clear solution was subsequently stirred at 40 °C for 72 hours. For work-up, all volatiles were removed *in vacuo* and residual off-white solids where recrystallized from acetone:hexane to give the product as a white solid (702 mg, 2.18 mmol, 68%).

^{1}H NMR ($CDCl_3$, 400.22 MHz, 300 K): δ = 1.30 (s, 9H, H16), 6.17 (s, 1H, H14), 6.73 (s, 1H, H8), 7.13-7.22 (m, 3H, H11 and H12), 7.28-7.34 (m, 4H, H2 and H10), 7.40-7.44 (m, 1H, H1), 7.74 (d, 2H, ^{3}J(H,H) = 7.3 Hz, H3), 8.08 (s, 1H, H6) ppm.
^{13}C{^{1}H} NMR ($CDCl_3$, 100.65 MHz, 300 K): δ = 28.7 (C16), 51.8 (C15), 125.3 (C8), 127.8 (C3), 128.7 (C12), 128.8 (C2/C11), 128.9 (C2/C11), 129.1 (C10), 131.1 (C7), 132.3 (C1), 133.2 (C4), 134.1 (C9), 165.5 (C13), 166.3 (C5) ppm.
HRMS (ESI): m/z calcd. for $C_{20}H_{22}N_2O_2$ $[M]^+$: 322.16813; found: 322.1678.
FTIR: $\tilde{\nu}$ = 688 (s), 1223 (s), 1281 (s), 1475 (s), 1627 (s), 1642 (s), 2871 (w), 2826 (w), 2967 (m), 3029 (w), 3059 (m), 3238 (bm) cm^{-1}.

7.4.16 PhCO-ΔPhe-NH^{i}Pr (47b)

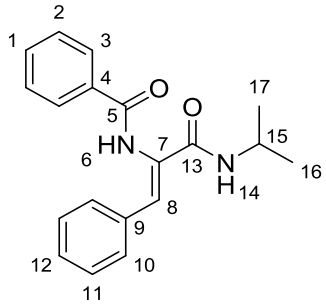

Azlactone **46** (200 mg, 0.80 mmol, 1.00 eq.) was dissolved in chloroform (5 ml). The clear solution was cooled in an ice bath and treated with isopropyl amine (245 µl, 4.01 mmol, 5.00 eq.). White solids precipitated soon after. Stirring was continued at room temperature for 72 hours. All volatiles were subsequently removed and residual solids were dissolved in acetone and precipitated with *n*-pentane to give the product as a white powder (171 mg, 556 µmol, 69%).

^{1}H NMR ($CDCl_3$, 598.61 MHz, 300 K): δ = 1.22 (d, 6H, ^{3}J(H,H) = 6.6 Hz, H16, H16'), 4.16 (ds, 1H, ^{3}J(H,H) = 6.7Hz, ^{3}J(H,H) = 6.9 Hz, H15), 6.20 (d, 1H, ^{3}J(H,H) = 6.8 Hz, H14), 6.97 (s, 1H, H8), 7.26-7.29 (m, 1H, H12), 7.31-7.34 (m, 2H, H11), 7.40-7.41 (m, 2H, H10), 7.44-7.46 (m, 2H, H2), 7.53-7.56 (m, 1H, H1), 7.84-7.85 (m, 2H, H3), 7.92 (s, 1H, H6) ppm.

$^{13}C\{^1H\}$ NMR ($CDCl_3$, 150.54 MHz, 300 K): δ = 22.8 (C16), 42.3 (C15), 126.2 (C8), 127.7 (C3), 128.9 (C2), 128.9 (C12), 129.0 (C11), 129.2 (C10), 130.2 C7), 132.5 (C1), 133.2 (C4), 134.0 (C9), 165.1 (C13), 166.3 (C5) ppm.
HRMS (ESI): m/z calcd. for $C_{19}H_{19}N_2O_2$ $[M-H]^-$: 307.14520; found: 307.14531.
FTIR: $\tilde{\nu}$ = 687.5 (s), 902 (m), 1277 (s), 1479 (s), 1512 (s), 1621 (s), 2873 (w), 2935 (w), 2969 (m), 3056 (m), 3214 (bs) cm^{-1}.

7.4.17 PhCO-ΔPhe-NHEt (47c)

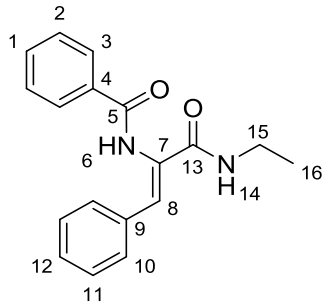

Azlactone **46** (200 mg, 0.80 mmol, 1.00 eq.) was dissolved in chloroform (5 ml). The clear solution was cooled in an ice bath and treated with ethylamine (2 M in ethanol, 2.00 ml, 4.00 mmol, 5.00 eq.) and white solids precipitated soon after. Stirring was continued at room temperature for 16 hours. All volatiles were subsequently removed and residual solids were washed with ethyl acetate (10 ml) to give the product as a white powder (172 mg, 583 µmol, 73%).

^1H NMR ($CDCl_3$, 399.87 MHz, 300 K): δ = 1.18 (t, 3H, $^3J(H,H)$ = 7.2 Hz, H16), 3.37 (dt, 1H, $^3J(H,H)$ = 13.1 Hz, $^3J(H,H)$ = 7.1 Hz, H15), 6.50 (s, 1H, H14), 6.99 (s, 1H, H8), 7.28-7.33 (m, 3H, H11 and H12), 7.38-7.43 (m, 2H, H10), 7.44-7.47 (m, 2H, H2), 7.54 (t, 1H, $^3J(H,H)$ = 7.5 Hz, H1), 7.85 (d, 2H, $^3J(H,H)$ = 8.3 Hz, H3), 8.05 (s, 1H, H6) ppm.
$^{13}C\{^1H\}$ NMR ($CDCl_3$, 100.54 MHz, 300 K): δ = 14.8 (C16), 35.1 (C15), 126.9 (C8), 127.7 (C3), 128.9 (C2), 128.9 (C11), 129.0 (C12), 129.2 (C10), 130.1 (C7), 132.4 (C1), 133.1 (C4), 134.0 (C9), 166.0 (C13), 166.5 (C5) ppm.
HRMS (ESI): m/z calcd. for $C_{18}H_{17}N_2O_2$ $[M-H]^-$: 293.12955; found: 293.12964.
FTIR: $\tilde{\nu}$ = 686 (s), 903 (m), 1274 (s), 1482 (s), 1482 (s), 1520 (s), 1630 (s), 2870 (w), 2932 (m), 2971 (m), 3073 (m), 3205 (bs), 3249 (bm) cm^{-1}.

7.4.18 Seeding experiments with bisphosphinite ligand 41a

A solution of ligand **41a** in dry and degassed THF-d8 was prepared and appropriate amounts of additive were added. For spectrum e), an aliquot of the final solution was taken and diluted.
The pure ligand shows similar properties to previously investigated bis(diamido)-substituted bisphosphine ligand. Two sets of signals, one sharp singlet and two broad singlets of equal intensity were found. In accordance with results from previous studies on the bisphosphine, it was concluded that they represent a monomeric ligand rotamer (S_{ax})-**41a** (sharp singlet) and a dimerized rotamer (R_{ax})-**41a** (two broad singlets). Addition of the additive substantially diminishes the S_{ax} rotamer, while the R_{ax} rotamer accumulates (newly formed singlet signal).

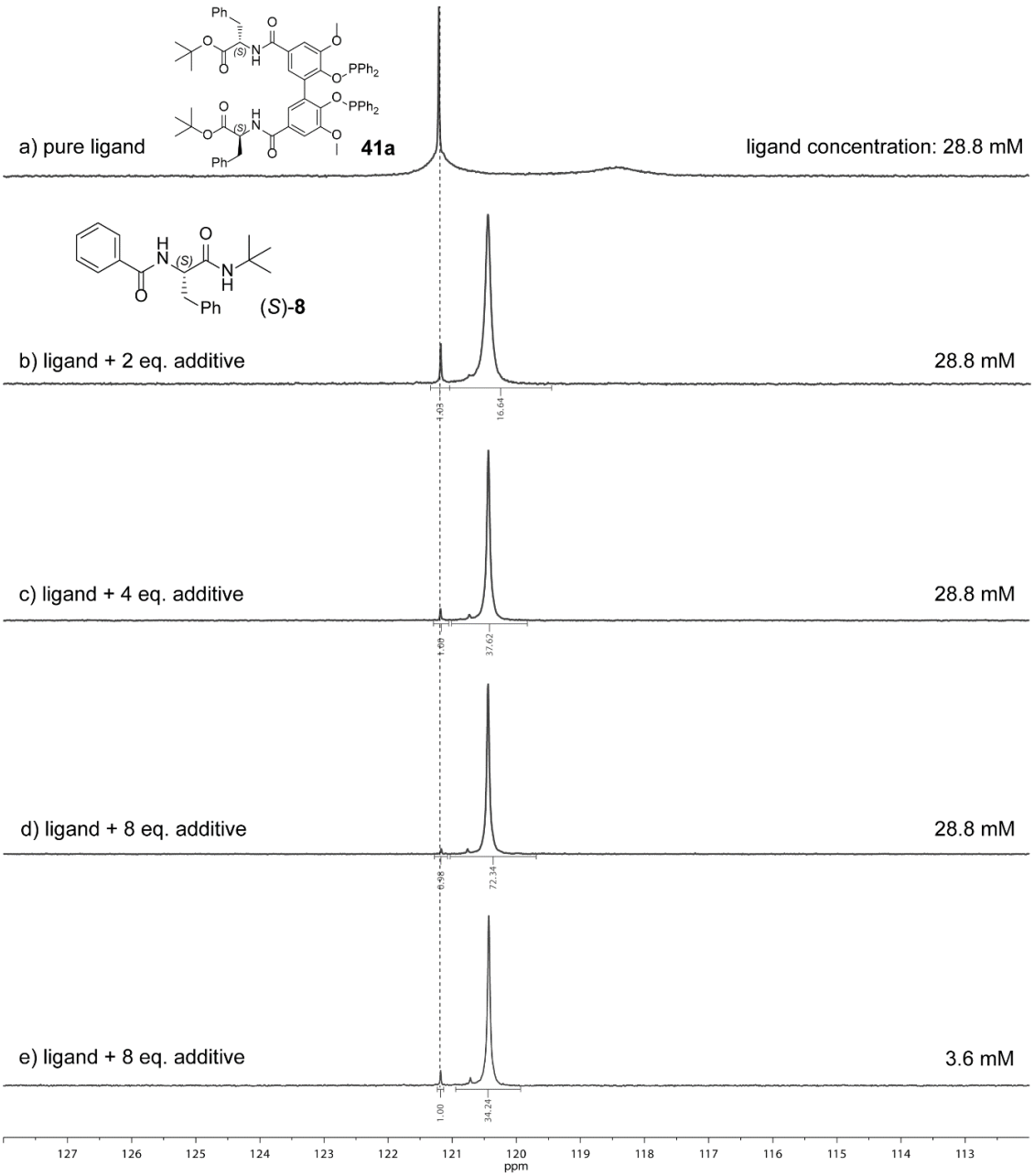

Figure 7-26: Interactions studies of ligand **41a** with different equivalents of diamide (*S*)-**25**.

7.4.19 Seeding experiments with bisphosphinite complex 42a

A solution of complex **42a** (4.3 mM) in dry and degassed $CDCl_3$ was prepared. For each seeding experiment, one additive was added in excess (5 eq. for compound **24**, 10 eq. for all other compounds) and clear solutions formed for all mixtures, but those containing compounds (*S*)-**9** and (*S*)-**35**, where the diamide only partly dissolved. Re-equilibration was monitored by ^{31}P NMR spectroscopy. All mixtures were found to reach their new equilibrium in less than 20 hours.

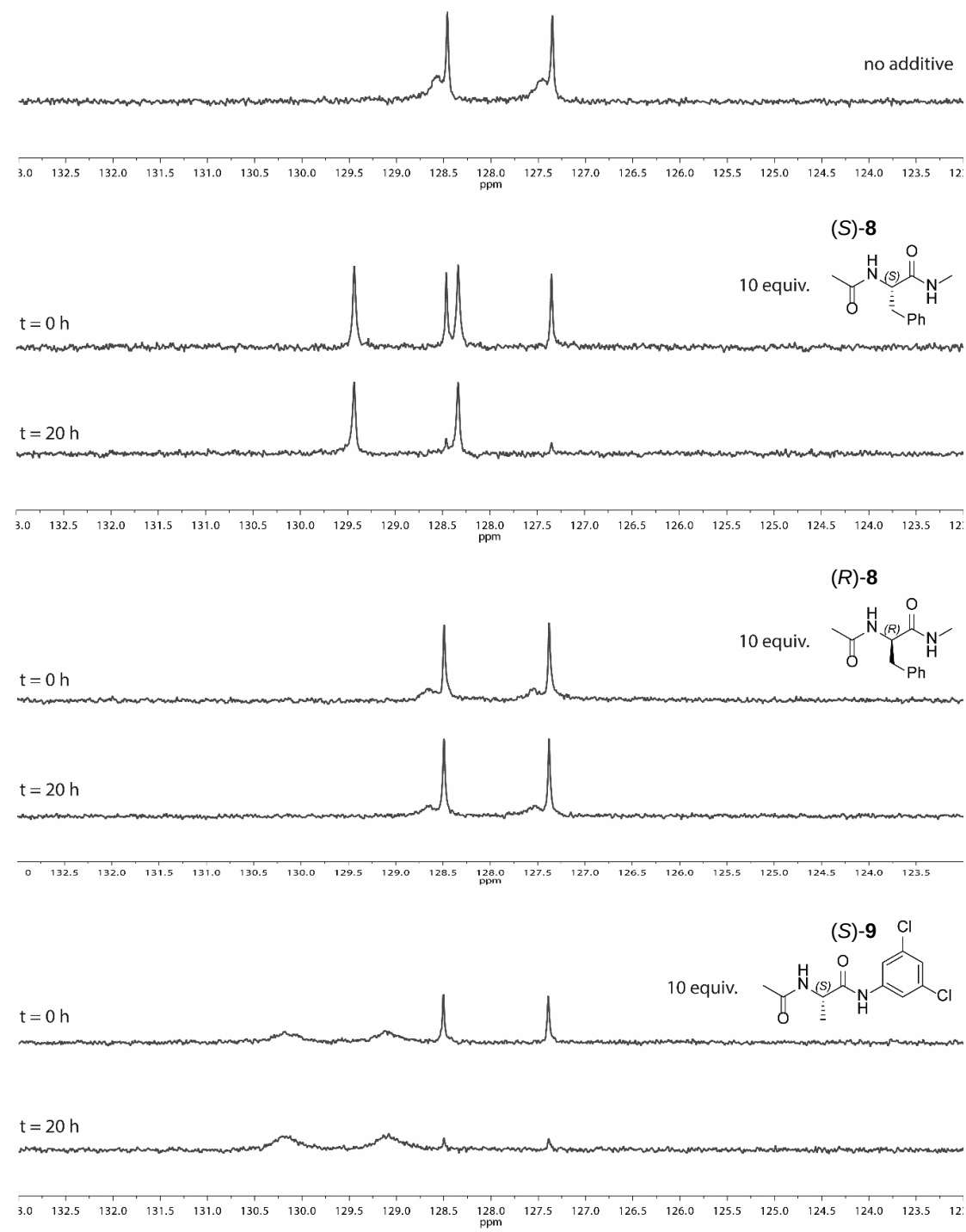
no additive
(S)-8
10 equiv.
t = 0 h
t = 20 h
(R)-8
10 equiv.
t = 0 h
t = 20 h
(S)-9
10 equiv.
t = 0 h
t = 20 h
ppm

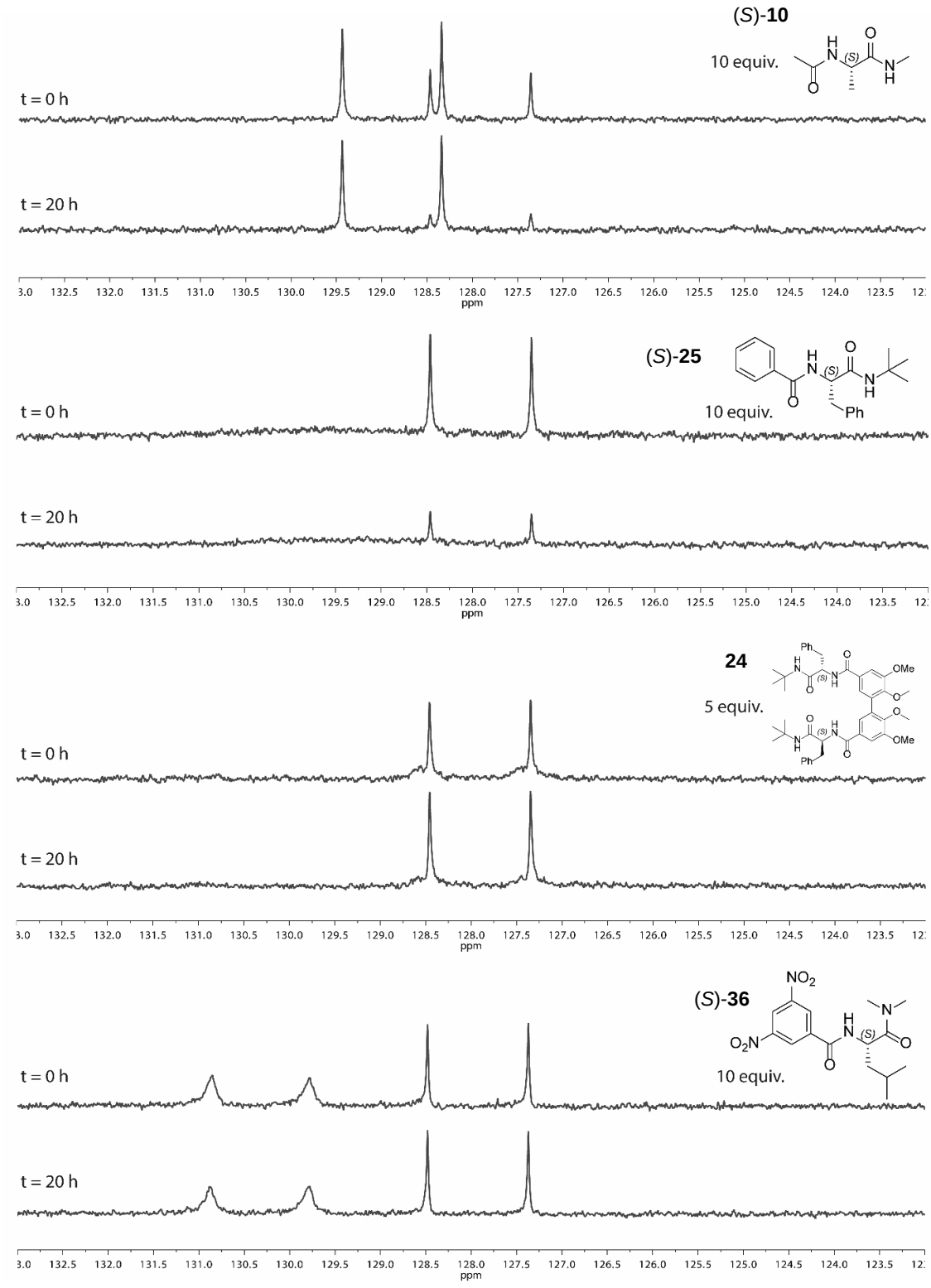
(S)-10
10 equiv.
t = 0 h
t = 20 h
ppm
(S)-25
10 equiv.
Ph
t = 0 h
t = 20 h
ppm
24
5 equiv.
OMe
t = 0 h
t = 20 h
ppm
(S)-36
10 equiv.
t = 0 h
t = 20 h
ppm

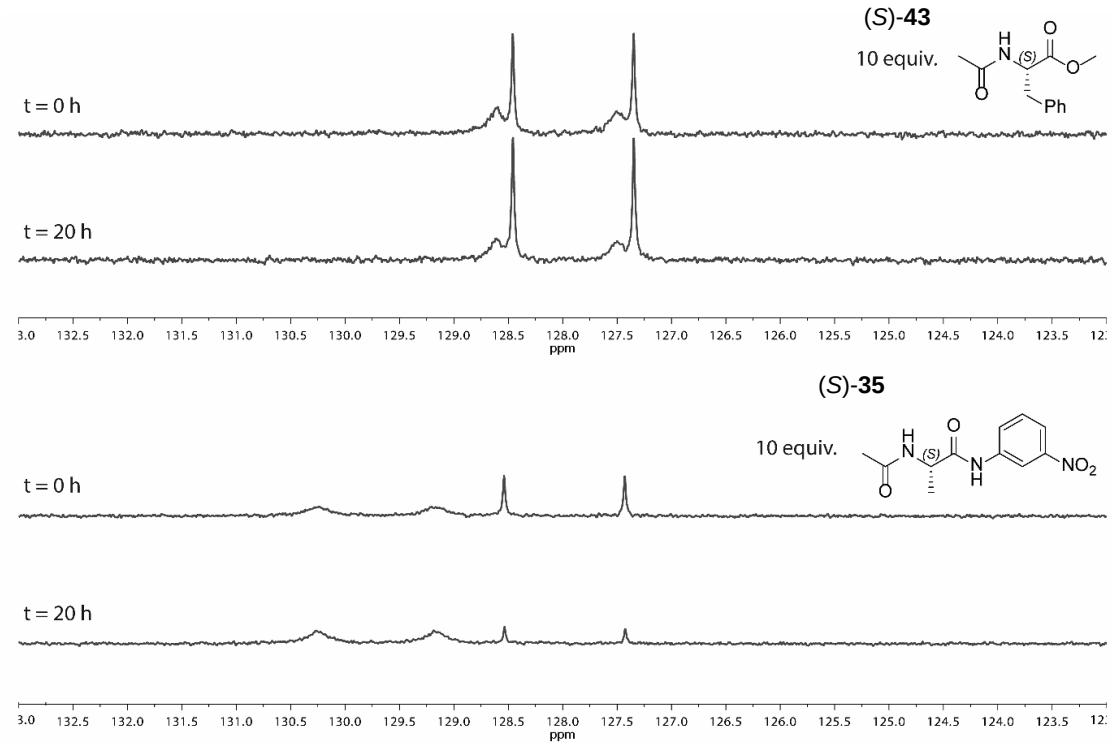

Figure 7-27: Equilibration of complex **42a** in presence of various amino acid-derived additives.

7.4.20 Seeding experiments with bisphosphinite complex 42b

A solution of complex **42b** (4.3 mM) in dry and degassed $CDCl_3$ was prepared. For each seeding experiment, one additive was added in excess (5 eq. for compound **24**, 10 eq. for the other compounds) and clear solutions formed for all mixtures, except for compound (*S*)-**9**, where the diamide only partly dissolved. Re-equilibration was monitored by ^{31}P NMR spectroscopy and all spectra shown below depict fully equilibrated mixtures. No significant change for the distribution of ligand rotamer species could be detected with any of the employed additives.

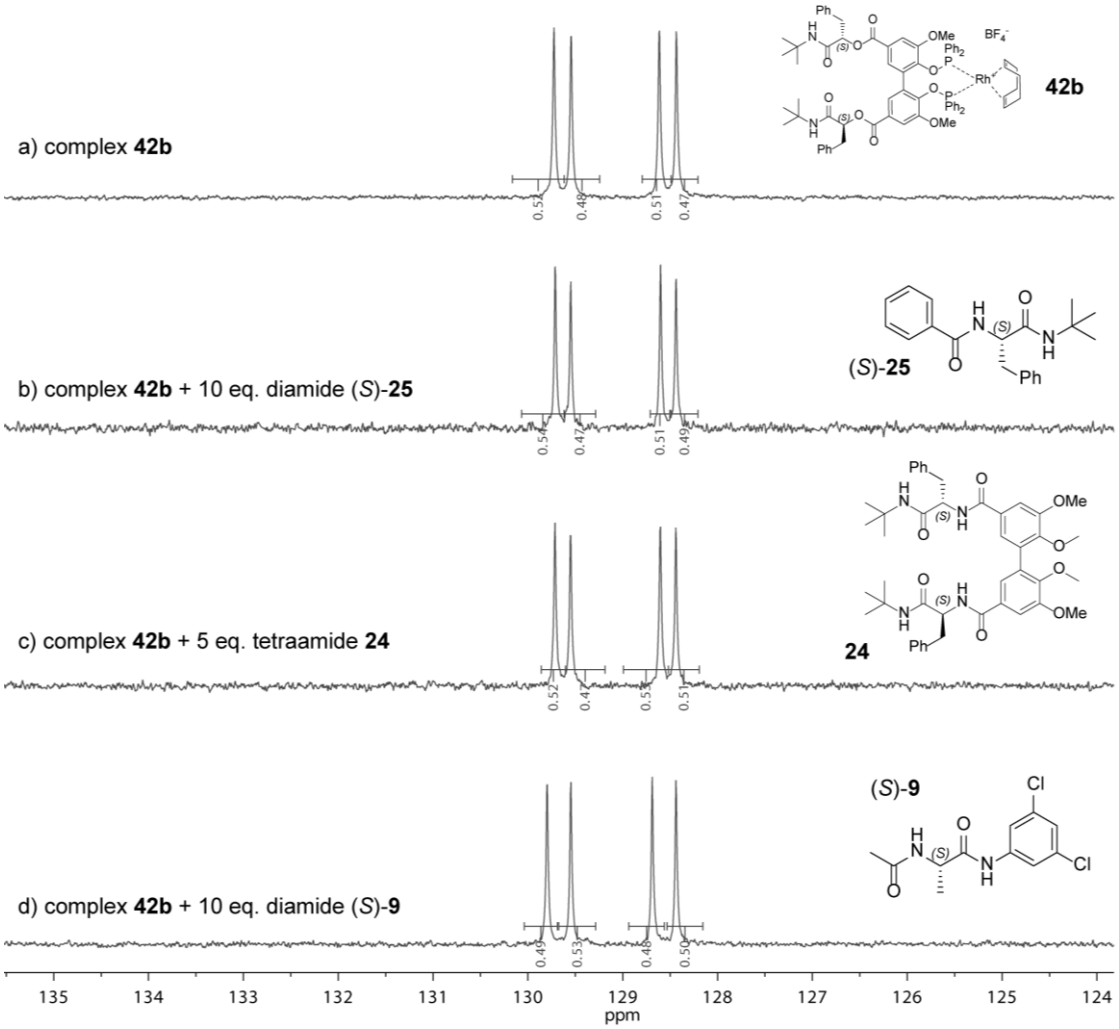

Figure 7-28: Equilibration of complex **42b** in presence of various amino acid derivatives.

7.4.21 Seeding experiments with phosphoramidite complex 45

A solution of complex **45** (4.3 mM) in dry and degassed $CDCl_3$ was prepared. For each seeding experiment, the appropriate amount of additive was added and clear solutions formed. The NMR spectrum of the pure complex shows a variety of signals which is in accordance with previously reported complexes of similar nature and potentially arises due to fast interconversion of different rotamers. See SI of this reference for further information.[40]
Addition of the *S* enantiomer of the chiral additive shows a distinct change of the spectrum, where the multitude of small signals is replaced by two potential doublets of different intensity. This also happens when a racemic mixture of the additive is employed, which proves that enantioselective interactions occur for this ligand, as well.

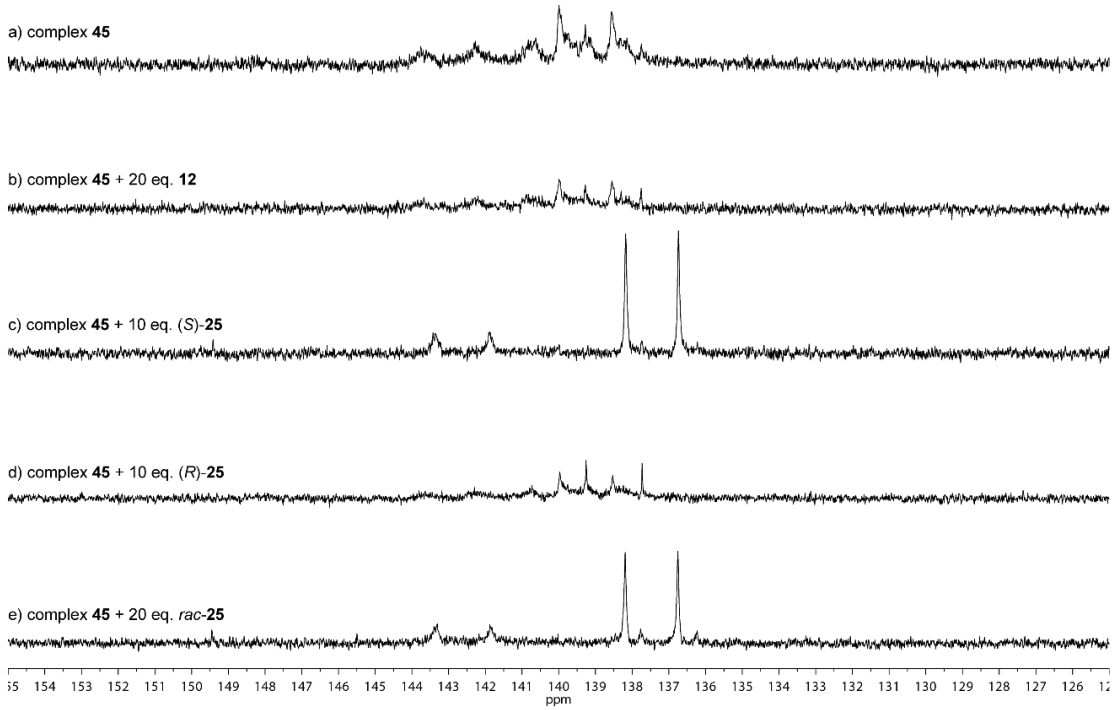

Figure 7-29: Interaction studies between phosphoramidite complex **45** and additives *(S)*- and *(R)*-**25**.

7.4.22 Hydrogenation experiments

For hydrogenation experiments with bisphosphinite catalysts **42a** and **42b**, methyl 2-acetamidoacrylate **12** (6.10 mg, 42.6 µmol, 20 eq. with respect to catalyst) was added to the equilibrated mixtures from the seeding experiments.
For hydrogenation experiments with phosphoramidite catalyst **45**, a J.Young NMR tube was charged with the appropriate amount of substrate and additive. The catalyst was added from a stock solution.
The prepared solution was transferred into a nitrogen-filled stainless steel reactor loaded with a standard NMR tube and a small stirring bar. The reactor was pressurized with hydrogen gas (50 bar in case of bisphosphinite complexes, 5 bar in case of phosphoramidite complexes, unless noted otherwise) to initiate the catalysis.

The autoclave was reopened after one day (two days in case of low catalyst concentrations). The solution was passed through a short pipet filled with silica (ca. 3 cm) using ethyl acetate as eluent. Evaporation gave the hydrogenation product as a yellow oil. Enantiomeric ratio was determined by chiral GC (compound **12**: (6-TBDMS-2,3-Ac)-β-CD, 25 m, i.d. 250 µm, film thickness 250 nm, prepared and coated in the Trapp group, 100 kPa helium, 130 °C, FID detection, k_R = 6.84, k_S = 9.07, α = 1.33) or chiral HPLC (compound **47a**: Chiralpak IE, hexane:isopropanol: 80:20, 1.0 ml/min, 20 °C, 254 nm, t_S = 5.2 min and t_R = 5.8 min; compound **47b**: Chiralpak IE, hexane:isopropanol: 80:20, 0.5 ml/min, 20 °C, 254 nm, t_S = 6.6 min and t_R = 7.2 min; **47c**: Chiralpak IC, hexane:isopropanol: 80:20, 1.0 ml/min, 10 °C, 254 nm, t_S = 7.2 min and t_R = 7.9 min;). Assignment of absolute configuration was accomplished by comparing measurements to those of previously prepared enantiopure samples. All reactions showed full conversion.

7.5 Experimental data for chapter 5

7.5.1 ^{t}BuNH-(*S*)Phe-NH fumarate (51)

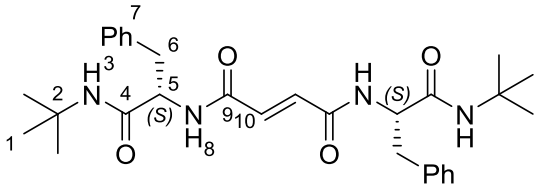

Fumaric acid (50.0 mg, 431 µmol 1.00 eq.) and HOBt (145 mg, 1.08 mmol, 2.50 eq.) were dissolved dry DMF (2 ml) and DIPEA (188 µl, 1.08 mmol, 2.50 eq.) was added. The clear solution was cooled in an ice bath and EDCI.HCl (206 mg, 1.08 mmol, 2.50 eq.) was added. Stirring was continued for 15 minutes and the solution turned orange. (*S*)-Phenylalanine *tert*-butylamide hydrochloride **S2c** (277 mg, 1.08 mmol, 2.50 eq.) was added and after another 15 minutes, the clear, orange solution was warmed to room temperature and stirring was continued. After 16 hours, the mixture was diluted with 25 ml ethyl acetate (25 ml) and solids precipitated. Solids were filtered off and washed with small quantities of fresh ethyl acetate. The organic layer was washed with HCl solution (2 x 25 ml), sat. $NaHCO_3$ solution (2 x 25 ml) and brine (1 x 25 ml). It was dried over sodium sulfate, filtrated and evaporated to give more white solids. Combined solids were finally dried at 50 °C *in vacuo* to yield the product as a beige solid (169 mg, 324 µmol, 75%).

^{1}H-NMR (DMSO-d6, 400 MHz, 298 K) δ = 1.20 (s, 9H, H1), 2.75 (dd, 1H, ^{2}J(H,H) = 13.6 Hz, ^{3}J(H,H) = 9.3, H6^a), 2.75 (dd, 1H, ^{2}J(H,H) = 13.6 Hz, ^{3}J(H,H) = 5.4, H6^b), 4.56 (dt, 1H, ^{3}J(H,H) = 8.9 Hz, ^{3}J(H,H) = 5.3, H5), 6.80 (s, 1H, H10), 7.14-7.26 (m, 5H, H7), 7.58 (s, 1H, H2), 8.53 (d, 1H, ^{3}J(H,H) = 8.6 Hz, H8) ppm.
^{13}C{^{1}H}-NMR (DMSO-d6, 100 MHz, 298 K) δ = 28.4 (C1), 38.2 (C6), 50.1 (C2), 54.4 (C5), 126.2 (C7^p), 127.9 (C7$^{o/m}$), 129.2 (C7$^{o/m}$), 132.7 (C10), 137.7 (C7^i), 163.2 (C9), 170.0 (C4) ppm.
HR-MS (ESI): m/z calcd. for $C_{30}H_{41}N_4O_4^+$, $[M+H]^+$: 521.31223; found: 521.31193.
FTIR: $\tilde{\nu}$ = 698 (s), 1224 (m), 1512 (s), 1632 (s), 2928 (w), 2967 (w), 3064 (w), 3281 (bm) cm^{-1}.

7.5.2 ^{t}BuNH-(*S*)Phe-NH *meso*-2,3-dibromo succinic amide (52)

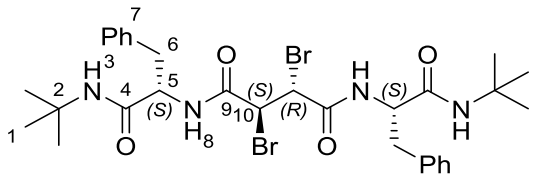

Alkene **51** (123 mg, 236 µmol 1.00 eq.) was suspended in chloroform (6 ml). Bromine was added and the suspension was stirred in the dark for 60 hours. The resulting clear solution was evaporated and the residue was dissolved in ethyl acetate:chloroform (1:1, 5 ml) and passed through a short pad of silica using ethyl acetate as eluent. The collected fraction was concentrated. Addition of *n*-hexane gave white solids that were dried *in vacuo* (159 mg, 235 µmol, 99%).

Additional splitting was observed for some signals, which is caused by the non-equivalence of both molecular halves. Respective signals are indicated as X and X'.

^{1}H-NMR (DMSO-d6, 400 MHz, 298 K) δ = 1.18 (s, 9H, H1), 1.19 (s, H9, H1'), 2.78 (dd, 2H, ^{2}J(H,H) = 13.7 Hz, ^{3}J(H,H) = 8.4, H6^{a}), 2.90 (dd, 2H, ^{2}J(H,H) = 13.7 Hz, ^{3}J(H,H) = 5.9, H6^{b}), 4.74 (dt, 1H, ^{3}J(H,H) = 8.4 Hz, ^{3}J(H,H) = 5.9, H5), 4.52 (dt, 1H, ^{3}J(H,H) = 8.4 Hz, ^{3}J(H,H) = 5.9, H5), 4.89 (s, 2H, H10), 7.14-7.22 (m, 10H, H7), 7.36 (s, 1H, H3'), 7.43 (s, 1H, H3'), 8.82 (d, 1H, ^{3}J(H,H) = 8.4 Hz, H8), 8.83 (d, 1H, ^{3}J(H,H) = 8.4 Hz, H8') ppm.

^{13}C{^{1}H}-NMR (DMSO-d6, 100 MHz, 298 K) δ = 38.2 (C1), 28.3 (C1'), 37.6 (C6), 38.0 (C6'), 44.7 (C10), 45.3 (C10'), 50.2 (C2), 54.2 (C5), 54.4 (C5'), 126.1 (C7^{p}), 126.2 (C7^{p}'), 127.9 (C7$^{o/m}$), 127.9 (C7$^{o/m}$'), 137.2 (C7^{i}), 137.2 (C7^{i}'), 165.4 (C9),165.4 (C9'), 169.2 (C4), 169.2 (C4') ppm.

HR-MS (ESI): m/z calcd. for $C_{30}H_{41}Br^{79}{}_2N_4O_4^+$, $[M+H]^+$: 679.14891; found: 679.14965. m/z calcd. for $C_{30}H_{41}Br^{81}{}_2N_4O_4^+$, $[M+H]^+$: 681.14716; found: 681.14686.

7.5.3 Oxazoline-protected fumaric acid (53)

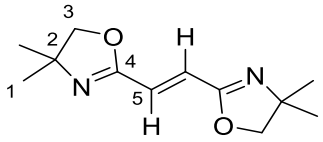

Fumaric acid (1.50 g, 12.9 mmol 1.00 eq.) was suspended in dry DCM (15 ml) and 15 drops of dry DMF were added. The suspension was treated with oxalyl chloride (2.77 ml, 32.3 mmol, 2.50 eq.) and gas evolved. The mixture was stirred at room temperature and a clear, orange solution had formed after 16 hours. In a separate, heat-gun dried flask, 2-amino-2,2-dimethylethanol was dissolved in dry DCM (15 ml) and cooled in an ice bath. The solution with the carboxylic acid chloride was added dropwise, upon which the solution turned yellow and thick solids formed. The suspension was subsequently warmed to room temperature and allowed to stir for another three hours. All volatiles were subsequently removed, residual white solids were placed on a plug of silica and the diol intermediate was eluated with tetrahydrofuran (1.5 L). Evaporation gave white solids.

Formation of the bisoxazoline was done according to a published procedure.[218] The isolated diol (500 mg, 1.94 mmol, 1.00 eq.) was suspended in dry THF (25 ml) and cooled to -78 °C. DAST was added dropwise and the mixture was kept stirring for four hours. For work-up, potassium carbonate (802 mg, 5.81 mmol, 3.00 eq.) was added, the mixture was warmed to room temperature and slowly poured into sat. $NaHCO_3$ solution (100 ml). The aqueous layer was extracted with DCM (3x 100 ml) Combined organic layers were dried over sodium sulfate and evaporated to give a beige solid. Further purification by column chromatography (silica, *n*-pentane:diethyl ether 1:1, R_f = 0.23) gave the product as a white solid (236 mg, 1.06 mmol, 25% over two steps).

^{1}H-NMR (CD_2Cl_2, 600 MHz, 298 K) δ = 1.27 (s, 6H, H1), 3.99 (s, 2H, H3), 6.69 (s, 1H, H5) ppm.
^{13}C{^{1}H}-NMR (CD_2Cl_2, 150 MHz, 298 K) δ = 28.31 (C1), 68.3 (C2), 79.3 (C3), 126.7 (C5), 160.6 (C4) ppm.
HR-MS (ESI): m/z calcd. for $C_{12}H_{19}N_2O_2^+$, $[M+H]^+$: 223.14410; found: 223.14392.
FTIR: $\tilde{\nu}$ = 726 (m), 989 (s), 1298 (s), 1637 (s), 2871 (w), 2894 (w), 2969 (s), 3053 (s) cm^{-1}.

7.5.4 *Meso*-2,3-diacetoxysuccinic acid (54)

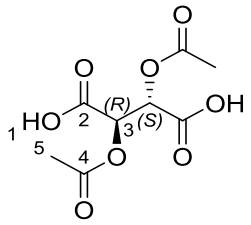

This compound was synthesized according to a known procedure, which was slightly adapted.[222] *Meso*-tartaric acid (1.00 g, 6.66 mmol, 1.00 eq.) and acetyl chloride (467 mg, 59.5 mmol, 42.5 ml, 10.0 eq.) were placed in a heat-gun dried round bottom flask and refluxed for 48 hours. After cooling to room temperature, all volatiles were removed under high vacuum. Last traces of solvent were then evaporated during three freeze-pump-thaw cycles to give the acetyl-protected anhydride as a yellow oil. It was dissolved in THF/H_2O (5:1, 24.0 ml) and stirred overnight at room temperature. The solvent was removed under high vacuum once more and the residue was washed with DCM to give the product as a beige solid that was dried at 50 °C *in vacuo* (1.49 g, 6.36 mmol, 96%).

^{1}H-NMR (DMSO-d6, 400 MHz, 298 K) δ = 2.10 (s, 3H, H5), 5.43 (s, 1H, H3) ppm. Carboxylic acid protons were not observed.
^{13}C{^{1}H}-NMR (DMSO-d6, 400 MHz, 298 K) δ = 20.4 (C5), 70.9 (C3), 167. (C2), 169.5 (C4) ppm.
HR-MS (ESI): m/z calcd. for $C_8H_9O_8^-$, $[M-H]^-$: 233.03029; found: 233.03024.
FTIR: $\tilde{\nu}$ = 656 (s), 683 (s), 769 (s), 805 (w), 879 (s), 923 (m), 1005 (w), 1046 (w), 1078 (s), 1210 (vs), 1277 (s), 1339 (m), 1375 (s), 1437 (m), 1720 (vs), 1738 (vs), 2539 (w), 2595 (w), 2650 (w), 2775 (w), 2874 (w), 2991 (w) cm^{-1}

7.5.5 ^{t}BuNH-(*S*)Phe-NH *meso*-2,3-diacetyloxy succinic amide (55)

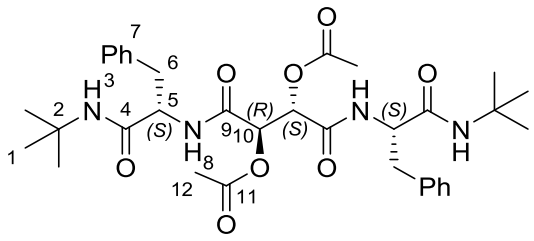

This compound was synthesized according to a known procedure.[223] Compound **54** (200 mg, 0.85 mmol, 1.00 eq.) was dissolved in DCM (2 ml, dry and degassed) and dry DMF (8 drops) were added. The clear solution was subsequently treated with oxalyl chloride (325 mg, 0.22 ml, 2.56 mmol, 3.00 eq.) under evolution of gas. After two hours, all volatiles were removed *in vacuo* and the residue was re-dissolved in DCM (2 ml, dry and degassed). In a second heat-gun dried flask, (*S*)-phenylalanine *tert*-butylamide hydrochloride **S2c** (548 mg, 2.14 mmol, 2.50 eq.) was dissolved in DCM (3 ml, dry and degassed) and DIPEA (662 mg, 0.89 ml, 5.12 mmol, 6.00 eq.) was added. The acetylated succinic acid chloride solution was subsequently added dropwise to the selector solution under formation of fumes. The reaction mixture was stirred for four hours at room temperature, then diluted with ethyl acetate (35 ml), washed with HCl solution (2M, 3 x 35 ml), sat. $NaHCO_3$ solution (2 x 35 ml) and brine (1 x 35 ml), dried over Na_2SO_4, filtered and finally concentrated under reduced pressure to give yellowish solids. These were re-dissolved in DCM and precipitated with *n*-pentane yielding compound **55** as a white powder (309 mg, 0.48 mmol, 57%).

Additional splitting was observed for some signals, which is caused by the non-equivalence of both molecular halves. Respective signals are indicated as X and X'.

^{1}H-NMR ($CDCl_3$, 600 MHz, 298 K) δ = 1.13 (s, 9H, H1), 1.31 (s, 9H, H1'), 2.04 (s, 3H, H12), 2.13 (s, 3H, H12'), 2.80 (dd, 1H, ^{2}J(H,H) = 13.5 Hz, ^{3}J(H,H) = 9.8 Hz, H6^{a}'), 2.93 (dd, 1H, ^{2}J(H,H) = 13.8 Hz, ^{3}J(H,H) = 7.4 Hz, H6^{a}), 3.23 (dd, 1H, ^{2}J(H,H) = 13.5 Hz, ^{3}J(H,H) = 5.1 Hz, H6^{b}'), 3.34 (dd, 1H, ^{2}J(H,H) = 13.8 Hz, ^{3}J(H,H) = 6.0 Hz, H6^{b}), 4.33 (ddd, 1H, ^{3}J(H,H) = 9.8 Hz, ^{3}J(H,H) = 7.3 Hz, ^{3}J(H,H) = 5.1 Hz, H5'), 4.54 (dt, 1H, ^{3}J(H,H) = 7.6 Hz, ^{3}J(H,H) = 5.9 Hz, H5), 4.83 (s, 1H, H3), 5.61 (d, 1H, ^{3}J(H,H) = 2.1 Hz, H10), 5.67 (d, 1H, ^{3}J(H,H) = 2.1 Hz, H10'), 6.06 (s, H, H3'), 6.90 (d, 1H, ^{3}J(H,H) = 7.9 Hz, H8), 7.19-7.34 (m, 10H, H7 and H7'), 7.46 (d, 1H, ^{3}J(H,H) = 7.4 Hz, H8') ppm.

^{13}C{^{1}H}-NMR ($CDCl_3$, 150 MHz, 298 K) δ = 20.6 (C12), 20.7 (C12'), 28.4 (C1), 28.6 (C1'), 37.6 (C6), 38.8 (C6'), 51.5 (C2), 51.6 (C2'), 54.5 (C5), 55.5 (C5'), 72.9 (C10), 127.1 (C7^{p}), 127.2 (C7^{p}'), 128.7 (C7$^{o/m}$), 128.8 (C7$^{o/m}$'), 129.4 (C7$^{o/m}$), 129.4 (C7$^{o/m}$'), 136.7 (C7^{i}), 136.9 (C7^{i}'), 165.1 (C9), 165.9 (C9'), 168.7 (C11), 168.9 (C4), 168.9 (C11'), 169.5 (C4') ppm.

HR-MS (ESI): m/z calcd. for $C_{34}H_{47}N_4O_8^+$, $[M^+H]^+$: 639.33884; found: 639.33901.

FTIR: $\tilde{\nu}$ = 679 (w), 698 (s), 742 (s), 800 (m), 758 (w), 846 (w), 886 (m), 909 (w), 922 (m), 986 (w), 1003 (w), 1044 (m), 1067 (w), 1085 (w), 1130 (m), 1152 (w), 1192 (w), 1216 (s), 1246 (w), 1263 (w), 1287 (w), 1303 (w), 1320 (w), 1365 (m), 1392 (w), 1414 (w), 1453 (s), 1486 (s), 1541 (s), 1596 (m), 1639 (s), 1661 (w), 2870 (w), 2933 (m), 2967 (m), 3030 (w), 3065 (w), 3083 (w), 3298 (s), 3368 (w) cm^{-1}.

7.5.6 ^{t}BuNH-(*S*)Phe-NH *meso*-2,3-dihydroxy succinic amide (56)

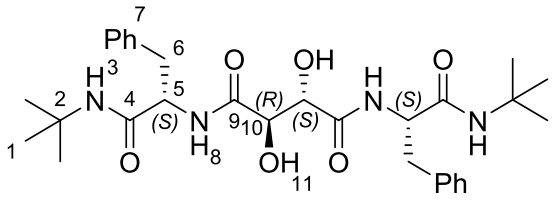

Deprotection was done according to a known protocol with a modified work-up procedure.[236] Compound **55** (500 mg, 783 µmol, 1.00 eq.) was dissolved in methanol (10 ml). K_2CO_3 (1.08 g, 7.83 mmol, 10.0 eq.) was added and the suspension was stirred at 40 °C for 1.5 hours. The suspension was poured onto a short plug of silica and the product was eluated with ethanol. Evaporation gave the desired diol **56** as a white solid (430 mg,780 µmol, quant).

Additional splitting was observed for some signals, which is caused by the non-equivalence of both molecular halves. Respective signals are indicated as X and X'.

^{1}H-NMR (DMSO-d6, 600 MHz, 298 K) δ = 1.13 (s, 9H, H1), 1.27 (s, 9H, H1'), 2.81 (dd, 1H, ^{2}J(H,H) = 13.6 Hz, ^{3}J(H,H) = 6.7 Hz, H6^{a}), 2.96 (dd, 1H, ^{2}J(H,H) = 13.6 Hz, ^{3}J(H,H) = 6.1 Hz, H6^{b}), 2.99-3.05 (m, 2H, H6^{a}' and H6^{b}'), 4.11 (s, 1H, H10'), 4.19 (s, 1H, H10), 4.36-4.43 (m, 2H, H5 and H5'), 6.62 (bs, 2H, H11 and H11'), 7.16-7.25 (m, 10H, H7 and H7'), 7.41 (s, 1H, H3), 7.48 (s, 1H, H3'), 7.52 (d, 1H, ^{3}J(H,H) = 8.1 Hz, H8), 7.60 (d, 1H, ^{3}J(H,H) = 8.6 Hz, H8') ppm.

^{13}C{^{1}H}-NMR (DMSO-d6, 100 MHz, 298 K) δ = 28.3 (C1), 28.5 (C1'), 37.1 (C6'), 38.3 (C6), 50.2 (C2), 50.4 (C2'), 53.3 (C5), 73.8 (C10'), 74.1 (C10), 126.2 (C7^{p}), 126.2 (C7^{p}'), 127.8 (C7$^{o/m}$), 128.1 (C7$^{o/m}$'), 129.2 (C7$^{o/m}$), 129.6 (C7$^{o/m}$'), 137.1 (C7^{i}), 137.9 (C7^{i}'), 169.0 (C4), 169.7 (C4'), 170.1 (C9'), 170.6 (C9) ppm.

HR-MS (ESI): m/z calcd. for $C_{30}H_{43}N_4O_6^+$, $[M+H]^+$: 555.31771; found: 555.31750.

FTIR: $\tilde{\nu}$ = 741 (s), 913 (m), 1080 (s), 1222 (s), 1364 (s), 1454 (s), 1514 (s), 1644 (s), 2873 (w), 2929 (w), 2969 (m), 3031 (w), 3064 (w), 3088 (w), 3308 (bs) cm^{-1}.

7.5.7 ^{t}BuNH-(*S*)Phe-NH *meso*-tartaric acid-derived bisphosphinite (49)

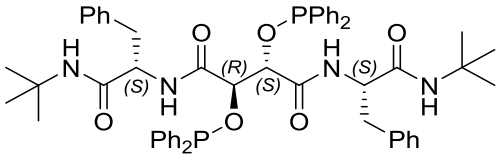

Long term experiment: Compound **56** (20.0 mg, 36.1 µmol, 1.00 eq.) and 4-dimethylaminopyridine (881 µg, 7.21 µmol, 0.20 eq.) were placed in a J. Young NMR tube and dissolved in dry and degassed THF-d8 (0.5 ml). Diethylamino diphenylphosphine (35.7 µl, 144.2 µmol, 4.00 eq.) was added and the mixture was heated to 70 °C and NMR spectra were collected periodically until no further reaction was observed.
Synthesis: Compound **56** (50.0 mg, 90.1 µmol, 1.00 eq.) was dissolved in dry and degassed THF (1.0 ml). Triethylamine (56.5 µl, 406 µmol, 4.50 eq.) was added and the mixture was cooled in an ice bath. Chlorodiphenylphosphine (50.9 µl, 297 µmol, 3.30 eq.) was added dropwise. The suspension was slowly warmed to room temperature and stirring was continued for another three hours. All volatiles were subsequently removed and crude solids washed with *n*-pentane (5 x 2 ml) to yield a grey powder. Traces of $Ph_2P(O)PPh_2$ (side product) still remained and could not be removed without significant loss of product.

^{31}P-NMR (THF-d_8, 161.98 MHz, 295.0 K) δ = 124.5 (s), 123.8 (bs) ppm.

7.6 Selector Preparation

7.6.1 General procedure for the preparation of selector amine hydrochlorides

The *N*-protected amino acid (1.00 eq.) was placed in a dried Schlenk tube and dissolved in dry DMF (about 4 ml/mmol amino acid). DIPEA (2.00 eq.) and the corresponding primary amine (1.10 eq.) were added and the clear solution was cooled in an ice bath. Addition of COMU (1.10 eq.) gave a bright yellow solution that was left stirring to slowly warm to room temperature overnight. For work-up, the solution was diluted with ethyl acetate (10 times the volume of DMF) and the organic layer was washed consecutively with HCl solution (1M, three times), saturated $NaHCO_3$ solution (two times) and brine (two times), dried over sodium sulfate and evaporated. Purification by column chromatography gave the BOC-protected amide as a white solid.
In order to ensure that no racemization occurred during amide formation, enantiopurity of the chiral amides was determined using chiral HPLC (Chiralpak IE, hexane:isopropanol 95:5). All coupling products were obtained with purities >99% *ee*.
For removal of the BOC group, the protected amide (1.00 eq.) was dissolved in THF (about 1 ml/mmol) and HCl in isopropanol (5 M, 10 eq.) was added slowly. The clear solution was stirred at room temperature for 20 hours. After all volatiles were removed, the residual oil was stirred in diethyl ether (100 ml) to give white solids that were filtered off , washed another two times with diethyl ether (100 ml each) and were finally dried *in vacuo*.

7.6.1.1 ^{t}BuNH-(*S*)Val-NH selector ((*S*)-S2a)

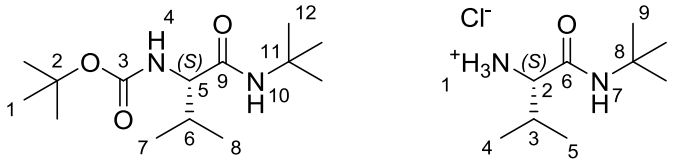

The compound was synthesized according to the general procedure described above using (*tert*-butoxycarbonyl)-L-valine (5.00 g, 23.0 mmol). After column chromatography (silica, *n*-pentane:ethyl acetate 3:1, R_f = 0.12), BOC-protected valine *tert*-butyl amide (*S*)-**S1a** was obtained as a white solid (4.20 g, 15.4 mmol, 67%).

Deprotection (4.20 g, 15.4 mmol) gave the corresponding amine hydrochloride (*S*)-**S2a** as a white, fluff y solid (3.12 g, 15.00 mmol, 97%).

Analytics for BOC protected amide:
^{1}H-NMR ($CDCl_3$, 400.13 MHz, 298 K): δ = 0.90 (d, 3H, ^{3}J(H,H) = 6.8 Hz, H7), 0.94 (d, 3H, ^{3}J(H,H) = 6.8 Hz, H8), 1.34 (s, 9H, H1), 1.43 (s, 9H, H12), 1.90-2.11 (m, 1H, H6), 3.70 (dd, 1H, ^{3}J(H,H) = 6.5 Hz, ^{3}J(H,H) = 8.8Hz, H5), 5.08 (s, 1H, H4), 5.69 (s, 1H, H10) ppm.
^{13}C{^{1}H}-NMR ($CDCl_3$, 100.66 MHz, 298 K): δ = 18.1 (C7), 19.4 (C8), 31.2 (C6), 51.6 (C11), 60.7 (C5), 1179.8 (C3), 156.1 (C3), 170.9 (C9) ppm.
HRMS (ESI): m/z calcd. for $C_{14}H_{28}N_2NaO_3$ $[M+Na]^+$: 295.19921; found: 295.19922.
FTIR: $\tilde{\nu}$ = 881 (w), 1010 (m), 1168 (s), 1251 (s), 1299 (s), 1364 (s), 1527 (s), 1650 (s), 2874 (w), 2933 (w), 2989 (m), 3295 (bs) cm^{-1}.
$[\alpha]_D^{20}$ -13.1 (c 1%, $CHCl_3$).

Analytics for hydrochloride:
^{1}H-NMR (DMSO-d6, 400.33 MHz, 300 K): δ = 0.92 (d, 3H, ^{3}J(H,H) = 6.9 Hz, H4), 0.93 (d, 3H, ^{3}J(H,H) = 6.9 Hz, H5), 1.28 (s, 9H, H9), 2.01-2.12 (m, 1H, H3), 3.55 (d, 1H, ^{3}J(H,H) = 5.9 Hz, H2), 8.14 (s, 1H, H7), 8.17 (s, 3H, H1) ppm.
^{13}C{^{1}H}-NMR (DMSO-d6, 100.66 MHz, 300 K): δ = 17.9 (C4), 18.3 (C5), 28.3 (C9), 29.8 (C3), 50.7 (C8), 57.4 (C2), 167.0 (C6) ppm.
HRMS (ESI): m/z calcd. for $C_9H_{21}N_2O$ $[M-Cl]^+$: 173.16484; found: 173.14938.
FTIR: $\tilde{\nu}$ = 905 (w), 1029 (w), 1224 (s), 1362 (s), 1493 (s), 1544 (s), 1684 (s), 2878 (bs), 2967 (bs), 3028 (bs), 3300 (bw), 3412 (bw) cm^{-1}.
$[\alpha]_D^{20}$ +30.6 (c 1%, MeOH).

7.6.1.2 1-AdNH-(*S*)Val-NH selector ((*S*)-S2b)

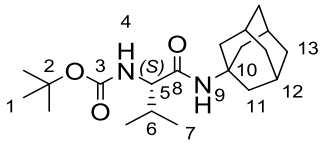
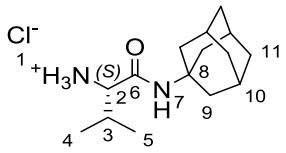

The compound was synthesized according to the general procedure described above using (*tert*-butoxycarbonyl)-L-valine (3.00 g, 13.8 mmol). After column chromatography (silica, *n*-pentane:diethyl ether 3:1, R_f = 0.19), BOC-protected valine adamantyl amide (*S*)-**S1b** was obtained as a white solid (3.78 g, 10.78 mmol, 78%).

Deprotection (3.60 g, 10.3 mmol) gave the corresponding amine hydrochloride (*S*)-**S2b** as a white, fluff y solid (2.74 g, 9.55 mmol, 87%).

Analytics for BOC protected amide:
^{1}H-NMR ($CDCl_3$, 400.13 MHz, 298 K): δ = 0.84 (d, 3H, ^{3}J(H,H) = 6.3 Hz, H8), 0.88 (d, 3H, ^{3}J(H,H) = 6.3 Hz, H7), 1.38 (s, 9H, H1), 1.58-1.63 (m, 6H, H14), 1.53-1.72 (m, 1H, H5), 1.91-1.96 (m, 6H, H12), 1.98-2.05 (m, 3H, H13), 3.58-3.74 (m, 1H, H5), 5.02 (s, 1H, H10), 5.42 (s, 1H, H4) ppm.
^{13}C{^{1}H}-NMR ($CDCl_3$, 100.66 MHz, 298 K): δ = 18.0 (C8), 19.3 (C7), 28.3 (C1), 29.4 (C13), 36.3 (C14), 41.6 (C14), 52.2 (C11), 60.5 (C5), 79.7 (C2), 155.9 (C3), 170.6 (C9) ppm.
HRMS (ESI): m/z calcd. for $C_{36}H_{56}N_4NaO_6$ $[2M+Na]^+$: 723.5031; found: 723.5035.
FTIR: $\tilde{\nu}$ = 881.3 (w), 1170 (s), 1242 (m), 1364 (m), 1522 (bm), 1647 (s), 1682 (m), 2852 (w), 2905 (s), 2972 (w), 3083 (w), 3292 (bs) cm^{-1}.
$[\alpha]_D^{20}$ -18.9 (c 1%, $CHCl_3$).

Analytics for hydrochloride:
^{1}H-NMR (CD_3OD, 400.33 MHz, 300 K): δ = 1.04 (d, 3H, ^{3}J(H,H) = 6.9 Hz, H4), 1.06 (d, 3H, ^{3}J(H,H) = 6.9 Hz, H5), 1.70-1.78 (m, 6H, H8), 2.04-2.09 (m, 9H, H10 and H11), 2.09-2.17 (m, 1H, H3), 3.51 (d, 1H, ^{3}J(H,H) = 5.94 Hz, H2) ppm. No NH protons were observed due to rapid HD exchange.
^{13}C{^{1}H}-NMR (CD_3OD, 100.66 MHz, 300 K): δ = 17.9 (C4), 19.0 (C5), 30.9 (C11), 31.7 (C3), 37.9 (C10), 42.3 (C9), 53.5 (C8), 60.0 (C2), 168.4 (C6) ppm.
HRMS (ESI): m/z calcd. for $C_{15}H_{27}N_2O$ $[M-Cl]^+$: 251.2188; found: 251.2144.
FTIR: $\tilde{\nu}$ = 742 (m), 899 (m), 1091 (s), 1395 (s), 1452 (s), 1507 (s), 1647 (s), 2849 (s), 2902 (s), 3366 (bw) 3428 (bw) cm^{-1}.
$[\alpha]_D^{20}$ +22.8 (c 1%, MeOH).

7.6.1.3 ^{t}Bu-(*S*)Phe-NH selector ((*S*)-S2c)

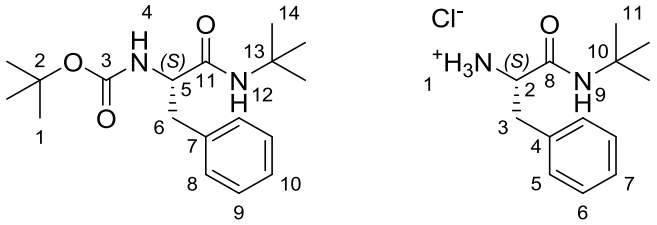

The compound was synthesized according to the general procedure described above using (*tert*-butoxycarbonyl)-L-phenylalanine (4.10 g, 15.5 mmol). After column chromatography (silica, *n*-pentane:diethyl ether 4:1, R_f = 0.14), BOC-protected phenylalanine tert-butyl amide (*S*)-**S1c** was obtained as a white solid (4.80 g, 15.0 mmol, 97%).

Deprotection (4.80 g, 15.0 mmol) gave the corresponding amine hydrochloride (*S*)-**S2c** as a white, fluff y solid (3.35 g, 13.0 mmol, 87%).

Analytics for BOC protected amide:
^{1}H-NMR ($CDCl_3$, 400.33 MHz, 298 K): δ = 1.20 (s, 9H, H14), 1.43 (s, 9H, H1), 2.91 (dd, 1H, ^{3}J(H,H) = 8.33 Hz, ^{2}J(H,H) = 13.45 Hz, H6a), 3.10 (dd, 1H, ^{3}J(H,H) = 5.72 Hz, ^{2}J(H,H) = 13.45 Hz, H6b), 4.14 (m, 1H, H5), 5.16 (bs, 1H, H4), 5.26 (bs, 1H, H12), 7.20-7.21 (m, 3H, H9 and H10), 7.28-7.32 (m, 2H, H8) ppm.
^{13}C{^{1}H}-NMR ($CDCl_3$, 100.66 MHz, 298 K): δ = 28.5 (C1), 28.7 (C14), 39.3 (C6), 51.4 (C13), 56.7 (C5), 80.2 (C2), 127.1 (C10), 128.8 (C9), 129.6 (C8), 137.3 (C7), 155.5 (C3), 170.1 (C11) ppm.
HRMS (ESI): m/z calcd. for $C_{36}H_{56}N_4NaO_6$ $[2M+Na]^+$: 663.4092; found: 663.4092.
FTIR: $\tilde{\nu}$ = 696 (s), 1021 (m), 1170 (s), 1363 (s), 1539 (s), 1653 (s), 2868 (w), 2931 (w), 2972 (m), 3066 (w), 3304 (bs) cm^{-1}.
$[\alpha]_D^{20}$ +8.7 (c 1%, $CHCl_3$).

Analytics for hydrochloride:
^{1}H-NMR ($CDCl_3$, 150.93 MHz, 298 K): δ = 1.15 (s, 9H, H14), 3.18-3.22 (m, 1H, H3a), 3.50-3.58 (m, 1H, H3b), 4.48-4.52 (m, 1H, H2), 6.46 (s, 1H, H9), 7.20-7.25 (m, 1H, H7), 7.26-7.35 (m, 2H, H6), 7.31-7.45 (m, 2H, H5), 8.54 (bs, 3H, H1) ppm.
^{13}C{^{1}H}-NMR ($CDCl_3$, 100.66 MHz, 298 K): δ = 28.6 (C11), 37.8 (C3), 52.1 (C10), 55.3 (C2), 127.6 (C7), 129.0 (C6), 130.1 (C5), 135.0 (C4), 167.1 (C8) ppm.
HRMS (ESI): m/z calcd. for $C_{13}H_{21}N_2O$ $[M-Cl]^+$: 221.1648; found: 221.1647.
FTIR: $\tilde{\nu}$ = 698 (s), 740 (s), 1221 (s), 1456 (s), 1295 (s), 1688 (s), 2899 (bs), 2969 (bs), 3209 (w) 3309 (w) cm^{-1}.
$[\alpha]_D^{20}$ +64.6 (c 1%, $CHCl_3$).

7.6.1.4 ^{t}Bu-(*R*)Phe-NH selector ((*R*)-S2c)

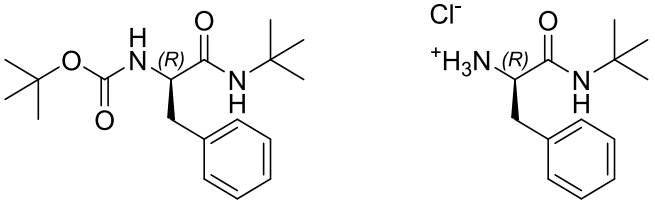

The compound was synthesized according to the general procedure described above using (*tert*-butoxycarbonyl)-D-phenylalanine (3.95 g, 14.9 mmol). After column chromatography (silica, *n*-pentane:diethyl ether 4:1, R_f = 0.14), BOC-protected phenylalanine *tert*-butyl amide (*R*)-S**1c** was obtained as a white solid (4.21 g, 13.1 mmol, 88%).

Deprotection (4.21 g, 13.1 mmol) gave the corresponding amine hydrochloride (*R*)-**S2c** as a white, fluff y solid (3.18 g, 12.3 mmol, 94%).

Analytical NMR, HR-MS and IR data was identical to that of the enantiomers.

Analytics for BOC protected amide:
[α]$_D^{20}$ +8.7 (c 1%, $CHCl_3$).

Analytics for hydrochloride:
[α]$_D^{20}$ +64.6 (c 1%, $CHCl_3$).

7.6.1.5 ^{t}BuNH-Gly-NH selector (S2d)

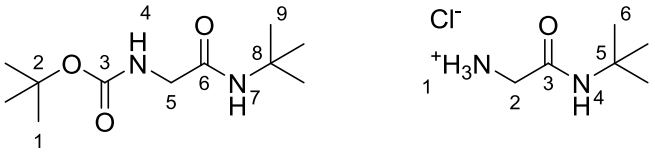

The compound was synthesized according to the general procedure described above using (*tert*-butoxycarbonyl)-glycine (4.92 g, 28.1 mmol). BOC protected glycine *tert*-butyl amide **S1d** was obtained as a white solid.

Deprotection of the amine gave the corresponding hydrochloride **S2d** as a white, fluff y solid (3.70 g, 22.2 mmol, 79% over two steps).

Analytics for crude BOC protected amide:
^{1}H-NMR ($CDCl_3$, 300.51 MHz, 298 K): δ = 1.35 (s, 9H, H9), 1.45 (s, 9H, H1), 3.67 (m, 2H, H5), 5.1 (bs, 1H, H4), 5.80 (s, 1H, H7) ppm.

Analytics for hydrochloride:
^{1}H-NMR (DMSO-d6, 400.13 MHz, 298 K): δ = 1.27 (s, 9H, H6), 3.44 (s, 2H, H2), 8.17 (bs, 3H, H1), 8.19 (s, 1H, H4) ppm.
^{13}C{^{1}H}-NMR (DMSO-d6, 100.66 MHz, 298 K): δ = 18.4 (C6), 30.3 (C5), 40.6 (C2), 155.0 (C3) ppm.
HRMS (EI): m/z calcd. for $C_6H_{15}N_2O$ [M-Cl]$^+$: 131.11789; found: 131.11790.

FTIR: $\tilde{\nu}$ = 705 (s), 925 (s), 1365 (s), 1488 (s), 1560 (s), 1678 (s), 2618 (m), 2680 (m), 2841 (bm), 3060 (bm), 3224 (w) cm^{-1}.

7.6.2 ^{t}BuNH-(*S*)Phe-O selector (S3)

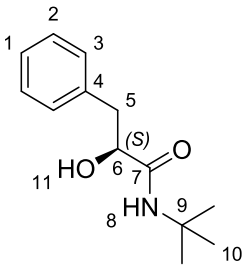

(*S*)-3-Phenyl lactic acid (5.00 g, 30.1 mmol, 1.00 eq.) and HOBt (4.47 g, 33.1 mmol, 1.10 eq.) were dissolved in dry DMF (60 ml). DIPEA (10.5 ml, 60.2 mmol, 2.00 eq.) was added, the solution was cooled in an ice bath and EDCI.HCl (6.34 g, 33.1 mmol, 1.10 eq.) was added. After 15 min, all solids had dissolved and the solution was treated with *tert*-butyl amine (3.48 ml, 33.1 mmol, 1.10 eq.). After 30 minutes at lower temperatures, the mixture was warmed to room temperature again and stirring was continued for 18 hours. The mixture was subsequently diluted with ethyl acetate (500 ml) and washed with HCl solution (2M, 3 x 300 ml), saturated bicarbonate solution (3 x 300 ml) and brine (1 x 300 ml), dried over sodium sulfate and evaporated to give the product as a yellow oil, that crystallized into an amorphous solid after prolonged drying (4.57 g, 20.7 mmol, 69%).

^{1}H NMR ($CDCl_3$, 800.34 MHz, 300 K): δ = 1.29 (s, 9H, H10), 2.78 (bs, 1H, H11), 2.93 (dd, 1H, ^{2}J(H,H) = 13.9 Hz, ^{3}J(H,H) = 7.6 Hz, H5'), 3.12 (dd, 1H, ^{2}J(H,H) = 13.9 Hz, ^{3}J(H,H) = 4.8 Hz, H5), 4.16 (dd, 1H, ^{3}J(H,H) = 7.6 Hz, ^{3}J(H,H) = 4.9 Hz, H6), 6.13 (s, 1H, H8), 7.24-7.26 (m, 3H, H3 and H1), 7.30-7.32 (m, 2H, H2) ppm.
^{13}C{^{1}H} NMR ($CDCl_3$, 201.24 MHz, 300 K): δ = 28.7 (C10), 41.1 (C5), 51.1 (C9), 72.9 (C6), 127.1 (C1), 128.8 (C2), 129.8 (C3), 137.1 (C4), 172.0 (C7) ppm.
HRMS (ESI): m/z calcd. for $C_{13}H_{18}NO_2$ $[M+H]^+$: 220.1343; found: 220.13439.
FTIR: $\tilde{\nu}$ = 697 (s), 742 (s), 1089 (s), 1186 (s), 1223 (s), 1454 (s), 1528 (s), 1642 (s), 1743 (s), 2929 (m), 2968 (m), 3030 (w), 3063 (w), 3088 (w), 3225 (bs), 3335 (w), 3397 (w) cm^{-1}.
$[\alpha]_D^{20}$ -56.5 (c 1%, $CHCl_3$).

7.7 Preparation of additives for chiral alignment

Additives (*S*)- and (*R*)-AcNH-Phe-NHMe (**8**) as well as AcNH-(*S*)Ala-NHMe (**13**) are known compounds and were prepared according to published protocols.[237] Similarly, Ac-(*S*)Phe-OMe (**43**)[237] and (3,5-dinitrobenzoyl)-(*S*)Leu-NMe_2 (**36**)[77] have previously been described elsewhere.

7.7.1 AcNH-(*S*)Ala-NH(3,5-dichlorophenyl) ((*S*)-9)

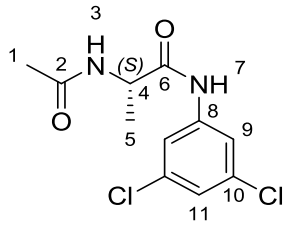

(*S*)-N-Acetyl alanine (200 mg, 1.53 mmol, 1.00 eq.) was suspended in dry DCM (5 ml). EDCI.HCl (322 mg, 1.68 mmol, 1.10 eq.) was added and the mixture was stirred for 15 min to give a clear solution. Subsequently, 3,5-dichloroaniline (260 mg, 1.60 mmol, 1.05 eq.) was added as a solid to give a dark purple solution from which solids precipitated shortly after. After 16 hours, the solids were collected by filtration. The mother liquor was evaporated and the residue slurried in warm acetonitrile from which another batch of solids was obtained. The combined crude product was finally dissolved in ethyl acetate (10 ml) at 65 °C and crystallized in the freezer. This was repeated twice to give the enantiomerically pure product (*S*)-**9** as a white, crystalline solid (150 mg, 1.53 mmol, 36%).

The enantiopurity of the compound was verified by chiral HPLC (Chiralpak IA, hexane:isopropanol 80:20, 1.0 ml/min, t_S = 5.10 min) and was found to be >99% *ee*.

^{1}H-NMR (CD_3OD, 600.24 MHz, 300 K): δ = 1.26 (d, 3H, ^{3}J(H,H) = 7.0 Hz, H5), 1.85 (s, 3H, H1), 4.31 (dt, 1H, ^{3}J(H,H) = 7.0Hz, ^{3}J(H,NH) = 6.9 Hz, H4), 7.27 (t, 1H, ^{3}J(H,H) = 1.8 Hz, H11), 7.67 (d, 2H, ^{3}J(H,H) = 1.8 Hz, H9), 8.24 (d, 1H, ^{3}J(H,H) = 6.9 Hz, H3), 10.33 (s, 1H, H7) ppm.
^{13}C{^{1}H}-NMR (CD_3OD, 150.93 MHz, 300 K): δ = 17.7 (C5), 22.4 (C1), 49.3 (C4), 117.4 (C9), 122.6 (C11), 134.1 (C10), 141.3 (C8), 169.4 (C2), 172.4 (C6) ppm.
HRMS (ESI): m/z calcd. for $C_{11}H_{12}Cl_2N_2NaO_2$ $[M+Na]^+$: 297.0168; found: 297.0170.
FTIR: $\tilde{\nu}$ = 668 (s), 1153 (s), 1409 (s), 1436 (s), 1526 (s), 1586 (s), 1642 (s), 2978 (w), 3086 (w), 3117 (w), 3181 (w), 3257 (w), 3343, (m) cm^{-1}.
$[\alpha]_D^{20}$ -34.9 (c 0.5%, MeOH).

7.7.2 *O,O'*-methylated ^{t}BuNH-(*S*)Phe-NH biphenol (24)

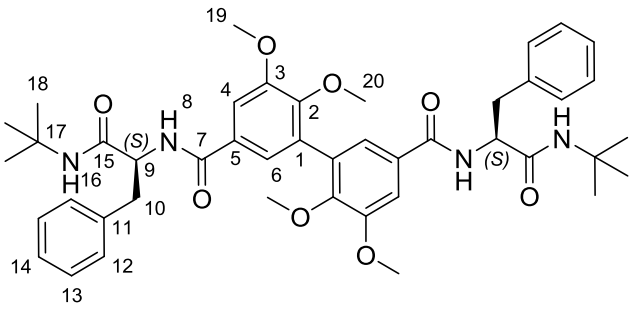

Compound **18c** (180 mg, 244 µmol, 1.00 eq.) was dissolved in dry acetone (20 ml). Caesium carbonate (188 mg, 975 µmol, 4.00 eq.) was added and the mixture was cooled in an ice bath. The cool solution was treated with iodomethane (303 µl, 4.87 mmol, 20.0 eq.) and turned into a gel-like mass. Stirring was continued at room temperature, the gel dissolved overtime and solids formed. After 72 hours, all volatiles were removed and the crude mix was partitioned between water and DCM (20 ml each). Layers were separated and the aqueous layer was extracted with

DCM (20 ml) another two times. Combined organic layers were subsequently washed with brine, dried over sodium sulfate and evaporated to give the methylated compound **24** as a white solid (160 mg, 209 µmol, 86%).

^{1}H-NMR ($CDCl_3$, 600.24 MHz, 298 K): δ = 0.98 (s, 9H, H18), 1.26 (s, 9H, H18‘), 2.98 (dd, 1H, ^{2}J(H,H) = 13.6 Hz, ^{3}J(H,H) = 10.0 Hz, H10b‘), 3.13-3.19 (m, 2H, H10a‘ and H10b), 3.43 (s, 3H, H20‘), 3.44-3.48 (m, 1H, H10a), 3.65 (s, 3H, H19), 3.72 (s, 3H, H20), 3.94 (s, 3H, H19‘), 4.47-4.51 (m, 1H, H9‘), 5.25 (s, 1H, H16‘), 5.54-5.58 (m, 1H, H9), 6.92 (d, 1H, ^{4}J(H,H) = 2.0 Hz, H4), 7.03-7.06 (m, 1H, H14), 7.09-7.12 (m, 2H, H13), 7.19-7.21 (m, 1H, H14‘), 7.23-7.24 (m, 1H, H6), 7.27-7.29 (m, 2H, H12‘ and H13‘), 7.67-7.68 (m, 2H, H12), 7.73 (d, 1H, ^{4}J(H,H) = 2.1 Hz, H6‘), 7.79 (d, 1H, ^{3}J(H,H) = 2.1 Hz, H4‘), 8.21 (s, 1H, H16), 9.34 (d, 1H, ^{3}J(H,H) = 6.3 Hz, H8‘), 9.89 (d, 1H, ^{3}J(H,H) = 9.2 Hz, H8) ppm.
^{13}C{^{1}H}-NMR ($CDCl_3$, 150.93 MHz, 289 K): δ = 27.9 (C18), 28.9 (C18‘), 38.3 (C10‘), 39.0 (C10), 51.0 (C17), 51.6 (C17‘), 55.3 (C19), 56.3 (C9), 56.3 (C19‘), 58.5 (C9‘), 60.7 (C20), 60.8 (C20‘), 111.5 (C4), 112.7 (C4‘), 119.7 (C6), 122.5 (C5‘), 126.4 (C14), 126.9 (C14‘), 127.9 (C13), 128.4 (C5), 128.5 (C13’), 128.8 (C5‘), 129.8 (C12‘), 130.2 (C12), 131.3 (C1‘), 133.2 (C1), 138.0 (C11‘), 139.3 (C11), 148.9 (C2), 150.1 (C2‘), 152.1 (C3), 152.8 (C3‘), 166.0 (C7’), 166.2 (C7), 172.5 (C15‘), 173.7 (C15) ppm.
HRMS (ESI): m/z calcd. for $C_{44}H_{55}N_4O_8$ $[M+H]^+$: 767.40144; found: 767.40033.
FTIR: $\tilde{\nu}$ = 697 (s), 1003 (s), 1223 (s), 1483 (s), 1543 (s), 1627 (s), 2837 (w), 2933 (m), 2967 (m), 3064 (w), 3284 (bm) cm^{-1}.

7.7.3 PhCO-(*S*)Phe-NH^{t}Bu ((*S*)-25)

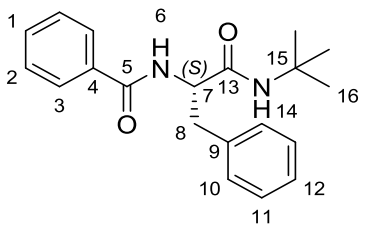

Benzoyl chloride (100 µl, 854 µmol, 1.00 eq.) and DIPEA (327 µl, 1.88 µmol, 2.20 eq.) were mixed in dry DCM (5 ml) and cooled in an ice bath. (*S*)-**2c** (241 mg, 939 µmol, 1.10 eq.) was added as a solid and the clear mixture was subsequently stirred at room temperature for 18 hours. For work-up, the clear solution was diluted in ethyl acetate (40 ml) and the organic layer was washed with HCl solution (40 ml, 2 M, three times), saturated bicarbonate solution (40 ml, two times) and brine (40 ml, once). Drying over sodium sulfate and evaporation gave the diamide (*S*)-**25** as a white, fluffy solid (257 mg, 792 µmol, 93%)

Enantiopurity of the compound was confirmed by chiral HPLC (Chiralpak IE, hexane:isopropanol 80:20, 1.0 ml/min, 20 °C, t_R = 5.2 min).

^{1}H-NMR ($CDCl_3$, 598.17 MHz, 298 K): δ = 1.19 (s, 9H, H16), 2.96 (dd, 1H, ^{3}J(H,H) = 9.3 Hz, ^{2}J(H,H) = 13.4 Hz, H8b), 3.31 (dd, 1H, ^{3}J(H,H) = 5.2 Hz, ^{2}J(H,H) = 13.4 Hz, H8a), 4.66 (ddd, 1H, ^{3}J(H,H) = 9.3 Hz, ^{3}J(H,H) = 7.3 Hz, ^{3}J(H,H) = 5.2 Hz, H7), 5.17 (s, 1H, H14), 7.98 (d, 1H, ^{3}J(H,H) = 7.3 Hz, H6), 7.25-7.28 (m, 1H, H12), 7.30-7.35 (m, 4H, H10 and H14), 7.41-7.44 (m, 2H, H2), 7.49-7.52 (m, 1H, H1), 7.78-7.80 (m, 2H, H3) ppm.

$^{13}C\{^{1}H\}$-NMR ($CDCl_3$, 150.65 MHz, 298 K): δ = 28.6 (C16), 39.6 (C8), 51.6 (C15), 55.7 (C7), 127.2 (C3), 127.2 (C12), 128.7 (C2), 128.9 (C11), 129.7 (C10), 131.9 (C1), 134.1 (C4), 137.2 (C9), 166.9 (C5), 169.6 (C13) ppm.
HRMS (ESI): m/z calcd. for $C_{20}H_{23}N_2O_2$ $[M-H]^-$: 323.17650; found: 323.17682.
FTIR: $\tilde{\nu}$ = 687 (s), 1224 (m), 1543 (s), 1636 (s), 2923 (w), 2970 (m), 3066 (bw), 3278 (bs) cm^{-1}.
$[\alpha]_D^{20}$ +7.01 (c 1 %, $CHCl_3$).

7.7.4 PhCO-(*R*)Phe-NH^{t}Bu ((*R*)-25)

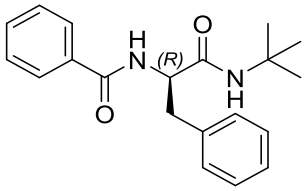

This compound was prepared according to the same procedure as its enantiomer using (*R*)-**S2c** (200 mg, 0.78 mmol) as substrate. The product was obtained as a white solid (230.9 mg, 0.71 mmol, quant.)

Analytical NMR, MS and IR data was identical to that of the enantiomers.

Analytics for diamide:
$[\alpha]^{D}_{20}$ -7.2 (c 1% in $CHCl_3$)

7.7.5 AcNH-(*S*)Ala-NH(3-nitrophenyl) ((*S*)-35)

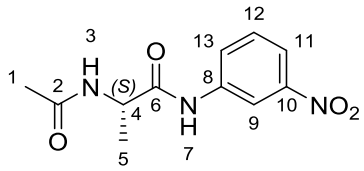

(*S*)-N-acetyl alanine (400 mg, 3.05 mmol, 1.00 eq.) was placed in a dried Schlenk flask and suspended in dry DCM (2 ml). The mixture was cooled in an ice bath and EDCI-HCl (643 mg, 3.36 mmol, 1.10 eq.) was added as a solid. After 15 minutes, all solids had dissolved and 3-nitroaniline (421 mg, 3.05 mmol, 1.00 eq.) was added. After stirring was continued for another 18 hours at room temperature, the solution was diluted more DCM (50 ml). The organic layer was washed with HCl solution (2 M, 3 x 50 ml), saturated bicarbonate solution (2 x 50 ml) and brine (1 x 50 ml), dried over sodium sulfate and evaporated. Resulting solids were recrystallized four times from hot ethyl acetate at 60 °C to give the enantiopure product as a white powder (300 mg, 1.19 mmol, 39 %).

Enantiopurity of the compound was confirmed by chiral HPLC (Chiralpak IE, hexane:isopropanol 80:20, 1.0 ml/min, 20 °C, t_S = 8.3 min).

^{1}H NMR (DMSO-d6, 400.33 MHz, 300 K): δ = 1.30 (d, 3H, $^{3}J(H,H)$ = 7.1 Hz, H5), 1.87 (s, 3H, H1), 4.37 (dq, 1H, $^{3}J(H,H)$ = 7.1 Hz, $^{3}J(H,H)$ = 7.0 Hz, H4), 7.60 (t, 1H, $^{3}J(H,H)$ = 8.2 Hz, H12),

7.89-7.94 (m, 2H, H11 and H13), 8.23 (d, 1H, ^{3}J(H,H) = 6.9 Hz, H3), 8.64 (t, 1H, ^{4}J(H,H) = 2.2 Hz, H9), 10.46 (s, 1H, H7) ppm.
^{13}C{^{1}H} NMR (DMSO-d6, 100.66 MHz, 300 K): δ = 17.7 (C5), 22.4 (C1), 49.3 (C4), 113.3 (C9), 117.8 (C13), 125.2 (C11), 130.2 (C12), 140.1 (C8), 148.0 (C10), 169.4 (C2), 172.3 (C6) ppm.
HRMS (ESI): m/z calcd. for $C_{22}H_{26}N_6NaO_8$ $[M+Na]^+$ 525.17043; found: 525.17131.
FTIR: $\tilde{\nu}$ = 729 (s), 740 (s), 820 (s), 1209 (s), 1294 (s), 1345 (s), 1526 (s), 1599 (s), 1647 (s), 1686 (s), 2950 (w), 3001 (w), 3103 (bm), 3136 (w), 3246 (m) cm^{-1}.
$[\alpha]_{880nm}^{20}$ -1.3 (c 1%, MeOH).

7.7.6 PhCO-(*S*)Phe-OMe (57)

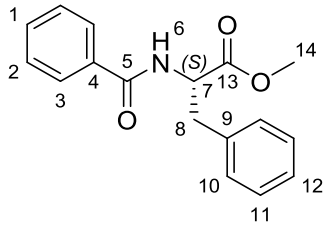

This compound was prepared according to the same procedure as PhCO-Phe-NH^{t}Bu **25**. Using (*S*)-phenylalanine methyl ester (1.10g, 5.09 mmol, 1.10 eq.), DIPEA (537 µl, 4.62 mmol, 2.20 eq.) and benzoic acid chloride (650 mg, 4.62 mmol, 1.00 eq.), the desired amido ester **57** was obtained as a white, waxy solid (1.15 g, 4.06 mmol, 88%).

^{1}H NMR ($CDCl_3$, 589.67 MHz, 300 K): δ = 3.23 (dd, 1H, ^{2}J(H,H) = 13.9 Hz, ^{3}J(H,H) = 5.4 Hz, H8'), 3.30 (dd, 1H, ^{2}J(H,H) = 13.9 Hz, ^{3}J(H,H) = 5.8 Hz, H8) 3.77 (s, 3H, H14), 5.10 (dt, 1H, ^{3}J(H,H) = 7.6 Hz, , ^{3}J(H,H) = 5.6 Hz, H7), 6.57 (d, 1H, ^{3}J(H,H) = 7.5 Hz, H6), 7.13-7.14 (m, 2H, H10), 7.25-7.27 (m, 1H, H12), 7.28-7.31 (m, 2H, H11), 7.41-7.44 (m, 2H, H2), 7.49-7.52 (m, 1H, H1), 7.71-7.73 (m, 2H, H3) ppm.
^{13}C{^{1}H} NMR ($CDCl_3$, 150.55 MHz, 300 K): δ = 37.9 (C8), 52.4 (C14), 53.5 (C7), 127.0 (C8), 127.2 (C12), 128.6 (C11 and C2), 129.3 (C10), 131.8 (C1), 133.9 (C4), 135.8 (C9), 166.8 (C5), 172.0 (C13) ppm.
HRMS (ESI): m/z calcd. for $C_{17}H_{18}NO_3$ $[M+H]^+$: 284.12812; found: 284.12797.
FTIR: $\tilde{\nu}$ = 693 (s), 1172 (s), 1214 (s), 1638 (s), 1739 (s), 2885 (w), 2950 (m), 3031 (w), 3063 (w), 3305 (bs) cm^{-1}.
$[\alpha]_D^{20}$ +105.5 (c 1%, $CHCl_3$).

7.7.7 PhCO-(*S*)Phe-NHEt (58)

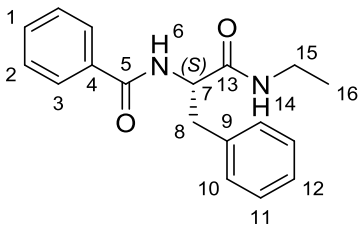

Amido ester **57** (100 mg, 353 µmol, 1.00 eq.) was dissolved in methanol (1 ml) and a solution of ethylamine in methanol (2 M, 1.8 ml) was added. The clear mixture was stirred for 72 hours

and white solids precipitated. All volatiles were subsequently removed and residual solids were re-precipitated from DCM:*n*-pentane to give the pure product as a white, fluffy solid (87.0 mg, 0.29 mmol, 83%).

Enantiopurity of the compound was confirmed by chiral HPLC (Chiralpak IE, hexane:isopropanol 80:20, 1 ml/min, 20 °C, t_R = 8.4 min).

^{1}H NMR ($CDCl_3$, 400.22 MHz, 300 K): δ = 1.01 (t, 3H, ^{3}J(H,H) = 7.3 Hz, H16), 3.08-3.32 (m, 4H, H8 and H8'and H15), 4.81 (dt, 1H, ^{3}J(H,H) = 8.1, ^{3}J(H,H) = 5.9 Hz, H7), 5.81 (s, 1H, H14), 7.04 (d, 1H, ^{3}J(H,H) = 7.7 Hz, H6), 7.25-7.34 (m, 5H, H10 and H11 and H12), 7.42-7.46 (m, 2H, H3), 7.51-7.53 (m, 1H, H1), 7.76-7.78 (m, 2H, H2) ppm.
^{13}C{^{1}H} NMR ($CDCl_3$, 100.65 MHz, 300 K): δ = 14.7 (C16), 34.6 (C15), 39.1 (C8), 55.3 (C7), 127.2 (C2), 128.7 (C3), 128.8 (C11), 129.5 (C10), 131.9 (C1), 133.9 (C4), 137.0 (C9), 167.2 (C5), 170.6 (C13) ppm.
HRMS (ESI): m/z calcd. for $C_{18}H_{19}N_2O_2$ $[M-H]^-$: 295.14520; found: 295.14539.
FTIR: $\tilde{\nu}$ = 699 (s), 1232 (m), 1291 (s), 1527 (s), 1634 (s), 2868 (w), 2929 (m), 2967 (m), 3031 (w), 3063 (w), 3264 (s), 3307 (s) cm^{-1}.
$[\alpha]_D^{20}$ -12.3 (c 1%, $CHCl_3$).

1.1.1 PhCO-(*S*)Phe-NH^{i}Pr (59)

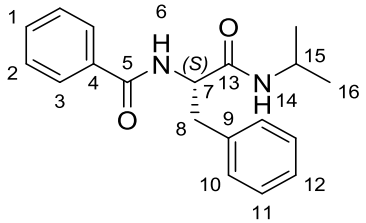

Amido ester **57** (100 mg, 353 µmol , 1.00 eq.) was dissolved in methanol (1 ml) and isopropylamine (0.60 ml, 7.06 mmol, 20.0 eq.) was added. The mixture was stirred at 50 °C for 7 days until no more substrate could be detected by TLC. After cooling to room temperature, all volatiles were removed and residual solids re-precipitated from ethyl acetate:*n*-pentane to give the product as a white solid (83.0 mg, 267 µmol, 76%).

Enantiopurity of the compound was confirmed by chiral HPLC (Chiralpak IE, hexane:isopropanol 80:20, 0.5 ml/min, 20 °C, t_R = 6.55 min).

^{1}H NMR ($CDCl_3$, 598.61 MHz, 300 K): δ = 0.94 (d, 3H, ^{3}J(H,H) = 6.6 Hz, H16), 0.96 (d, 3H, ^{3}J(H,H) = 6.6 Hz, H16'), 3.03 (ddd, 1H, ^{2}J(H,H) = 13.5, ^{3}J(H,H) = 8.9, ^{4}J(H,H) = 1.9 Hz, 8H), 3.26 (ddd, 1H, ^{2}J(H,H) = 13.5, ^{3}J(H,H) = 5.7, ^{4}J(H,H) = 3.3 Hz, H8'), 3.92-4.00 (m, 1H, H15), 4.77 (tdd, 1H, ^{3}J(H,H) = 8.3, ^{3}J(H,H) = 5.6, ^{3}J(H,H) = 2.7 Hz, H7), 5.54-5.62(m, 1H, H14), 7.07-7.08 (m, 1H, H6), 7.22-7.31 (m, 5H, H10 and H11 and H12), 7.41-7.44 (m, 2H, H2), 7.49-7.52 (m, 1H, H19, 7.76-7.78 (m, 2H, H3) ppm.
^{13}C{^{1}H} NMR ($CDCl_3$, 150.54 MHz, 300 K): δ = 22.5 (C16), 22.6 (C16'), 39.4 (C8), 44.7 (C15), 55.4 (C7), 127.2 (C12), 127.2 (C3), 128.7 (C11), 128.8 (C2), 129.6 (C10), 131.9 (C1), 134.0 (C4), 137.0 (C9), 167.0 (C5), 169.8 (C13) ppm.
HRMS (ESI): m/z calcd. for $C_{19}H_{21}N_2O_2$ $[M+H]^+$: 309.16085; found: 309.16095.

FTIR: $\tilde{\nu}$ = 690 (s), 1255 (m), 1327 (m), 1536 (s), 1630 (s), 2872 (w), 2926 (w), 2971 (m), 3023 (w), 2061 (m), 3284 (bs) cm^{-1}.
$[\alpha]_{880nm}^{20}$ +1.6 (c 1%, MeOH).

7.8 Crystallographic data

7.8.1 Compound (R_{ax})-7

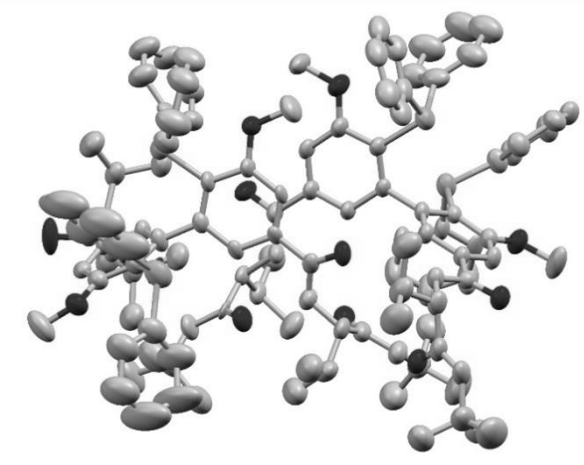

Identification code	jfs2sq
Empirical formula	$C_{60.73}H_{66.74}Cl_{8.21}N_4O_6P_2$
Formula weight	1301.63
Temperature	200(2) K
Wavelength	0.71073 Å
Crystal system	monoclinic
Space group	$P2_1$
Z	4
Unit cell dimensions	
a =	17.729(3) Å α = 90 deg.
b =	17.746(4) Å β = 96.724(5) deg.
c =	24.008(5) Å γ = 90 deg.
Volume	7501(3) $Å^3$
Density (calculated)	1.15 g/cm^3
Absorption coefficient	0.40 mm^{-1}
Crystal shape	polyhedron
Crystal size	0.170 x 0.160 x 0.160 mm^3
Crystal colour	colourless
Theta range for data collection	1.6 to 17.4 deg.
Index ranges	-14≤h≤14, -14≤k≤13, -20≤l≤18
Reflections collected	21959
Independent reflections	8569 (R(int) = 0.1005)
Observed reflections	5441 (I > 2σ(I))
Absorption correction	Semi-empirical from equivalents
Max. and min. transmission	0.95 and 0.84
Refinement method	Full-matrix least-squares on F^2
Data/restraints/parameters	8569 / 2858 / 1482
Goodness-of-fit on F^2	1.02
Final R indices (I>2sigma(I))	R1 = 0.095, wR2 = 0.226
Absolute structure parameter	0.12(8)
Largest diff. peak and hole	0.36 and -0.34 $eÅ^{-3}$

7.8.2 Compound (*S*)-9

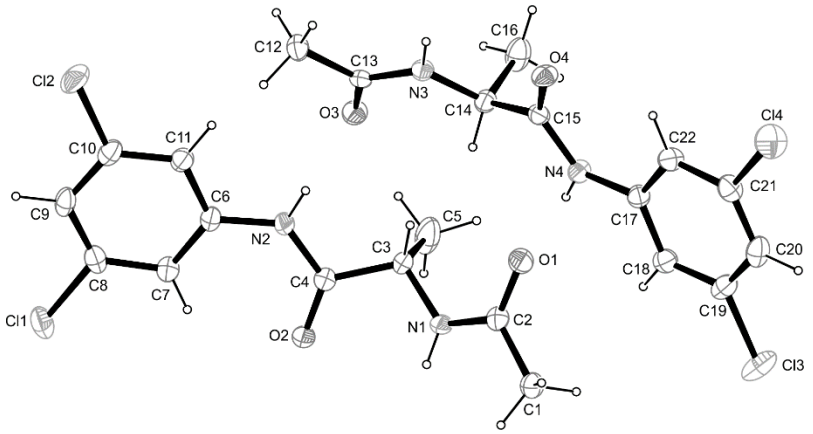

ID	xv019_trapp	refls. measured	37014
net formula	$C_{11}H_{12}Cl_2N_2O_2$	R_{int}	0.0544
M_r/g mol^{-1}	275.13	mean σ(I)/I	0.0351
crystal size/mm	0.100 × 0.030 × 0.020	θ range	2.860–27.101
T/K	110.(2)	observed refls.	5024
radiation	MoKα	x, y (weighting scheme)	0.0248, 0.8813
diffractometer	'Bruker D8 Venture TXS'	hydrogen refinement	H(C) constr, H(N) refall
crystal system	orthorhombic	Flack parameter	0.00(2)
space group	'P 21 21 21'	refls in refinement	5515
a/Å	9.4676(3)	parameters	327
b/Å	12.6190(4)	restraints	0
c/Å	20.9371(8)	$R(F_{obs})$	0.0302
α/°	90	$R_w(F^2)$	0.0721
β/°	90	S	1.054
γ/°	90	shift/error$_{max}$	0.001
V/Å^3	2501.39(15)	max electron density/e Å^{-3}	0.240
Z	8		
calc. density/g cm^{-3}	1.461		
μ/mm^{-1}	0.510		
absorption correction	Multi-Scan		
transmission factor range	0.82–0.99		

7.8.3 Compound 19d

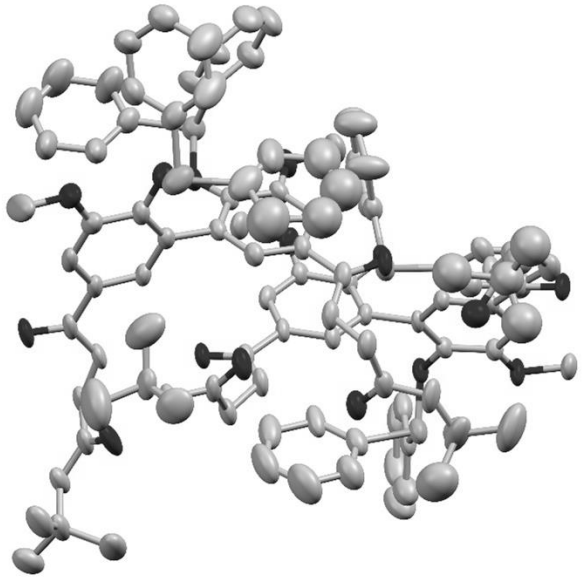

ID	vv186_trapp	refls. measured	43408
net formula	$C_{53.75}H_{58}N_4O_8P_2$	R_{int}	0.0623
M_r/g mol^{-1}	949.98	mean σ(I)/I	0.0941
crystal size/mm	0.100 × 0.080 × 0.050	θ range	3.143–25.338
T/K	100.(2)	observed refls.	23005
radiation	MoKα	x, y (weighting scheme)	0.2000, 0.0000
diffractometer	'Bruker D8 Venture TXS'	hydrogen refinement	constr
crystal system	triclinic	refls in refinement	43408
space group	'P -1'	parameters	2376
a/Å	18.7366(15)	restraints	132
b/Å	25.531(2)	$R(F_{obs})$	0.1038
c/Å	27.891(2)	$R_w(F^2)$	0.3365
α/°	65.696(3)	S	1.090
β/°	82.215(3)	shift/error$_{max}$	0.001
γ/°	80.709(3)	max electron density/e Å^{-3}	1.466
V/Å^3	11964.7(17)	min electron density/e Å^{-3}	−1.151
Z	8		
calc. density/g cm^{-3}	1.055		
μ/mm^{-1}	0.121		
absorption correction	Multi-Scan		
transmission factor range	0.8989–0.9705		

7.8.4 Compound 24

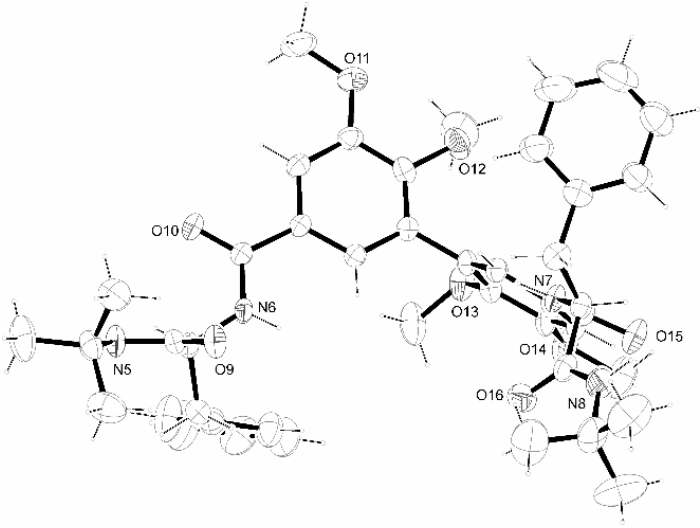

ID	wq035_trapp	absorption correction	Multi-Scan
net formula	$C_{47.15}H_{57.60}N_4O_8$	transmission factor range	0.93–1.00
M_r/g mol^{-1}	808.37	refls. measured	41085
crystal size/mm	0.100 × 0.090 × 0.040	R_{int}	0.0508
T/K	296.(2)	mean σ(I)/I	0.0648
radiation	MoKα	θ range	2.332–25.350
diffractometer	'Bruker D8Quest'	observed refls.	10885
crystal system	orthorhombic	x, y (weighting scheme)	0.0573, 2.1296
space group	'P 21 21 21'	hydrogen refinement	constr
a/Å	17.3902(6)	Flack parameter	−1.0(6)
b/Å	22.2927(10)	refls in refinement	16733
c/Å	23.9010(11)	parameters	1114
α/°	90	restraints	54
β/°	90	$R(F_{obs})$	0.0612
γ/°	90	$R_w(F^2)$	0.1504
V/Å^3	9265.8(7)	S	1.024
Z	8	shift/error$_{max}$	0.001
calc. density/g cm^{-3}	1.159	max electron density/e Å^{-3}	0.291
μ/mm^{-1}	0.079	min electron density/e Å^{-3}	−0.296

7.8.5 Compound (*S*)-25

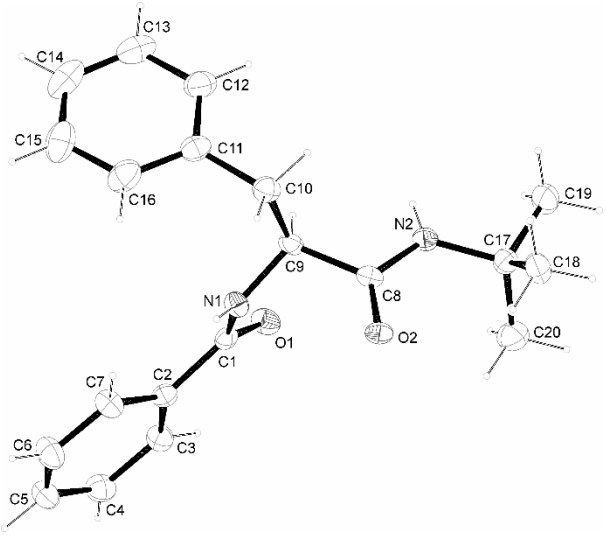

ID	wv089_trapp	absorption correction	Multi-Scan
net formula	$C_{20}H_{24}N_2O_2$	transmission factor range	0.95–1.00
M_r/g mol^{-1}	324.41	refls. measured	47885
crystal size/mm	0.100 × 0.020 × 0.020	R_{int}	0.0488
T/K	100.(2)	mean σ(I)/I	0.0635
radiation	MoKα	θ range	3.136–25.348
diffractometer	'Bruker D8 Venture TXS'	observed refls.	13654
crystal system	monoclinic	x, y (weighting scheme)	0.0343, 0.2107
space group	'P 1 21 1'	hydrogen refinement	H(C) constr, H(N) restr
a/Å	20.9315(6)	Flack parameter	−0.4(4)
b/Å	10.3250(3)	refls in refinement	17123
c/Å	22.0184(6)	parameters	1136
α/°	90	restraints	46
β/°	99.6730(10)	$R(F_{obs})$	0.0428
γ/°	90	$R_w(F^2)$	0.0848
V/Å^3	4690.9(2)	S	1.036
Z	10	shift/error$_{max}$	0.001
calc. density/g cm^{-3}	1.148	max electron density/e Å^{-3}	0.158
μ/mm^{-1}	0.074	min electron density/e Å^{-3}	−0.204

7.8.6 Compound 47a

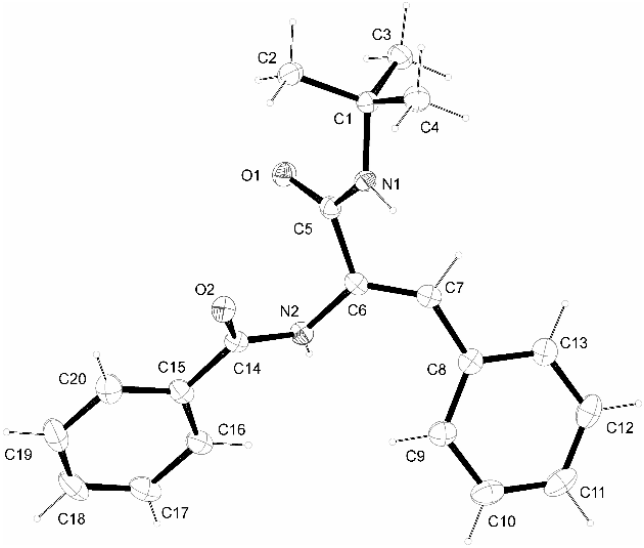

ID	vv796_trapp	absorption correction	Multi-Scan
net formula	$C_{20}H_{22}N_2O_2$	transmission factor range	0.92–1.00
M_r/g mol^{-1}	322.39	refls. measured	4157
crystal size/mm	0.100 × 0.030 × 0.030	R_{int}	0.0517
T/K	103.(2)	mean σ(I)/I	0.0412
radiation	MoKα	θ range	3.271–26.367
diffractometer	'Bruker D8 Venture TXS'	observed refls.	3601
crystal system	tetragonal	x, y (weighting scheme)	0.0517, 3.3665
space group	'I 41 c d'	hydrogen refinement	H(C) constr, H(N) refall
a/Å	23.7003(9)	Flack parameter	0.5
b/Å	23.7003(9)	refls in refinement	4157
c/Å	14.6413(7)	parameters	228
α/°	90	restraints	1
β/°	90	$R(F_{obs})$	0.0443
γ/°	90	$R_w(F^2)$	0.1074
V/Å^3	8224.1(7)	S	1.074
Z	16	shift/error$_{max}$	0.001
calc. density/g cm^{-3}	1.042	max electron density/e Å^{-3}	0.234
μ/mm^{-1}	0.068	min electron density/e Å^{-3}	−0.183

7.8.7 Compound 47c

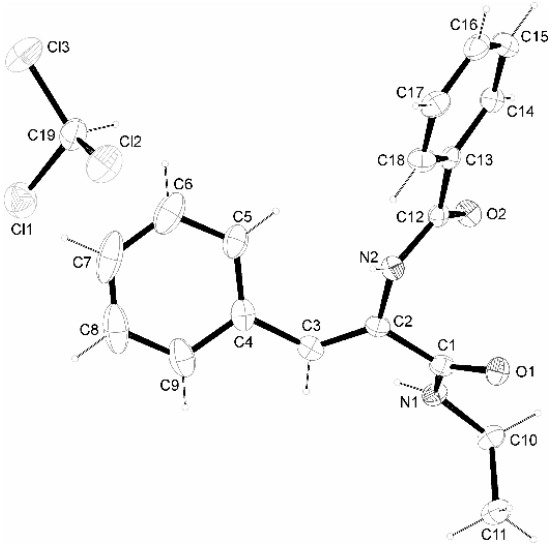

ID	wv096_trapp	absorption correction	Multi-Scan
net formula	$C_{19}H_{19}Cl_3N_2O_2$	transmission factor range	0.91–0.98
M_r/g mol^{-1}	413.71	refls. measured	20081
crystal size/mm	0.100 × 0.050 × 0.040	R_{int}	0.0392
T/K	100.(2)	mean σ(I)/I	0.0343
radiation	MoKα	θ range	3.217–26.363
diffractometer	'Bruker D8 Venture TXS'	observed refls.	3209
crystal system	tetragonal	x, y (weighting scheme)	0.0286, 9.6216
space group	'I 41/a'	hydrogen refinement	H(C) constr, H(N) refall
a/Å	23.4372(6)	refls in refinement	4211
b/Å	23.4372(6)	parameters	244
c/Å	15.0532(4)	restraints	0
α/°	90	$R(F_{obs})$	0.0389
β/°	90	$R_w(F^2)$	0.0860
γ/°	90	S	1.030
V/Å^3	8268.8(5)	shift/error$_{max}$	0.001
Z	16	max electron density/e Å^{-3}	0.406
calc. density/g cm^{-3}	1.329	min electron density/e Å^{-3}	−0.380
μ/mm^{-1}	0.458		

7.8.8 Compound 51

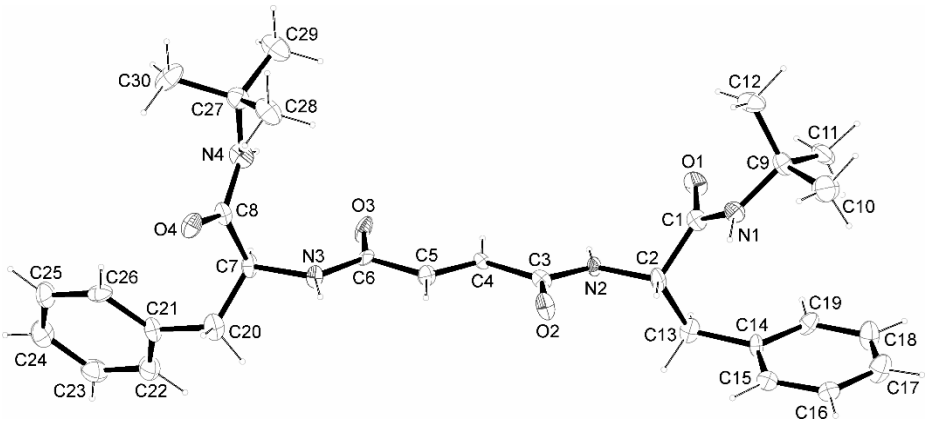

ID	wv070_trapp	absorption correction	Multi-Scan
net formula	$C_{30}H_{40}N_4O_4$	transmission factor range	0.88–1.00
M_r/g mol^{-1}	520.66	refls. measured	51785
crystal size/mm	0.100 × 0.030 × 0.020	R_{int}	0.1049
T/K	100.(2)	mean σ(I)/I	0.1514
radiation	MoKα	θ range	3.141–25.137
diffractometer	'Bruker D8 Venture TXS'	observed refls.	12450
crystal system	monoclinic	x, y (weighting scheme)	0.0633,
space group	'P 1 21 1'	hydrogen refinement	constr
a/Å	9.7167(7)	Flack parameter	−1.0(8)
b/Å	33.897(2)	refls in refinement	19807
c/Å	17.4040(10)	parameters	1394
α/°	90	restraints	13
β/°	90.041(3)	$R(F_{obs})$	0.0665
γ/°	90	$R_w(F^2)$	0.1611
V/Å^3	5732.3(6)	S	1.007
Z	8	shift/error$_{max}$	0.001
calc. density/g cm^{-3}	1.207	max electron density/e Å^{-3}	0.353
μ/mm^{-1}	0.081	min electron density/e Å^{-3}	−0.296

7.8.9 Compound 59

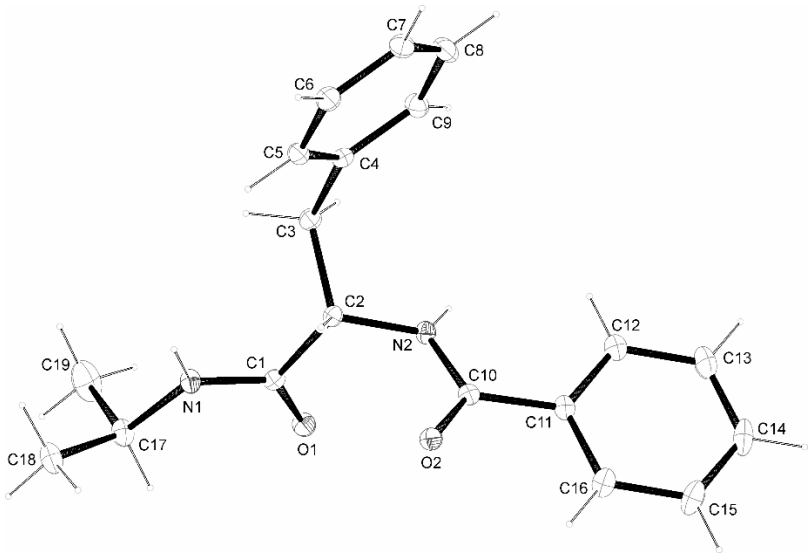

ID	wv422_trapp	absorption correction	Multi-Scan
net formula	$C_{19}H_{22}N_2O_2$	transmission factor range	0.96–1.00
M_r/g mol^{-1}	310.38	refls. measured	18067
crystal size/mm	0.060 × 0.040 × 0.030	R_{int}	0.0461
T/K	110.(2)	mean σ(I)/I	0.0589
radiation	MoKα	θ range	2.890–26.372
diffractometer	'Bruker D8 Venture TXS'	observed refls.	5263
crystal system	triclinic	x, y (weighting scheme)	0.0327, 0.7272
space group	'P -1'	hydrogen refinement	H(C) constr, H(N) refall
a/Å	10.8890(15)	refls in refinement	6961
b/Å	11.6708(16)	parameters	430
c/Å	15.8451(15)	restraints	1
α/°	73.396(4)	$R(F_{obs})$	0.0470
β/°	78.461(3)	$R_w(F^2)$	0.1145
γ/°	62.592(4)	S	1.043
V/Å^3	1707.5(4)	shift/error$_{max}$	0.001
Z	4	max electron density/e Å^{-3}	0.237
calc. density/g cm^{-3}	1.207	min electron density/e Å^{-3}	−0.246
μ/mm^{-1}	0.079		

7.9 Concepts of stereoinduction

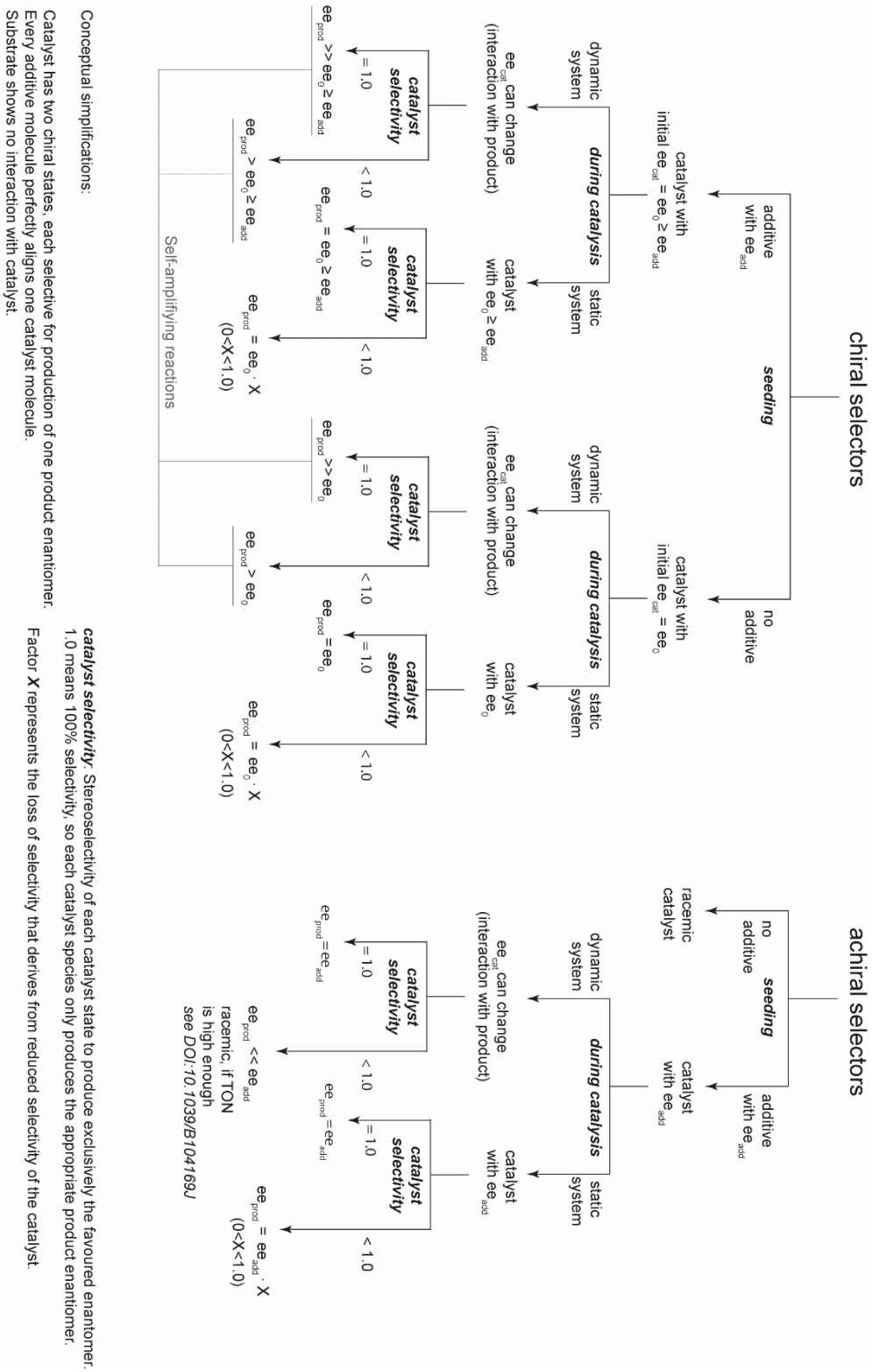

Conceptual simplifications:

Catalyst has two chiral states, each selective for production of one product enantiomer.
Every additive molecule perfectly aligns one catalyst molecule.
Substrate shows no interaction with catalyst.

catalyst selectivity: Stereoselectivity of each catalyst state to produce exclusively the favoured enantiomer. 1.0 means 100% selectivity, so each catalyst species only produces the appropriate product enantiomer.

Factor ***X*** represents the loss of selectivity that derives from reduced selectivity of the catalyst.

8 Bibliography

[1] J. Bailey, *Orig. Life Evol. Biospheres*, **2001**, *31*, 167-183.
[2] P. D. Bailey, *J. Chem. Soc., Chem. Commun.*, **1995**, 1797-1798.
[3] R. G. Cooks, D. Zhang, K. J. Koch, F. C. Gozzo and M. N. Eberlin, *Anal. Chem.*, **2001**, *73*, 3646-3655.
[4] A. Saghatelian, Y. Yokobayashi, K. Soltani and M. R. Ghadiri, *Nature*, **2001**, *409*, 797-801.
[5] H. Moser, G. Ryhs and Hp.Sauter, *Z. Naturforsch.*, **1982**, *B*, 451.
[6] K. Roth, *Chem. unserer Zeit*, **2005**, *39*, 212-217.
[7] O. Trapp, G. Schoetz and V. Schurig, *J. Pharm. Biomed. Anal.*, **2002**, *27*, 497-505.
[8] G. Schoetz, O. Trapp and V. Schurig, *Electrophoresis*, **2001**, *22*, 3185-3190.
[9] T. Eriksson, S. Björkman, B. Roth, Å. Fyge and P. Höuglund, *Chirality*, **1995**, *7*, 44-52.
[10] D. J. Ager, A. H. M. de Vries and J. G. de Vries, *Chem. Soc. Rev.*, **2012**, *41*, 3340-3380.
[11] N. B. Johnson, I. C. Lennon, P. H. Moran and J. A. Ramsden, *Acc. Chem. Res.*, **2007**, *40*, 1291-1299.
[12] L. A. Saudan, *Acc. Chem. Res.*, **2007**, *40*, 1309-1319.
[13] C. Jaekel and R. Paciello, Preparation of optically active aldehydes and ketones via asymmetric hydrogenation, *WO2006040096A1*, **2006**.
[14] W. S. Knowles, *Acc. Chem. Res.*, **1983**, *16*, 106-112.
[15] W. S. Knowles, *J. Chem. Educ.*, **1986**, *63*, 222.
[16] J. L. Bada, *Nature*, **1995**, *374*, 594-595.
[17] S. Mason, *Nature*, **1985**, *314*, 400-401.
[18] W. E. Elias, *J. Chem. Educ.*, **1972**, *49*, 448.
[19] G. Wald, *Ann. N.Y. Acad. Sci.*, **1957**, *69*, 352-368.
[20] F. C. Frank, *Biochim. Biophys. Acta*, **1953**, *11*, 459-463.
[21] R. R. E. Steendam, J. M. M. Verkade, T. J. B. van Benthem, H. Meekes, W. J. P. van Enckevort, J. Raap, F. Rutjes and E. Vlieg, *Nat. Commun.*, **2014**, *5*, 5.
[22] E. Havinga, *Biochim. Biophys. Acta*, **1954**, *13*, 171-174.
[23] T. Satyanarayana, S. Abraham and H. B. Kagan, *Angew. Chem. Int. Ed.*, **2009**, *48*, 456-494.
[24] J. E. Hein and D. G. Blackmond, *Acc. Chem. Res.*, **2012**, *45*, 2045-2054.
[25] M. Klussmann, H. Iwamura, S. P. Mathew, D. H. Wells, U. Pandya, A. Armstrong and D. G. Blackmond, *Nature*, **2006**, *441*, 621-623.
[26] M. H. Todd, *Chem. Soc. Rev.*, **2002**, *31*, 211-222.
[27] E. N. Jacobsen, A. Pfaltz and H. Yamamoto, *Comprehensive Asymmetric Catalysis*, Springer-Verlag Berlin Heidelberg, Heidelberg, **1999**.
[28] T. P. Yoon and E. N. Jacobsen, *Science*, **2003**, *299*, 1691-1693.
[29] R. Noyori and H. Takaya, *Acc. Chem. Res.*, **1990**, *23*, 345-350.
[30] W. Zhang, Y. Chi and X. Zhang, *Acc. Chem. Res.*, **2007**, *40*, 1278-1290.
[31] H. Brunner, *J. Organomet. Chem.*, **1986**, *300*, 39-56.
[32] R. Noyori, *Chem. Soc. Rev.*, **1989**, *18*, 187-208.
[33] K. Maruoka and H. Yamamoto, *J. Am. Chem. Soc.*, **1989**, *111*, 789-790.
[34] J. W. Faller and M. Tokunaga, *Tetrahedron Lett.*, **1993**, *34*, 7359-7362.
[35] J. W. Faller and J. Parr, *J. Am. Chem. Soc.*, **1993**, *115*, 804-805.
[36] T. Ohkuma, H. Doucet, T. Pham, K. Mikami, T. Korenaga, M. Terada and R. Noyori, *J. Am. Chem. Soc.*, **1998**, *120*, 1086-1087.
[37] K. Mikami, M. Terada, T. Korenaga, Y. Matsumoto, M. Ueki and R. Angelaud, *Angew. Chem. Int. Ed.*, **2000**, *39*, 3532-3556.
[38] M. Oeki, *Topics in Stereochemistry*, Wiley, **1983**.
[39] K. Mikami and S. Matsukawa, *Nature*, **1997**, *385*, 613-615.
[40] G. Storch and O. Trapp, *Nat. Chem.*, **2017**, *9*, 179-187.

[41] G. Storch and O. Trapp, *Chirality*, **2018**, *30*, 1150-1160.
[42] G. Storch, F. Maier, P. Wessig and O. Trapp, *Eur. J. Org. Chem.*, **2016**, *2016*, 5123-5126.
[43] O. Desponds and M. Schlosser, *Tetrahedron Lett.*, **1996**, *37*, 47-48.
[44] J. J. Becker, P. S. White and M. R. Gagné, *J. Am. Chem. Soc.*, **2001**, *123*, 9478-9479.
[45] K. Mikami, T. Korenaga, M. Terada, T. Ohkuma, T. Pham and R. Noyori, *Angew. Chem. Int. Ed.*, **1999**, *38*, 495-497.
[46] K. Mikami, K. Aikawa and Y. Yusa, *Org. Lett.*, **2001**, *4*, 95-97.
[47] K. Aikawa, M. Kojima and K. Mikami, *Angew. Chem. Int. Ed.*, **2009**, *48*, 6073-6077.
[48] J. W. Faller and J. C. Wilt, *J. Organomet. Chem.*, **2006**, *691*, 2207-2212.
[49] T. Punniyamurthy, M. Mayr, A. S. Dorofeev, C. J. Bataille, S. Gosiewska, B. Nguyen, A. R. Cowley and J. M. Brown, *Chem. Commun.*, **2008**, 5092-5094.
[50] M. Schmitkamp, D. Chen, W. Leitner, J. Klankermayer and G. Francio, *Chem. Commun.*, **2007**, 4012-4014.
[51] P. Oczipka, D. Muller, W. Leitner and G. Francio, *Chem. Sci.*, **2016**, *7*, 678-683.
[52] J. Yu, T. V. RajanBabu and J. R. Parquette, *J. Am. Chem. Soc.*, **2008**, *130*, 7845-7847.
[53] G. Storch and O. Trapp, *Angew. Chem. Int. Ed.*, **2015**, *54*, 3580-3586.
[54] M. Siebert, G. Storch, F. Rominger and O. Trapp, *Synthesis*, **2017**, *49*, 3485-3494.
[55] S. Carboni, C. Gennari, L. Pignataro and U. Piarulli, *Dalton Trans.*, **2011**, *40*, 4355-4373.
[56] M. Raynal, P. Ballester, A. Vidal-Ferran and P. W. N. M. van Leeuwen, *Chem. Soc. Rev.*, **2014**, *43*, 1660-1733.
[57] J. Wieland and B. Breit, *Nat Chem*, **2010**, *2*, 832-837.
[58] K. M. Wenz, G. Leonhardt- Lutterbeck and B. Breit, *Angew. Chem. Int. Ed.*, **2018**, *57*, 5100-5104.
[59] Z. Kokan and S. I. Kirin, *Eur. J. Org. Chem.*, **2013**, *2013*, 8154-8161.
[60] Z. Kokan, Z. Glasovac, M. Majerić Elenkov, M. Gredičak, I. Jerić and S. I. Kirin, *Organometallics*, **2014**, *33*, 4005-4015.
[61] A. C. Laungani and B. Breit, *Chem. Commun.*, **2008**, 844-846.
[62] P. Dydio, C. Rubay, T. Gadzikwa, M. Lutz and J. N. H. Reek, *J. Am. Chem. Soc.*, **2011**, *133*, 17176-17179.
[63] M. M. Green, M. P. Reidy, R. D. Johnson, G. Darling, D. J. O'Leary and G. Willson, *J. Am. Chem. Soc.*, **1989**, *111*, 6452-6454.
[64] L. Brunsveld, A. P. H. J. Schenning, M. A. C. Broeren, H. M. Janssen, J. A. J. M. Vekemans and E. W. Meijer, *Chem. Lett.*, **2000**, *29*, 292-293.
[65] A. R. A. Palmans, J. A. J. M. Vekemans, E. E. Havinga and E. W. Meijer, *Angew. Chem. Int. Ed. Engl.*, **1997**, *36*, 2648-2651.
[66] L. J. Prins, J. Huskens, F. de Jong, P. Timmerman and D. N. Reinhoudt, *Nature*, **1999**, *398*, 498-502.
[67] L. J. Prins, P. Timmerman and D. N. Reinhoudt, *J. Am. Chem. Soc.*, **2001**, *123*, 10153-10163.
[68] J. J. L. M. Cornelissen, M. Fischer, N. A. J. M. Sommerdijk and R. J. M. Nolte, *Science*, **1998**, *280*, 1427.
[69] B. M. W. Langeveld-Voss, R. J. M. Waterval, R. A. J. Janssen and E. W. Meijer, *Macromolecules*, **1999**, *32*, 227-230.
[70] Y. Nagata, S. Ohashi and M. Suginome, *J. Polym. Sci., Part A: Polym. Chem.*, **2012**, *50*, 1564-1571.
[71] Y. Z. Ke, Y. Nagata, T. Yamada and M. Suginome, *Angew. Chem. Int. Ed.*, **2015**, *54*, 9333-9337.
[72] Y. Nagata, T. Nishikawa and M. Suginome, *J. Am. Chem. Soc.*, **2015**, *137*, 4070-4073.
[73] Y. Akai, T. Yamamoto, Y. Nagata, T. Ohmura and M. Suginome, *J. Am. Chem. Soc.*, **2012**, *134*, 11092-11095.
[74] Y. Nagata, T. Nishikawa and M. Suginome, *ACS Macro Lett.*, **2016**, *5*, 519-522.
[75] F. Maier and O. Trapp, *Angew. Chem. Int. Ed. Engl.*, **2014**, *53*, 8756-8760.

[76] G. Storch, M. Siebert, F. Rominger and O. Trapp, *Chem. Commun.*, **2015**, *51*, 15665-15668.
[77] W. H. Pirkle, P. G. Murray, D. J. Rausch and S. T. McKenna, *J. Org. Chem.*, **1996**, *61*, 4769-4774.
[78] W. H. Pirkle, P. G. Murray and S. R. Wilson, *J. Org. Chem.*, **1996**, *61*, 4775-4777.
[79] H. Frank, G. J. Nicholson and E. Bayer, *J. Chromatogr. Sci.*, **1977**, *15*, 174-176.
[80] P. A. Levkin, A. Levkina and V. Schurig, *Anal. Chem.*, **2006**, *78*, 5143-5148.
[81] G. Uccello-Barretta, S. Nazzi, F. Balzano, P. A. Levkin, V. Schurig and P. Salvadori, *Eur. J. Org. Chem.*, **2007**, *2007*, 3219-3226.
[82] B. Feibush, *J. Chem. Soc. D*, **1971**, 544-545.
[83] H. Frank, G. J. Nicholson and E. Bayer, *Angew. Chem.*, **1978**, *90*, 396-398.
[84] V. Schurig and W. Buerkle, *J. Am. Chem. Soc.*, **1982**, *104*, 7573-7580.
[85] P. A. Levkin, A. Ruderisch and V. Schurig, *Chirality*, **2006**, *18*, 49-63.
[86] P. A. Levkin, A. Levkina, H. Czesla and V. Schurig, *Anal. Chem.*, **2007**, *79*, 4401-4409.
[87] P. A. Levkin, A. Levkina, H. Czesla, S. Nazzi and V. Schurig, *J. Sep. Sci.*, **2007**, *30*, 98-103.
[88] E. Mann, A. Montero, M. A. Maestro and B. Herradón, *Helv. Chim. Acta*, **2002**, *85*, 3624-3638.
[89] B. Herradon, A. Montero, E. Mann and M. A. Maestro, *CrystEngComm*, **2004**, *6*, 513-521.
[90] T. Moriuchi, A. Nomoto, K. Yoshida, A. Ogawa and T. Hirao, *J. Am. Chem. Soc.*, **2001**, *123*, 68-75.
[91] D. R. van Staveren, T. Weyhermuller and N. Metzler-Nolte, *Dalton Trans.*, **2003**, 210-220.
[92] S. I. Kirin, H.-B. Kraatz and N. Metzler-Nolte, *Chem. Soc. Rev.*, **2006**, *35*, 348-354.
[93] M. Rieger and F. H. Westheimer, *J. Am. Chem. Soc.*, **1950**, *72*, 19-28.
[94] K. Aikawa, Y. Miyazaki and K. Mikami, *Bull. Chem. Soc. Jpn.*, **2012**, *85*, 201-208.
[95] J. M. Hopkins, S. A. Dalrymple, M. Parvez and B. A. Keay, *Org. Lett.*, **2005**, *7*, 3765-3768.
[96] D. A. Rankic, J. M. Hopkins, M. Parvez and B. A. Keay, *Synlett*, **2009**, *2009*, 2513-2517.
[97] L. S. Melvin, *Tetrahedron Lett.*, **1981**, *22*, 3375-3376.
[98] N. Kornblum and D. L. Kendall, *J. Am. Chem. Soc.*, **1952**, *74*, 5782-5782.
[99] E. F. Pettersen, T. D. Goddard, C. C. Huang, G. S. Couch, D. M. Greenblatt, E. C. Meng and T. E. Ferrin, *J. Comput. Chem.*, **2004**, *25*, 1605-1612.
[100] J.-C. Hierso, *Chem. Rev.*, **2014**, *114*, 4838-4867.
[101] S. D. Pastor, S. P. Shum, R. K. Rodebaugh, A. D. Debellis and F. H. Clarke, *Helv. Chim. Acta*, **1993**, *76*, 900-914.
[102] A. Wu and L. Isaacs, *J. Am. Chem. Soc.*, **2003**, *125*, 4831-4835.
[103] M. A. Masood, E. J. Enemark and T. D. P. Stack, *Angew. Chem. Int. Ed.*, **1998**, *37*, 928-932.
[104] Y. Ishida and T. Aida, *J. Am. Chem. Soc.*, **2002**, *124*, 14017-14019.
[105] E. Murguly, R. McDonald and N. R. Branda, *Org. Lett.*, **2000**, *2*, 3169-3172.
[106] X. Shi, J. C. Fettinger, M. Cai and J. T. Davis, *Angew. Chem. Int. Ed.*, **2000**, *39*, 3124-3127.
[107] J.-M. Vincent, C. Philouze, I. Pianet and J.-B. Verlhac, *Chem. - Eur. J.*, **2000**, *6*, 3595-3599.
[108] A. T. ten Cate, P. Y. W. Dankers, R. P. Sijbesma and E. W. Meijer, *J. Org. Chem.*, **2005**, *70*, 5799-5803.
[109] O. Trapp, *Anal. Chem.*, **2006**, *78*, 189-198.
[110] C. E. Dalgliesh, *J. Chem. Soc.*, **1952**, 3940-3942.
[111] G. Wells, A. Seaton and M. F. Stevens, *J. Med. Chem.*, **2000**, *43*, 1550-1562.
[112] M. Dindaroğlu, A. Falk and H.-G. Schmalz, *Synthesis*, **2013**, *45*, 527-535.
[113] S. H. Gellman, G. P. Dado, G. B. Liang and B. R. Adams, *J. Am. Chem. Soc.*, **1991**, *113*, 1164-1173.

[114] E. S. Stevens, N. Sugawara, G. M. Bonora and C. Toniolo, *J. Am. Chem. Soc.*, **1980**, *102*, 7048-7050.
[115] G. Fischer, *Chem. Soc. Rev.*, **2000**, *29*, 119-127.
[116] M. J. Deetz, J. E. Fahey and B. D. Smith, *J. Phys. Org. Chem.*, **2001**, *14*, 463-467.
[117] D. G. Davis and A. Bax, *J. Magn. Reson.*, **1985**, *64*, 533-535.
[118] J. Jeener, B. H. Meier, P. Bachmann and R. R. Ernst, *J. Chem. Phys.*, **1979**, *71*, 4546-4553.
[119] Y.-G. Zhou and X. Zhang, *Chem. Commun.*, **2002**, 1124-1125.
[120] T. Saito, T. Yokozawa, T. Ishizaki, T. Moroi, N. Sayo, T. Miura and H. Kumobayashi, *Adv. Synth. Catal.*, **2001**, *343*, 264-267.
[121] S. Wu, W. Wang, W. Tang, M. Lin and X. Zhang, *Org. Lett.*, **2002**, *4*, 4495-4497.
[122] L. R. Steffel, T. J. Cashman, M. H. Reutershan and B. R. Linton, *J. Am. Chem. Soc.*, **2007**, *129*, 12956-12957.
[123] C. K. Woodward and B. D. Hilton, *Annu Rev Biophys Bioeng*, **1979**, *8*, 99-127.
[124] J. M. Brunel, *Chem. Rev.*, **2005**, *105*, 857-898.
[125] Y. Chen, S. Yekta and A. K. Yudin, *Chem. Rev.*, **2003**, *103*, 3155-3212.
[126] F.-Y. Zhang, C.-W. Yip, R. Cao and A. S. C. Chan, *Tetrahedron: Asymmetry*, **1997**, *8*, 585-589.
[127] A. S. C. Chan, F.-Y. Zhang and C.-W. Yip, *J. Am. Chem. Soc.*, **1997**, *119*, 4080-4081.
[128] D. Seebach, D. A. Plattner, A. K. Beck, Y. M. Wang, D. Hunziker and W. Petter, *Helv. Chim. Acta*, **1992**, *75*, 2171-2209.
[129] M. Kitamura, S. Suga, K. Kawai and R. Noyori, *J. Am. Chem. Soc.*, **1986**, *108*, 6071-6072.
[130] K. Soai, A. Ookawa, T. Kaba and K. Ogawa, *J. Am. Chem. Soc.*, **1987**, *109*, 7111-7115.
[131] M. Yoshioka, T. Kawakita and M. Ohno, *Tetrahedron Lett.*, **1989**, *30*, 1657-1660.
[132] in *eLS*.
[133] C.-J. Tsai and R. Nussinov, *PLOS Comput. Biol.*, **2014**, *10*, e1003394.
[134] A. W. Fenton, *Trends Biochem. Sci*, **2008**, *33*, 420-425.
[135] J.-P. Changeux, *Annu. Rev. Biophys.*, **2012**, *41*, 103-133.
[136] V. Blanco, D. A. Leigh and V. Marcos, *Chem. Soc. Rev.*, **2015**, *44*, 5341-5370.
[137] M. Vlatković, B. S. L. Collins and B. L. Feringa, *Chem. - Eur. J.*, **2016**, *22*, 17080-17111.
[138] M. Samanta, V. Siva Rama Krishna and S. Bandyopadhyay, *Chem. Commun.*, **2014**, *50*, 10577-10579.
[139] F. Würthner and J. Rebek, *Angew. Chem. Int. Ed. Engl.*, **1995**, *34*, 446-448.
[140] S. L. Balof, S. J. P'Pool, N. J. Berger, E. J. Valente, A. M. Shiller and H.-J. Schanz, *Dalton Trans.*, **2008**, 5791-5799.
[141] V. Blanco, A. Carlone, K. D. Hänni, D. A. Leigh and B. Lewandowski, *Angew. Chem. Int. Ed.*, **2012**, *51*, 5166-5169.
[142] E. M. Broderick, N. Guo, T. Wu, C. S. Vogel, C. Xu, J. Sutter, J. T. Miller, K. Meyer, T. Cantat and P. L. Diaconescu, *Chem. Commun.*, **2011**, *47*, 9897-9899.
[143] I. M. Lorkovic, R. R. Duff and M. S. Wrighton, *J. Am. Chem. Soc.*, **1995**, *117*, 3617-3618.
[144] J. Gregoliński, M. Hikita, T. Sakamoto, H. Sugimoto, H. Tsukube and H. Miyake, *Inorg. Chem.*, **2016**, *55*, 633-643.
[145] G. Romanazzi, L. Degennaro, P. Mastrorilli and R. Luisi, *ACS Catal.*, **2017**, *7*, 4100-4114.
[146] J. Wang and B. L. Feringa, *Science*, **2011**, *331*, 1429-1432.
[147] S. F. Pizzolato, P. Štacko, J. C. M. Kistemaker, T. van Leeuwen, E. Otten and B. L. Feringa, *J. Am. Chem. Soc.*, **2018**, *140*, 17278-17289.
[148] D. Zhao, T. M. Neubauer and B. L. Feringa, *Nat. Commun.*, **2015**, *6*, 6652.
[149] C.-T. Chen, C.-C. Tsai, P.-K. Tsou, G.-T. Huang and C.-H. Yu, *Chem. Sci.*, **2017**, *8*, 524-529.
[150] Y. Nagata, T. Yamada, T. Adachi, Y. Akai, T. Yamamoto and M. Suginome, *J. Am. Chem. Soc.*, **2013**, *135*, 10104-10113.

[151] L. A. Joyce, M. S. Maynor, J. M. Dragna, G. M. da Cruz, V. M. Lynch, J. W. Canary and E. V. Anslyn, *J. Am. Chem. Soc.*, **2011**, *133*, 13746-13752.
[152] P. Zhang and C. Wolf, *Chem. Commun.*, **2013**, *49*, 7010-7012.
[153] T. Yamamoto, R. Murakami, S. Komatsu and M. Suginome, *J. Am. Chem. Soc.*, **2018**, *140*, 3867-3870.
[154] J. M. Zimbron, X. Caumes, Y. Li, C. M. Thomas, M. Raynal and L. Bouteiller, *Angew. Chem. Int. Ed. Engl.*, **2017**, *56*, 14016-14019.
[155] X. Chen, C. Yamamoto and Y. Okamoto, *Pure Appl. Chem.*, **2007**, *79*, 1561.
[156] Y. Okamoto, R. Aburatani and K. Hatada, *J. Chromatogr. A*, **1987**, *389*, 95-102.
[157] G. Storch, S. Pallmann, F. Rominger and O. Trapp, *Beilstein J. Org. Chem.*, **2016**, *12*, 1453-1458.
[158] G. Storch, L. Deberle, J.-M. Menke, F. Rominger and O. Trapp, *Chirality*, **2016**, *28*, 744-748.
[159] D. J. Frank, A. Franzke and A. Pfaltz, *Chem. - Eur. J.*, **2013**, *19*, 2405-2415.
[160] D. Gaude, R. L. Goaller and J. L. Pierre, *Synth. Commun.*, **1986**, *16*, 63-68.
[161] S. Aiba, N. Takamatsu, T. Sasai, Y. Tokunaga and T. Kawasaki, *Chem. Commun.*, **2016**, *52*, 10834-10837.
[162] B. L. Feringa and R. A. van Delden, *Angew. Chem. Int. Ed.*, **1999**, *38*, 3418-3438.
[163] W. Langenbeck and G. Triem, *Z. Phys. Chem.*, **1936**, *177*, 401-408.
[164] V. A. Pavlov and E. I. Klabunovskii, *Curr. Org. Chem.*, **2014**, *18*, 93-114.
[165] L.-C. Sogutoglu, R. R. E. Steendam, H. Meekes, E. Vlieg and F. P. J. T. Rutjes, *Chem. Soc. Rev.*, **2015**, *44*, 6723-6732.
[166] J. S. Siegel, *Chirality*, **1998**, *10*, 24-27.
[167] W. H. Mills, *Chem. Ind.* , **1932**, 750–759
[168] K. Mislow, *Collect. Czech. Chem. Commun.*, **2003**, *68*, 849-864.
[169] G. Storch, M. Haas and O. Trapp, *Chem. - Eur. J.*, **2017**, *23*, 5414-5418.
[170] T. Williams, R. G. Pitcher, P. Bommer, J. Gutzwiller and M. Uskokovic, *J. Am. Chem. Soc.*, **1969**, *91*, 1871-1872.
[171] A. Tait, E. Colorni and M. Di Bella, *Tetrahedron: Asymmetry*, **1997**, *8*, 2199-2207.
[172] K. C. Cundy and P. A. Crooks, *J. Chromatogr. A*, **1983**, *281*, 17-33.
[173] J. Martens and R. Bhushan, *Helv. Chim. Acta*, **2014**, *97*, 161-187.
[174] V. A. Soloshonok, C. Roussel, O. Kitagawa and A. E. Sorochinsky, *Chem. Soc. Rev.*, **2012**, *41*, 4180-4188.
[175] A. Horeau, *Tetrahedron Lett.*, **1969**, *10*, 3121-3124.
[176] A. Horeau and J. P. Guetté, *Tetrahedron*, **1974**, *30*, 1923-1931.
[177] N. S. Bowman, G. T. McCloud and G. K. Schweitzer, *J. Am. Chem. Soc.*, **1968**, *90*, 3848-3852.
[178] C. Puchot, O. Samuel, E. Dunach, S. Zhao, C. Agami and H. B. Kagan, *J. Am. Chem. Soc.*, **1986**, *108*, 2353-2357.
[179] D. Guillaneux, S.-H. Zhao, O. Samuel, D. Rainford and H. B. Kagan, *J. Am. Chem. Soc.*, **1994**, *116*, 9430-9439.
[180] M. E. Noble-Terán, T. Buhse, J.-M. Cruz, C. Coudret and J.-C. Micheau, *ChemCatChem*, **2016**, *8*, 1836-1845.
[181] M. Kitamura, S. Okada, S. Suga and R. Noyori, *J. Am. Chem. Soc.*, **1989**, *111*, 4028-4036.
[182] A. H. Alberts and H. Wynberg, *J. Am. Chem. Soc.*, **1989**, *111*, 7265-7266.
[183] H. Wynberg and B. Feringa, *Tetrahedron*, **1976**, *32*, 2831-2834.
[184] Y. Shvo, M. Gal, Y. Becker and A. Elgavi, *Tetrahedron: Asymmetry*, **1996**, *7*, 911-924.
[185] H. Danda, H. Nishikawa and K. Otaka, *J. Org. Chem.*, **1991**, *56*, 6740-6741.
[186] M. Szlosek and B. Figadère, *Angew. Chem. Int. Ed.*, **2000**, *39*, 1799-1801.
[187] D. P. Heller, D. R. Goldberg and W. D. Wulff, *J. Am. Chem. Soc.*, **1997**, *119*, 10551-10552.
[188] K. Soai, T. Shibata, H. Morioka and K. Choji, *Nature*, **1995**, *378*, 767-768.
[189] I. Sato, H. Urabe, S. Ishiguro, T. Shibata and K. Soai, *Angew. Chem. Int. Ed.*, **2003**, *42*, 315-317.

[190] K. Soai, T. Kawasaki and A. Matsumoto, *Acc. Chem. Res.*, **2014**, *47*, 3643-3654.
[191] K. Kaneko, Y. Miwa and N. Nakamura, *J. Appl. Polym. Sci.*, **2007**, *105*, 2474-2481.
[192] B. Feibush, *Chirality*, **1998**, *10*, 382-395.
[193] K. Mikami and M. Yamanaka, *Chem. Rev.*, **2003**, *103*, 3369-3400.
[194] K. Aikawa and K. Mikami, *Chem. Commun.*, **2012**, *48*, 11050-11069.
[195] F. Maier and O. Trapp, *Angew. Chem.*, **2014**, *126*, 8901-8905.
[196] Y. Imai, W. Zhang, T. Kida, Y. Nakatsuji and I. Ikeda, *Tetrahedron Lett.*, **1997**, *38*, 2681-2684.
[197] C. Bolm, M. Zehnder and D. Bur, *Angew. Chem. Int. Ed. Engl.*, **1990**, *29*, 205-207.
[198] Q. Jing, C. A. Sandoval, Z. Wang and K. Ding, *Eur. J. Org. Chem.*, **2006**, *2006*, 3606-3616.
[199] K. Mikami, K. Wakabayashi and K. Aikawa, *Org. Lett.*, **2006**, *8*, 1517-1519.
[200] K. Mikami, K. Wakabayashi, Y. Yusa and K. Aikawa, *Chem. Commun.*, **2006**, 2365-2367.
[201] M. Kranenburg, Y. E. M. van der Burgt, P. C. J. Kamer, P. W. N. M. van Leeuwen, K. Goubitz and J. Fraanje, *Organometallics*, **1995**, *14*, 3081-3089.
[202] T. J. Davis, J. Balsells, P. J. Carroll and P. J. Walsh, *Org. Lett.*, **2001**, *3*, 2161-2164.
[203] G. J. Rowlands, *Isr. J. Chem.*, **2012**, *52*, 60-75.
[204] E. Yashima, N. Ousaka, D. Taura, K. Shimomura, T. Ikai and K. Maeda, *Chem. Rev.*, **2016**.
[205] T. P. Dang and H. B. Kagan, *J. Chem. Soc. D*, **1971**, 481-481.
[206] M. D. Fryzuk and B. Bosnich, *J. Am. Chem. Soc.*, **1977**, *99*, 6262-6267.
[207] R. M. Pitzer, *Acc. Chem. Res.*, **1983**, *16*, 207-210.
[208] M. ŌKi, *Proc. Jpn. Acad., Ser. B*, **2010**, *86*, 867-883.
[209] G. A. Bootsma and J. C. Schoone, *Acta Crystallogr.*, **1967**, *22*, 522-532.
[210] U. Rychlewska, N. Wascinska, B. Warzajtis and J. Gawronski, *Acta Crystallogr., Sect. B*, **2008**, *64*, 497-503.
[211] A. M. Costa, C. Jimeno, J. Gavenonis, P. J. Carroll and P. J. Walsh, *J. Am. Chem. Soc.*, **2002**, *124*, 6929-6941.
[212] J. Freiberg, A. Weigt and H. Dilcher, *J. Prakt. Chem. /Chem-Ztg*, **1993**, *335*, 337-344.
[213] U. Nagel, *Angew. Chem.*, **1984**, *96*, 425-426.
[214] A. Terfort, *Synthesis*, **1992**, *1992*, 951-953.
[215] C. Hedberg, K. Källström, P. Brandt, L. K. Hansen and P. G. Andersson, *J. Am. Chem. Soc.*, **2006**, *128*, 2995-3001.
[216] J. L. Bookham, D. M. Smithies, A. Wright, M. Thornton-Pett and W. McFarlane, *J. Chem. Soc., Dalton Trans.*, **1998**, 811-818.
[217] M. A. Shaw and J. C. Tebby, *J. Chem. Soc. C*, **1970**, 5-9.
[218] A. J. Phillips, Y. Uto, P. Wipf, M. J. Reno and D. R. Williams, *Org. Lett.*, **2000**, *2*, 1165-1168.
[219] R. Luisi, V. Capriati, P. Di Cunto, S. Florio and R. Mansueto, *Org. Lett.*, **2007**, *9*, 3295-3298.
[220] B. Das, Y. Srinivas, C. Sudhakar, K. Damodar and R. Narender, *Synth. Commun.*, **2008**, *39*, 220-227.
[221] R. Rodebaugh, J. S. Debenham, B. Fraser-Reid and J. P. Snyder, *J. Org. Chem.*, **1999**, *64*, 1758-1761.
[222] D. K. MacFarland and C. R. Landis, *Organometallics*, **1996**, *15*, 483-485.
[223] E. P. Peçanha, L. J. O. Figueiredo, R. M. Brindeiro, A. Tanuri, A. R. Calazans and O. A. C. Antunes, *Il Farmaco*, **2003**, *58*, 149-157.
[224] M. Karplus, *J. Am. Chem. Soc.*, **1963**, *85*, 2870-2871.
[225] G. R. Fulmer, A. J. M. Miller, N. H. Sherden, H. E. Gottlieb, A. Nudelman, B. M. Stoltz, J. E. Bercaw and K. I. Goldberg, *Organometallics*, **2010**, *29*, 2176-2179.
[226] O. Trapp, *J. Chromatogr. B*, **2008**, *875*, 42-47.
[227] O. Trapp, ChemOrganizer MMXIII, *Ruprecht-Karls-Universität Heidelberg*,
[228] M. J. Frisch, G. W. Trucks, H. B. Schlegel, G. E. Scuseria, M. A. Robb, J. R. Cheeseman, G. Scalmani, V. Barone, G. A. Petersson, H. Nakatsuji, X. Li, M. Caricato,

A. V. Marenich, J. Bloino, B. G. Janesko, R. Gomperts, B. Mennucci, H. P. Hratchian, J. V. Ortiz, A. F. Izmaylov, J. L. Sonnenberg, Williams, F. Ding, F. Lipparini, F. Egidi, J. Goings, B. Peng, A. Petrone, T. Henderson, D. Ranasinghe, V. G. Zakrzewski, J. Gao, N. Rega, G. Zheng, W. Liang, M. Hada, M. Ehara, K. Toyota, R. Fukuda, J. Hasegawa, M. Ishida, T. Nakajima, Y. Honda, O. Kitao, H. Nakai, T. Vreven, K. Throssell, J. A. Montgomery Jr., J. E. Peralta, F. Ogliaro, M. J. Bearpark, J. J. Heyd, E. N. Brothers, K. N. Kudin, V. N. Staroverov, T. A. Keith, R. Kobayashi, J. Normand, K. Raghavachari, A. P. Rendell, J. C. Burant, S. S. Iyengar, J. Tomasi, M. Cossi, J. M. Millam, M. Klene, C. Adamo, R. Cammi, J. W. Ochterski, R. L. Martin, K. Morokuma, O. Farkas, J. B. Foresman and D. J. Fox, Gaussian 16, *Wallingford, CT*, **2016**.

[229] A. D. Becke, *J. Chem. Phys.*, **1993**, *98*, 5648-5652.

[230] S. Grimme, S. Ehrlich and L. Goerigk, *J. Comput. Chem.*, **2011**, *32*, 1456-1465.

[231] T. H. D. Jr., *J. Chem. Phys.*, **1989**, *90*, 1007-1023.

[232] D. E. Woon and T. H. D. Jr., *J. Chem. Phys.*, **1993**, *98*, 1358-1371.

[233] C. Monti, C. Gennari, U. Piarulli, J. G. de Vries, A. H. de Vries and L. Lefort, *Chem. - Eur. J.*, **2005**, *11*, 6701-6717.

[234] A. H. M. de Vries, A. Meetsma and B. L. Feringa, *Angew. Chem. Int. Ed. Engl.*, **1996**, *35*, 2374-2376.

[235] H. Hey and H. J. Arpe, *Angew Chem Int Edit*, **1973**, *12*, 928-929.

[236] J. J. Plattner, R. D. Gless and H. Rapoport, *J. Am. Chem. Soc.*, **1972**, *94*, 8613-&.

[237] T. H. Applewhite and C. Niemann, *J. Am. Chem. Soc.*, **1959**, *81*, 2208-2213.

9 Danksagung

An erster Stelle möchte ich mich bei meinem Doktorvater Prof. Dr. Oliver Trapp dafür bedanken, dass er mir die Möglichkeit gegeben hat, diese Arbeit in seinem Arbeitskreis anzufertigen. Seine andauernde Unterstützung und die vielen konstruktiven Diskussionen haben maßgeblich zur Entfaltung des Themas beigetragen und seine motivierende und aufrichtende Art habe ich während meiner Zeit im Arbeitskreis sehr zu schätzen gelernt.
Ich danke Prof. Dr. Paul Knochel, der sich bereit erklärt hat, die Aufgabe des Zweitgutachters für meine Dissertation zu übernehmen.
Ich danke der Max-Planck-Gesellschaft für die finanzielle Unterstützung.
Weiterer Dank gilt den Mitarbeitern der Analytiklabore der Universität Heidelberg unter der Leitung von Dr. Jürgen Graf (NMR-Spektroskopie), Dr. Rominger (Kristallstrukturanalyse) und Dr. Jürgen Gross (Massenspektrometrie), sowie der Ludwig-Maximilians-Universität München unter der Leitung von Dr. Stephenson (NMR-Spektroskopie), Dr. Mayer (Kristallstrukturanalyse), Dr. Kempf (Elementaranalyse) und Dr. Spahl (Massenspektrometrie) für die Ausführung der analytischen Messungen und für die kompetente Beratung bei analytischen Problemstellungen. Ebenso unverzichtbar waren Ute Gärtner und Christiane Hölscher in Heidelberg und Dr. Claudia Meier, Brigitte Janker, Carrie Louis und Hildegart Lipfert in München, bei denen ich im Falle organisatorischer Fragen und bei der Bewältigung der kleinen und großen Probleme des universitären Arbeitsalltags stets Hilfe gefunden habe.
Ich danke allen Mitgliedern und Ehemaligen der AMPCAT-Gruppe, im Besonderen Max Siebert und Golo Storch, für die zahlreichen, gewinnbringenden Diskussionen rund um stereodynamische Systeme und die asymmetrische Katalyse, und des Weiteren Alexander Siegle, Max Siebert, Max Seibicke, Stefanie Auras, Jan Menke und Golo Storch für das Engagement bei der Korrektur meiner Manuskripte.
Danken möchte ich außerdem meinen ForschungspraktikantInnen Florian Kromm, Christian Schiwek, Fabian Pilz, Gloria Betzenbichler und Christian Bini für ihre Arbeit, ihr Engagement und ihre Anregungen.
Außerhalb des Fachlichen möchte ich allen Arbeitskreismitgliedern aus Heidelberg und München meinen Dank dafür aussprechen, dass ich meine Zeit als Doktorand mit ihnen teilen durfte: Claudia Meier, Brigitte Janker, Carrie Louis, Hildegart Lipfert, Kai Kohler, Elina Fuks, Saskia Lamour, Maren Haas, Sebastian Pallmann, Florian Kruse, Gloria Betzenbichler, Fabian Sauer, Alexander Siegle, Jennifer Teichert, Anna Closs, Sophia Schwarz, Jan Menke, Stefanie Auras, Max Siebert, Max Seibicke, Constanze Sydow, Golo Storch, Jana Šteflová, Regina Berg, Michael Ziegler, Skrollan Stockinger, Marie-Louise Morkos, Julia Gmeiner, Kerstin Zawatzky, Ute Gärtner und Sarah Wiesner. Ich danke Kai für das Teilen seiner Kaffee-Kochkünste, Maren für den geteilten Spaß auf der Skipiste. Elina, Felix und Basti danke ich für die sportliche Motivation beim Badmintonspiel, Fabi und Alex für die geilte Freude an Erdnussbutter und körperlicher Selbstkasteiung. Bei MJ bedanke ich mich für die vielen anregenden Gespräche, die witzigen Wow-Momente und die musikalische Weiterbildung und beim schönen Max für die vielen Komplimente. Jan und Steffi danke ich als Labornachbarn für die lockere Atmosphäre und den herzlichen Umgang, der so manchen frustrierenden Nachmittag erträglicher gemacht hat.
Besonders danken möchte ich an dieser Stelle Golo. Für die charakterbildenden Kochabende und Autofahrten, sowie für andere gemeinsame, freundschaftliche Unternehmungen und bestandene Abenteuer in Mannheim, Heidelberg und München.

Gleiches gilt für Saskia. Als Mitstreiterin vom ersten Tag meiner Doktorarbeit an habe ich deine ehrliche und offene Art sehr schätzen gelernt und liebgewonnen. Vielen Dank für die gemeinsame Zeit bei Spieleabenden, die lehrreichen Gespräche über den Ernst des Lebens und deine beständige Anteilnahme.
Mein spezieller Dank geht weiterhin an Yuri. Deine Freundschaft und Kameradschaftlichkeit während der Zeit an der Uni war unersetzlich. Ich bedanke mich für die zahlreichen Erlebnisse abseits der Laborbank, für die langen Abende mit horizonterweiternden Streitgesprächen auf der einen und mit geistigen Exkursen von fragwürdiger Sinnhaftigkeit auf der anderen Seite. Und für russisches Frühstück.
In besonderem Maße bedanken möchte ich mich auch bei Basti. Ich danke dir für die gemeinsame, schöne Zeit als Mitbewohner und Kollege und darüber hinaus für die entgegengebrachte Freundschaft, die mich gestützt und die vergangenen Jahre maßgeblich mitgeprägt hat. Vielen Dank für die vielen gemeinsamen Serien- und Musikabende, die Unternehmungen, für Gesprächen über Gott und die Welt und für ein offenes Ohr in guten und in schwierigen Zeiten.
Ich bedanke mich bei allen, deren Freundschaft ich aus Kassel und Heidelberg mit nach München genommen habe, die mich während meines gesamten Studiums begleitet, mir zahlreiche unvergessliche Abende und manchmal auch die notwendige Ablenkung beschert haben.
Mein besonderer Dank gebührt außerdem Ariane Laferrière. Deine Unterstützung ist unbezahlbar und ich danke dir dafür, dass du trotz deiner räumlichen Ferne jeden Tag Anteil an meiner Freude und meiner Sorge genommen hast, die ich mit nach Hause gebracht habe.
Zuletzt möchte ich meiner Familie danken. Ohne Euch wäre der Weg bis hierher nicht möglich gewesen. Ich danke Euch für euren andauernden Rückhalt und es tut gut zu wissen, dass ihr immer hinter mir steht.